Oxidation of Glutathione, Cysteinesulfinic Acid and N,N-dimethylhydroxylamine Hydrochloride by Transition Metals

by

Nootan Prasad Bhattarai

A dissertation submitted to the Graduate Faculty of
Auburn University
In partial fulfillment of the
Requirements for the Degree of
Doctor of Philosophy

Auburn, Alabama
August 03, 2013

Keywords: Electron-transfer, glutathione, cysteinesulfinic acid, N,N-dimethylhydroxylamine, stopped-flow

Approved by

David M. Stanbury, Chair, Professor of Chemistry and Biochemistry
German Mills, Associate Professor of Chemistry and Biochemistry
Holly Ellis, Associate Professor of Chemistry and Biochemistry
Christian Goldsmith, Assistant Professor of Chemistry and Biochemistry

Abstract

The aqueous oxidations of glutathione (GSH) by the substitutionally inert outer-sphere oxidants $[IrCl_6]^{2-}$, $[Fe(bpy)_2(CN)_2]^{+}$ and $[Fe(bpy)(CN)_4]^{-}$ have been investigated at 25 °C and ionic strength (μ) = 0.1 M between pH 1 and 11. All these reactions are catalyzed by trace amounts of Cu^{2+} ions. Such catalysis can be effectively prevented with addition of 1 mM dipic for the reduction of $[IrCl_6]^{2-}$ and $[Fe(bpy)_2(CN)_2]^{+}$ and is completely impeded with 5 mM EDTA for the reduction of $[Fe(bpy)(CN)_4]^{-}$. The kinetic reactions with Fe^{III} are mildly inhibited by the product Fe^{II} at low pH and are controlled by the use of spin trap PBN (N-tert-butyl-α-phenylnitrone). $[IrCl_6]^{2-}$ oxidizes GSH yielding $[IrCl_6]^{3-}$ and GSO_3^- with some GSSG in presence of O_2; in the absence of O_2, the Fe^{III} compounds are reduced to their corresponding Fe^{II} products with almost quantitative formation of GSSG. All three reactions have common rate laws that are first order in [oxidant] and [reductant]. The general rate law is $-d[M_{ox}]/dt = k_{obs}[M_{ox}]$ with

$k_{obs} = k[GSH]_t = k_1[HGSH^+] + k_2[GSH^0] + k_3[GSH\text{-}H^-] + k_4[GSH\text{-}2H^{2-}] + k_5[GSH\text{-}3H^{3-}]$.

Inclusion of all respective pK_a terms of tetra-protic GSH leads to

$$k_{obs} = \left[\frac{k_1[H^+]^4 + k_2K_{a1}[H^+]^3 + k_3K_{a1}K_{a2}[H^+]^2 + k_4K_{a1}K_{a2}K_{a3}[H^+] + k_5K_{a1}K_{a2}K_{a3}K_{a4}}{[H^+]^4 + K_{a1}[H^+]^3 + K_{a1}K_{a2}[H^+]^2 + K_{a1}K_{a2}K_{a3}[H^+] + K_{a1}K_{a2}K_{a3}K_{a4}}\right][GSH]_t$$

where K_{a1}, K_{a2}, K_{a3} and K_{a4} are the successive acid dissociation constants of GSH. The rate laws show a general increase in rate with increasing pH. The pH resolved rate constants are described with a mechanism having rate-limiting outer-sphere electron transfer from the various thiolate forms of GSH.

An investigation of oxidation of cysteinesulfinic acid ($CysSO_2H$) by $[IrCl_6]^{2-}$ is described at 25 °C and ionic strength (μ) = 0.1 M between pH 3 and 5.6 adjusted with acetate buffers. This reaction is unaffected by the trace metal ions Cu^{2+} and Fe^{2+}, as observed with thiols. ^{1}H-NMR analysis shows that $CysSO_2H$ is quantitatively oxidized to the corresponding sulfonic acid and UV-vis data indicate the reduction of $[IrCl_6]^{2-}$ to $[IrCl_6]^{3-}$. The rate law is first order in $[CysSO_2H]$ and second order in $[IrCl_6]^{2-}$ with simple pH independent kinetics and an inverse dependence on $[IrCl_6]^{3-}$. The rate law is

$$\text{rate} = -\frac{d[\mathrm{IrCl_6^{2-}}]}{dt} = \frac{k[\mathrm{IrCl_6^{2-}}]^2[\mathrm{CysSO_2H}]_t}{[\mathrm{IrCl_6^{3-}}]}.$$

The oxidation of N,N-dimethylhydroxylamine by $[IrCl_6]^{2-}$ has been examined within the pH range 3.6-7.8 applying suitable buffers and keeping ionic strength at 0.1 M ($NaClO_4$). These reactions are catalyzed by Cu^{2+} and Fe^{2+} ions and the catalysis can be inhibited with 1 mM $[C_2O_4^{2-}]$. The rate law is

$$-\frac{d[\mathrm{Ir^{IV}}]}{dt} = k_{obs}\,[\mathrm{Ir^{IV}}]$$

where $k_{obs} = [\frac{k_1 K_{a1}}{[H^+] + K_{a1}} + \frac{k' K_{a1}}{[H^+]\{[H^+] + K_{a1}\}}][DMH]_t$. The pH resolved rate constants are k_1 = $(5.19 \pm 0.15) \times 10^2$ M^{-1} s^{-1} and k' = $(4.45 \pm 0.28) \times 10^{-5}$ s^{-1}.

Acknowledgements

First and foremost, I would like to offer my profound gratitude and deep regards to my supervisor, Professor David M. Stanbury for the patient guidance, support and advice throughout my time as his student. Without his helpful guidance and impressive teaching, I would not be able to complete my Ph. D. work along with attitude to be a scientist. Indeed, he played roles of an effective academic guardian. I am grateful to my committee members, Dr. German Mills, Dr. Holly Ellis and Dr. Christian Goldsmith for their kind and appropriate suggestions regarding my research and career. I also thank Dr. Michel Meadows and Dr. Yonnie Wu for helping NMR processing and mass spectrometry respectively. Dr. Na Song is also thanked for her help during my work.

I never forget my parents: my mother, father, wife, son, daughter and other family members for their encouragements and unconditional love in spite of all the time it took me away from them. It was a long and difficult journey for them. My mother's inspiration and contribution to acquire higher degree led me to this position. The support, patience and practical understanding of my loving wife Jhenuka always energized me to move ahead. I am deeply indebted to all of my family members.

I would like to thank almighty and beloved Swami, **Satya Saibaba** who always responded to my prayers all the time and guided me spiritually to live a disciplined life.

Finally, my thanks go to all people who have supported to accomplish the research work directly or indirectly.

Table of Contents

List of Tables

List of Schemes

List of Figures

Chapter 1

Literature Review

1.1. Redox reactions (electron transfer processes). Redox reactions are some of the key chemical processes through which energy can be produced and utilized in industry and in living organisms. A key feature of redox reactions is electron transfer between two reactants. These reactions are equally important in chemistry as well as in biological processes such as respiration, photosynthesis, oxygen binding, nitrogen fixation and phosphorylation.[1-4] Fig 1.1 depicts fields that involve electron-transfer reactions and their importance.[1a]

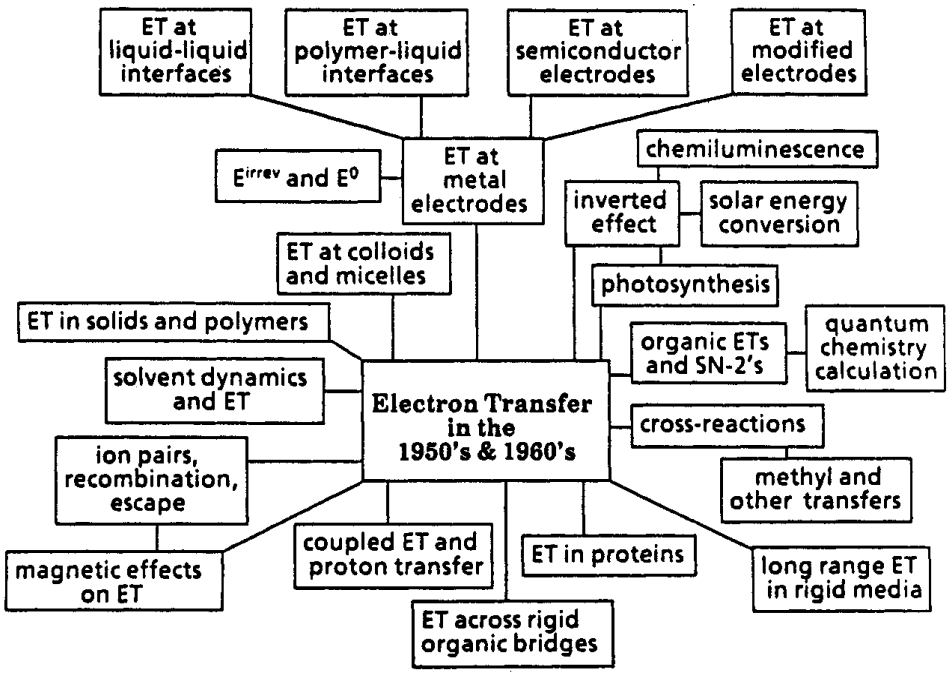

Fig 1.1. Examples of numerous topics in the electron transfer field.[1a]

Such reactions are complementary or non-complementary. In complementary reactions the change in oxidation state of both oxidant and reductant is equal whereas in non-complementary reactions the change is different.[5] The mechanism of electron transfer can be classified as either inner-sphere or outer-sphere, according to Taube.[6,7] Inner-sphere processes involve the sharing of a ligand in the first coordination sphere of the oxidant and reductant during the transition state as in Scheme 1.1.[6,7,8]

$$L_5M^{III}X + M^{II}(Y)_6 \rightarrow L_5M^{III}\text{-----}X\text{ ------ }M^{II}(Y)_5 + Y \rightarrow \text{Products.}$$

Scheme 1.1

The "X" ligand of the acceptor is acting as a bridge in the above scheme.

In the outer-sphere mechanism the two reactants do not form a common ligated bridge between donor and acceptor atoms. The assumption here is that the weak interaction of two relevant orbitals of the two centers restrict the sharing of the ligand.[3]

A reaction occurs only when two reactants come closer enough to each other so that the coupling of their electronic orbitals can take place. This phenomenon is described via the collision theory developed by Debye in 1942. This theory considers the reacting species, acceptor atom (A) and donor (D), as colliding spheres having specific charge(s) and radius. The collision between donor and acceptor is diffusion controlled.[9] If the colliding spheres D and A have their radii r_1 and r_2 with charge p and q respectively then the electrostatic force/energy (w_{12}) between them, when they are in equilibrium, is described by in eq 1.1

$$w_{12} = \frac{pqe^2}{Dr_{12}(1+\beta r_{12}\sqrt{\mu})} \qquad (1.1)$$

where the β = reciprocal Debye radius, separation distance ($r_{12} = r_1 + r_2$), e = electron charge, D = dielectric constant of the medium and μ = ionic strength.[10] A representation of the colliding sphere model is shown in Scheme 1.2 [9]

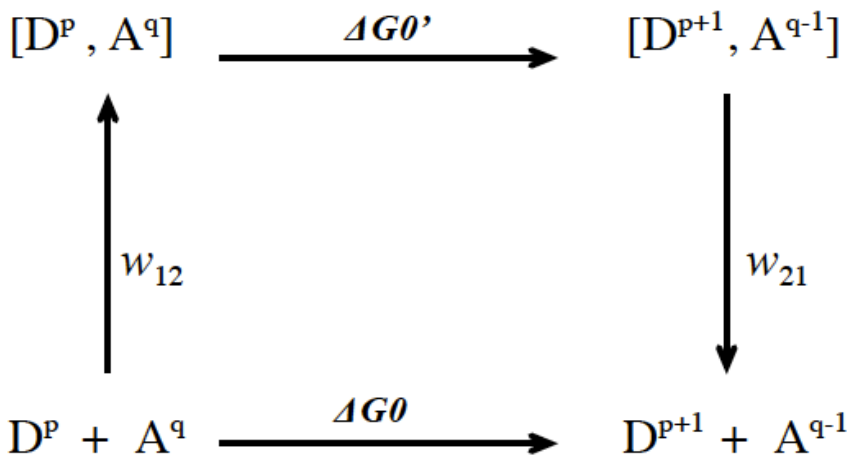

Scheme 1.2. Electron transfer process

The short lived reactant pair formed after collision is represented by precursor **$[D^p, A^q]$,** electron transfer results in another transient pair, successor **$[D^{p+1}, A^{q-1}]$**. Dissociation of the latter yields the final product, **$[D^{p+1} + A^{q-1}]$**. w_{21} is the energy involved to form the product and is obtained via equation 1.2.

$$w_{21} = \frac{(p+1)(q-1)e^2}{Dr_{12}(1+\beta r_{12}\sqrt{\mu})} \qquad (1.2)$$

Marcus[11] and others[12] have given extended explanation of this model. In Scheme 1.2, there are two free energy terms ΔG^0 and $\Delta G^{0'}$. $\Delta G^{0'}$ is the corrected Gibbs free energy which is obtained from equation 1.3.

$$\Delta G^{0'} = \Delta G^0 + w_{21} - w_{12} \qquad (1.3)$$

(where $w_{21} = w_{\text{product}}$ and $w_{12} = w_{\text{reactant}}$)

If the standard reduction potentials of the reductant and oxidant are available, the ΔG^0 can be derived using equation 1.4[9]

$$\Delta G^0 = -nFE^0_{cell} \qquad (1.4)$$

where $E^0_{cell} = (E^0_{\text{oxidant}} - E^0_{\text{reductant}})$, n = number of electron exchanged and F = Faraday constant.

1.1.1. Marcus Theory of Electron Transfer. The mechanism of electron transfer between molecules in solution was developed by R. A. Marcus and for which he was awarded the Nobel Prize of the year 1992. His theory is equally applicable to chemistry and biology.[9,13-18] Many articles and texts have outlined and reviewed the theory of electron transfer in solutions.[19-27] During electron transfer, several structural alterations (reorganizational activities) take place, due to change in electronic properties and charge distribution of reactant molecules and solution medium that facilitate the transfer process. According to Marcus and Sutin, such a phenomenon is best explained using Fig 1.2a-c.[3]

Fig 1.2a-c illustrates the three different electronic energy levels of the electron on the two reactant atoms, i.e. donor atom (1) and acceptor atom (2), with corresponding nuclear energy curves. Initially, the electron is localized on atom (1). The equilibrium position for this case is located at point (A) in the nuclear potential energy diagram (Fig 1.2a, right). The dashed lines indicate the electronic energy level relationship of the two. Before electron transfer, a fluctuation of positions of both nuclei occurs producing a new nuclear configuration (B) (Fig 1.2b, right). At this point, there is no electronic energy level difference between the two reactants. This occurs because of the rise of electronic orbital energy of the donor atom and lowering of the same of the acceptor atom. This is the suitable condition for electron transfer to take place. After the transfer of electron the entire system undergoes further rearrangements attaining a new nuclear configuration leading to a new equilibrium (C) for the products as shown in Fig 1.2c

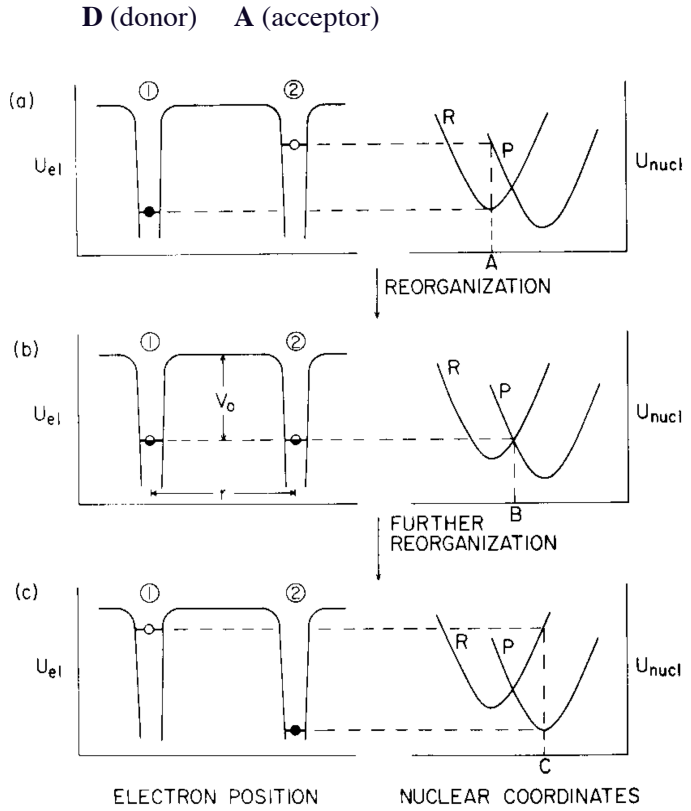

Fig 1.2. Illustration of the electron transfer process showing electronic potential energy curves along with the corresponding nuclear potential energy curves. Figure taken from ref.[3]

Following the Marcus theory, $\Delta G^{\ddagger}$ is given by equation 1.5

$$\Delta G^{\ddagger} = w_{12} + \frac{\lambda}{4}\left(1 + \frac{\Delta G^{0\prime}}{\lambda}\right)^2 \qquad (1.5)$$

where, $\lambda = \lambda_i + \lambda_0$; λ_i *and* λ_0 correspond to reorganizational energy of reactants and solvent respectively. Fig 1.3 provides the schematic representation of potential energy diagram involving $\Delta G^{\ddagger}$, λ and $\Delta G^{0'}$.

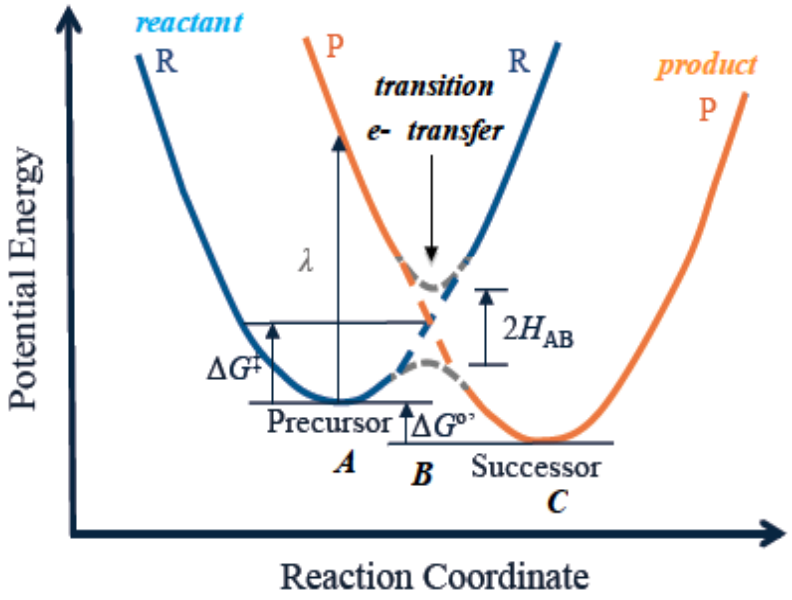

Fig 1.3. Potential energy profile surfaces for reactants and products with their corresponding environment in outer-sphere electron transfer reaction.[3a]

The transition state in Fig 1.3 is the meeting point of the two parabolas representing reactant (R) and product (P) where there is a maximum chance of an electron to be transferred following the well-known Frank-Condon Principle which states that the relative positions and momenta of the atoms are preserved during electronic transitions (electronic transitions in the range 10^{-15} s whereas vibration of molecules 10^{-13} s). The orbitals of the donor and acceptor atoms may mix together due to weak electronic interactions to produce electronic coupling.[3] $\Delta G^{\ddagger}$, the free energy of activation and the rate constant (k_{et}) have a relationship with each other as in equation 1.6.

$$k_{et} = k\, Z \exp(-\Delta G^{\ddagger}/RT) \qquad (1.6)$$

where, Z and κ are collision frequency ($Z = 1 \times 10^{11}$ M^{-1} s^{-1}) and the transmission coefficient ($\kappa = 1$ in an adiabatic reaction) respectively.

1.1.2. Application of Marcus Theory (Marcus Cross Relationship). In spite of the several approximations of the model, Marcus theory has been successful to treat the rates of outer-sphere electron transfer reactions. This model works well for the reactions that occur between compounds which are weakly charged and have substitutionally inert and saturated coordination shells in their respective reduced and oxidized forms. [28]

In Marcus's cross relationship, the rate constant for the electron transfer is

$$k_{12} = (k_{11}\, k_{22}\, K_{12}\, f_{12})^{1/2}\, W_{12} \tag{1.7}$$

$$lnf_{12} = \frac{[lnK_{12} + \frac{w_{12} - w_{21}}{RT}]^2}{4[\ln(\frac{k_{11}k_{22}}{Z^2}) + (\frac{w_{11} + w_{22}}{RT})} \tag{1.8}$$

$$lnW_{12} = -[(w_{12} + w_{21} - w_{11} - w_{22}) / 2RT] \tag{1.9}$$

In the above equations, the individual work terms (w_{12}, w_{21}, w_{11}, w_{22}) are obtained as:

$$w_{ij} = \frac{p_i q_j e^2}{Dr_{ij}(1 + \beta r_{ij}\sqrt{\mu})} \tag{1.10}$$

K_{12} is the equilibrium constant, W_{12} and f_{12} are factors, which rely on radii and charge of the reactants, medium of the reaction and ionic strength.

Self exchange rate constants k_{11} and k_{22} are calculated from the following reactions:

$$^{*}D^{p} + D^{p+1} \rightleftharpoons D^{p} + {}^{*}D^{p+1} \qquad k_{11},\ \lambda_{11} \qquad (1.11)$$

$$^{*}A^{q} + A^{q-1} \rightleftharpoons A^{q} + {}^{*}A^{q-1} \qquad k_{22},\ \lambda_{22} \qquad (1.12)$$

$$\text{Precursor } [D^{p}, A^{q}] \rightleftharpoons \text{successor}[D^{p+1}, A^{q-1}] \qquad k_{12},\ \lambda_{12} \qquad (1.13)$$

The donor D and acceptor A atoms have their corresponding oxidized and reduced forms as shown in eq 1.11 and 1.12. k_{11} and k_{22} are the self exchange rates of D and A respectively. λ is reorganizational energy.

In self exchange reactions, $\Delta G^{0'}$ is 0 and in such case, eq 1.5 reduces to eq 1.14

$$\Delta G^{\ddagger} = w_{12} + \frac{\lambda}{4} \qquad (1.14)$$

λ_{12} is supposed to be an average of λ_{11} and λ_{22} as in eq 1.15 [3, 29]

$$\lambda_{12} = \frac{\lambda_{12} + \lambda_{22}}{2} \qquad (1.15)$$

1.1.3. Tools and Techniques. To complete this research work, several tools and techniques were used. The techniques mostly used are ^{1}H-NMR, UV-vis spectroscopy, cyclic voltammetry, mass spectrometry and stopped-flow spectrophotometry. Cyclic voltammetry was used to check the purity and standard electrode potential of the synthesized and purchased metal compounds. It was also used to analyze the product related with Ir^{IV} reactions. ^{1}H-NMR was useful to check the purity of the glutathione (GSH), dimethyl hydroxylamine hydrochloride (DMH), and cysteinesulfinic acid. It was

a good tool to analyze the products as well. Likewise, UV-vis spectroscopy was used to identify the metallic products related to Fe^{II}, determine the stoichiometric ratio, check the stability of the oxidants and reductants and to follow reactions with slow kinetics.

Stopped-flow spectrometry was used for fast reactions. The schematic diagram of this technique is depicted in Fig 1.4.

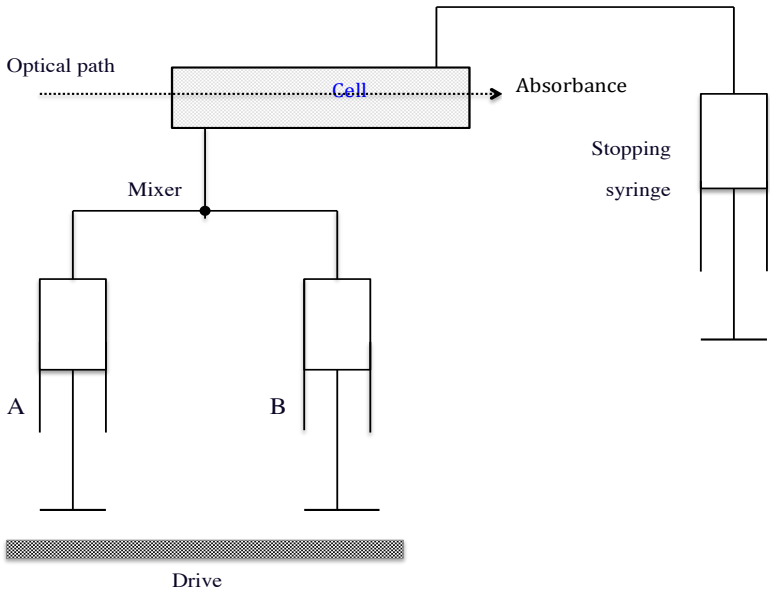

Fig 1.4. Sketch of stopped-flow instrumentation.

The stopped-flow instrument was designed with two separate sample drive syringes, A and B (Fig 1.4) along with a stopping syringe. Equal volumes of each reagent solutions are rapidly driven through the mixer into an observation cell and then to the stopping syringe. As soon as the stopping syringe is filled, the flow system stops and activates the data acquisition process. An appropriate drive system, for example, air pressure is used to inject the solutions. The input volume is controlled by the stop syringe to enhance the

stopped-flow mechanism.[30,31]The absorbance of reactants or products at a particular wavelength is recorded as a function of time.

1.2. Thiols. Thiols play crucial roles in important biological processes.[32-37] Examples of some thiols are homocysteine, L-cysteine and glutathione, shown in Scheme 1.3a-c.

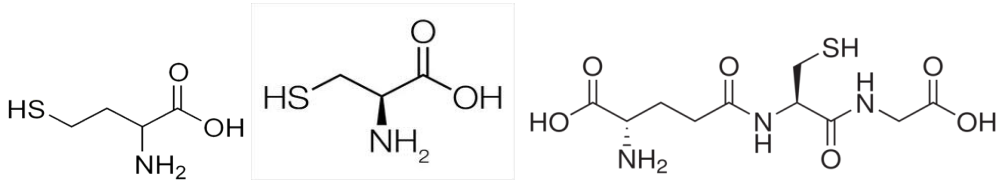

a. Homocysteine b. L-cysteine c. Glutathione

Scheme 1.3

Thiols are distinguishable by their thiol functional group (–SH) in which the sulfur atom is bonded to a carbon atom i.e. R-SH. The C-S bonds are not easily cleaved. Once the thiols undergo oxidation to their respective disulfide they can be reduced back for further use.[38,39] Sulfur atoms have electronic configuration of $[Ne]3s^2 3p^4$ and possible vacant d-orbitals (?) for bonding, which allows then to attain multiple oxidation states ranging from (-2 to +6). They are large in size, polarizable and electron rich as well. These properties make them good electrophiles, and in most of the cases it is their thiolate form (RS^-) that is responsible for the chemical reactivities.[40] Fig 1.5 shows the various sulfur oxidation states relevant to thiol oxidation.[39,41,42]

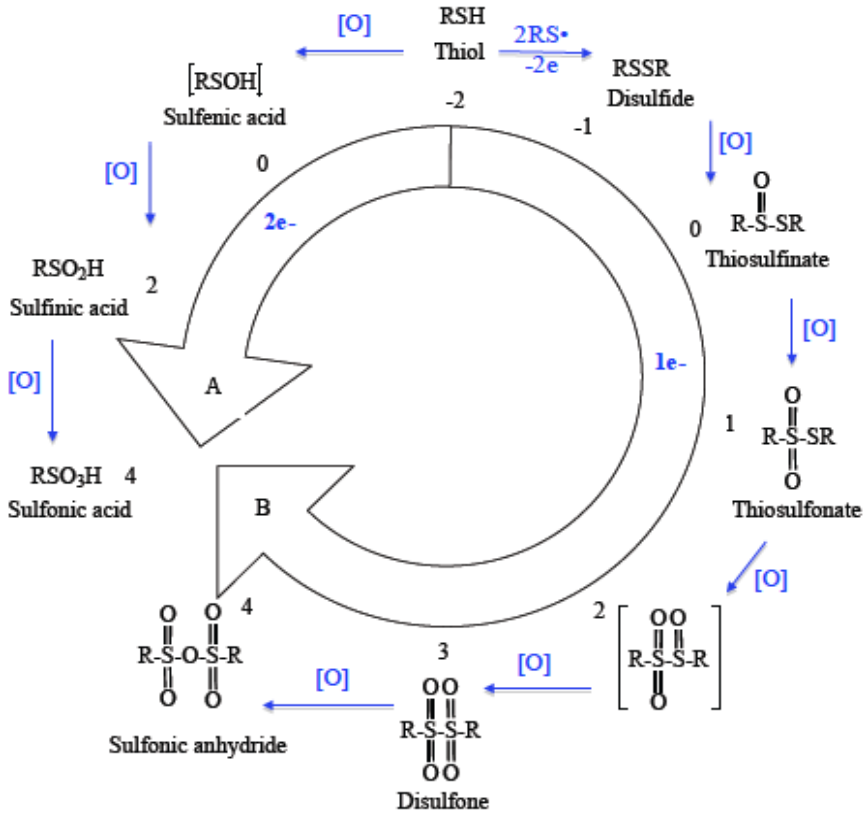

Fig 1.5. Various oxidation states of sulfur in different thiol oxidation products and intermediates.[42a]

Thiols have their roles as protectants for the cellular damage from reactive oxygen species (ROS) and reactive nitrogen species (RNS; •NO, $•NO_2$), toxic metal ions[43,44,45] and photolysis.[46,47] Some of these reactions are shown in equations 1.16 -1.21.

$$O_2 + e^- \rightarrow O_2^{\bullet -} \qquad (1.16)$$

$$O_2^{\bullet -} + 2H^+ + e^- \rightarrow H_2O_2 \qquad (1.17)$$

$$H_2O_2 + H^+ + e^- \rightarrow {}^{\bullet}OH + H_2O \qquad (1.18)$$

$$RSSR + h\nu \rightarrow 2RS^{\bullet} \quad (1.19)$$

$$RSH + M^{n} \rightarrow RS^{\bullet} + M^{n-1} + H^{+} \quad (1.20)$$

$$Fe^{2+}/Cu^{1+} + H_2O_2 \rightarrow Fe^{3+}/Cu^{2+} + {}^{\bullet}OH + OH^{-} \quad (1.21)$$

Such toxic species deplete the thiols producing free radicals (RS·) which are harmful and must be destroyed before they cause damage to the cells. The way how thiols fight against these free radicals is mostly through electron transfer, hydrogen atom transfer etc., reactions as in equations[43,48] (1.22-1.23)

$$RS^{-} + R'^{\bullet} \rightarrow RS^{\bullet} + R'^{-} \quad (1.22)$$

$$RSH + R'^{\bullet} \rightarrow RS^{\bullet} + R'H \quad (1.23)$$

In the equations 1.21 and 1.22 R'• is any destructive radical, R'H and R'- are products. The scavenging of R'· by thiols produces another highly reactive thiyl radical (RS·); however, thiyl radicals may undergo reduction to regenerate the thiolate ion (eq 1.24), or thiol (eq 1.25) or may combine with a thiolate ion to produce disulfide a radical anion (eq 1.26) leading to the disulfide product (eq 1.27).[43,49,50]

$$RS^{\bullet} + e^{-} \rightarrow RS^{-} \quad (1.24)$$

$$RS^{\bullet} + e^{-} + H^{+} \rightarrow RSH \quad (1.25)$$

$$RS^{\bullet} + RS^{-} \rightarrow RSSR^{\bullet -} \quad (1.26)$$

$$RSSR^{\bullet -} \rightarrow RSSR + e^{-} \quad (1.27)$$

1.2.1. Glutathione (GSH). Glutathione, a pervasive non-protein thiol, is an intracellular as well as extracellular tri-peptide composed of three simple common amino acids glutamate, glycine and cysteine. GSH functions as an antioxidant and protects cells against the cellular damage from endogenous and exogenous toxins by undergoing oxidation to save cells.[51,52,53,] It is extensively spread in the tissues of all living organisms.[54,55] This small molecule has been studied extensively (GSH was identified 100 years ago[55]) to observe its multifunctional properties such as biosynthesis of macromolecules, oxygen toxicity, transport, environmental toxins, drug metabolism, cancer, immune phenomena etc.[56,57] The thiol group (-SH) of the GSH cysteine moiety is biologically active and is associated with a variety of glutathione functions and intracellular stability. The glutamate side linkage also plays roles in the GSH diverse functionality.[58] GSH production takes place in the cystosol from precursor amino acids. The GSH concentration in cells of living systems (mammalian etc.) is in the millimolar range (0.5- 10 mM)[57], while in human blood plasma it is in the micromolar range (≅ 2.8 μM).[59]

One of the major functions of GSH, apart from cysteine storage,[60] signal transduction,[61] apoptosis[62] and others as already mentioned above, is to maintain redox balance in the cell.[63] The free reduced form of GSH in the cell amounts to about 98% of the total GSH and the oxidized disulfide (GSSG) form corresponds to only about 2%. The glutathione status in the cell is indicative of its functionality and viability. The redox equilibrium ratio of thiol/disulfide (GSH/GSSG) in the plasma can be used to assess the oxidative stress.[64,65,66] The redox potential of this system is obtained from the Nerst equation (eq 1.28)

$$E = E_0 + \frac{RT}{nF} \ln \left[\frac{\text{GSSG}}{2\text{GSH}}\right] \quad (1.28)$$

where, E^0 = standard potential of the redox couple (E^0 = -240 mV at pH 7.0, for the couple 2GSH/GSSG),[67] n = number of electron(s) exchanged, R = gas constant, F = Faraday's constant and T = temperature.

Glutathione undergoes 1e⁻ oxidation according to Scheme 1.4 [52]

$$2\text{GSH} + \text{oxidant} \underset{+2e^-}{\overset{-2e^-}{\longleftrightarrow}} \text{GSSG} + \text{reductant}$$

Scheme 1.4

A higher redox potential of the cell means higher usage of GSH. It is due to over-production of ROS and RNS which increases the oxidative/nitrosative stress. The system creates some of the disulfide formed as a product back to GSH (Scheme 1.4) using glutathione reductase: however, the disulfide is exported to some extent resulting in GSH depletion. Fig 1.6 shows how GSH is produced and destroyed in neurons as in other cells.[68,69,70] Ultimately a decreased GSH level limits its protecting function, the effect of which has been linked to various types of diseases such as cardiovascular risk,[71] type-2 diabeties,[72] respiratory disorder,[73] and Parkinson's disease.[68] Many factors can cause a decrease of GSH concentration in the body. These are chemical and environmental threats, disease, lifestyle (abuse of alcohol, smoking), aging, diet etc. For all these

reasons a healthy balance between the needs and availability of glutathione must be preserved, which can be achieved through proper diet, for instance, fresh fruits, vegetables, nuts, and eliminating processed and canned foods.[74]

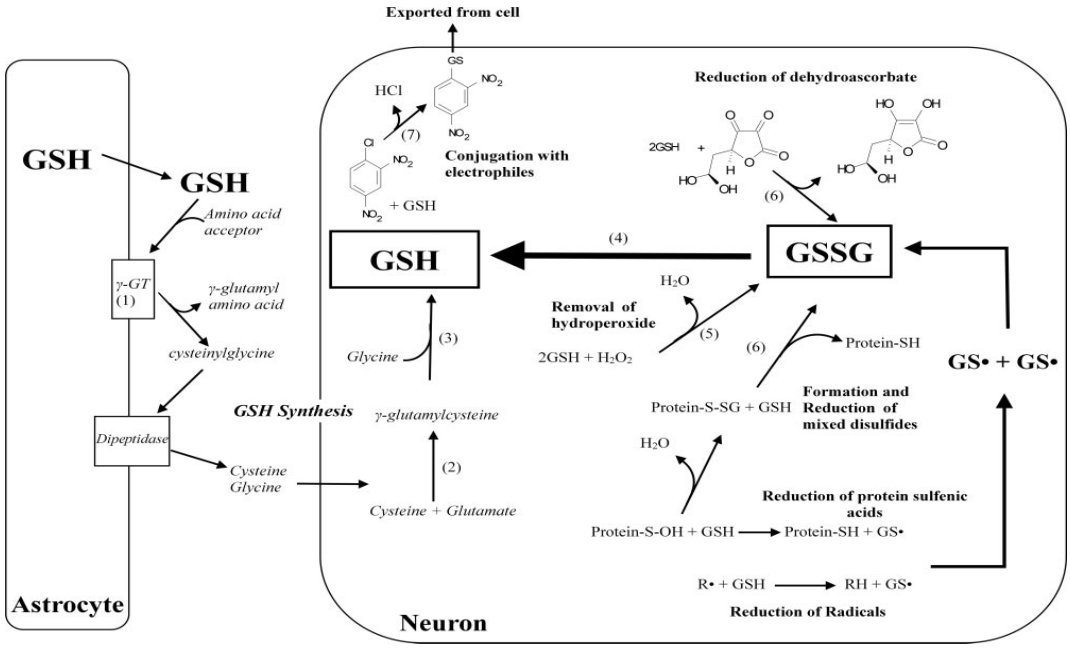

Fig 1.6. Synthesis and metabolism of glutathione in the central nervous system. [Ref 68,69,70]

Fig (1) Ecto-enzyme g-GT. (2) Glutamate-cysteine ligase (GCL). (3) GSH synthase. (4). The oxidized GSSG is reduced back by GSH-reductase and NADPH from the pentose phosphate shunt. (5) GSH-peroxidase. (6) glutaredoxin. (7) glutathione *S*-transferase (GST).

The maintenance of the redox environment in living systems involves electron transfer reactions and GSH does play an important role to remove deleterious oxidants by undergoing oxidation through electron donation processes. Therefore, it is essential to understand and explain the mechanism of such electron transfer processes. To probe the

mechanism of kinetic behavior of GSH with oxidants, three substitutionally inert and weakly charged transitional metal compounds have been chosen in this research.

In chapter two (2), the reaction between GSH and $(NH_4)_2IrCl_6$ in a pH range (1 – 7) is described using various buffers to fulfill the pH requirements. The reaction was found to be first order in both oxidant and reductant. On the basis of the pH dependent kinetics, product analysis and observed stoichiometric ratio, the pathway for the electron transfer between GSH and Ir^{IV} has been proposed.[75]

Similarly, in chapter (3) mixed-ligand iron Fe^{III} complexes (both of which are singly charged but exibit opposite charges) were synthesized and used to oxidize glutathione within the the pH range of 1-11. This chapter incorporates the reactions of all kinetically active deprotonated forms of GSH. The oxidation product was disulfide in contrast to the reaction with Ir^{IV} where the over-oxidation product sulfonic acid was formed.[75]

Likewise, chapter (4) presents an interesting reaction of cysteinesulfinic acid and Ir^{IV} which was found to have pH independent kinetics, with a rate law that was 2^{nd} order in $[Ir^{IV}]$ and inversely proportional to the concentration of metallic product Ir^{III} with no trace metal catalysis.

1.2.2. Trace metal catalysis. Trace metal catalysis (mainly by Cu^{2+} and Fe^{2+}) is always expected in the oxidation of thiols, possibly through the formation of metal-thiol adducts.[76,77,78] Such metal catalysis in the reactions of thiols has been observed since the 1930's.[79,80] It is necessary to suppress the catalytic action of impurity level metals in any

reaction to explain the non-catalyzed reaction mechanism. Suitable inhibitors through chelation can serve this purpose. Ethylenediaminetetraacetic acid (EDTA) seems to be in practice since long ago.[81-85] However, EDTA is susceptible to oxidation, and the M-EDTA complex reserves the risk of being catalytic.[86,87] Alternative effective chelaters, in use, are disodium salt of bathophenanthroline disulfonate, cyclam and 2, 6-pyridinedicarboxylic acid (dipic)[88-92] (Scheme 1.5).

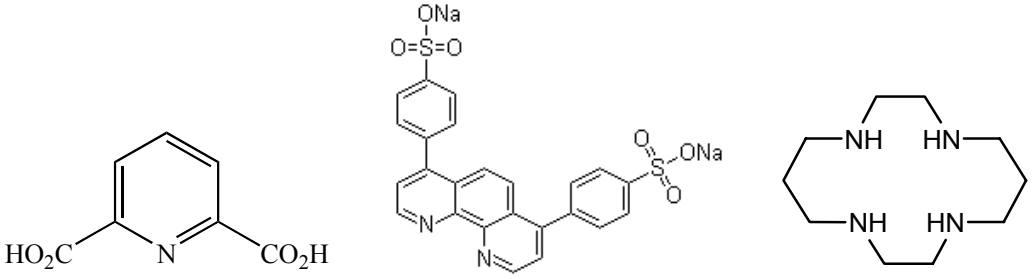

Dipicolinic acid (dipic) Bathophenanthroline disulfonate Cyclam

Scheme 1.5

In this research dipic and EDTA were applied to prevent such adventitious catalysis in the reaction of GSH with various oxidants, and sodium oxalate ($Na_2C_2O_4$)[93] in the reaction of N,N-dimethylhydroxylamine hydrochloride with Ir^{IV}. Details about these chelators are provided in respective chapters.

1.3. $Fe^{II/III}$ and Ir^{IV} Compounds in Redox Reactions. The development of electron transfer processes dates back to the late 1940s. The early studies, in this field

were made on 'self-exchange reactions' (that were based on isotopic exchange reactions as shown in Scheme 1.6 and, later 'cross reactions'.[1,94]

$$Fe^{2+} + Fe^{*3+} \longrightarrow Fe^{*3+} + Fe^{2+}$$

Scheme 1.6 [Ref 94]

Since then, numerous Fe(II/III) compounds with various ligands, including mixed ligands, have been made and used to study kinetics and mechanisms of $1e^-$ electron transfer reactions. Some examples of which include ferricytochrome c,[95] ferric salts,[96] $[Fe(bpy)_3]^{3+}$ and $[Fe(phen)_3]^{3+}$,[97] $[Fe(CN)_6]^{3-}$,[98] Fe(II) and its substituted tris-(1,10-Phenthroline),[99] $Fe(H_2O)_6^{2+}$,[100] Substituted 1,10-Phenanthroline, 2,2'-Dipyridine and 2,2',2″-tripyridine complexes of Fe(III),[101] polypyridine complexes of Fe(III).[102,103] $[Fe(bpy)_2(CN)_2]^+$ and $[Fe(bpy)(CN)_4]^-$,[91] etc. Likewise, use of iridium compound in the redox reactions includes $[IrCl_6]^{2-}$.[92,93,104-112]

In this research work, two one-electron substitution inert low spin d^5 Fe^{III} compounds $[Fe^{III}(bpy)_2(CN)_2]^+$ and $[Fe^{III}(bpy)(CN)_4]^-$,[91,113-115] are synthesized and used to oxidize glutathione. Commercially available $[Ir^{IV}Cl_6]^{2-}$, a substitution inert outer-sphere oxidant is also used to oxidize glutathione, cystienesulfinic acid and N,N-dimethylhydroxylamine after recrystallization. Chapter 5 describes the reaction of N, N-dimethylhydroxylamine hydrochloride with Ir^{IV}. The reaction is highly susceptible to metal ion catalysis that can be effectively inhibited with sodium oxalate, first order in both reductant and oxidant and pH dependent.

References.

1. Marcus, R. A., *Pure and Applied Chemistry* **1997**, *69*, 13.

   (1a). Marcus, R. A. and Siddarth, P. in *Photoprocessess in Transition Metal Complexes, Biosystems and Other Molecules*: *Experiment and theory*, E. Kochanski, ed., Kluwer, Massachusetts, **1992**, pp 49.

2. Chance, B.; Nishimura, M. *Proc. Natl. Acad. Sci. USA* **1960**, *46*, 19.

3. Marcus, R. A.; Sutin, N. *Biochim. Biophys. Acta* **1985**, *811*, 265.

   3a. Song, N. in *Mechanisms and kinetics of Proton-Coupled Electron-Transfer Oxidation of Phenols*, PhD Thesis, Auburn University, **2011**, pp 5.

4. Grimes, C. J.; Piszkiewicz, D.; Fleischer, E. B. *Proc. Natl. Acad. Sci. USA* **1974**, *71*, 1408.

5. Jordan, R. B. *Reaction mechanisms of Inorganic and Organometallic Systems*; 3rd ed.; Oxford University Press: New York, **2007**, pp 253.

6. Taube, H.; Myers, H.; Rich, R. L. *J. Am. Chem. Soc*. **1953**, *75*, 4118.

7. Taube, H; Myers, H. *J. Am. Chem. Soc*. **1954**, *76*, 2103.

8. Jordan, R. B. *Reaction mechanisms of Inorganic and Organometallic Systems*; 3rd ed.; Oxford University Press: New York, **2007**, pp 254.

9. Weinstock, I. A. *Chem Rev.* **1998**, *98*, 113.

10. Kozik, M.; Baker, L. C. W. *J. Am. Chem. Soc.* **1990,** *112*, 7604.

11. Marcus, R. A. *J. Phys. Chem.* **1963**, *67*, 853.

12. Marcus, R. A. *Annu. Rev. Phys. Chem.* **1964**, *15*, 155.

13. Marcus, R. A. *J. Phys. Chem.* **1968**, *72*, 891.

14. Fukuzumi, S.; Wong, C. L.; Kochi, J. K. *J. Am. Chem. Soc.* **1980**, *102*, 2928.

15. Hwang, J. K.; Warshel, A. *J. Am. Chem. Soc.* **1987**, *109,* 715.

16. Arnaut, L. G.; Formosinho, S. J. *J. photochem. Photobiol. A: Chem.* **1993**, *75*, 1.

17. Roth, J. P.; Yoder, J. C.; Won, T. J.; Mayer, J. M. *Science,* **2001**, *294*, 2524.

18. Barzykin, A. V.; Frantsuzov, P. A.; Seki, K.; Tachiya, M. *Adv. Chem. Phys*. **2002**, *123*, 511.

19. Reynolds, W. L. and Lumry, R. W. *Mechanisms of Electron Transfer,* Ronald Press, New York, **1966**.

20. Sutin, N. *Progr. Inorg. Chem.* **1983,** *30*, 441.

21. DeVault, D. *Quantum- Mechanical Tunnelling in Biological Systems*, 2nd ed., Cambridge University Press, New York, **1984**.

22. Sutin, N. *Inorganic Biochemistry* Eichhorn, G. L., ed., Elsevier, New York, **1973**, *vol 2*, p 611.

23. Newton, M. D.; Sutin, N. *Annu. Rev. Phys. Chem*. **1984**, *35*, 437.

24. Marcus, R. A. in *light-induced charge separation in Biology and Chemistry,* Eds, Gerischer, H.; Katz, J. J., Verlag Chemie , **1979**, 15.

25. Marcus, R. A. *Annu. Rev. Phys. Chem*. **1964**, *15*, 155.

26. Marcus, R. A. *J. Chem. Phys.* **1957**, *26*, 867.

27. Marcus, R. A. *Faraday Disc. Chem. Soc.* **1982**, *74*, 7.

28. Wilmarth, K. W.; Stanbury, D. M.; Byrd, J. E.; Po, H. N.; Chua, C. P. *Coord. Chem. Rev.* **1983**, *51*, 155.

29. Marcus, R. A. *J. Chem. Phys.* **1965**, *43*, 679.

30. Jordan, R. B. *Reaction mechanisms of Inorganic and Organometallic Systems*; 3rd ed.; Oxford University Press: New York, Oxford, **2007**, pp 423.

31. Laidler, K. J. *Chemical Kinetics*, 3rd ed.; Harper & Row, Publishers, New York, **1987**, pp 34.

32. Moriarty, S. E.; Jones, D. P. *Annu. Rev. Nutr.* **2004**, *24*, 481.

33. Jacob, C.; Giles, G. I.; Giles, N. M.; Sies, H. *Angew. Chem. Int. Ed.* **2003**, *42*, 4742.

34. Hand, C. E.; Honek, J. F. *J. Nat. Prod.* **2005**, *68*, 293.

35. Tsuchiya, K.; Kirima, K.; Yoshizumi, M.; Houchi, H.; Tamaki, T.; Mason, R. P. *Biochem. J.* **2002**, *367*, 771.

36. Jacob, C.; Knight, I.; Winyard, P. G. *Biol. Chem.* **2006**, *387*, 1385.

37. Jocelyn, P. C. *Biochemistry of the SH group,* Academic press: London, **1972**, pp 190-226.

38. Jocelyn, P. C. *Biochemistry of the SH group,* Academic press: London, **1972**, pp 94-115.

39. Darkwa, J.; Olojo, R.; Chikwana, E.; Simoyi, R. H. *J. Phys. Chem. A* **2004**, *108*, 5576.

40. Reddie, K. G.; Carrol, K. S. *Current Opinion in Chemical Biology,* **2008,** *12*, 746.

41. Huxtable, R. J. *Biochemistry of Sulfur*, Plenum Press: New York, **1986**; p 207.

42. Harman, L. S.; Mottley, C.; Mason, R. P. *J. Biol. Chem.* **1984**, *259*, 5606.

42a. Hung, M. in *Mechanisms and kinetics of the Oxidation of Thiols in Anaerobic Aqueous Media*, PhD Thesis, Auburn University, **2004**, pp 6.

43. Wlodek, L. *Pol. J. Pharm.* **2002**, *54*, 215.

44. Ercal, N.; Gurer, H.; Aykin, N. *Current Topics in Medicinal Chemistry*, **2001**, *1*, 529.

45. Battin, E. E.; Brumaghim, J. L. *J. Inorg. Biochem.* **2008,** *102*, 2036.

45a. Meneghini, R. *Free. Rad. Biol. Med*. **1997**, *23*, 783.

46. Romantsev, E. F. *Radiation and Chemical Protection*; The Clearinghouse for Federal Scientific and Technical Information, National Bureau of Standards, U. S. Department of Commerce: Springfield, Virginia, **1964**, pp 221.

47. Lal, M. *Radiat. Phys. Chem.* **1994**, *43*, 595.

48. Giles, N. M.; Giles, G. I.; Jacob, C. *Biochem. Biophys. Res. Commun*. **2003**, *300*, 1.

49. Wardman, P. in *Biothiols in Health and Diseases*, Eds, Parker, L.; Cadenas, E.; Marcel Dekker Inc., New York, **1995**, 1-21.

50. Winterbourn, C. C. in *Biothiols in Health and Diseases*, Eds, Parker, L.; Cadenas, E.; Marcel Dekker Inc., New York, **1995**, 117-134.

51. Pastore, P.; Federici, G.; Bertini, E.; Piemonte, F. *Clin. Chim. Acta*. **2003**, *333*, 19.

52. Dickinson, D. A.; Forman, H. J. *Biochem. Pharma*. **2002**, *64*, 1019.

53. Zeevalk, G. D.; Razmpour, R.; Bernard, L. P. *Biomed. Pharmacother*. **2008**, *62*, 236.

54. Meister, A. *Trends Biochem. Sci*. **1988**, *13*, 185.

55. Meister, A. *J. Biol. Chem*. **1988**, *263*, 17205.

56. Krezel, A.; Bal, W. *Org. Biomol. Chem.* ***2003****, 1,* 3885.

57. Meister, A.; Anderson, M. E. *Ann. Rev. Biochem.* **1983**, *52,* 711.

58. Arias, I. M.; Jakoby, W. B. (eds), *Glutathione, Metabolism and Function,* Raven Press, New York, **1976**, pp 2.

59. Jones, D. P.; Carlson, J. L.; Mody, V. C.; Cai, J.; Lynn, M. J.; Sternberg, P. *Free Rad. Biol. Med.* **2000**, *28*, 625.

60. Meister, A. *Glutathione,* in *The Liver: Biology and Pathology,* eds, Arias, I. M.; Jacoby, W. B.; Popper, H.; Schachter, D.; Shafritz, D. A., New York, Raven Press, **1988**, 2nd ed, 401.

61. Fideius, R. K.; Tsan, M. F. *Immunology*, **1987**, *61*, 503.

62. Filomeny, G.; Rotilio, G.; Ciriolo, M. R. *Biochem. Pharmacol.* **2002**, *64*, 1057.

63. Lu, S. C. *FASEB J*. **1999**, *13*, 1169.

64. Jones, D. P. *Antioxidant and Redox Signaling*, **2006**, *8*, 1865.

65. Kemp, M.; Go, Y - M.; Jones, D. P. *Free Rad. Biol. Med*. **2008**, *44,* 921.

66. Schafer, F. Q.; Bettner, G. R. *Free Rad. Biol. Med*. **2001**, *30,* 1191.

67. Rost, J.; Rapoport, S. *Nature*, **1964**, *201*, 185.

68. Martin, H. L.; Teismann, P. *FASEB J*. **2009**, *23*, 3263.

69. Dringen, R. *Prog. Neurobio*. **2000**, *62*, 649.

70. Griffith, O. W. *Free Rad. Biol. Med*. **1999**, *27,* 922.

71. Ashfaq, S.; Abramson, J. L.; Jones, D. P.; Rhodes, S. D.; Wentraub, W. S.; Hooper, W. C.; Vaccarino, V.; Harrison, D. G.; Quyyumi, A. A. *J. Am. Coll. Cardiol*. **2006**, *47*, 1005.

72. Samiec, P. S.; Drews- Botsch, C.; Flagg, E. W.; Kurtz, J. C.; Sternberg, P.; Reed, R. L.; Jones, D. P. *Free Rad. Biol. Med*. **1998**, *24,* 699

73. Yeh, M. Y.; Burnham, E. L.; Moss, M.; Brown, L. A. S. *Am. J. Respir. Crit. Care Med.* **2007**, *176*, 270.

74. Jones, D. P. "*The Health Dividend of Glutathione"*, *Natural Medicine Journal*, **2011**(Feb)**,** *3(2)*.

75. Bhattarai, N.; Stanbury, D. M. *Inorg Chem*. **2012**, *51*, 13303.

76. Shaikh, N.; Panja, A.; Banerjee, P. *Int. J. Chem. Kinetics* **2004**, *36*, 170.

77. Yordanov, N. D.; Antov, L.; Grampp, G. *Inorg. Chim. Acta* **1998**, *272*, 291.

78. Bagiyan, G. A.; Koroleva, I. K.; Soroka, N. V.; Uinsev, A. V. *Russian Chemical Bulletin, Int. Ed.* **2003**, *52*, 1135.

79. Bernheim, F.; Bernheim, M. L. C. *Cold Spring Harbor Symposia Quan. Biol.* **1939**, *7*, 174.

80. Kharasch, M. S.; Legault, R. R.; Wilder, A. B.; Gerard, R. W. *J. Biol. Chem.* **1936**, *113*, 537.

81. Guczi, L.; Gal, D. *Z. Physik Chem.* **1959**, *212*, 235.

82. Gal, D.; Guczi, L. *Radioisotopes Phy. Sci. Ind. Proc. Conf. Use, Copenhagen* **1960**, *3*, 217.

83. Bridgart, G. J.; Wilson, I. R. *J. Chem. Soc., Dalton Trans.* **1973**, 1281.

84. Mapstone, G. E. *J. appl. Chem. Biotechnol.* **1973**, *23*, 893.

85. Albergoni, V.; Cassini, A. *FEBS Lett.* **1975**, *55*, 261.

86. Bandy, B.; Walter, P. B.; Moon, J.; Davison, A. J. *Arch. Biochem. Biophys.* **2001**, *389*, 22.

87. Bridgart, G. J.; Waters, W. A.; Wilson**,** I. R. *J. Chem. Soc., Dalton Trans.* **1973**, 1582.

88. Fornaro, A.; Coichev, N. *J. Coord. Chem.* **1999**, *46*, 519.

89. Hung, M.; Stanbury, D. M., *Inorg Chem*., **2005**, *44,* 3541.

90. Saha, B.; Hung, M.; Stanbury, D. M. *Inorg. Chem*., **2002**, *41*, 5538.

91. Wang, X.; Stanbury, D. M. *Inorg. Chem.*, **2008**, *47*, 1224.

92. Sun, J. F.; Stanbury, D. M. *J. Chem. Soc., Dalton Trans.* **2002,** 785.

93. Makarycheva-Mikhailova, A. V.; Stanbury, D. M.; Mckee, M. L. *J. Phys. Chem. B*, **2007**, *111*, 6942.

94. Campion, R. J.; Deck, C. F.; King, P.; Wahl, A. C. *Inorg. Chem*. **1967**, *6*, 672.

95. Everse, J.; Kujundzic, N. *Biochemistry* **1979**, *18*, 2668.

96. Hamed, M. Y.; Silver, J.; Wilson, M. T. *Inorg. Chim. Acta* **1983**, *78*, 1.

97. Ayoko, G. A.; Iyun, J. F.; Ekubo, A. T. *Indian J. Chem.* **1993**, *32A*, 616.

98. Stochel, G.; Martinez, P.; van Eldik, R. *J. Inorg. Biochem.* **1994**, *54*, 131.

99. Dulz, G.; Sutin, N. *Inorg. Chem.* **1963**, *2*, 917.

100. Braddock, N.; Meyer, T. J. *J. Am. Chem. Soc.* **1973,** *95,* 3158.

101. Ford-Smith, M. H.; Sutin, N. *J. Am. Chem. Soc.* **1961,** *83,* 1830.

102. Cramer, J. L.; Meyer, T. J. *Inorg. Chem.* **1974,** *13,* 1250.

103. Adedinsewo, C. O.; Adegite, A. *Inorg. Chem.* **1979,** *18,* 3597.

104. Stanbury, D. M.; Wilmarth, W. K.; Khalaf, S. Po, H. N.; Byrd, J. E. *Inorg. Chem.* **1980,** *19,* 2715.

105. Sarala, R.; Stanbury, D. M. *Inorg. Chem.* **1992**, *31,* 2771.

106. Ram, M. S.; Stanbury, D. M. *J. Phys. Chem.* **1986**, *90,* 3691.

107. Hung, M.; Mckee, M. L.; Stanbury, D. M. *Inorg. Chem.* **1994**, *33,* 5108.

108. Stanbury, D. M. *Inorg. Chem.* **1984**, *23,* 2879.

109. Ram, M. S.; Stanbury, D. M. *Inorg. Chem.* **1985**, *24,* 2954.

110. Doona, C. J.; Stanbury, D. M. *Inorg. Chem.* **1996**, *35, 3*210.

111. Song, N.; Stanbury, D. M. *Inorg. Chem.* **2008**, *47,* 11458.

112. Song, N.; Stanbury, D. M. *Inorg. Chem.*, **2011**, *50*, 12762.

113. Oshio, H.; Tamada, O.; Onodera, H.; Ito, T.; Ikoma, T.; Tero-Kubota, S. *Inorg. Chem*. **1999**, *38*, 5686.

114. Lescouezec, R.; Lloret, F.; Julve, M.; Vaissermann, J.; Verdaguer, M. *Inorg. Chem.* **2002**, *41*, 818.

115. Schilt, A. A. *J. Am. Chem. Soc.* **1960**, *82*, 3000.

Chapter 2

Oxidation of Glutathione by Hexachloroiridate(IV)

This chapter is based on the following paper and reprints were made with permission from American Chemical Society.

Bhattarai, N.; Stanbury, D. M., *Inorg. Chem.* **2012**, *51*, 13303-13311.

2.1. Introduction

Glutathione (GSH) (the tripeptide glutamyl-cysteinyl-glycine, Scheme 2.1) is the principal soluble thiol in plants and animals, and it has extensive roles in cellular functions.[1, 2] Prominent among these is its redox reactivity, including its important roles as a redox buffer and radical scavenger. When GSH functions as a radical scavenger it usually undergoes one-electron oxidation, which typically occurs initially at the cysteinyl sulfur group and yields the GS• thiyl radical. Reports on the kinetics of aqueous oxidation of glutathione by one-electron reagents include ferricytochrome c,[3] ferric salts,[4] Cu^{2+},[5] $[Co^{III}W_{12}O_{40}]^{5-}$,[6] $[Cu(TAAB)]^{2+}$,[7] Cr(VI),[8] $[Fe(bpy)_3]^{3+}$ and $[Fe(phen)_3]^{3+}$,[9] $[(Ru(bpy)_2(OH_2))_2O]^{4+}$,[10] $[Ru(edta)pz]^{-}$,[11] $[Fe(CN)_6]^{3-}$,[12] $[Fe^{IV}(O)(N4Py)]^{2+}$,[13] $[Mn^{III}(cdta)]^{-}$,[14] $[CrOO]^{2+}$,[15] $[Ru^{III}(NH_3)_5Cl]^{2+}$,[16] $[Ru^{III}(H_2O)_4Cl_2]^{+}$,[17] $[PV^{V}W_{11}O_{40}]^{4-}$ and $[PV^{V}_2W_{10}O_{40}]^{5-}$,[18] ClO_2•,[19] NO_2•,[20] N_3•,[21, 22] CO_3•$^-$,[23, 24] Br_2•$^-$,[25] O_2•$^-$,[26] OH•,[27] CH_3•,[28] several alcohol radicals,[29] and the tyrosine phenoxyl radical.[30] These reports indicate a great diversity of rate laws and mechanisms, from which it is difficult to assemble a systematic understanding.

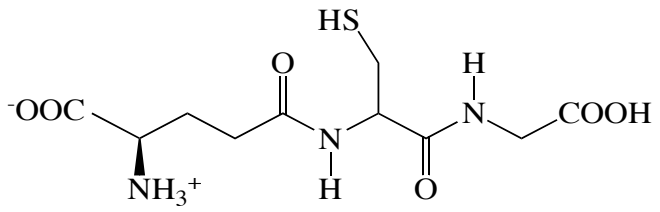

Scheme 2.1

In principle, outer-sphere electron transfer could be an important pathway in GSH oxidations. An understanding of this pathway would contribute to building a systematic overview of GSH oxidations, since such reactions are well understood at the theoretical level, and there is a predictive framework (Marcus theory) for describing their rates. Studies of this type have already been published for two relatively simple thiols: the diprotic thioglycolic acid,[31-33] and the triprotic cysteine amino acid.[34, 35] GSH, a tetraprotic acid, is the subject of the current study, which presents investigations of the oxidation of GSH by the well-established outer-sphere reagent: $[IrCl_6]^{2-}$. The results show that the reaction is highly sensitive to Cu^{2+} catalysis, and that the catalysis can be thoroughly inhibited with a suitable chelating agent. The uncatalyzed reaction has a common rate law with the rate-limiting steps corresponding to oxidation of the thiolate forms of GSH to the GS• radical, and the rates are consistent with Marcus theory.

2.2. Experimental Section

2.2.1. Reagents and Solutions. NH_4Cl, acetic acid, monochloroacetic acid, $CuSO_4 \cdot 5H_2O$, $(NH_4)_2Fe(SO_4)_2 \cdot 6H_2O$, cacodylic acid ($(CH_3)_2AsO_2H$)), D_2O, glutathione sulfonic acid (GSO_3H), and glycylglycine hydrochloride (gly-gly) (all from Sigma), and N-tert-butyl-α-phenylnitrone (PBN, 98%), 2-6-pyridine dicarboxylic acid (dipic), 2,2'-bipyridyl (bpy), L-glutathione (GSH, > 99%), L-glutathione disulfide (GSSG), 3-(trimethylsilyl)-1-propane sulfonic acid sodium salt (DSS), and $(NH_4)_3IrCl_6 \cdot H_2O$ (all from Aldrich) were used without further purification. Cl_2 gas (Matheson), NaOH pellets ("SigmaUltra", Sigma-Aldrich), HCl, ethanol, diethyl ether and Dowex 50-X8 resin (J. T. Baker) were used without further purification. $LiClO_4$ (GFS), and $NaClO_4$ (Fisher) were recrystallized from hot water. Anhydrous Na_3PO_4 was prepared from $Na_3PO_4 \cdot 12H_2O$ (99.6% Fisher) by melting it in a muffle furnace at 150 °C followed by cooling, pulverization, and repeated heating at 150 °C for several hours.

$(NH_4)_2IrCl_6$ (Aldrich) was recrystallized by adding a saturated solution of NH_4Cl to a hot saturated solution of $(NH_4)_2IrCl_6$ (100 mg/14 mL H_2O). After cooling the mixture in an ice bath, the crystals were collected by vacuum filtration and washed with 20% $NH_4Cl_{(aq)}$ solution. Crystals were again washed with 95% ethanol two times (10 mL at a time) and finally with diethyl ether (10 mL portion two times). The crystals were air dried first and then vacuum dried.[36] Yield = 85%.

Deionized water was purified with a Barnstead Nanopure Infinity system and used to prepare all solutions. Freshly prepared solutions were used to run all experiments except for stock solutions of $NaClO_4$, $LiClO_4$, $HClO_4$, HCl and some buffers. For all

studies the reactant solutions were purged with argon gas on a bubbling line prior to use and transferred via glass syringes with Teflon or Pt needles, except where noted.

Stock solutions of $LiClO_4$ and $NaClO_4$ were standardized by titration. An aliquot was passed through a cation exchange column which had been packed with Dowex 50-X8 resin and regenerated with conc HCl. The eluate was then titrated with a standard $NaOH_{(aq)}$ solution.

2.2.2. Methods. A HP-8453 diode array spectrophotometer equipped with a Brinkman Lauda RM6 thermostated system was used to record all UV-vis spectra at 25 ± 0.1 °C; 10 mm quartz cells were used. All pH measurements were performed on a Corning 450 pH/ion meter with a Mettler Toledo Inlab 421 combination pH electrode (3 M NaCl), calibrated with standard buffers.

^1H NMR spectra were obtained on a Brucker AV 400 MHz spectrometer. Chemical shifts (δ, ppm) in D_2O were relative to DSS. In determining the product ratio for the anaerobic reaction of GSH with Ir^{IV}, noise was reduced by applying 0.3 Hz of line broadening (LB = 0.3); a value of LB = 2 was used for the experiment with exposure to O_2.

Electrochemical measurements were conducted on a BAS 100B electrochemical analyzer equipped with a BAS C3 cell stand provided with an N_2 purging and stirring system. The cell used a 3.2 mm diameter glassy carbon disc as a working electrode, a Ag/AgCl (3 M NaCl) reference electrode ($E°$ = 0.205 V vs NHE),[37] and a Pt wire auxiliary electrode.

Kinetic studies were done at 25 ± 0.1 °C on a Hi-Tech SF-51 stopped-flow spectrophotometer in the 1 cm path length configuration with Olis 4300 data acquisition and analysis software. The reactions of GSH with $(NH_4)_2IrCl_6$ was monitored at 488 nm, always maintaining at least a 10-fold molar excess of GSH relative to the oxidant. All rate constants reported are the average of at least four runs unless and otherwise stated; shot-to-shot variation in k_{obs} was typically ± 1-3%. Least-squares fits of the pseudo-first-order rate constants were performed with the Prism 5 software package,[38] weighting the data proportionally to the inverse square of k_{obs}. When fitting the pH-dependent rate laws, proton concentrations were calculated with the approximation $[H^+] = 10^{-pH}$.

Electrospray mass spectra were recorded with a Waters Q-Tof Premier mass spectrometer. Samples for positive-ion spectroscopy were acidified with 0.1% formic acid. Samples were injected via a 10 μL sample loop directly into the ESI source at a flow rate of 50 μL/min with 50% acetonitrile as the mobile phase.

2.3. Results.

2.3.1. Solution Properties of $[IrCl_6]^{2-}$. The UV-vis analysis for the purity test was performed with 0.1 mM $(NH_4)_2IrCl_6$ in 0.1 M $HClO_4$. This complex exibits a characteristic UV-vis spectrum with a peak at 488 nm, in good agreement with prior reports[39-41](Fig 2.1). The value for $\varepsilon_{488}(Ir^{IV}) = 3.98 \times 10^3\ M^{-1}\ cm^{-1}$ has an estimated uncertainty of ± 4% based on the range in prior reports.[41-44]

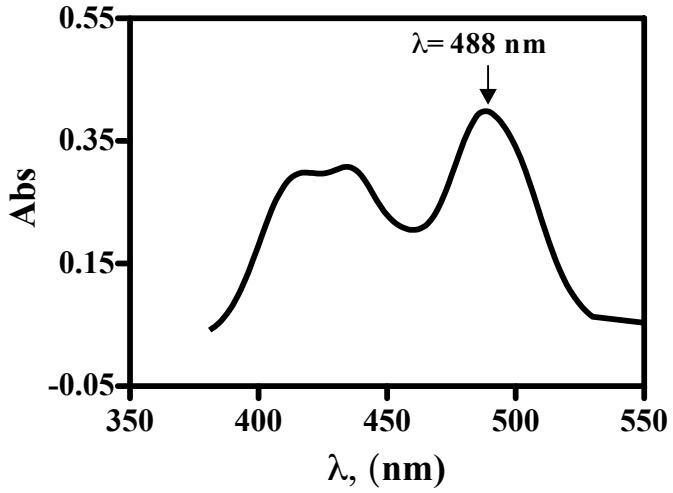

Fig 2.1. UV-vis spectrum, $[Ir^{IV}] = 0.10$ mM / 0.1 M ($HClO_4$)

Similarly, its electrochemistry ($Ir^{IV} = 0.10$ mM / 0.1 M ($HClO_4$) shows a reversible CV (cyclic voltammogram) corresponding to reduction to $[IrCl_6]^{3-}$ with $\Delta E_{p/p} = 64$ mV ($E_{1/2} =$ 704 mV vs Ag/AgCl) (Fig 2.2a). Osteryoung square-wave voltamogram (OSWV) of the same yielded $E_p = 688$ mV and $E_{1/2} = 0.89$ V vs NHE at $\mu = 0.1$ M, also in good agreement with prior results,[45] is shown in Fig 2.2b.

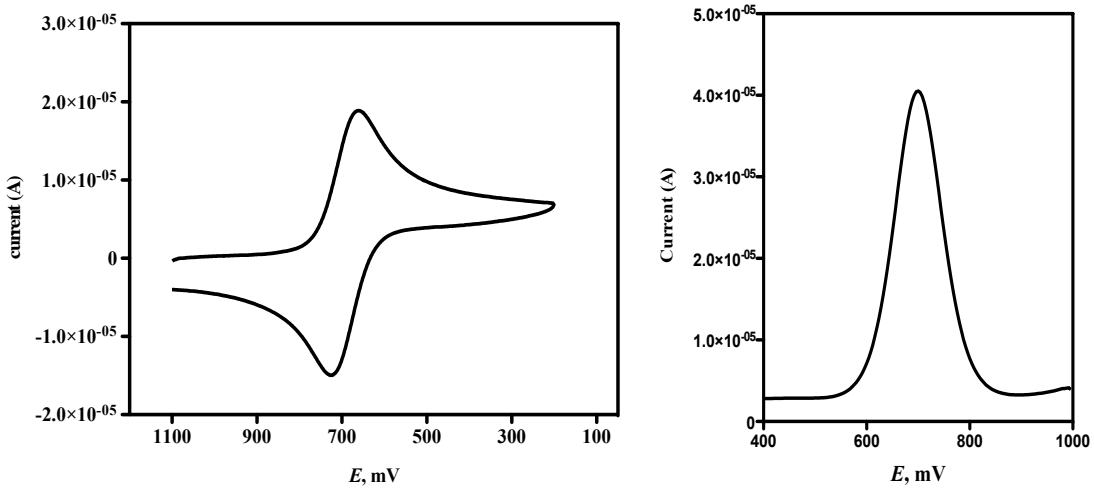

Fig 2.2. a. Cyclic voltammogram of 0.1 mM Ir^{IV} /0.1 M $HClO_4$ **b**. Osteryoung square wave voltammogram

2.3.2. Qualitative Features of the GSH Reactions with Ir^{IV}. Rapid color changes ensue upon mixing a solution of GSH with the oxidant $[IrCl_6]^{2-}$. Reduction of $[IrCl_6]^{2-}$ is signaled by the loss of absorbance at 488 nm. Fig 2.3 illustrates the kinetic decay spectra in the reaction of 0.1 mM Ir^{IV} with 1.0 mM GSH obtained using a diode array spectrophotometer. The solution included 1 mM dipic, 0.1 M $NaClO_4$ and was unbuffered at pH = 2.36 ($HClO_4$), run time = 600 sec with cycle time = 3 sec. The inset shows a kinetic trace for the reaction.

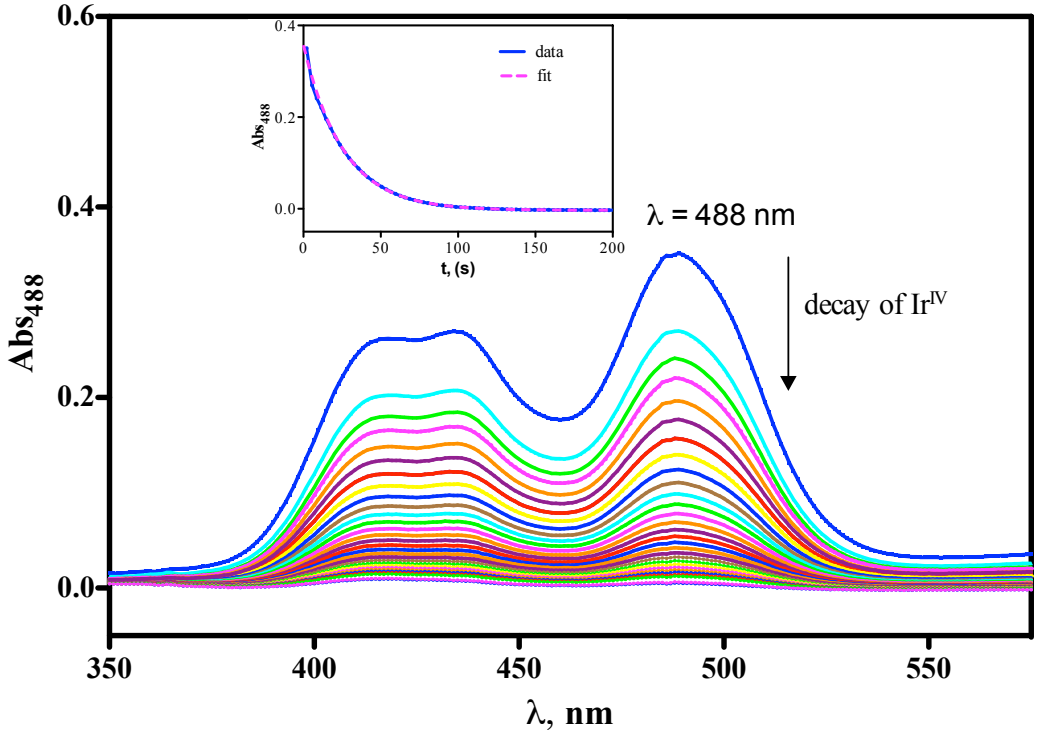

Fig 2.3. Kinetic decay of Ir^{IV} in the reaction with GSH using a diode array spectrophotometer. Inset: kinetic trace for the reaction. $[Ir^{IV}]_0$ = 0.1 mM, [GSH] = 1 mM, [dipic] = 1 mM, $[NaClO_4]$ = 0.1 M, unbuffered solution at pH 2.36 ($HClO_4$), run time = 600 sec with cycle time = 3 sec.

2.3.2.1. Metal Ion Catalysis. As is typical of thiol oxidations by inert one-electron oxidants,[31-35] this reaction is highly susceptible to catalysis by copper ions. For example, the addition of 1 μM $CuSO_4$ led to a four-fold rate increase in the oxidation of GSH by $[IrCl_6]^{2-}$ at pH 4.6, (Table 2.1, Fig A1). On the other hand, the addition of 1 mM 2,6-dipicolinic acid (dipic), a well-established inhibitor of copper catalysis,[31, 32, 34, 35] led to a 3-fold reduction in the rate of the $[IrCl_6]^{2-}$ reaction. Moreover, in the presence of 1 mM dipic the $[IrCl_6]^{2-}$ reaction rate was unaffected by the addition of 5 μM $CuSO_4$.

These results show that trace levels of Cu^{2+} ions as impurities are sufficient to dominate the reaction kinetics and that copper catalysis can be completely suppressed by the addition of suitable chelating agents. All results described below were obtained in the presence of dipic inhibitor. In the reaction of $[IrCl_6]^{2-}$ at pH 4.6, variation of the dipic concentration from 1 to 8 mM had no effect on the rates (Table 2.2, Fig A2); accordingly, 1 mM dipic was deemed adequate. EDTA could also scavenge copper but it is oxidized by $[IrCl_6]^{2-}$. We have used it with $[Fe^{III}(bpy)(CN)_4]^-$ (chapter 3) as this is a significantly weaker oxidant.

Table 2.1. Cu^{2+} Catalysis of the Reaction of Ir^{IV} with GSH[a]

Expt	$[Cu^{2+}]$, μM	[dipic], mM	$t_{1/2}$, s	k_{obs}, s^{-1}	fit
1.	0.0	0.0	0.85	0.90	bad
2.	1.0	0.0	0.16	3.52	bad
3.	5.0	0.0	0.03	15.8	bad
4.	5.0	1.0	2.00	0.37	good
5.	0.0	1.0	1.90	0.39	good

[a] $[GSH]_t$ = 1.0 mM, $[Ir^{IV}]_0$ = 0.10 mM, acetate buffer (10 mM), pH = 4.6 and μ = 0.1 M ($NaClO_4$).

Table 2.2. Kinetic Data for the Test of Dipicolinic acid Concentration Effect in the Reaction of Ir^{IV} with $[GSH]_t$.[a]

Expt	[dipic], mM	$t_{1/2}$, s	k_{obs}, s^{-1}
1.	1.0	1.67	0.45
2.	2.0	1.63	0.46
3.	4.0	1.63	0.46
4.	8.0	1.53	0.49

[a] $[Ir^{IV}]_0 = 0.10$ mM, $[GSH]_t = 1.0$ mM, acetate buffer at pH = 4.6 , $\mu = 0.1$ M ($NaClO_4$) .

2.3.3. Product Analysis and Stoichiometry

2.3.3.1 Product Analysis with $[IrCl_6]^{2-}$. Using excess GSH over $[IrCl_6]^{2-}$, the Ir-containing product was identified and determined from UV-vis spectroscopy and electrochemistry (OSWV). For the UV-vis study, an un-buffered solution of 0.10 mM Ir^{IV} with 1 mM dipic and 0.1 M $NaClO_4$ was prepared and the spectrum was recorded. Then, sufficient solid GSH was added to the Ir^{IV} solution to make a 1 mM GSH solution, and the spectrum recorded after the reaction showed complete consumption of Ir^{IV} and the product spectrum was consistent with conversion to $[IrCl_6]^{3-}$ (Fig 2.4). Upon chlorination of this product the original $[IrCl_6]^{2-}$ spectrum was recovered in full yield, confirming that reduction of $[IrCl_6]^{2-}$ by GSH proceeds without loss of bound chloride

(Fig 2.5). This inference is based on the well-established evidence that chlorination of aquated derivatives of $[IrCl_6]^{3-}$ yields the corresponding Ir^{IV} products, which have distinct UV-vis spectra.[41]

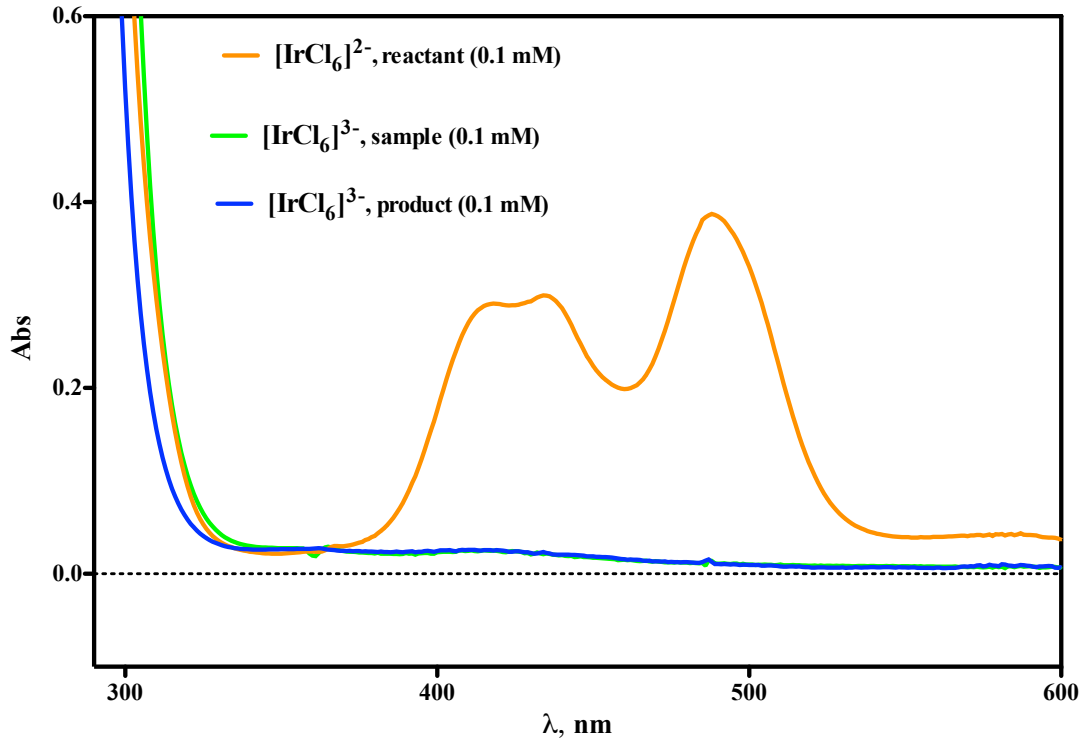

Fig 2.4. UV-vis spectral changes in the reaction of GSH with Ir^{IV}. Orange = Ir^{IV}; green = Ir^{III} and blue = product solution. The Ir^{IV} spectrum is of a 0.1 mM solution of Ir^{IV} in 1 mM dipic with 0.1 M $NaClO_4$. The product solution (pH 3.0) was obtained by adding solid GSH to the above Ir^{IV} solution sufficient to make $[GSH]_t$ = 1 mM. The Ir^{III} spectrum is of a 0.10 mM solution of $(NH_4)_3IrCl_6$ in 1 mM dipic with 0.1 M $NaClO_4$.

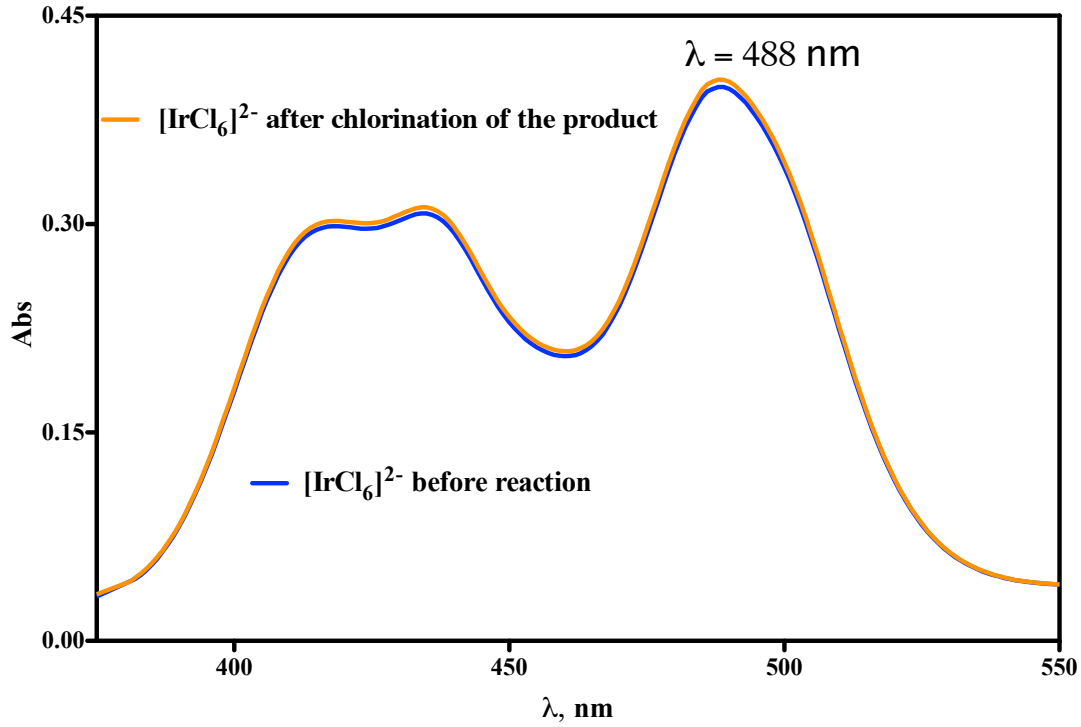

Fig 2.5. Comparison of UV-vis spectra of the Ir^{IV} reactant and the chlorinated product solution. Product obtained from the reaction of Ir^{IV} and GSH was chlorinated to recover the Ir^{IV}. At 488 nm the absorbance is 0.398 before and 0.404 after chlorination, indicatingcomplete recovery of the starting $[IrCl_6]^{2-}$. The product spectrum is obtained by chlorinating a mixture of 4.0 mL of (0.2 mM Ir^{IV} in 0.1 M $HClO_4$) plus 4.0 mL of (2.0 mM GSH in 2 mM dipic). The "reactant" spectrum is of the Ir^{IV} reactant solution diluted with an equal volume of H_2O. Thus, the Ir concentration is 0.1 mM for both spectra.

Further evidence that the coordination sphere of $[IrCl_6]^{2-}$ remains intact during reduction by GSH is provided by OSWV (Osteryoung square ware voltammetry) (Figure 2.6): here, a product solution was prepared from the reaction 0.1 mM Ir^{IV} and 1 mM GSH in 0.1 M

$HClO_4$ and in the presence of 1 mM dipic. The solution was then chlorinated to remove the interfering excess GSH and oxidize the Ir^{III} to Ir^{IV}. OSWV analysis of this solution yielded a voltammogram having a peak potential and current closely consistent with an authentic sample of $[IrCl_6]^{2-}$. The aquo derivatives of $[IrCl_6]^{2-}$ have significantly higher $E°$ values.[46]

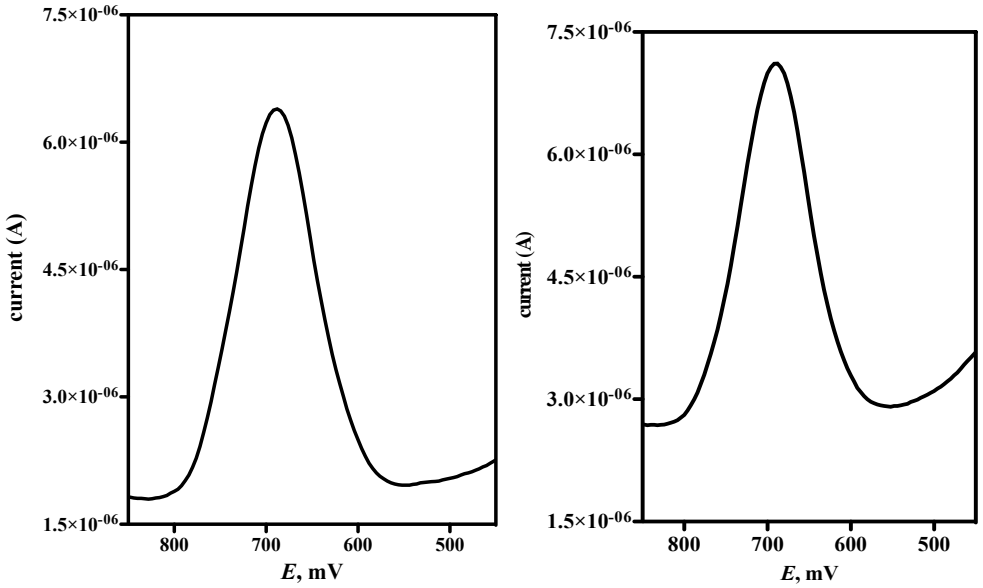

Fig 2.6. OSWV analysis of the products of the oxidation of GSH by Ir^{IV}.

Reference electrode = Ag/AgCl. a) 0.10 mM Ir^{IV} in 0.1 M $HClO_4$. E_p = + 688 mV. b) product after chlorination: $[Ir^{IV}]_0$ = 0.10 mM and $[GSH]_t$ = 1.0 mM, 0.1 M $HClO_4$, 1 mM dipic. E_p = + 688 mV.

Sulfur-containing products were determined by electrospray mass spectrometry and ^{1}H NMR spectroscopy. Positive-ion mass analysis was performed on the products arising from the reaction of 1.0 mM GSH and 4.0 mM Ir^{IV} with 1 mM dipic at pH 2.6 where the reactants were exposed to O_2. Prominent peaks are evident at *m/z* 613.12 corresponding to GSSG and at *m/z* 356.068 corresponding to GSO_3H (Fig 2.7a &b).

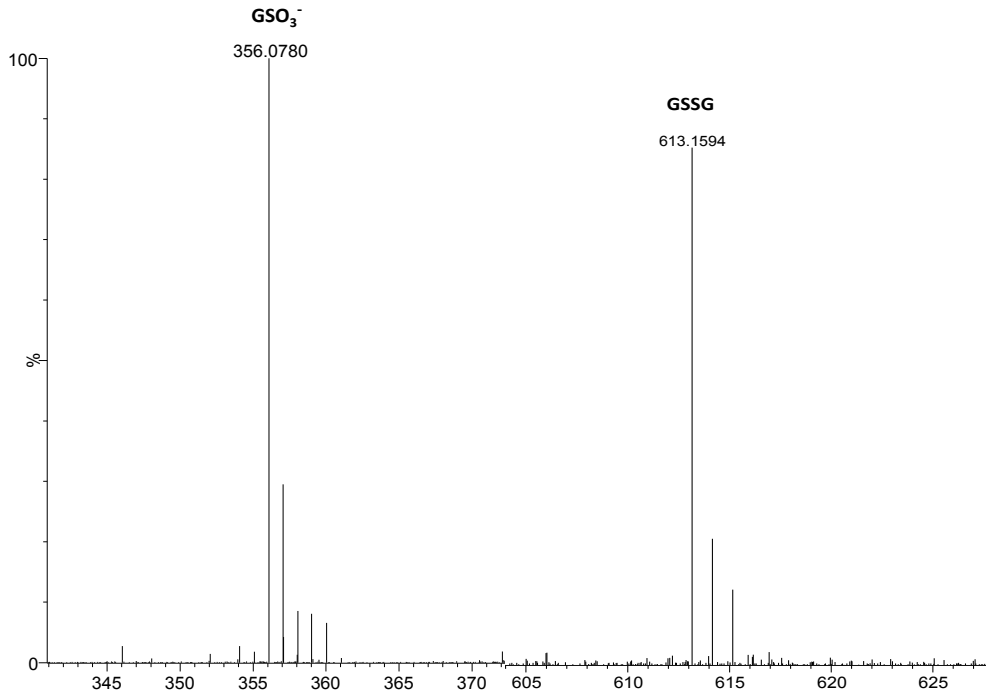

Fig 2.7a. Electrospray mass spectra. 0.5 mM GSH + 2.25 mM Ir^{IV}+ 1 mM dipic in H_2O, unbuffered solution at pH 2.6, reactants exposed to O_2. Sample diluted 10-fold for analysis. Left: Positive-ion spectrum of GSO_3H in product. Right: Positive-ion spectrum of GSSG.

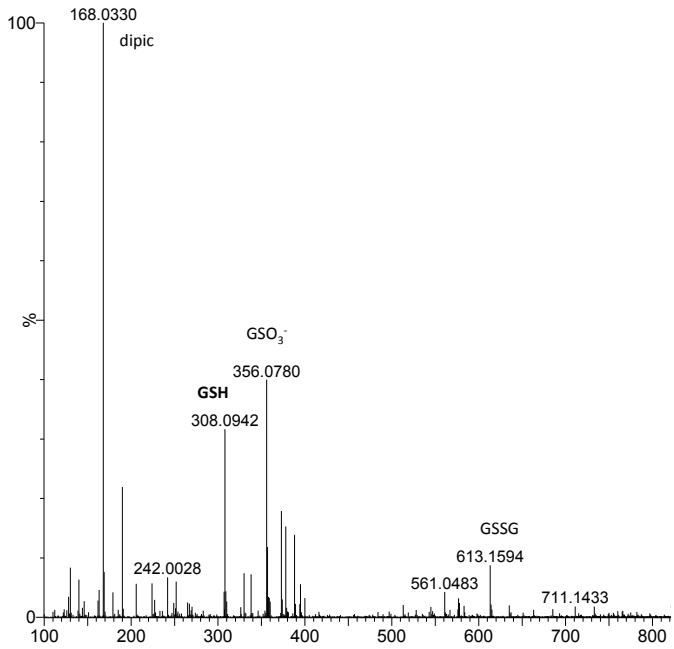

Fig 2.7. b. Electrospray mass spectra. 0.5 mM GSH + 2.25 mM Ir^{IV}+ 1 mM dipic in H_2O, un-buffered solution at pH 2.6, reactants exposed to O_2. Sample diluted 10-fold for analysis. Overall product spectrum.

^{1}H NMR analysis was performed on a solution of 1 mM GSH, 4.9 mM Ir^{IV}, and 1 mM dipic with a little DSS in D_2O that was allowed to react. The ^{1}H NMR spectrum of the product mixture (Fig 2.8) shows complete consumption of the GSH and two different sets of peaks that are assigned to GSSG and glutathione sulfonate (GSO_3^-). These two products have overlapping peaks in most regions of the spectrum, but they can be distinguished in the region between δ 3.2 and 3.5 ppm. In particular, GSO_3^- has an isolated doublet of doublets centered at 3.42 ppm corresponding to the cysteine C_β-H_b proton. The region between δ 3.23 and 3.32 ppm comprises a doublet of doublets due to

the GSO_3^- cysteine C_β-H_a proton and an overlapping doublet of doublets arising from the pair of GSSG cysteine C_β-H_a protons.[47] An estimate of the product ratio, $[GSO_3^-]/[GSSG] = 6.4$, can be calculated from the peak integrals as $2I_{3.42}/(I_{3.23\text{-}3.32} - I_{3.42})$. When a similar experiment was performed with solutions exposed to O_2 the $[GSO_3^-]/[GSSG]$ ratio was 2.1.

2.3.3.2. Stoichiometry. A spectrophotometric titration was conducted at pH 4.8 (acetate buffer) with 1 mM dipic. 2.0 mL of 0.276 mM GSH was placed in a cuvette and titrated under Ar with a 4.7 mM solution of Ir^{IV} (Fig 2.9). These spectra show a weak absorbance increase at 420 nm associated with the formation of Ir^{III};[41] at the end point the spectra begin to show a much larger absorbance increase which is due to the accumulation of excess Ir^{IV}. The titration curve at 488 nm has a well-defined end point, corresponding to a molar consumption ratio $\Delta(Ir^{IV})/\Delta(GSH)$ of (7.1 ± 0.3) where the uncertainty reflects the precision of the end point and the uncertainty in the molar absorptivity of Ir^{IV}. When the titration was performed with exposure to O_2 the consumption ratio (= 4.2) was significantly smaller.

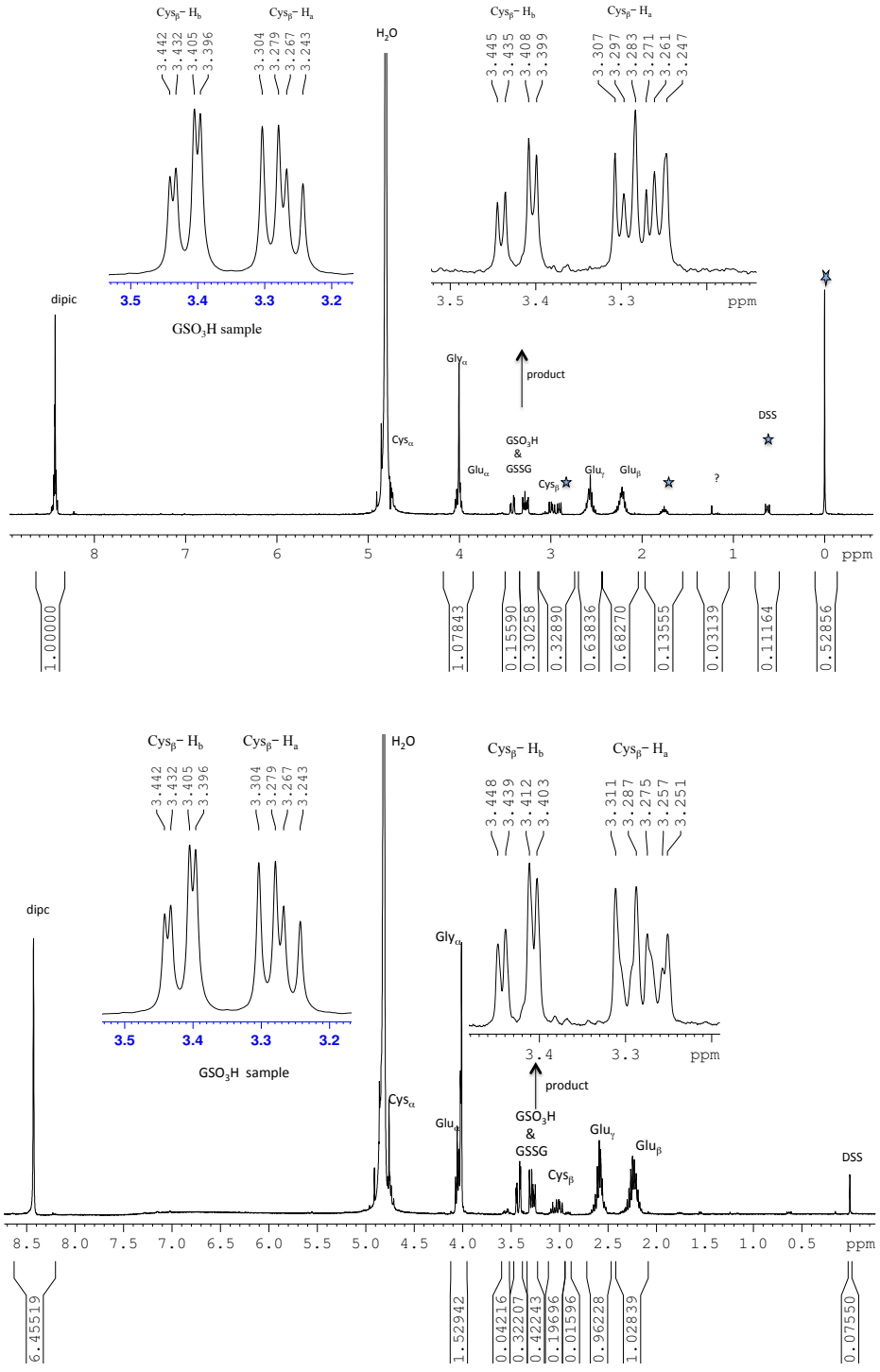

Fig 2.8. Top: ^{1}H NMR spectra of the products of the reaction of 4.5 mM Ir^{IV} with 1 mM GSH in D_2O with 1 mM dipic and DSS, reactants exposed to O_2. Left inset: reference spectrum of GSO_3^-. Right inset: expanded portion of the product spectrum, showing overlapping resonances of GSSG and GSO_3^-. Bottom: Analogous reaction with 4.9 mM Ir^{IV} and with rigorous exclusion of O_2.

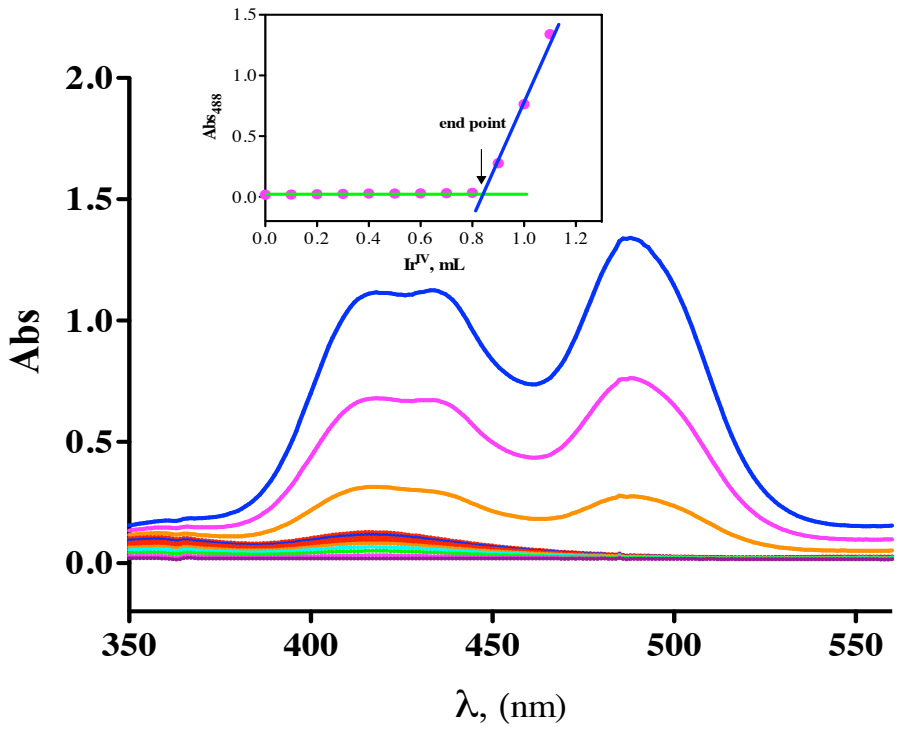

Fig 2.9. Anaerobic titration of GSH by Ir^{IV}. Inset: plot of titration data. pH = 4.8 (acetate buffer), [dipic] = 1 mM. [Ir^{IV}] = 4.67 mM and 2.0 mL of 0.276 mM $[GSH]_t$. Endpoint at 0.84 mL of Ir^{IV}.

From these observations it is evident that the overall oxidation of GSH by $[IrCl_6]^{2-}$ under anaerobic conditions is given primarily by

$$6[IrCl_6]^{2-} + GSH + 3H_2O \rightarrow 6[IrCl_6]^{3-} + GSO_3^- + 7H^+ \qquad (2.1)$$

A minor component of the reaction is disulfide formation:

$$2[IrCl_6]^{2-} + 2GSH \rightarrow 2[IrCl_6]^{3-} + GSSG + 2H^+ \qquad (2.2)$$

The slight excess over 6 for the stoichiometric ratio obtained from the spectrophotometric titrations indicates a small degree of oxidation beyond the GSO_3^- stage, although the products were not identified.

2.3.4. Kinetics.

2.3.4.1. General Features. As described above, copper ions are strongly catalytic in the reaction of Ir^{IV} with GSH. Accordingly, all kinetic results described below are obtained from reactions conducted in the presence of inhibitors that completely suppress the catalysis. The reactions were generally studied with a flooding excess of GSH over oxidant, which led to pseudo-first-order kinetics. The pseudo-first-order rate constant (k_{obs}) is defined by eq 2.3.

$$-\frac{d[\mathrm{Ir^{IV}}]}{dt} = k_{obs}\,[\mathrm{Ir^{IV}}] \qquad (2.3)$$

GSH has four acidic protons, with pK_{a1} = 2.12, pK_{a2} = 3.512, pK_{a3} = 8.73 and pK_{a4} = 9.65 at ionic strength 0.1 M.[19,48] Thus, GSH potentially has five kinetically distinguishable protonation states: cationic (protonated), neutral, mono-anionic, di-anionic and tri-anionic forms depending upon pH, which are represented as $HGSH^+$, GSH^0, $GSH\text{-}H^-$, $GSH\text{-}2H^{2-}$ and $GSH\text{-}3H^{3-}$, respectively. In principle, each of these protonation states could be reactive. The total GSH concentration is designated $[GSH]_t$. Under the assumption that these protonation states are rapidly interconverted and that each protonation state reacts

with simple mixed second-order kinetics, the general rate law is eq 2.4.

$k_{obs} = k[GSH]_t =$

$$k_1[HGSH^+] + k_2[GSH^0] + k_3[GSH\text{-}H^-] + k_4[GSH\text{-}2H^{2-}] + k_5[GSH\text{-}3H^{3-}] \quad (2.4)$$

The k_{obs} obtained in the reaction of $Ir^{IV}$with $[GSH]_t$ is the sum of the rate contributed by all these species as in eq 2.4.

Inclusion in eq 2.4 of all respective pK_a terms leads to eq 2.5.

$$k_{obs} = \left[\frac{k_1[H^+]^4 + k_2K_{a1}[H^+]^3 + k_3K_{a1}K_{a2}[H^+]^2 + k_4K_{a1}K_{a2}K_{a3}[H^+] + k_5K_{a1}K_{a2}K_{a3}K_{a4}}{[H^+]^4 + K_{a1}[H^+]^3 + K_{a1}K_{a2}[H^+]^2 + K_{a1}K_{a2}K_{a3}[H^+] + K_{a1}K_{a2}K_{a3}K_{a4}}\right][GSH]_t \quad (2.5)$$

At a given pH eq 2.5 simplifies to

$$k_{obs} = k_{pH}[GSH]_t \quad (2.6)$$

Deviations from rate law (eq 2.3) can be anticipated for weak oxidants under acidic conditions, when inhibition by the product M_{red} can occur in thiol oxidations.[31,32,34,35] No such inhibition was detected in the current study with $[IrCl_6]^{2-}$ as the oxidant.

A typical kinetic trace with an excellent pseudo-first-order fit is obtained for the reaction of Ir^{IV} with GSH under the conditions $[Ir^{IV}]$ = 0.1 mM, $[GSH]_t$ = 1.0 mM, pH = 4.6 (10 mM acetate buffer), [dipic] = 1.0 mM and μ = 0.1 M ($NaClO_4$) (Fig 2.10). In another experiment under these conditions the buffer concentration was reduced by a factor of 10

(1 mM buffer), and virtually identical results were obtained. This latter result implies that the rate law is independent of buffer concentration. Further details about catalytic effect of various buffer concentration are given in appendix B.

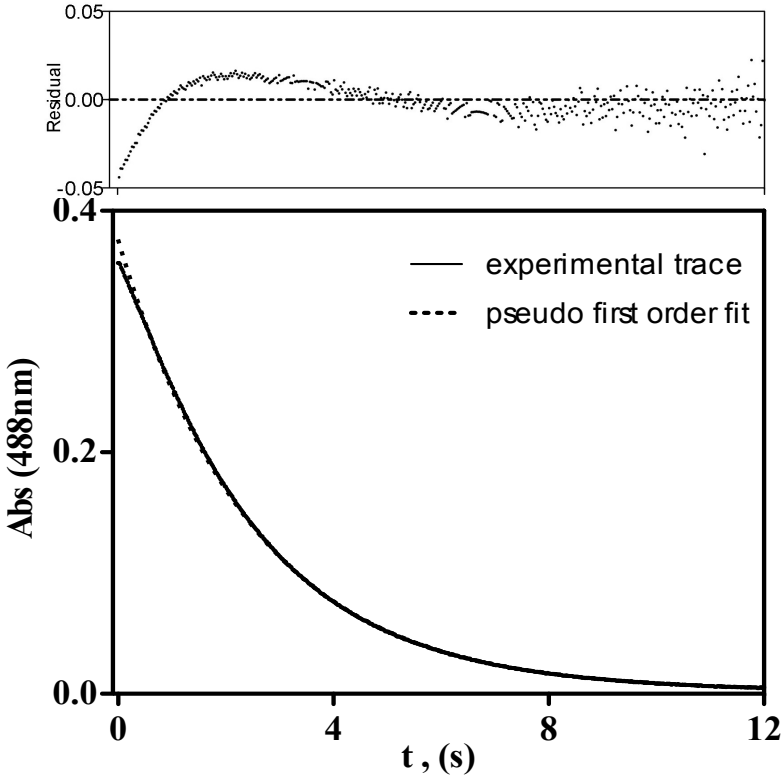

Fig 2.10. Kinetic trace of oxidation of glutathione by 1.0×10^{-4} M $[IrCl_6]^{2-}$ at pH 4.6 (acetate buffer). The lower box shows the experimental reaction trace (solid line) with pseudo first order fit (dashed line). $[GSH]_t = 1.0 \times 10^{-3}$ M, $\mu = 0.1$ M ($NaClO_4$) and dipic = 1 mM. Upper box: residual.

2.3.4.2. GSH Dependence. The dependence on $[GSH]_t$ was investigated over a ten-fold range in GSH concentration, with the conditions 0.1 mm $[Ir^{IV}]_0$, 1 mM dipic, $[GSH]_t$ = 1.0 -10 mM at pH 4.5 ± 0.1 (acetate buffer) and 0.1 M ionic strength ($NaClO_4$). Table 2.3 lists all the kinetic data. The linear plot of k_{obs} vs $[GSH]_t$ with a slope (7.42 ± 0.15) × 10^2 M^{-1} s^{-1} and intercept (0.14 ± 0.03) s^{-1} displayed in Fig 2.11 confirms the rate law to be first order with respect to $[GSH]_t$ as in eq 2.7.

$$k_{obs} = k[\mathrm{GSH}]_t \tag{2.7}$$

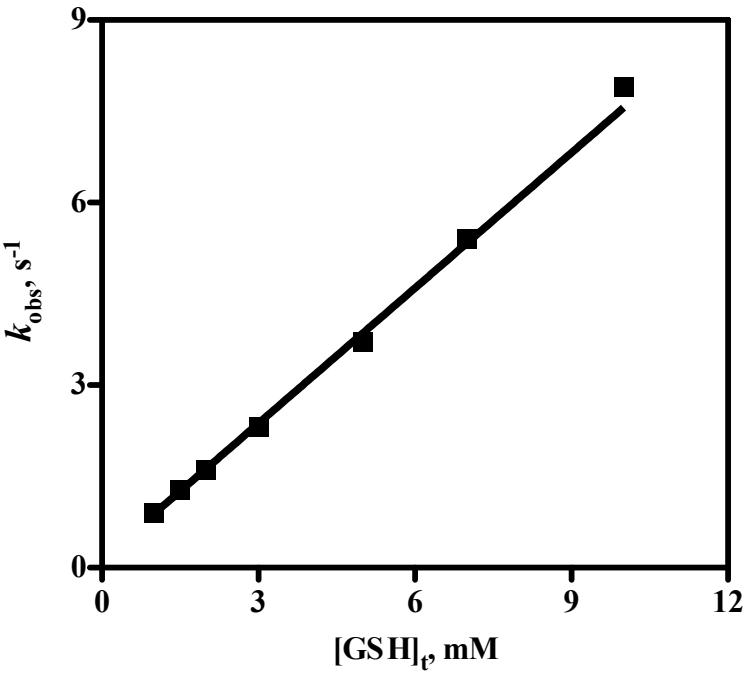

Fig 2.11. Glutathione dependence of k_{obs} in the reaction of $[IrCl_6]^{2-}$ with GSH. Solid line is a linear fit. $[Ir^{IV}]_0$ = 0.01 mM, $[GSH]_t$ = 1.0–10 mM, acetate buffer at pH 4.5 ± 0.1, with 1 mM dipic, μ = 0.1 M ($NaClO_4$). Standard deviations of the shot-to-shot k_{obs} values are smaller than the square data points. Slope = (7.42 ± 0.15) × 10^2 M^{-1} s^{-1} and intercept = 0.14 ± 0.03 s^{-1}

Table 2.3. Glutathione Dependence of the Kinetics of the Reaction Between Ir^{IV} and GSH[a]

Expt.	$[GSH]_t$, mM	$t_{1/2}$, s	k_{obs}, s^{-1}	SD[b]
1.	1.0	0.84	0.90	0.017
2.	1.5	0.60	1.27	0.022
3.	2.0	0.48	1.60	0.450
4.	3.0	0.33	2.31	0.240
5.	5.0	0.21	3.70	0.017
6.	7.0	0.13	5.40	0.230
10.	10.0	0.09	7.90	0.310

[a] $[Ir^{IV}]_0$ = 0.01 mM, $[GSH]_t$ = 1.0 – 10.0 mM, acetate buffer at pH 4.5 ± 0.1, μ = 0.1 M ($NaClO_4$).

$$SD = \sqrt{\frac{\sum(X - M)^2}{n - 1}}$$

[b]SD = standard deviation, X = individual scores, M = mean and n = # samples (shots)

2.3.4.3. pH Dependence. The pH dependence was studied over the pH range of 1.2- 7.07, keeping the conditions 0.5–1.0 mM $[GSH]_t$, 1.0 mM dipic and 0.1 M ionic strength. Appropriate buffers were used to maintain pH between pH 2.4 and pH 7.1. Above pH 2.4 the ionic strength was maintained by $NaClO_4$, but, in order to minimize the effects of specific activity coefficients, below pH 2.4 the ionic strength was maintained with $LiClO_4$. All kinetic data are summarized in (Table 2.4). The plot of $\log(k_{obs}/[GSH]_t)$

vs pH shown in Fig 2.12 indicates a complex dependence on pH with an irregular trend of increasing rate with increasing pH, including a narrow plateau region at around pH 4.5. Parenthetically, the slowest rates, obtained at low pH, were mildly sensitive to the purity of the $[IrCl_6]^{2-}$, presumably because of catalysis by aquated derivatives of this oxidant; similar catalysis has been reported for the oxidation of NH_2OH by $[IrCl_6]^{2-}$.[49] The data in Fig 2.12 were analyzed in accordance with eq 2.5, holding K_{a1}, K_{a2}, K_{a3} and K_{a4} at their literature values (relationship used: pKa = -log K_a and $K_a = 10^{-pKa}$). Initial attempts to fit all five rate constants failed to converge, but an excellent fit to this equation was obtained by holding $k_5 = 0$. The pH-resolved second-order rate constants are $k_1 = 1.1 \pm 1.0\ M^{-1}\ s^{-1}$, $k_2 = 36 \pm 4\ M^{-1}\ s^{-1}$, $k_3 = (2.9 \pm 0.2) \times 10^2\ M^{-1}\ s^{-1}$ and $k_4 = (4.73 \pm 0.18) \times 10^6\ M^{-1}\ s^{-1}$ Thus, k_1 is zero within its uncertainty, and k_5 is also undefined. In principle, k_5 could have been measured by conducting experiments at higher pH, but the rates become too fast to measure with our instrument under such conditions.

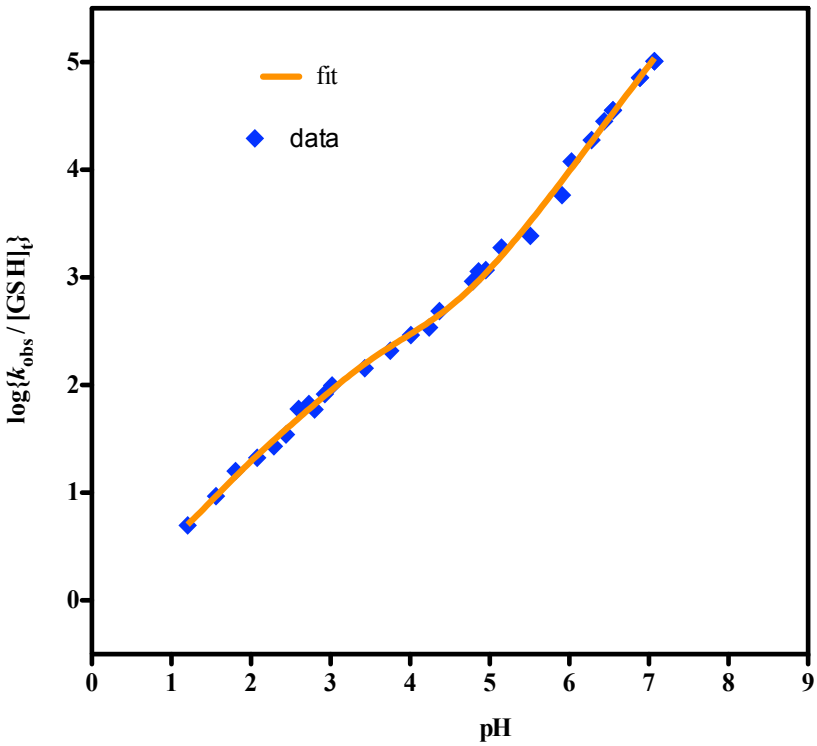

Fig 2.12. Plot of log(k_{obs}/[GSH]$_t$) vs pH for the reactions of GSH with $[IrCl_6]^{2-}$. Solid lines are the fits to eq 2.8. Standard deviations of the shot-to-shot k_{obs} values are smaller than the data points. $[Ir^{IV}]_0$ = 0.10 mM, [dipic] = 1 mM. pH from 1.2 to 2.29 was maintained by $HClO_4$ and μ = 0.1 M ($LiClO_4$). At higher pH appropriate 10 mM buffers were used with μ = 0.1 M ($NaClO_4$). Chloroacetate buffer (2.4-3.4), acetate buffer (3.7-4.9), cacodylate buffer (5.1-6.8) and gly-gly buffer (7.0).

$$k_{obs} = \left[\frac{k_1[H^+]^4 + k_2K_{a1}[H^+]^3 + k_3K_{a1}K_{a2}[H^+]^2 + k_4K_{a1}K_{a2}K_{a3}[H^+]}{[H^+]^4 + K_{a1}[H^+]^3 + K_{a1}K_{a2}[H^+]^2 + K_{a1}K_{a2}K_{a3}[H^+] + K_{a1}K_{a2}K_{a3}K_{a4}}\right] \quad (2.8)$$

Table 2.4. pH Dependent Kinetics of the Reaction of Ir^{IV} With GSH[a]

pH	k_{obs}, s^{-1}	$[GSH]_t$, mM	$k_{obs}/[GSH]_t$, M^{-1} s^{-1}	$\log\{k_{obs}/[GSH]_t\}$
1.20	2.49×10^{-2}	5.0	4.99	0.698
1.56	4.65×10^{-2}	5.0	9.30	0.969
1.81	7.96×10^{-2}	5.0	15.9	1.20
2.08	1.05×10^{-1}	5.0	21.1	1.32
2.29	1.34×10^{-1}	5.0	27.0	1.43
2.44[b]	1.74×10^{-1}	5.0	34.8	1.54
2.60[b]	6.00×10^{-2}	1.0	60.0	1.78
2.73[b]	3.33×10^{-1}	5.0	66.6	1.82
2.93[b]	4.14×10^{-1}	5.0	82.7	1.20
3.02[b]	4.95×10^{-1}	5.0	99.1	2.00
3.43[b]	7.16×10^{-1}	5.0	1.43×10^{2}	2.16
3.75[c]	2.09×10^{-1}	1.0	2.09×10^{2}	2.32
4.01[c]	2.92×10^{-1}	1.0	2.92×10^{2}	2.46
4.24[c]	3.42×10^{-1}	1.0	3.42×10^{2}	2.53
4.37[c]	4.87×10^{-1}	1.0	4.87×10^{2}	2.69
4.79[c]	9.23×10^{-1}	1.0	9.23×10^{2}	2.97
4.86[c]	1.14	1.0	1.14×10^{3}	3.06
4.95[c]	1.27	1.0	1.27×10^{3}	3.10

Table 2.4. pH Dependent Kinetics of the Reaction of Ir^{IV} With GSH[a] contd…

pH	k_{obs}, s^{-1}	$[GSH]_t$, mM	$k_{obs}/[GSH]_t$, M^{-1} s^{-1}	$\log\{k_{obs}/[GSH]_t\}$
5.15[d]	1.90	1.0	1.90×10^3	3.28
5.51[d]	2.44	1.0	2.44×10^3	3.39
5.91[d]	5.81	1.0	5.81×10^3	3.76
6.03[d]	11.9	1.0	1.19×10^4	4.08
6.28[d]	18.9	1.0	1.89×10^4	4.28
6.44[d]	28.3	1.0	2.83×10^4	4.45
6.55[d]	35.6	1.0	3.56×10^4	4.55
6.89[d]	71.8	1.0	7.18×10^4	4.86
7.07[e]	1.02×10^2	1.0	1.02×10^5	5.01

[a]$[Ir^{IV}]_0$ = 0.10 mM, [dipic] = 1 mM. pH from 1.2 to 2.29 was maintained by $HClO_4$ and μ = 0.1 M ($LiClO_4$). At higher pH appropriate 10 mM buffers were used with μ = 0.1 M ($NaClO_4$). [b]Chloroacetate buffer. [c]Acetate buffer. [d]Cacodylate buffer. [e]Gly-gly buffer.

The reaction of GSSG with $[IrCl_6]^{2-}$ was investigated in a separate experiment, since GSSG is one of the products of reaction of GSH with $[IrCl_6]^{2-}$ and its oxidation could conceivably lead to the formation of GSO_3^-. The experiment was performed at pH 5.0 (cacodylate buffer) with 0.17 mM $[IrCl_6]^{2-}$ and 0.15 mM GSSG. No appreciable loss of $[IrCl_6]^{2-}$ was detected over one hour (Fig 2.13), which means that the second-order rate constant for reaction of GSSG with $[IrCl_6]^{2-}$ is less than 0.5 M^{-1} s^{-1} at pH 5. This is considerably slower than the rate of reaction of $[IrCl_6]^{2-}$ with GSH at any pH.

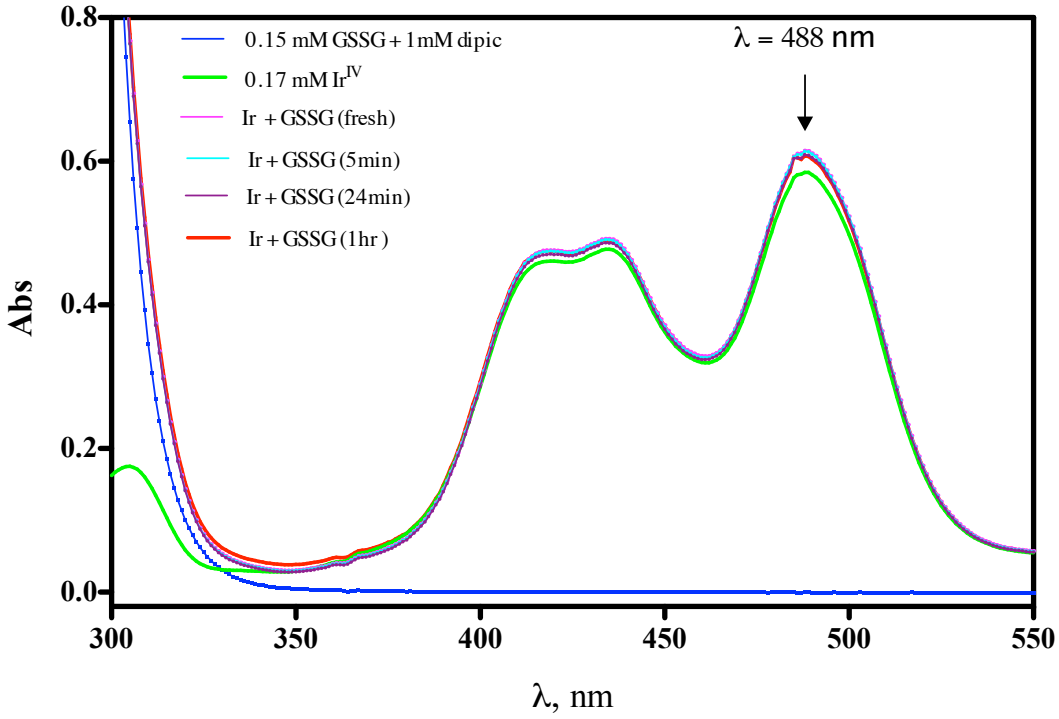

Fig 2.13. The reaction of GSSG with $[IrCl_6]^{2-}$. 2 mL (0.3 mM) GSSG with 2 mM dipic + 2 mL (0.34 mM) Ir^{IV} = 4 mL 0.15 mM GSSG and 0.17 mM Ir^{IV} with 1 mM dipic in the reaction. Ir^{IV} solution prepared in cacodylate buffer at pH 5.0. 'Ir' in the above figure = $[IrCl_6]^{2-}$.

2.4. Discussion.

In the oxidation of GSH by the strong oxidant $[IrCl_6]^{2-}$, over-oxidation (formation of GSO_3^- rather than GSSG) occurred. The over-oxidation trend is observed in the oxidation of thioglycolate by $[IrCl_6]^{2-}$ which over-oxidizes to give the product sulfonate.[33] Since $[IrCl_6]^{2-}$ reacts much more slowly (if at all) with GSSG than with GSH, it is clear that GSO_3^- must be produced from reaction intermediates before they generate GSSG.

A simplified general mechanism for reaction of GSH with the oxidant (Ir^{IV}) is given below. Details relating to the pH dependence of the rate-limiting steps are discussed further below.

$$Ir^{IV} + GSH \rightleftharpoons Ir^{III} + GS\bullet + H^+ \quad (2.9)$$

$$GS\bullet + GSH \rightleftharpoons GSSG\bullet^- + H^+ \quad (2.10)$$

$$Ir^{IV} + GSSG\bullet^- \longrightarrow Ir^{III} + GSSG \quad (2.11)$$

$$2GS\bullet \longrightarrow GSSG \quad (2.12)$$

$$Ir^{IV} + GS\bullet + H_2O \longrightarrow Ir^{III} + GSOH + H^+ \quad (2.13)$$

$$GSOH + 2H_2O \longrightarrow GSO_3^- + 4e^- + 5H^+ \quad (2.14)$$

Reaction 2.9 is the rate-limiting step, which generates the well-known glutathione thiyl radical. Reversible association of GS• with GSH to form $GSSG\bullet^-$ in the next step (eq 2.10) is quite well established.[27, 50, 51] Two routes to GSSG are depicted in reactions 2.11

and 2.12. The first of these, oxidation of $GSSG^{\bullet -}$ by Ir^{IV}, is expected to have a large rate constant and to be predominant at higher pH. At lower pH, where reaction 2.10 is unfavorable, dimerization of GS• could become significant. Formation of GSO_3^- is proposed to occur through the direct reaction of GS• with Ir^{IV} as in eq 2.13; this reaction would lead initially to GSOH. Conversion of GSOH to GSO_3^- is indicated in eq 2.14, although the details of this conversion are unknown.

By analogy with cysteine, it can be expected that GSOH reacts with GSH to form GSSG:[52]

$$GSOH + GSH \longrightarrow GSSG + H_2O \qquad (2.15)$$

The yield of GSO_3^- should thus be determined by the competition between reactions 2.15 and 2.14.

It is well known that the glutathione radical GS• undergoes a reversible internal carbon-to-sulfur hydrogen-atom transfer reaction to yield •GSH.[53] It is possible that under acidic conditions where reaction 2.10 is disfavored and with weak oxidants where reaction 2.13 is insignificant, this internal hydrogen atom transfer could become competitive with GS• dimerization. This could lead to more highly oxidized products. Although no such products were detected in the current study, the high stoichiometric ratio obtained for the Ir^{IV}/GSH reaction might be a consequence of this reaction pathway.

The effect of O_2 on the stoichiometry of the reaction of GSH with Ir^{IV} can be rationalized as a consequence of O_2 oxidizing the $GSSG^{-\bullet}$ radical:

$$GSSG^{-}\bullet + O_2 \longrightarrow GSSG + O_2^{-}\bullet \qquad (2.16)$$

This type of reaction is very rapid ($k = 5.1 \times 10^8$ M^{-1} s^{-1}) [54] because the $GSSG^{-}\bullet$ radical is strongly reducing.[55, 56]

Glutathione has four acid/base sites: two carboxylates, a primary amine, and a thiol. In its cationic form, $HGSH^{+}$, all four sites are protonated. pK_{a1} and pK_{a2} lead to production of GSH^0 and $GSH\text{-}H^{-}$, which are primarily deprotonated at the carboxylate sites. pK_{a3} (= 8.73) corresponds to formation of $GSH\text{-}2H^{2-}$, which is mostly in the thiolate form. The primary amine site is the most strongly basic and is deprotonated at pK_{a4}.[57] The three intermediate protonation states can exist as various tautomers, and some of the microscopic equilibrium constants among them have been determined.[57] The pH dependence of the kinetics is accounted for by a model in which the various protonation states of GSH react with the oxidants:

$$GSH^0 + Ir^{IV} \longrightarrow GS\bullet + Ir^{III} \qquad k_2 \qquad (2.17)$$

$$GSH\text{-}H^{-} + Ir^{IV} \longrightarrow GS\bullet + Ir^{III} \qquad k_3 \qquad (2.18)$$

$$GSH\text{-}2H^{2-} + Ir^{IV} \longrightarrow GS\bullet + Ir^{III} \qquad k_4 \qquad (2.19)$$

$$GSH\text{-}3H^{3-} + Ir^{IV} \longrightarrow GS\bullet + Ir^{III} \qquad k_5 \qquad (2.20)$$

Despite considerable effort, we were unable to find evidence for reaction of $HGSH^{+}$ (k_1) with Ir^{IV}. This species is fully protonated and provides no possibility for tautomerization

to expose a reactive thiolate form. On the other hand, the trianion GSH-3H^{3-} is fully deprotonated, so it is unambiguously a thiolate. Reaction via this species is demonstrated by the well-resolved value of k_5 for [Fe(bpy)(CN)$_4$]$^-$ in the Chapter 3 . It is inferred that the values of k_2, k_3, and k_4 in Table 2.5 all refer to reactions of the oxidant with the associated thiolate forms of GSH. Since the dianion GSH-2H^{2-} is primarily in the thiolate form, the value of k_4 is the actual bimolecular rate constant for the thiolate. On the other hand, for the species GSH^0 and GSH-H$^-$ the thiolate forms are the minor tautomers with the respective tautomerization equilibrium constants K_{Tn} and K_{Ta} being much less than unity:

$$HS–(NH_3^+)(COOH)(COO^-) \rightleftharpoons {}^-S–(NH_3^+)(COOH)_2 \qquad K_{Tn} \quad (2.21)$$

$$HS–(NH_3^+)(COO^-)_2 \rightleftharpoons {}^-S–(NH_3^+)(COOH)(COO^-) \qquad K_{Ta} \quad (2.22)$$

$$^-S–(NH_3^+)(COOH)_2 + Ir^{IV} \longrightarrow \bullet S–(NH_3^+)(COOH)_2 + Ir^{III} \qquad k_{2a} \quad (2.23)$$

$$^-S–(NH_3^+)(COOH)(COO^-) + Ir^{IV} \longrightarrow \bullet S–(NH_3^+)(COOH)(COO^-) + Ir^{III} \quad k_{3a} \quad (2.24)$$

These considerations lead to the relationships $k_2 = k_{2a}K_{Tn}$ and $k_3 = k_{3a}K_{Ta}$. A value of about 10^{-5} can be estimated for K_{Tn} and K_{Ta} from the known values for pK_{a2} and pK_{a3}. Values of the corrected bimolecular rate constants for the thiolate forms are $k_{2a} = 4 \times 10^6$ M^{-1} s^{-1} and $k_{3a} = 3 \times 10^7$ M^{-1} s^{-1}.

An electron-transfer mechanism is assigned above to the reactions of the thiolate forms of GSH. This assignment is based on the observation that the metal complex is reduced by one electron while retaining its coordination sphere intact.

An estimate for the electron-transfer equilibrium constants can be made, making use of the $E°$ ($RT\ln K = nFE^{0}_{cell}$) values for the oxidant and $E°$ ($GS•/GS^-$) for the GSH thiyl radical. This latter quantity is estimated to be about 0.82 ± 0.02 V vs NHE.[58] The value for the derived electron-transfer equilibrium constant is 15 for $[IrCl_6]^{2-}$. The values for the rate constants for reverse electron-transfer can be calculated from the forward rate constants (summary Table 2.5) and the equilibrium constant. The derived rate constant values are well below the limits of diffusion control. These calculations provide further evidence that these reactions have an electron-transfer mechanism.

As mentioned above, with $[IrCl_6]^{2-}$ as an oxidant, the thiolate electron-transfer equilibrium constant is about 15, i.e., mildly favorable for products. The corresponding rate constants in Table 2.5 are several orders of magnitude smaller than the diffusion-controlled values, so a significant kinetic barrier can be inferred. If it is assumed that these electron-transfer reactions follow an outer-sphere mechanism, then the cross relationship of the Marcus theory should apply to the rate constants. When this relationship is applied in its usual form including work terms,[59] we calculate a self-exchange rate constant of 1×10^6 M^{-1} s^{-1} for the $GSH\text{-}2H^{2-}/GS•$ redox couple. This calculation is based on the value for k_4 in Table 2.5 for $[IrCl_6]^{2-}$, a self-exchange rate constant of 2×10^5 M^{-1} s^{-1} for $[IrCl_6]^{2-/3-}$, and radii of 4.1 Å for $[IrCl_6]^{2-}$ and 3 Å for GSH. Given the considerable uncertainties involved, this calculated self-exchange rate constant is quite similar to the value of 7×10^6 M^{-1} s^{-1} that was reported for the analogous cysteine self-exchange rate constant.[34]

These results are broadly consistent with those previously reported for oxidation of GSH by ClO_2•,[19] NO_2•,[20] CO_3•$^-$,[23, 24] and N_3•,[21, 22] in that it is the thiolate forms of GSH that are the reactive species.

Table 2.5. Rate Constants for the Oxidation of the Thiolate Forms of GSH[a]

Parameter	$[IrCl_6]^{2-}$
E_f, V vs NHE	0.89
k_{11}, M^{-1} s^{-1}	2×10^5[b]
k_{2a}, M^{-1} s^{-1}	4×10^6
k_{-2a}, M^{-1} s^{-1}	2.7×10^5
k_{3a}, M^{-1} s^{-1}	3×10^7
k_{-3a}, M^{-1} s^{-1}	2×10^6
k_4, M^{-1} s^{-1}	4.7×10^6

[a] 25.0 °C, μ = 0.1 M. Values for k_{2a} and k_{3a} derived from the values for k_2 and k_3 by adjusting for tautomerization. Likewise k_{-2a} and k_{-3a} from the relation $k_{2a}/k_{-2a} = K_{eq} = 15$.

[b] Reference [60].

2.5. Conclusions.

Oxidation of glutathione by $[IrCl_6]^{2-}$ is sensitive to Cu^{2+} ion catalysis, but 1 mM dipic is enough to remove the Cu^{2+} and inhibit this side reaction. Dipic has no effect on the Ir^{IV} reaction. The rate law for the un-catalyzed reaction is first order in both Ir^{IV} and GSH. The pH dependence of the reaction kinetics is complex due to the tetraprotic nature of glutathione, with a trend of increasing rates with increasing pH. The un-catalyzed reaction proceeds by a rate limiting outer-sphere electron transfer from the thiolate forms of GSH to generate thiyl radicals. The sulphur containing product is the corresponding sulfonic acid due to over-oxidation with negligible amount of disulfide (GSSG) whereas the metal containing product is $[IrCl_6]^{3-}$.

References.

1. Sies, H. *Free Rad. Biol. Med.* **1999**, *27*, 916.

2. Meister, A.; Anderson, M. E. *Ann. Rev. Biochem.* **1983**, *52*, 711.

3. Everse, J.; Kujundzic, N. *Biochemistry* **1979**, *18*, 2668.

4. Hamed, M. Y.; Silver, J.; Wilson, M. T. *Inorg. Chim. Acta* **1983**, *78*, 1.

5. Scarpa, M.; Momo, F.; Viglino, P.; Vianello, F.; Rigo, A. *Biophys. Chem.* **1996**, *60*, 53.

6. Ayoko, G. A.; Olatunji, M. A. *Inorg. Chim. Acta* **1983**, *80*, L15-L17, 287.

7. Labuda, J.; Vanickova, M.; Pavlishchuk, V. V.; Kolchinskii, A. G. *Chem. Papers* **1994**, *48*, 78.

8. Bose, R. N.; Moghaddas, S.; Gelerinter, E. *Inorg. Chem.* **1992**, *31*, 1987.

9. Ayoko, G. A.; Iyun, J. F.; Ekubo, A. T. *Indian J. Chem.* **1993**, *32A*, 616.

10. Ayoko, G. A.; Iyun, J. F.; Ekubo, A. T. *Transition Met. Chem.* **1993**, *18*, 6.

11. Chatterjee, D.; Pal, U.; Ghosh, S.; van Eldik, R. *Dalton Trans* **2011**, *40*, 1302.

12. Stochel, G.; Martinez, P.; van Eldik, R. *J. Inorg. Biochem.* **1994**, *54*, 131.

13. Campanali, A. A.; Kwiecien, T. D.; Hryhorczuk, L.; Kodanko, J. J. *Inorg. Chem.* **2010**, *49*, 4759.

14. Gangopadhyay, S.; Ali, M.; Dutta, A.; Banerjee, P. *J. Chem. Soc., Dalton Trans.* **1994**, 841.

15. Perez-Benito, J. F.; Arias, C. *J. Phys. Chem. A* **1998**, *102*, 5837.

16. Frasca, D. R.; Clarke, M. J. *J. Am. Chem. Soc.* **1999**, *121*, 8523.

17. Nayak, S.; Brahma, G. S.; Reddy, K. V. *Aust. J. Chem.* **2012**, *65*, 113.

18. Sami, P.; Anand, T. D.; Premanathan, M.; Rajasekaran, K. *Transition Met. Chem.* **2010**, *35*, 1019.

19. Ison, A.; Odeh, I. N.; Margerum, D. W. *Inorg. Chem.* **2006**, *45*, 8768.

20. Ford, E.; Hughes, M. N.; Wardman, P. *Free Radical Biol. Med.* **2002**, *32*, 1314.

21. Abedinzadeh, Z.; Gardes-Albert, M.; Ferradini, C. *Radiat. Phys. Chem.* **1991**, *38*, 1.

22. Zhao, R.; Lind, J.; Merényi, G.; Eriksen, T. E. *J. Am. Chem. Soc.* **1994**, *116*, 12010.

23. Chen, S.-N.; Hoffman, M. Z. *Radiat. Res.* **1973**, *56*, 40.

24. Eriksen, T. E.; Fransson, G. *Radiat. Phys. Chem.* **1988**, *32*, 163.

25. Candeias, L. P.; Folkes, L. K.; Dennis, M. F.; Patel, K. B.; Everett, S. A.; Stratford, M. R. L.; Wardman, P. *J. Phys. Chem.* **1994**, *98*, 10131.

26. Winterbourn, C. C.; Metodiewa, D. *Free Rad. Biol. Med.* **1999**, *27*, 322.

27. Mezyk, S. P. *J. Phys. Chem.* **1996**, *100*, 8861.

28. Huston, P.; Espenson, J. H.; Bakac, A. *Inorg. Chem.* **1992**, *31*, 720.

29. Schöneich, C.; Asmus, K. D.; Bonifacic, M. *J. Chem. Soc., Faraday Trans.* **1995**, *91*, 1923.

30. Folkes, L. K.; Trujillo, M.; Bartesaghi, S.; Radi, R.; Wardman, P. *Arch. Biochem. Biophys.* **2011**, *506*, 242.

31. Hung, M.; Stanbury, D. M. *Inorg. Chem.* **2005**, *44*, 9952.

32. Saha, B.; Hung, M.; Stanbury, D. M. *Inorg. Chem.* **2002**, *41*, 5538.

33. Sun, J.; Stanbury, D. M. *J. Chem. Soc., Dalton Trans.* **2002**, 785.

34. Wang, X.; Stanbury, D. M. *Inorg. Chem.* **2008**, *47*, 1224.

35. Hung, M.; Stanbury, D. M. *Inorg. Chem.* **2005**, *44*, 3541.

36. Kauffman, G. B.; Teter, L. A. *Inorg. Synth.* **1966**, *8*, 223.

37. Sawyer, D. T.; Sobkowiak, A.; Roberts, J. L. *Electrochemistry for Chemists, 2nd ed,* John Wiley and Sons: New York, 1995; pp 192.

38. *Prism 5,* GraphPad Software, Inc.: San Diego, CA, 2010;

39. Chang, J. C.; Garner, C. S. *Inorg. Chem.* **1965**, *4*, 209.

40. Jorgensen, C. K. *Acta Chem. Scand.* **1957**, *11*, 151.

41. Poulsen, I. A.; Garner, C. S. *J. Am. Chem. Soc.* **1962**, *84*, 2032.

42. Sarala, R.; Stanbury, D. M. *Inorg. Chem.* **1990**, *29*, 3456.

43. Stapp, E. L.; Carlyle, D. W. *Inorg. Chem.* **1974**, *13*, 834.

44. Wilmarth, W. K.; Stanbury, D. M.; Byrd, J. E.; Po, H. N.; Chua, C.-P. *Coord. Chem. Rev.* **1983**, *51*, 155.

45. Margerum, D. W.; Chellappa, K. L.; Bossu, F. P.; Burce, G. L. *J. Am. Chem. Soc.* **1975**, *97*, 6894.

46. Cecil, R.; Littler, J. S.; Easton, G. *J. Chem. Soc. B* **1970**, 626.

47. Harwood, D. T.; Nimmo, S. L.; Kettle, A. J.; Winterbourn, C. C.; Ashby, M. T. *Chem. Res. Toxicol.* **2008**, *21*, 1011.

48. Krezel, A.; Bal, W. *Org. Biomol. Chem.* **2003**, *1*, 3885.

49. Makarycheva-Mikhailova, A. V.; Stanbury, D. M.; McKee, M. L. *J. Phys. Chem. B* **2007**, *111*, 6942.

50. Hoffman, M. Z.; Hayon, E. *J. Phys. Chem.* **1973**, *77*, 990.

51. Mezyk, S. P.; Armstrong, D. A. *J. Chem. Soc., Perkin Trans. 2* **1999**, 1411.

52. Nagy, P.; Ashby, M. T. *J. Am. Chem. Soc.* **2007**, *129*, 14082.

53. Hofstetter, D.; Nauser, T.; Koppenol, W. H. *Chem. Res. Toxicol.* **2010**, *23*, 1596.

54. Prütz, W. A.; Butler, J.; Land, E. J. *Biophys. Chem.* **1994**, *49*, 101.

55. Asmus, K.-D.; Bonifacic, M. in *S-Centered Radicals;* Alfassi, Z. B., Ed.; John Wiley & Sons: New York, 1999; pp 141.

56. Quintiliani, M.; Badiello, R.; Tamba, M.; Esfandi, A.; Gorin, G. *Int. J. Radiat. Biol.* **1977**, *32*, 195.

57. Rabenstein, D. L. *J. Am. Chem. Soc.* **1973**, *95*, 2797.

58. Madej, E.; Wardman, P. *Arch. Biochem. Biophys.* **2007**, *462*, 94.

59. Zuckerman, J. J. *Inorganic Reactions and Methods, vol. 15,* VCH: Deerfield Beach, FL, 1986; pp 13.

60. Hurwitz, P.; Kustin, K. *Trans. Faraday Soc.* **1966**, *62*, 427.

Chapter 3

Oxidation of Glutathione by Dicyanobis(bipyridine)iron(III), and Tetracyano(bipyridine)iron(III)

This chapter is based on the following paper and reprints were made with permission from American Chemical Society.

Bhattarai, N.; Stanbury, D. M., *Inorg. Chem.* **2012**, *51*, 13303-13311.

3.1. Introduction

Glutathione (GSH, Scheme 2.1 chapter 2) composed of glutamyl-cysteinyl-glycine, is a ubiquitous tri-peptide found in the cell of living systems. This tri-peptide is involved in detoxification and protection from oxidative damage to the cell. Among various important roles of GSH are as an antioxidant, a redox buffer, radical scavenger etc.[1-3] The oxidation of glutathione by one-electron metal complexes and other reagents has been widely investigated proposing varieties of mechanisms.[4-31]

In chapter 2 GSH oxidation by $[IrCl_6]^{2-}$ has been described where the sulfur-containing product was glutathione sulfonic acid. In this chapter two relatively weak one-electron substitution inert oxidants bearing small charges, $[Fe(bpy)_2(CN)_2]^{+}$ and $[Fe(bpy)(CN)_4]^{-}$, have been selected to oxidize GSH under a wide range of pH (1-11) and maintaining various experimental conditions with a view to suggesting a possible reaction mechanism. These Fe^{III} compounds oxidized GSH yielding disulfide products.

3.2. Experimental Sections

3.2.1. Reagents and Solutions. Acetic acid, monochloroacetic acid, $CuSO_4 \cdot 5H_2O$, $(NH_4)_2Fe(SO_4)_2 \cdot 6H_2O$, HNO_3, H_2SO_4, KCN and chloroform (all from Fisher), cacodylic acid ($(CH_3)_2AsO_2H$)), D_2O, and glycylglycine hydrochloride (gly-gly) (from Sigma), N-tert-butyl-α-phenylnitrone (PBN, 98%), 2-6-pyridine dicarboxylic acid (dipic), 2,2'-bipyridyl (bpy), L-glutathione (GSH, > 99%), L-glutathione disulfide (GSSG), 3-(trimethylsilyl)-1-propane sulfonic acid sodium salt (DSS), and tetraphenylphosphonium chloride (PPh_4Cl, all from Aldrich) were used without further purification. $NaCF_3SO_3$ (98%, GFS), EDTA (MCB), $K_3[Fe(CN)_6]$ (certified, Fisher), Cl_2 gas (Matheson), NaOH pellets ("SigmaUltra", Sigma-Aldrich), HCl, $NaHCO_3$ and Dowex 50-X8 resin (J.T. Baker) were used without further purification. $LiClO_4$ (GFS), and $NaClO_4$ (Fisher) were recrystallized from hot water. Anhydrous Na_3PO_4 was prepared from $Na_3PO_4 \cdot 12H_2O$ (99.6% Fisher) as described in chapter 2.

Deionized water was purified with a Barnstead Nanopure Infinity system and used to prepare all solutions. Freshly prepared solutions were used to run all experiments except for stock solutions of $NaClO_4$, $LiClO_4$, $HClO_4$, HCl and some buffers. For all studies the reactant solutions were purged with argon gas on a bubbling line prior to use and transferred via glass syringes with Teflon or Pt needles, except where noted.

Stock solutions of $LiClO_4$ and $NaClO_4$ were standardized by titration. An aliquot was passed through a cation exchange column which had been packed with Dowex 50-X8 resin and regenerated with conc HCl. The eluate was then titrated with standard $NaOH_{(aq)}$ solution.

3.2.2. Preparation of Fe^{III} Complexes.

3.2.2.1. $[Fe^{II}(bpy)_2(CN)_2]\bullet 3H_2O$ was prepared as described in the literature.[32,33] A solution of 2,2'-bipyridine and $(NH_4)_2Fe(SO_4)_2\bullet 6H_2O$ in 3:1 mole ratio was prepared in 40 mL water. Immediately after heating the resulting dark red solution to below the boiling point, a freshly prepared KCN solution (excess) was added to it, stirred for fifteen minutes and cooled to room temperature. Through vacuum filtration the dark violet crystals were collected, washed with water and dried in vacuum. Yield obtained was 96%.

3.2.2.2. $[Fe^{III}(bpy)_2(CN)_2]NO_3 \bullet 2H_2O$. This compound was made by oxidizing $[Fe^{II}(bpy)_2(CN)_2]$ with conc. HNO_3 following Schilt's standard procedures.[32-34] 0.3 g $[Fe^{II}(bpy)_2(CN)_2]$ was dissolved in 1 mL concentrated nitric acid, gently warmed, diluted to 40 mL and filtered. The filtrate was kept in a refrigerator overnight and produced glistering red crystals which were recovered by filtration following vacuum drying at room temperature with the yield of 53%.

3.2.2.3. $K_2[Fe(bpy)(CN)_4]\bullet 3H_2O$. Schilt's standard procedure[32-34] was used to synthesize it according to which $[Fe^{II}(bpy)_2(CN)_2]$ and KCN (in 1: 3 mole ratio) were mixed together in 150 mL water and refluxed for 25 hours in a water bath. The resulting solution was cooled, filtered and extracted with chloroform to remove any residual $[Fe^{II}(bpy)_2(CN)_2]$. The aqueous phase was evaporated to reduce the volume, kept in a refrigerator overnight, and the resulting dark orange brown crystals were collected by suction filtration. The crystals were dried in a vacuum dessicator.

3.2.2.4. $Li[Fe(bpy)(CN)_4]\bullet 2.5H_2O$ was prepared with a slight modification of a published procedure:[34,35] A solution of $K_2[Fe(bpy)(CN)_4]$ was oxidized via sparging with

an excess of Cl_2 gas. Then to the resulting solution was added saturated hot solution of PPh_4Cl in a 1:1 mole ratio. The solution color turned dirty yellow, which was kept hot with constant stirring for about fifteen minutes, becoming a clear solution. This solution was cooled, and the resulting solid was collected by vacuum filtration. The formed $PPh_4[Fe^{III}(bpy)(CN)_4]$ was dissolved in acetonitrile, and then anhydrous $LiClO_4$ powder in excess was added, keeping the ratio of 1:1.5 moles (1.5 mole $LiClO_4$) A precipitate of $Li[Fe(bpy)(CN)_4]\bullet 2.5H_2O$ formed in high purity. Yield was 67%.

3.2.3. Methods. A HP-8453 diode array spectrophotometer equipped with a Brinkman Lauda RM6 thermostated system was used to record all UV-vis spectra at 25 ± 0.1 °C; 10 mm quartz cells were used. All pH measurements were performed on a Corning 450 pH/ion meter with a Mettler Toledo Inlab 421 combination pH electrode (3 M NaCl), calibrated with standard buffers.

^1H NMR spectra were obtained on a Brucker AV 400 MHz spectrometer. Chemical shifts (δ, ppm) in D_2O were relative to DSS.

Electrochemical measurements were conducted on a BAS 100B electrochemical analyzer equipped with a BAS C3 cell stand provided with an N_2 purging and stirring system. The cell used a 3.2 mm diameter glassy carbon disc as a working electrode, a Ag/AgCl (3 M NaCl) reference electrode ($E°$ = 0.205 V vs NHE),[36] and a Pt wire auxiliary electrode.

Kinetic studies were done at 25 ± 0.1 °C on a Hi-Tech SF-51 stopped-flow spectrophotometer in the 1 cm path length configuration with Olis 4300 data acquisition and analysis software. The reactions of GSH with $[Fe(bpy)_2(CN)_2]NO_3$ and $Li[Fe(bpy)(CN)_4]$ were monitored at 522 and 482 nm respectively, always maintaining at least a 10-fold molar excess of GSH relative to the oxidant. All rate constants reported are the average of at least four runs unless and otherwise stated; the shot-to-shot variation in k_{obs} was typically ± 1-3%. Least-squares fits of the pseudo-first-order rate constants were performed with the Prism 5 software package,[37] weighting the data proportionally to the inverse square of k_{obs}. When fitting the pH-dependent rate laws, proton concentrations were calculated with the approximation $[H^+] = 10^{-pH}$.

3.3. Results.

3.3.1. Characterization of Fe^{III} complexes. The prepared Fe^{III} complexes, **$[Fe^{III}(bpy)_2(CN)_2]NO_3$ and $Li[Fe^{III}(bpy)(CN)_4]$,** were analyzed as follows; the preparation of Fe^{III} complexes was a multi step process during which $[Fe^{II}(bpy)_2(CN)_2]$ and $K_2[Fe^{II}(bpy)(CN)_4]$ were also made to achieve the target compounds. These intermediate compounds were also checked with UV-vis, CV, OSWV and ^{1}H-NMR. All of these results are presented below.

3.3.1.1. $[Fe^{II}(bpy)_2(CN)_2]$. $[Fe^{II}(bpy)_2(CN)_2]$ has limited aqueous solubility (ca. 1 mM), which is a significant constraint on studies where it is involved. It was studied with the tools UV-vis (Fig A-4), CV (Fig A-5), and ^{1}H-NMR (Fig A-6). All results were in accordance with those described in the literature.[32,34,38]

3.3.1.2. $K_2[Fe^{II}(bpy)(CN)_4]$. UV-vis (Fig A-7), CV (Fig A-8) and ^{1}H-NMR (Fig A-9) tests were conducted separately for this compound. The details of results with corresponding figures are introduced in the appendix.

3.3.1.3. $[Fe^{III}(bpy)_2(CN)_2]NO_3$. This compound is very stable in neutral solution. The stability of a 3.4×10^{-4} M solution was monitored with UV-vis and was found unchanged for about 24 hours (Fig A-10 and A-3) The UV-vis spectrum was obtained with a 5.7×10^{-5} M solution of $[Fe^{III}(bpy)_2(CN)_2]^+$ in water. As reported in the literature, [32,34] the two peaks at wavelengths 394 and 544 nm were observed with molar extinction coefficient $\varepsilon_{394} = 1382$ and $\varepsilon_{544} = 269$ M^{-1} cm^{-1} respectively (Fig 3.1).

CV and OSWV voltammograms of $[Fe^{III}(bpy)_2(CN)_2]^+$ are presented in Fig 3.2a & b. They were obtained using a 1.3×10^{-3} M aqueous solution in 0.1 M $NaCF_3SO_3$. The $\Delta E_{p/p} = 61$ mV confirms that the electrochemistry of $[Fe^{III}(bpy)_2(CN)_2]^+$ is reversible. The derived $E_{1/2}$ is 564 mV vs Ag/AgCl and $E_{1/2}$ = 0.77 V vs NHE, which is in good agreement with $E_P = 556$ mV obtained from OSWV.

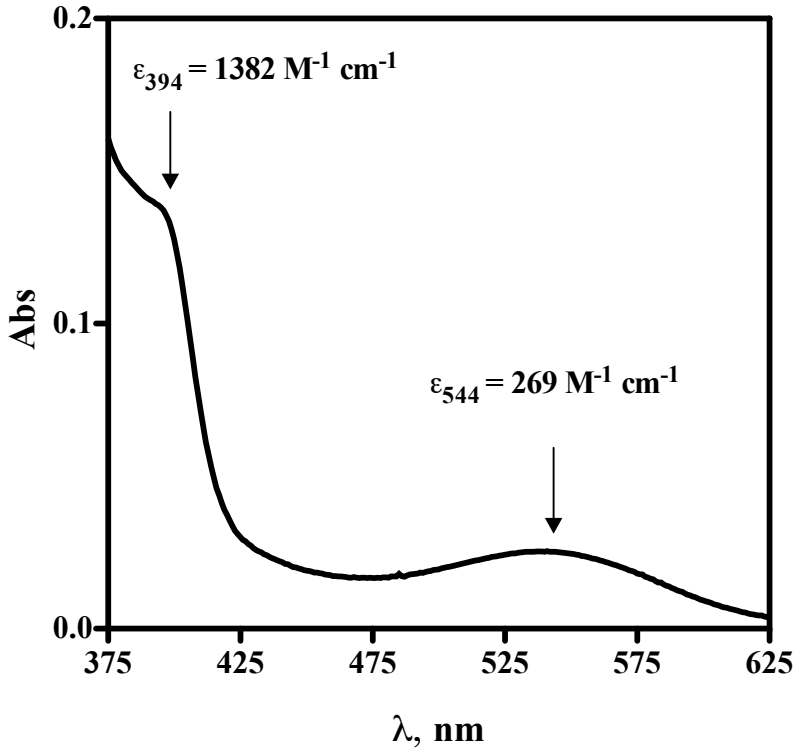

Fig 3.1. UV-vis spectrum of dicyanobis(bipyridine)iron(III). ($[Fe^{III}(bpy)_2(CN)_2]NO_3$) = 5.7×10^{-5} M in water. $T = 25\ ^0$C and pathlength (l) = 1 cm. Molar extinction coefficient values (ε) are in $M^{-1}\ cm^{-1}$.

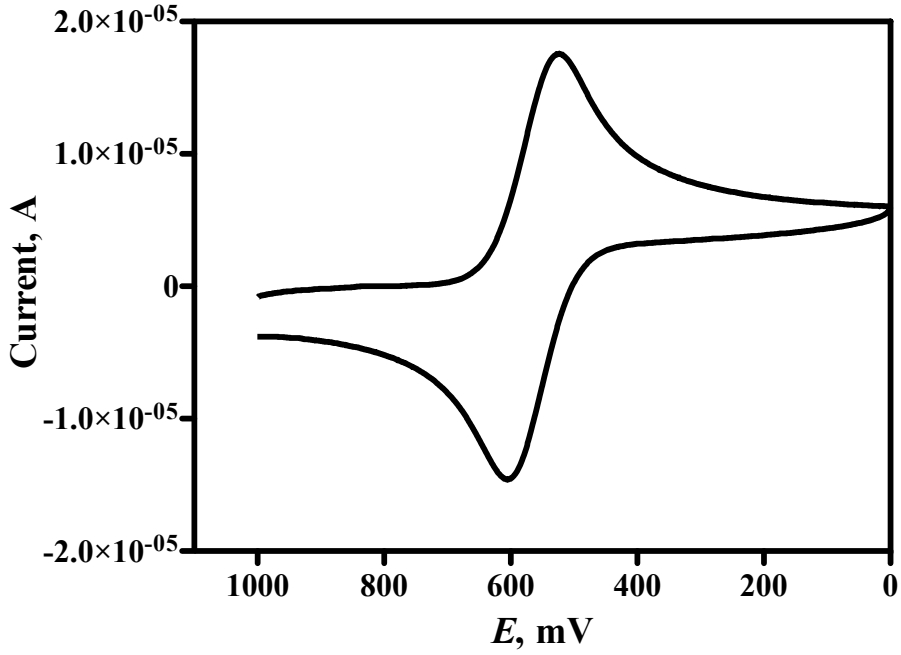

Fig 3.2a. Cyclic voltammogram of dicyanobis(bipyridine)iron(III).

$[[Fe^{III}(bpy)_2(CN)_2]NO_3] = 1.3 \times 10^{-4}$ M in 0.1 M $NaCF_3SO_3$

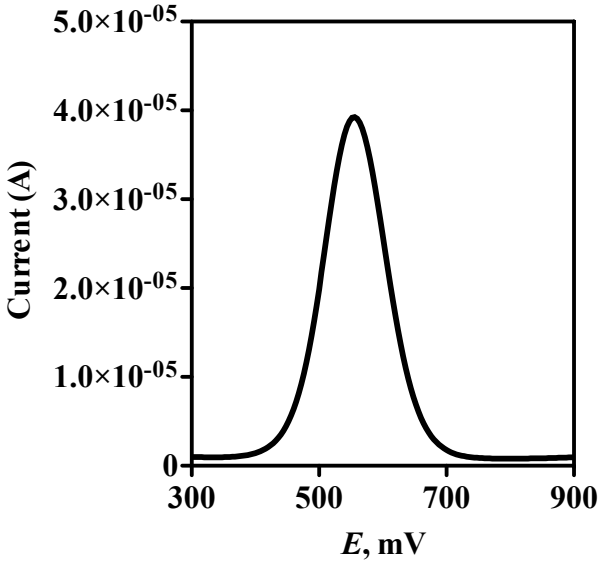

Fig 3.2b. OSWV of dicyanobis(bipyridine)iron(III).

$[[Fe^{III}(bpy)_2(CN)_2]NO_3] = 1.3 \times 10^{-4}$ M in 0.1 M $NaCF_3SO_3$ (aq)

3.3.1.4. Li[Fe^{III}(bpy)$(CN)_4$]. The stability of this compound ($[Fe^{III}(bpy)(CN)_4]^-$ = 5.8×10^{-4} M) in water was monitored with UV-vis. The data (Table A-4) and (Fig A-11) show that it is quite stable for two hours. Being paramagnetic, no NMR measurements were attempted. Another UV-vis examination performed on a 8.4×10^{-5} M solution at pH 6.0 (cacodylate buffer) with added 0.1 M $NaClO_4$ and 5.0×10^{-4} M EDTA showed that Li[Fe^{III}(bpy)$(CN)_4$] is a quite stable compound at slightly acidic pH for almost two days (Fig A-12 and Table A-5).

In an another test, the absorbance spectrum of a 5.0×10^{-5} M solution in water displayed two peaks characteristic of Li[Fe^{III}(bpy)$(CN)_4$] at 375 and 416 nm with ε_{375} = 1467 and ε_{482} = 975 M^{-1} cm^{-1} which are in good agreement with the literature values [34] (Fig 3.3).

The cyclic voltammogram of Li[Fe^{III}(bpy)$(CN)_4$] obtained with 9.0×10^{-4} M compound in a 0.1 M aqueous sodium triflate exhibited redox reversibility ($\Delta E_{p/p}$ = 67 mV) and $E_{1/2}$ = 350 mV ($E_{1/2}$ = 0.55 V vs NHE), also in good agreement with prior reports (Fig 3.4)[34]. A summary of the properties of the Fe^{III} complexes in aqueous solution is given in Table 3.1.

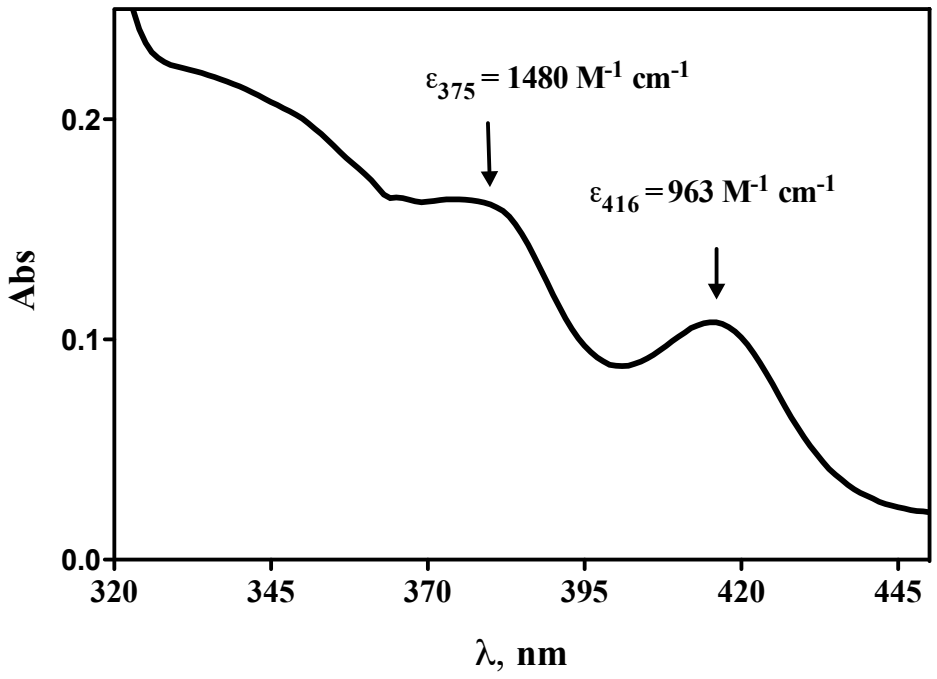

Fig 3.3. UV-vis spectrum of $Li[Fe^{III}(bpy)(CN)_4]$. $[Li[Fe^{III}(bpy)(CN)_4]] = 5.0 \times 10^{-5}$ M/H_2O

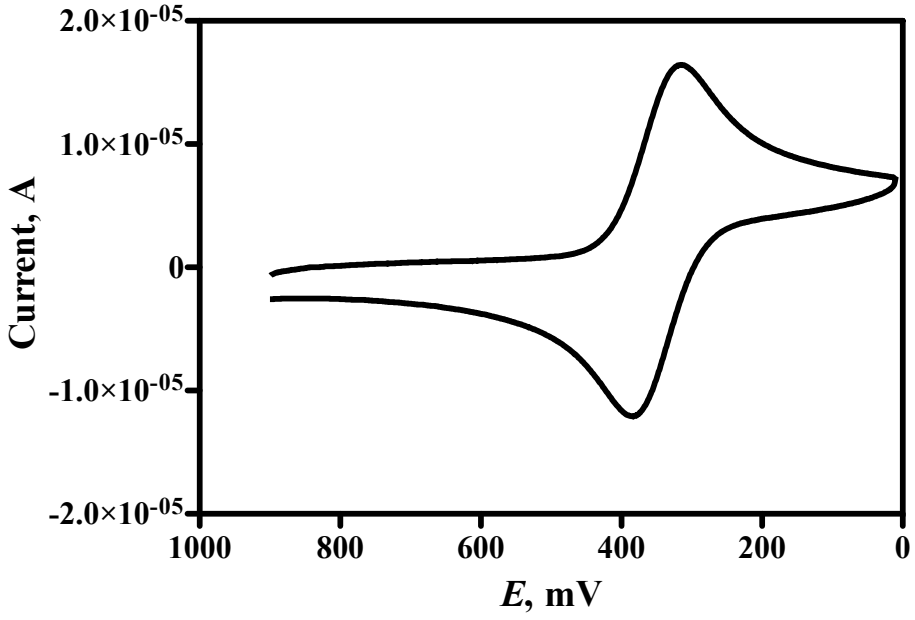

Fig 3.4. Cyclic voltammogram of $Li[Fe^{III}(bpy)(CN)_4]$

$[Li[Fe^{III}(bpy)(CN)_4]] = 9.0 \times 10^{-4}$ M in 0.1 M aqueous sodium triflate ($NaCF_3SO_3$)

Table 3.1. Summary of Properties of the Fe^{III} complexes in Aqueous Solution

Compound	band	λ_{max}, nm	ε, M^{-1} cm^{-1}	$E_{1/2}$, mV[a]
$Fe^{II}(bpy)_2(CN)_2$	I	352	5.56×10^3	566
	II	522	5.85×10^3	
$[Fe^{III}(bpy)_2(CN)_2]NO_3$	I	394	1.38×10^3	566
	II	544	2.69×10^2	
$K_2[Fe^{II}(bpy)(CN)_4]$	I	346	3.20×10^3	351
	II	482	2.62×10^3	
$Li[Fe^{III}(bpy)(CN)_4]$	I	375	1.48×10^3	350
	II	416	9.63×10^2	

[a] μ = 0.1 M, mV vs Ag/AgCl.

3.3.2. Qualitative Features of the GSH Reactions. Rapid color changes result upon mixing solutions of GSH with these two oxidants. Reductions of $[Fe^{III}(bpy)_2(CN)_2]^+$ and $[Fe^{III}(bpy)(CN)_4]^-$ occur with absorbance increases at 522 and 482 nm, respectively. Illustrations of these changes are depicted in Fig 3.5 and Fig 3.6 for $[Fe^{III}(bpy)_2(CN)_2]^+$ and $[Fe^{III}(bpy)(CN)_4]^-$ respectively.

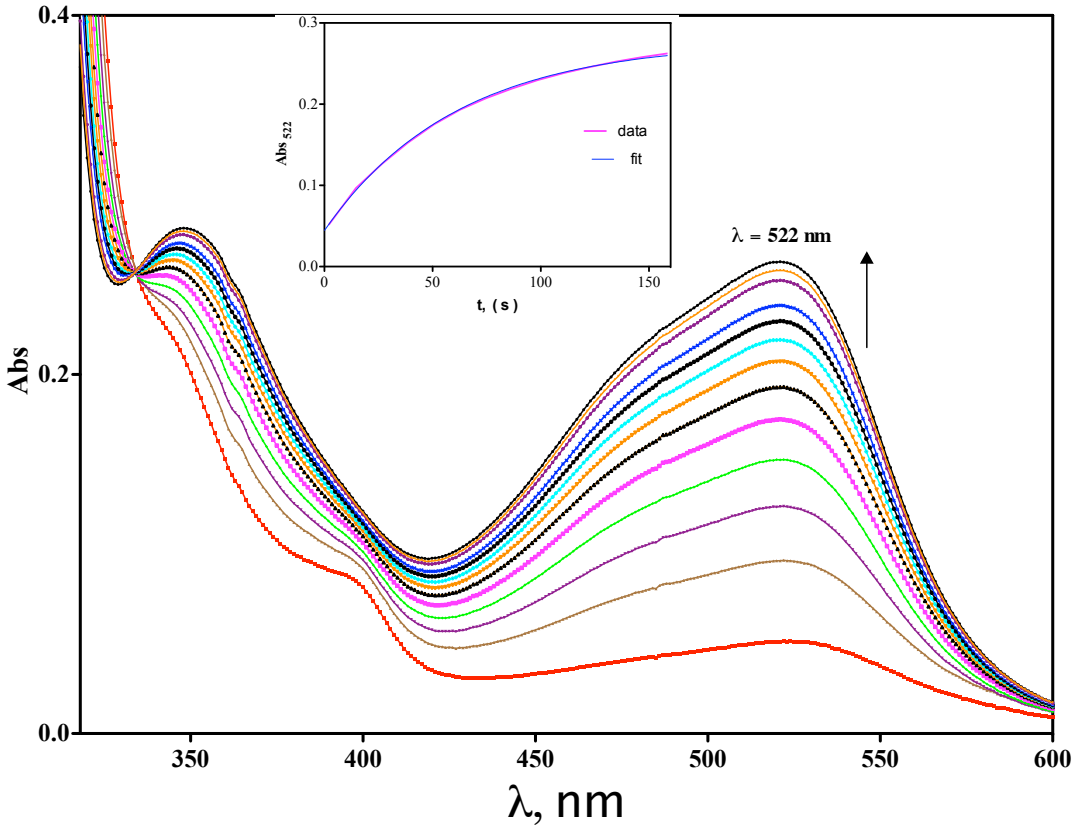

Fig 3.5. Kinetic formation of the spectra of $[Fe^{II}(bpy)_2(CN)_2]$ at 522 nm in the reaction of Fe^{III} with GSH using a diode array spectrophotometer . Inset: the kinetic trace for the reaction. $[[Fe^{III}(bpy)_2(CN)_2]^+]$ = 0.05 mM, [GSH] = 1 mM, [dipic] = 1 mM, no PBN, $[NaClO_4]$ = 0.1 M, unbuffered solution at pH = 3.2, run time = 160 sec and cycle time = 12 sec.

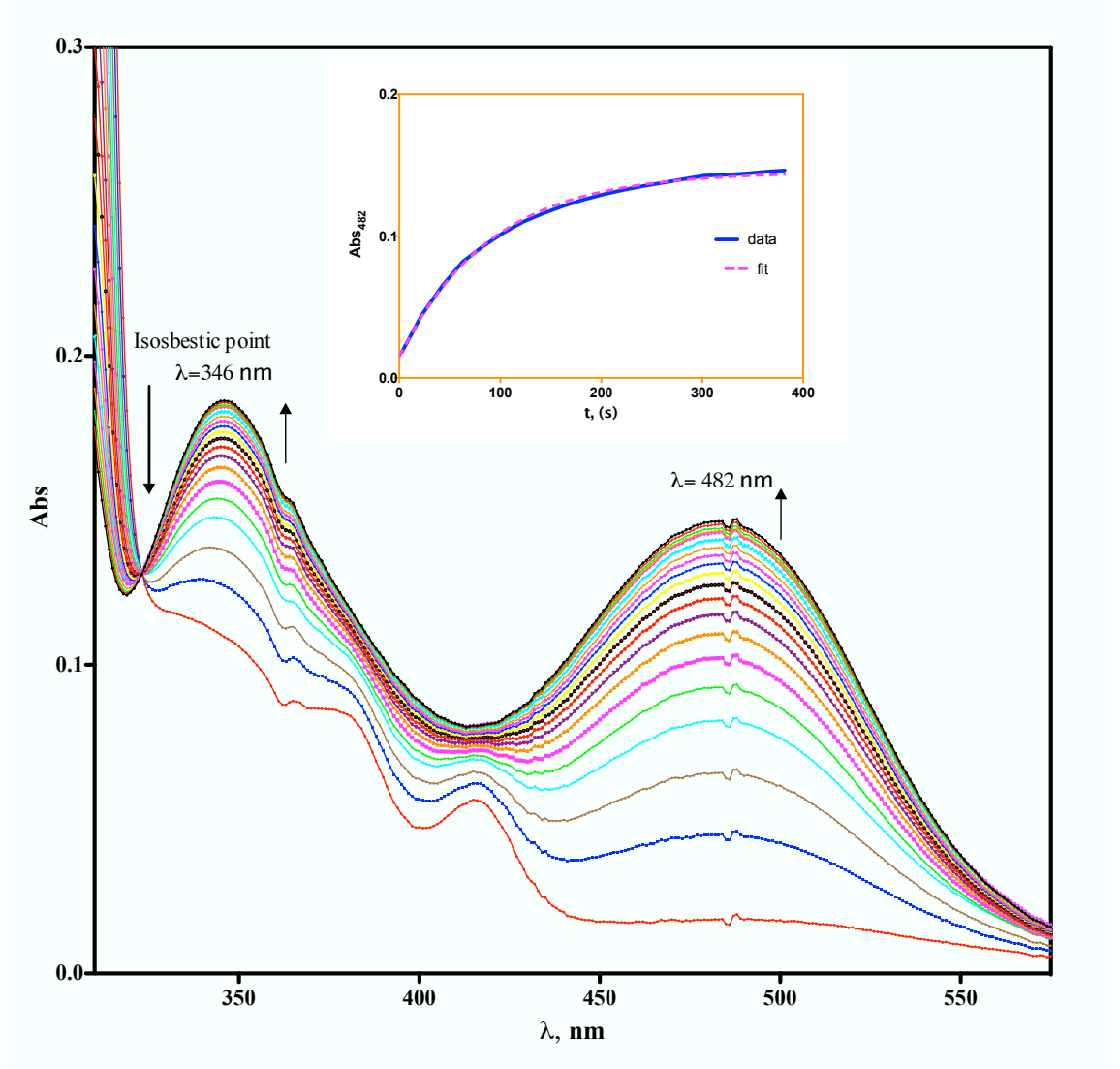

Fig 3.6. Kinetic formation of the spectra of $[Fe^{II}(bpy)(CN)_4]^{2-}$ at 482 nm in the reaction of $[Fe(bpy)(CN)_4]^-$ with $[GSH]_t$ using a diode array spectrophotometer. Inset: kinetic trace for the reaction. $[[Fe(bpy)(CN)_4]^-] = 0.055$ mM, $[GSH]_t = 1.0$ mM, [dipic] = 1 mM, ionic strength = 0.1 M ($NaClO_4$) at pH 6.2 cacodylate buffer (20 mM), run time = 400 sec with 20 second cycle time.

3.3.2.1. Trace metal catalysis. As is typical of thiol oxidations by inert one-electron oxidants,[34,39-42] these two reactions are highly susceptible to catalysis by copper ions. For example, the addition of 1 μM $CuSO_4$ led to a three-fold rate increase in the oxidation by $[Fe^{III}(bpy)_2(CN)_2]^+$ at pH 4.7, and a 12-fold rate increase in the oxidation by $[Fe^{III}(bpy)(CN)_4]^-$ at pH 7.0 (Tables 3.2 & 3.3; kinetic traces Fig A-13 & A-14). On the other hand, the addition of 1 mM 2,6-dipicolinic acid (dipic), a well-established inhibitor of copper catalysis,[34,39,40,42] led to a reduction in the rate of the $[Fe^{III}(bpy)_2(CN)_2]^+$ reaction. Likewise, 2 mM dipic or 5 mM EDTA reduced the rate of the $[Fe^{III}(bpy)(CN)_4]^-$ reaction by a factor of ten. Moreover, in the presence of 5 mM EDTA the $[Fe^{III}(bpy)(CN)_4]^-$ reaction was unaffected by 5 μM $CuSO_4$. These results show that trace levels of Cu^{2+} ions as impurities are sufficient to dominate the reaction kinetics and that copper catalysis can be completely suppressed by the addition of suitable chelating agents. All results described below were obtained in the presence of these inhibitors. In the reaction of $[Fe^{III}(bpy)_2(CN)_2]^+$ 1 mM dipic was deemed adequate; EDTA is unsuitable for

Table 3.2. Cu^{2+} Catalysis of the Oxidation of GSH by $[Fe(bpy)_2(CN)_2]^{+a}$

Expt.	$[Cu^{2+}]$, μM	$t_{1/2}$, s	[dipic], mM	k_{obs}, s^{-1}
1.	0.0	1.77	0.0	0.377
2.	1.0	0.62	0.0	1.46
3.	5.0	0.055	0.0	17.6
4.	0.0	2.26	1.0	0.297

[a] $[GSH]_t$ = 0.50 mM, $[Fe^{III}]_0$ = 0.05 mM, acetate buffer, pH = 4.7, μ = 0.1 M ($NaClO_4$).

use with stronger oxidants because it is oxidized directly. At pH higher than 7 dipic did not work, the dipic may not bind metal strongly in basic pH, and EDTA was used with $[Fe^{III}(bpy)(CN)_4]^-$ because this is a significantly weaker oxidant.

Table 3.3. Cu^{2+} Catalysis in the Reaction of $[Fe(bpy)(CN)_4]^-$ with GSH[a]

Expt	$[Cu^{2+}]$, μM	[EDTA], mM	[dipic], mM	$t_{1/2}$, s	k_{obs}, s^{-1}	fit
1.	0.0	0.0	0.0	2.23	0.30	bad
2.	1.0	0.0	0.0	0.29	3.72	bad
3.	5.0	0.0	0.0	0.013	36.0	bad
4.	0.0	1.0	0.0	21.0	2.82×10^{-2}	bad
5.	0.0	3.0	0.0	20.0	3.01×10^{-2}	good
6.	0.0	5.0	0.0	19.4	3.21×10^{-2}	good
7.	5.0	5.0	0.0	17.4	3.51×10^{-2}	good
8.	0.0	0.0	2.0	23.0	2.54×10^{-2}	bad

[a] $[GSH]_t = 0.5$ mM, $[Fe(bpy)(CN)_4]^- = 0.05$ mM, cacodylate buffer, pH = 7.0, $\mu = 0.1$ M ($NaClO_4$).

3.3.3. Product Analysis and Stoichiometry.

3.3.3.1. Product analysis with $[Fe(bpy)_2(CN)_2]^+$. The ^{1}H-NMR spectrum of the reaction products arising from an equimolar mixture of GSH and $[Fe^{III}(bpy)_2(CN)_2]^+$ shows that the Fe^{III} reagent is cleanly reduced to $[Fe^{II}(bpy)_2(CN)_2]$ (Fig 3.7). This

conclusion is based on the chemical shift values in the region 7.2-9.4 ppm, which are characteristic of $[Fe(bpy)_2(CN)_2]$.[38] The sharpness of these peaks is an indication that there is no residual Fe^{III} in the product mixture. The same NMR spectrum displays peaks due to GSSG at δ 3.291, 3.279, 3.255 and 3.244 ppm, and the lack of other peaks indicates that GSSG is the major oxidation product. UV-vis analysis of the reaction of 0.05 mM Fe^{III} with 0.5 mM GSH shows quantitative production (>95% yield) of $[Fe(bpy)_2(CN)_2]$ with its characteristic peak at 522 nm (Fig 3.8).

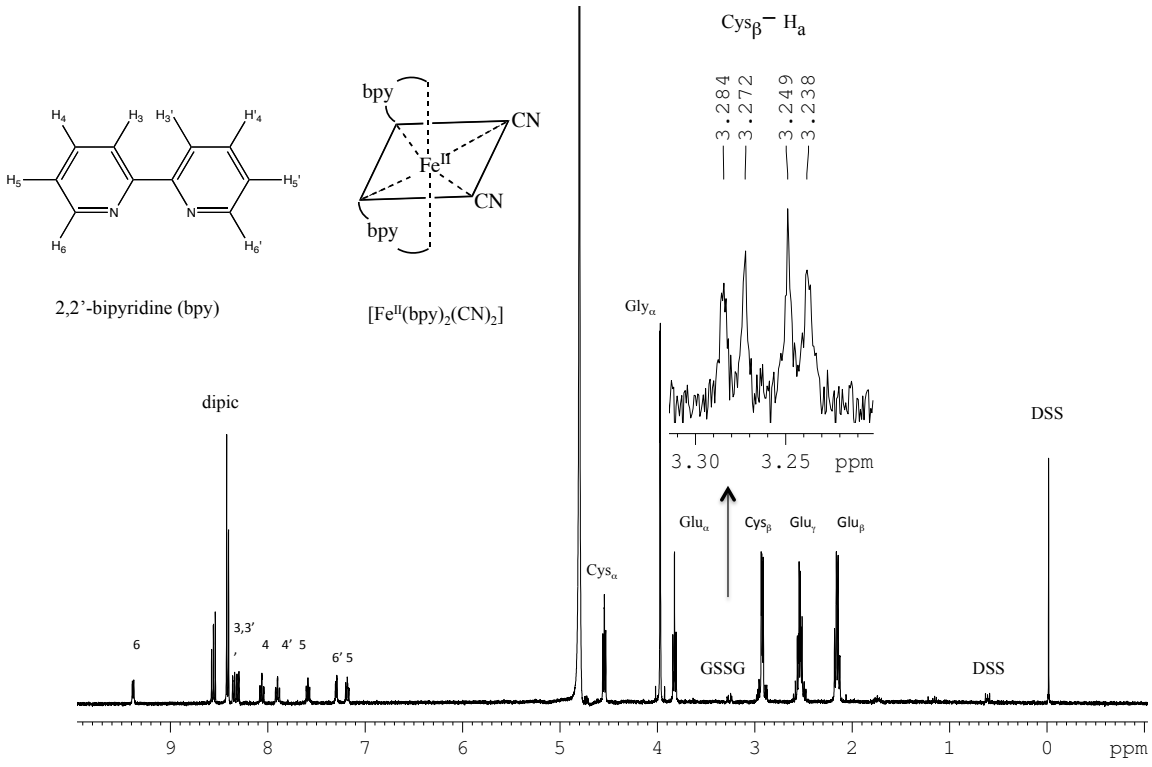

Fig 3.7. Product analysis of the reaction of GSH with $[Fe(bpy)_2(CN)_2]^+$ by ^1H NMR. Unbuffered solution in D_2O with DSS, $[Fe^{III}]_0$ = 1 mM, $[GSH]_0$ = 1 mM, [dipic] = 1 mM. Some Fe^{II} product precipitated.

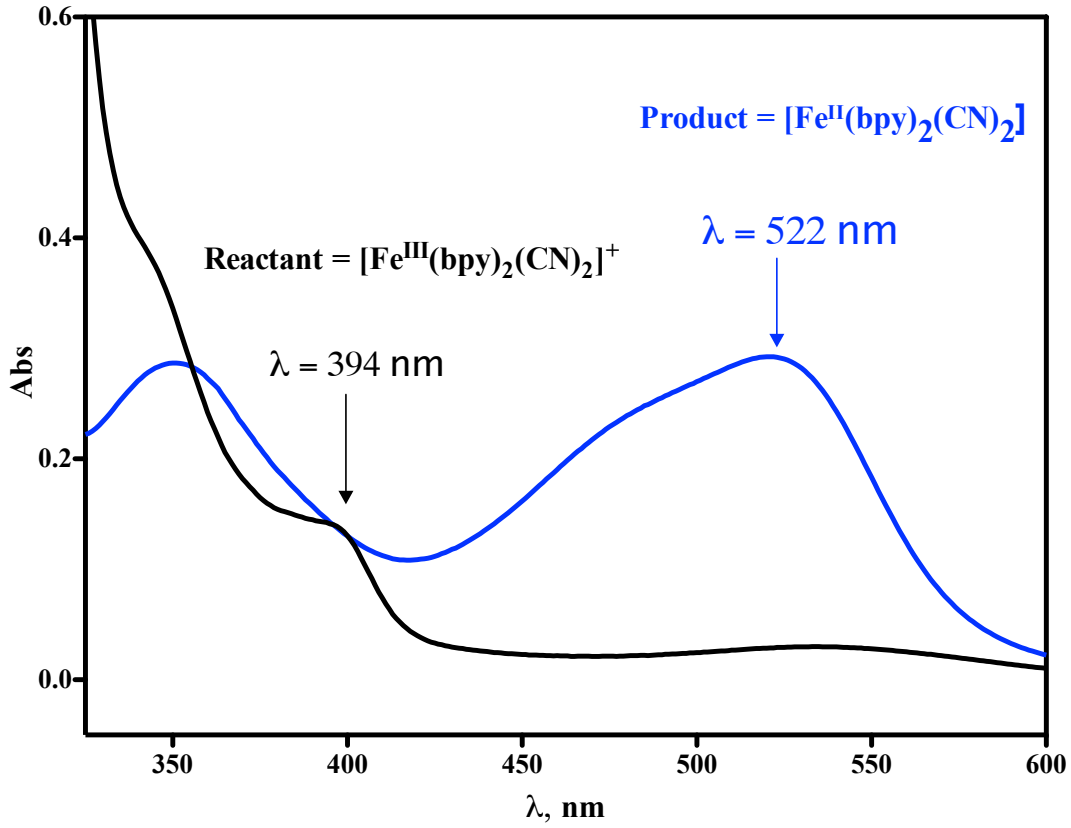

Fig 3.8. UV-vis spectral changes in the reaction of GSH with $[Fe^{III}(bpy)_2(CN)_2]^+$.

$[Fe^{III}]_0$ = 0.525 mM, $[GSH]_t$ = 0.50 mM, [dipic] = 1 mM, μ = 0.1 M ($NaClO_4$).

3.3.3.2. Stoichiometry. The consumption ratio ($\Delta[Fe(III)]/\Delta[GSH]_t$ = 1.5 ± 0.5) was obtained when a spectrophotometric titration at pH 4.7 including 1 mM dipic and 0.1 M ionic strength ($NaClO_4$) with 9.9 × 10^{-7} moles of $[GSH]_t$ was run against a 2.45 mM Fe^{III} solution. At the end point 1.5 × 10^{-6} moles of Fe^{III} were found to be consumed (Fig 3.9 and Table A-6). Thus the stoichiometric ratio, $\frac{n[Fe(III)}{n[GSH]t}$, was determined to be 1.5 ± 0.5.

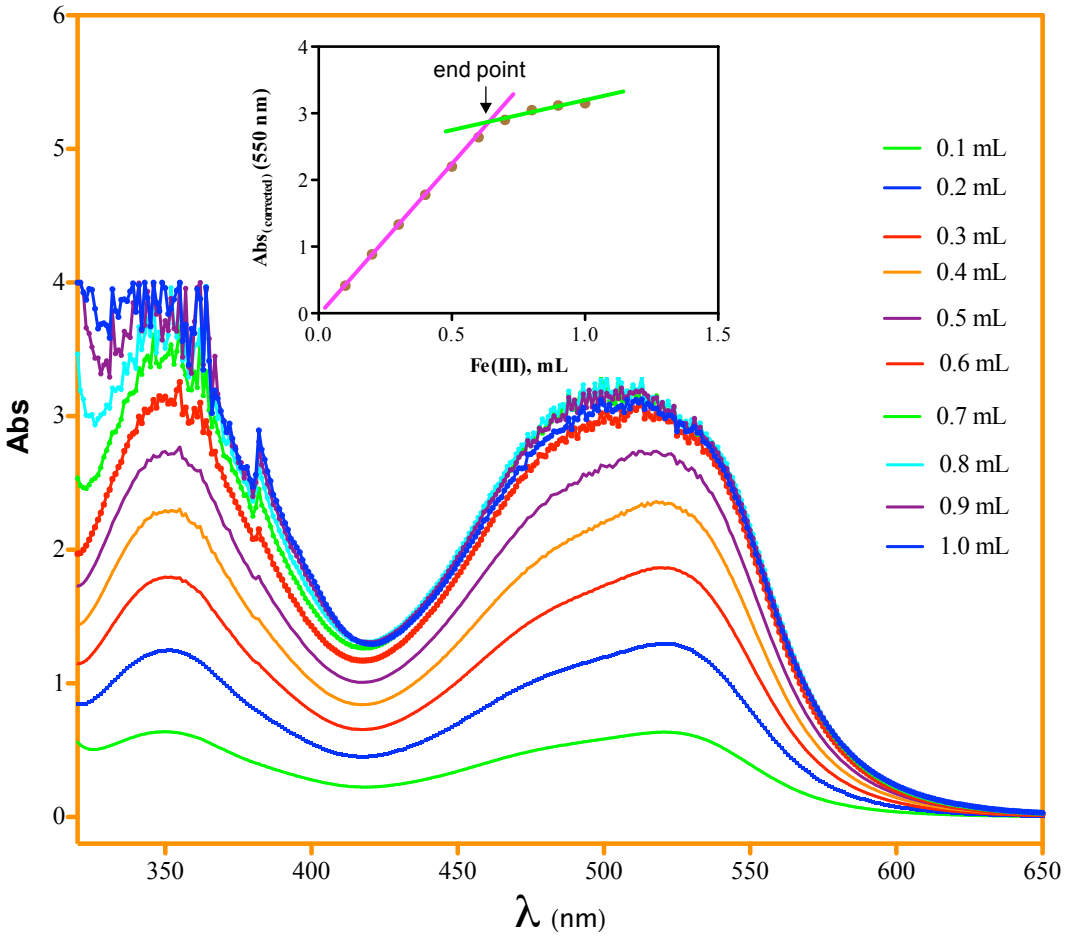

Fig 3.9. Spectrophotometric titration of GSH with $[Fe(bpy)_2(CN)_2]^+$. 2.0 mL of 0.495 M $[GSH]_t$ in acetate buffer at pH 4.7 with [dipic] = 1 mM, titrated with 0.0495 mM Fe^{III}. Absorbances corrected for dilution.

These results imply that the major overall reaction in excess GSH is

$$2[Fe^{III}(bpy)_2(CN)_2]^+ + 2GSH \rightarrow GSSG + 2[Fe^{II}(bpy)_2(CN)_2] + 2H^+ \quad (3.1)$$

A minor degree of over-oxidation (oxidation beyond GSSG) is inferred from the excess consumption of Fe^{III}.

3.3.3.3. Product Analysis with $[Fe^{III}(bpy)(CN)_4]^-$. Quantitative conversion (≥ 92%) of $[Fe^{III}(bpy)(CN)_4]^-$ to $[Fe^{II}(bpy)(CN)_4]^{2-}$ with excess GSH was observed by UV-vis spectroscopy (Fig 3.10). This result was obtained when 0.05 mM Fe^{III} reacted with 2.0 mM GSH at pH 7.2 (gly-gly buffer). The product spectrum exhibited peaks at 346 and 482 nm characteristic of $[Fe^{II}(bpy)(CN)_4]^{2-}$, the yield of Fe^{II} being determined from the molar absorptivity at 482 nm. Conversion of $[Fe^{III}(bpy)(CN)_4]^-$ to $[Fe^{II}(bpy)(CN)_4]^{2-}$ is confirmed by the ^1H NMR product spectrum obtained under similar conditions, as shown in Fig 3.11. This NMR spectrum also shows that GSSG is the only detected reaction product derived from GSH.

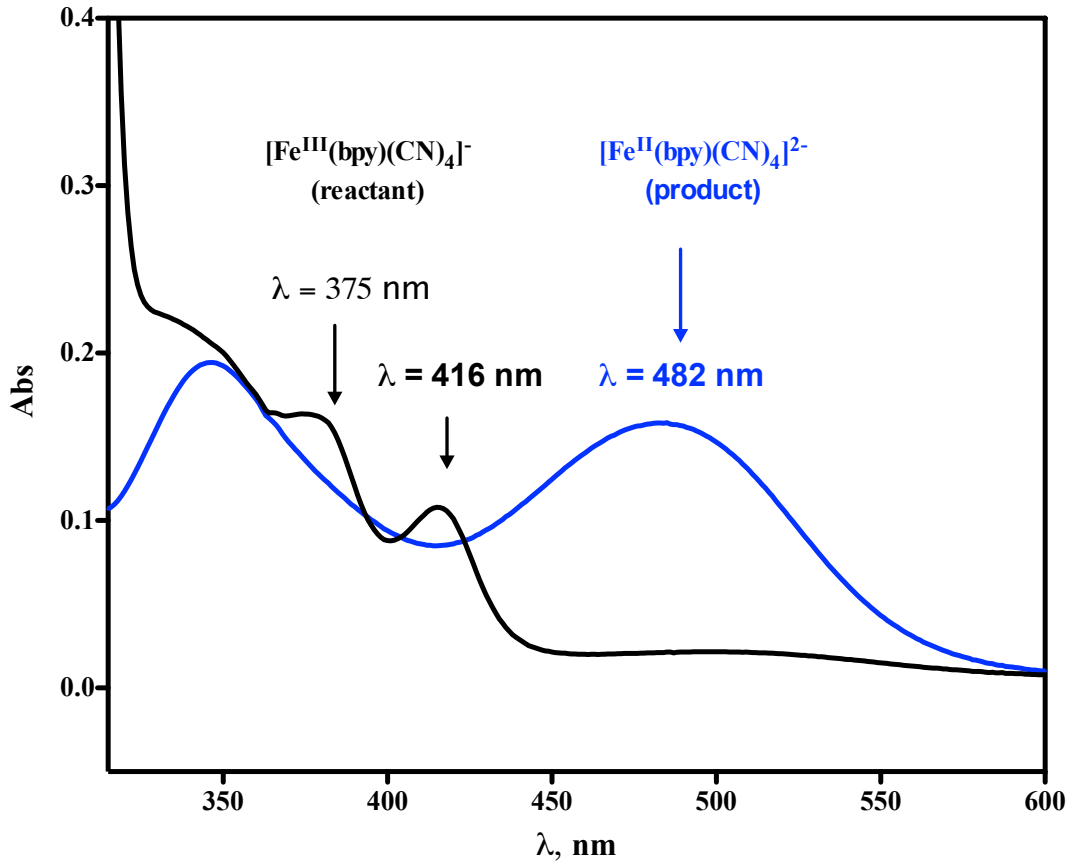

Fig 3.10. UV-vis spectral changes in the reaction of GSH with $[Fe^{III}(bpy)(CN)_4]^-$. The black spectrum is the Fe^{III} reactant. The blue spectrum is the product's. 2.0 mM $[GSH]_t$ vs 0.05 mM $[Fe^{III}(bpy)(CN)_4]^-$; gly-gly buffer (pH = 7.2), [dipic] = 1 mM and μ = 0.1 M ($NaClO_4$).

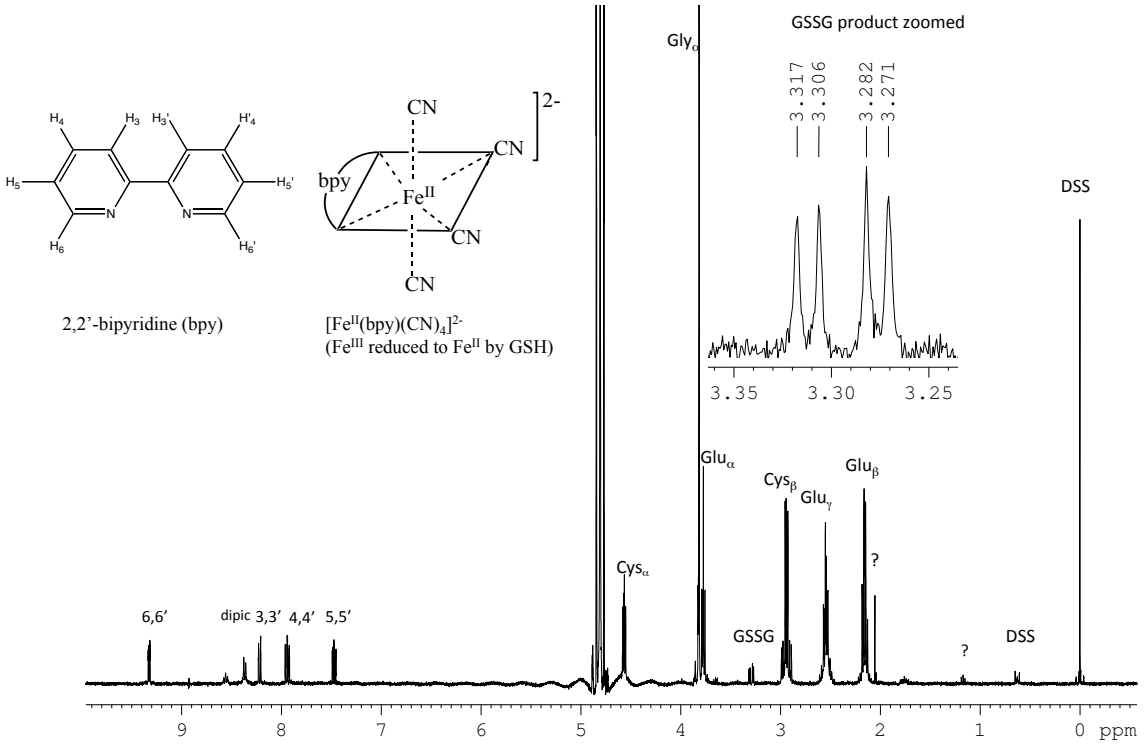

Fig 3.11. ^{1}H NMR spectrum of the product mixture formed in the reaction of $[Fe^{III}(bpy)(CN)_4]^-$ with GSH. 2 mM GSH with 1.2 mM Fe^{III}, 1 mM dipic, pH = 7.5 (Na_3PO_4), and a small amount of DSS as internal standard in D_2O

3.3.3.4. Stoichiometry. The consumption ratio in the reaction of $[Fe^{III}(bpy)(CN)_4]^-$ with GSH was determined at pH 6.3 by spectrophotometric titration of GSH, monitoring the absorbance at 482 nm (Fig 3.12). 2.0×10^{-6} moles of GSH consumed 2.41×10^{-6} moles of Fe^{III} at the endpoint indicating a stoichiometric ratio of 1.2 ± 0.2 (= $\Delta[Fe^{III}]/\Delta[GSH]_t$).

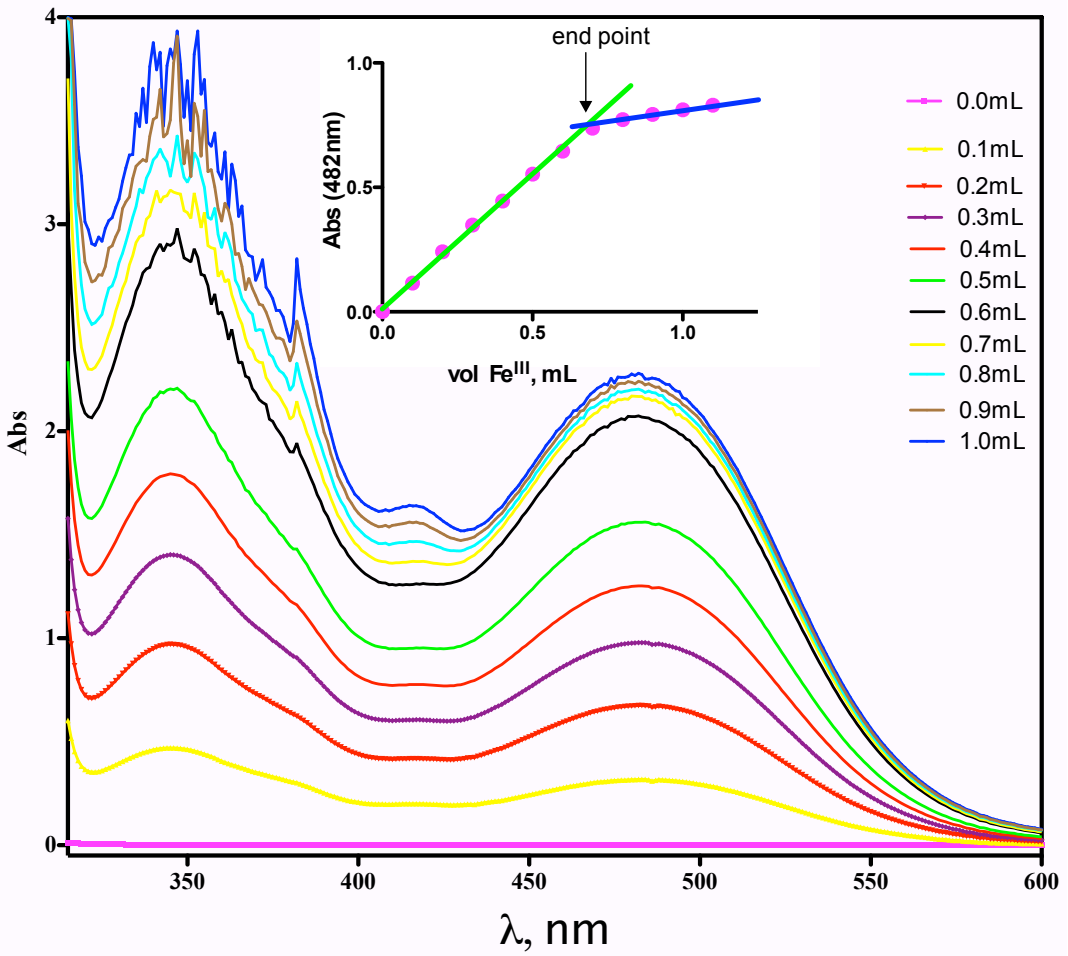

Fig 3.12. Spectrophotometric titration of GSH with $[Fe(bpy)(CN)_4]^-$. pH 6.3 (cacodylate buffer), [dipic] = 1 mM. 2.0 mL of 1.0 mM GSH titrated with 0.35 mM $Li[Fe(bpy)(CN)_4]$.

In view of the spectroscopic and titration results described above, the overall reaction is described by eq 3.2:

$$2[Fe^{III}(bpy)(CN)_4]^- + 2GSH \rightarrow GSSG + 2[Fe^{II}(bpy)(CN)_4]^{2-} + 2H^+ \qquad (3.2)$$

3.3.4. Kinetics.

3.3.4.1. General Features. As described above, copper ions are strongly catalytic in the reactions of these two oxidants with GSH. Accordingly, all kinetic results described below are obtained from reactions conducted in the presence of inhibitors that completely suppress the catalysis. The reactions were generally studied with a 10-fold excess of GSH over oxidant, which led to pseudo-first-order kinetics. The pseudo-first-order rate constant (k_{obs}) is defined by eq 3.3,

$$\text{Rate} = -\frac{d[\text{Fe}^{\text{III}}]}{dt} = k_{obs}[\text{Fe}^{\text{III}}] \quad (3.3)$$

GSH has four acidic protons, with pK_{a1} = 2.12, pK_{a2} = 3.512, pK_{a3} = 8.73 and pK_{a4} = 9.65 at ionic strength 0.1 M.[20,39] Thus, GSH potentially has five kinetically distinguishable protonation states: cationic (protonated), neutral, mono-anionic, di-anionic and tri-anionic forms depending upon pH, which are represented as [$HGSH^+$], [GSH^0], [$GSH\text{-}H^-$], [$GSH\text{-}2H^{2-}$] and [$GSH\text{-}3H^{3-}$], respectively. In principle, each of these protonation states could be reactive. The total GSH concentration is designated $[GSH]_t$. The k_{obs} obtained in the reactions of Fe^{III} with [GSH] is the sum of the rate contributed by all these species as in eq 3.4:

$$k_{obs} = k[GSH]_t = k_1[HGSH^+] + k_2[GSH^0] + k_3[GSH\text{-}H^-] + k_4[GSH\text{-}2H^{2-}] + k_5[GSH\text{-}3H^{3-}] \quad (3.4)$$

Inclusion in eq 3.4 of all respective pK_a terms leads to eq 3.5:

$$k_{\text{obs}} = \left[\frac{k_1[\text{H}^+]^4 + k_2K_{\text{a1}}[\text{H}^+]^3 + k_3K_{\text{a1}}K_{\text{a2}}[\text{H}^+]^2 + k_4K_{\text{a1}}K_{\text{a2}}K_{\text{a3}}[\text{H}^+] + k_5K_{\text{a1}}K_{\text{a2}}K_{\text{a3}}K_{\text{a4}}}{[\text{H}^+]^4 + K_{\text{a1}}[\text{H}^+]^3 + K_{\text{a1}}K_{\text{a2}}[\text{H}^+]^2 + K_{\text{a1}}K_{\text{a2}}K_{\text{a3}}[\text{H}^+] + K_{\text{a1}}K_{\text{a2}}K_{\text{a3}}K_{\text{a4}}}\right][\text{GSH}]_{\text{t}} \quad (3.5)$$

At a given pH eq 3.5 simplifies to eq 3.6:

$$k_{\text{obs}} = k_{\text{pH}}[\text{GSH}]_{\text{t}} \quad (3.6)$$

Deviations from rate law 3.3 can be anticipated for weak oxidants under acidic conditions, when inhibition by the product M_{red} can occur in thiol oxidations.[34,39,40,42] Mild product inhibitions were detected in the current study of GSH reactions with $[Fe(bpy)_2(CN)_2]^+$, and $[Fe(bpy)(CN)_4]^-$. Following prior practice, [34,39,40,42] these effects were eliminated by means of the radical spin trap PBN.

3.3.4.2. Kinetics with $[Fe(bpy)_2(CN)_2]^+$. A typical kinetic trace is shown in Fig 3.13, and was obtained in the reaction of 0.05 mM $[Fe^{III}(bpy)_2(CN)_2]^+$ with 1.0 mM $[GSH]_t$ at pH 6.6 in cacodylate buffer with 0.1 M ionic strength and 1 mM dipic. The kinetics of oxidation of GSH by $[Fe^{III}(bpy)_2(CN)_2]^+$ is mildly inhibited by $[Fe^{II}(bpy)_2(CN)_2]$ at lower pH. For example, the reaction of 0.5 mM GSH with 0.05 mM Fe^{III} at pH 6.0 occurred with k_{obs} = 4.3 s^{-1}, but k_{obs} decreased to 3.3 s^{-1} with 0.10 mM

added Fe^{II} (Table 3.4 & Fig 3.14). At pH 6.7 the effect of Fe^{II} is weaker (Table 3.5). At pH 3.2 the effect is strong enough to cause significant departures from pseudo-first-order kinetics (Fig 3.15). The addition of 0.1 mM PBN is sufficient to prevent Fe^{II} inhibition, leading to excellent pseudo-first-order kinetics (Fig 3.15 & Table A-8). Accordingly, 0.1 mM PBN was included in all further kinetic measurements at pH 4.4 and below (Table A-9). Further details about PBN experiments are introduced in the appendix (Fig A-15).

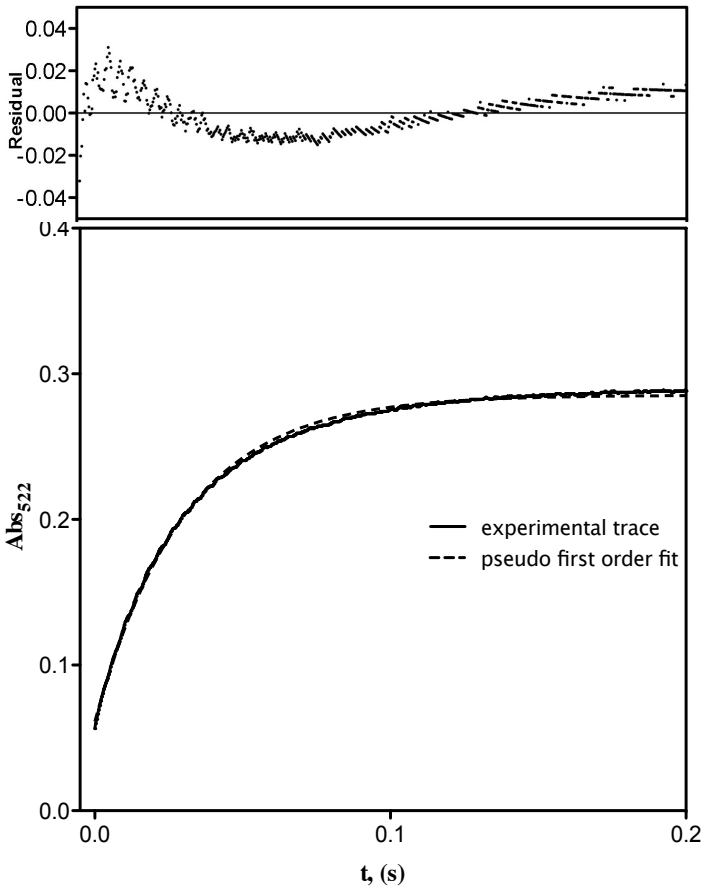

Fig 3.13. Kinetic trace for the reaction of $[Fe(bpy)_2(CN)_2]^+$ with $[GSH]_t$ at pH = 6.6 cacodylate buffer, $[Fe(bpy)_2(CN)_2]^+$ = 0.05 mM, $[GSH]_t$ = 1.0 mM , μ = 0.1 M ($NaClO_4$) and [dipic] = 1 mM. Upper box shows the residuals and lower box shows the experimental trace with pseudo-first order fit.

Table 3.4. Product Inhibition Test in the Reaction of $[Fe(bpy)_2(CN)_2]^+$ with $[GSH]_t$ [a]

Expt.	$[Fe(bpy)_2(CN)_2]$, mM	$t_{1/2}$, s	k_{obs}, s^{-1}
1.	0.00	0.14	4.3
2.	0.05	0.16	4.1
3.	0.10	0.24	3.3

[a] $[GSH]_t$ = 0.50 mM, $[[Fe(bpy)_2(CN)_2]NO_3]$ = 0.05 mM, cacodylate buffer, pH = 6.0, [dipic] = 1 mM, μ = 0.1 M ($NaClO_4$).

Table 3.5 Product Inhibition not Significant at pH 6.7 in the Reaction of $[Fe(bpy)_2(CN)_2]^+$ with $[GSH]_t$ [a]

Expt.	$[Fe(bpy)_2(CN)_2]_0$, mM	$t_{1/2}$, s	k_{obs}, s^{-1}
1.	0.00	0.028	20.8
2.	0.05	0.033	17.2
3.	0.10	0.037	16.1

[a] $[GSH]_t$ = 0.50 mM, $[[Fe(bpy)_2(CN)_2]^+]$ = 0.05 mM, cacodylate buffer, pH = 6.7, [dipic] = 1 mM, μ = 0.1 M ($NaClO_4$).

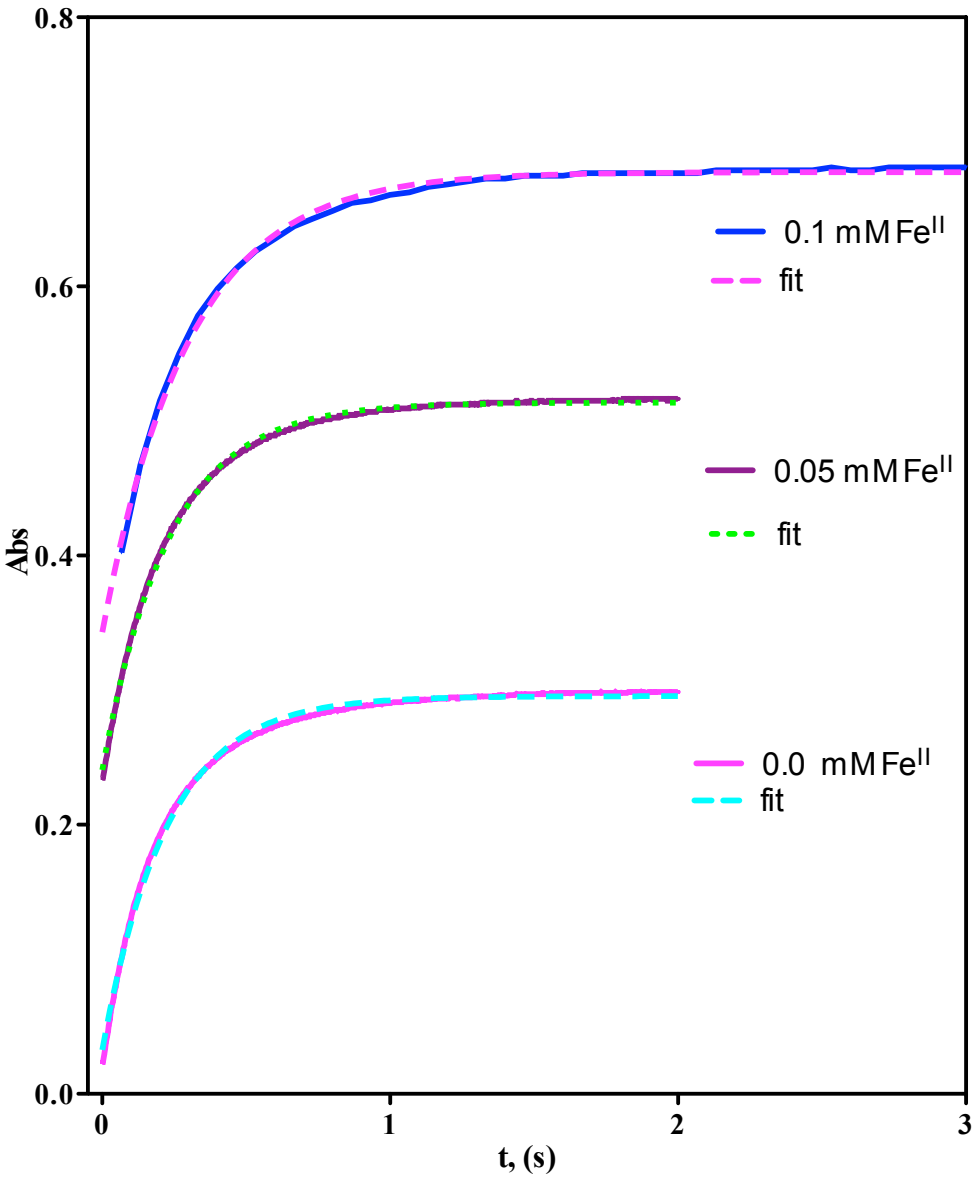

Fig 3.14. Product inhibition test in the reaction of $[Fe(bpy)_2(CN)_2]^+$ with $[GSH]_t$ at pH 6.0 , cacodylate buffer. $[[Fe(bpy)_2(CN)_2]^+] = 0.05$ mM, $[GSH]_t = 0.50$ mM, [dipic] = 1 mM $Fe^{II} = [Fe^{II}(bpy)_2(CN)_2]$.

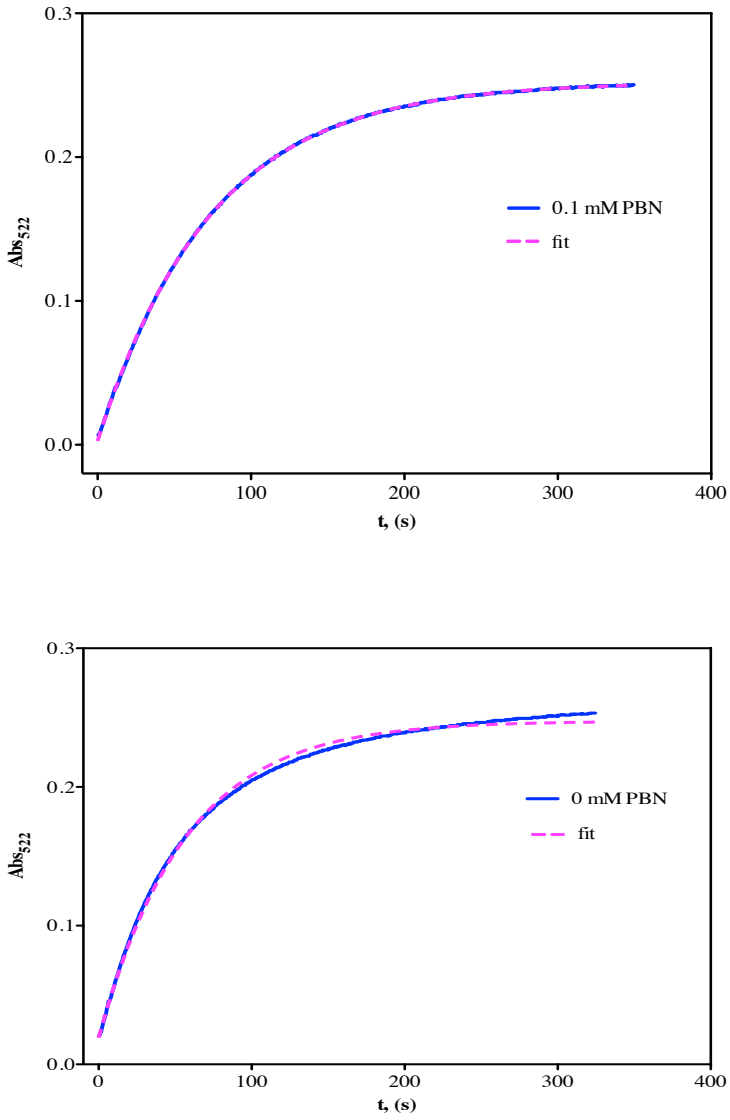

Fig 3.15. Kinetic traces for the oxidation of GSH by $[Fe(bpy)_2(CN)_2]^+$ showing departures from pseudo-first-order behavior and the effect of PBN. 0.5 mM $[GSH]_t$ with 0.05 mM $[Fe(bpy)_2(CN)_2]^+$, 1 mM dipic and 0.1 M ionic strength ($NaClO_4$) at pH 3.2 (acetate buffer).Top: With added 0.1 mM PBN. For ease of comparison these data were converted from delta absorbance to absorbance by adding a constant.

3.3.4.2.1. GSH Dependence. The dependence of k_{obs} on $[GSH]_t$ was determined at pH 4.3 (acetate buffer), maintaining the conditions $[Fe^{III}]$ = 0.05 mM, $[GSH]_t$ = 0.50–6.0 mM, [dipic] = 1.0 mM, [PBN] = 0.1 mM and μ = 0.1 M ($NaClO_4$) (Table 3.6). These data demonstrate a linear dependence of k_{obs} on $[GSH]_t$ with a slope of 198 ± 4 M^{-1} s^{-1} and a nearly insignificant intercept of 0.02 ± 0.005 s^{-1} (Fig 3.16). Such linearity of the data requires the rate law to be first order with respect to $[GSH]_t$ as in eqn 3.7

$$k_{obs} = k[\mathrm{GSH}]_t \tag{3.7}$$

Table 3.6. Glutathione Dependence of k_{obs} in the Reaction Between $[Fe(bpy)_2(CN)_2]^+$ and GSH[a]

Expt.	$[GSH]_t$, mM	k_{obs}, s^{-1}
1.	0.50	0.126
2.	1.0	0.228
3.	1.5	0.329
4.	2.0	0.405
5.	3.0	0.602
6.	4.0	0.780
7.	5.0	1.06
8.	6.0	1.27

[a] $[Fe^{III}]_0$ = 0.05 mM, $[GSH]_t$ = 0.5 – 6.0 mM, acetate buffer at pH 4.3, μ = 0.1 M ($NaClO_4$), [dipic] = 1 mM.

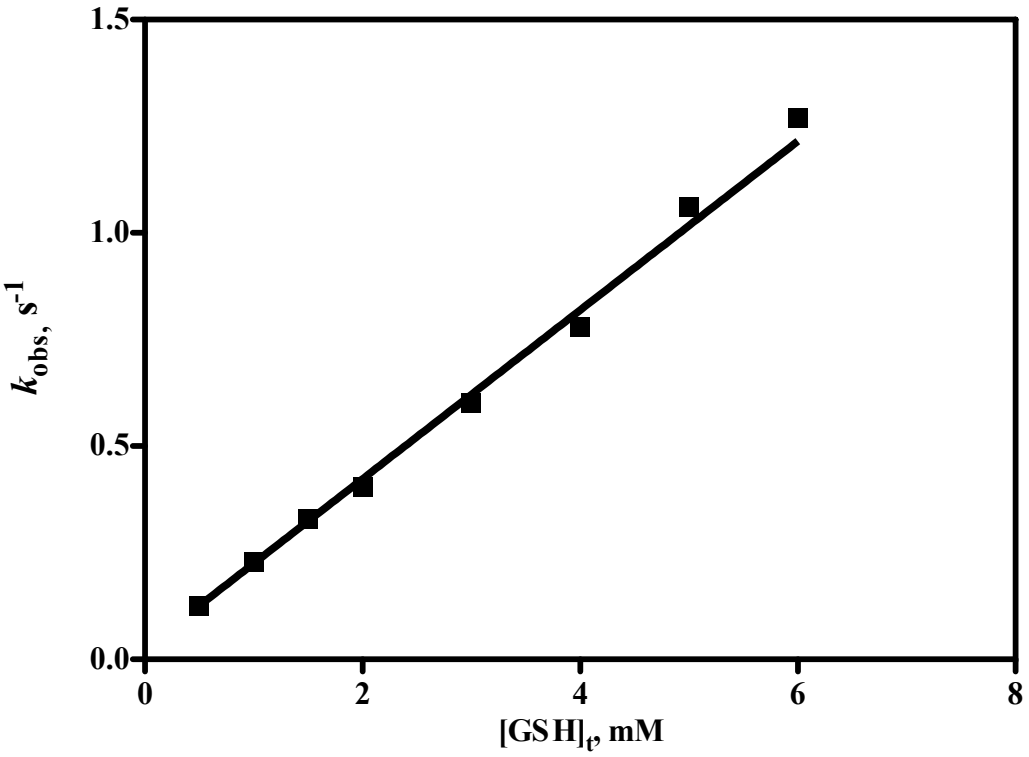

Fig 3.16. $[GSH]_t$ dependent kinetics in the reaction of $[Fe(bpy)_2(CN)_2]^+$ with GSH at pH = 4.3. $[GSH]_t = 0.5 – 6.0$ mM, $[Fe^{III}]_0 = 0.05$ mM, $\mu = 0.1$ M ($NaClO_4$), [dipic] = 1 mM, acetate buffer, [PBN] = 0.1 mM.

3.3.4.2.2. pH Dependence. In a separate set of experiments, a study of the pH dependence of k_{obs} was performed over a broad range of pH (1.4-7.0) with $[Fe^{III}]_0 = 0.05$ mM, $[GSH]_t = 1.0$ mM, [dipic] = 1.0 mM, $\mu = 0.1$ M (Li- or $NaClO_4$) and [PBN] = 0.1 mM (up to pH 4.4). The kinetic data are presented in Table 3.7. The plot of this pH dependence shown in Fig 3.17 indicates a complex dependence on pH with an irregular trend of increasing rate, including a narrow plateau region at around pH 4.5, with increasing pH. This complication is due to the five potentially reactive states of $[GSH]_t$. This is rather similar to that for the oxidation by $[IrCl_6]^{2-}$ (Chapter 2, Fig 2.12), except

that the rates are somewhat slower and the plateau at around pH 4 is less evident. Fits of the data to the general rate law (eq 3.5) failed to converge when holding K_{a1}, K_{a2}, K_{a3} and K_{a4} at their literature values and allowing all five rate constants to be optimized. On the other hand, an excellent fit was obtained when the k_1 and k_5 terms were excluded from the rate law (eq 3.8). The derived rate constants are $k_2 = 4.4 \pm 0.5$ M^{-1} s^{-1}, $k_3 = 59 \pm 6$ M^{-1} s^{-1} and $k_4 = (3.3 \pm 0.2) \times 10^6$ M^{-1} s^{-1} (also collected in Table 3.11).

$$\frac{k_{obs}}{[GSH]_t} = \left[\frac{k_2K_{a1}[H^+]^3 + k_3K_{a1}K_{a2}[H^+]^2 + k_4K_{a1}K_{a2}K_{a3}[H^+]}{[H^+]^4 + K_{a1}[H^+]^3 + K_{a1}K_{a2}[H^+]^2 + K_{a1}K_{a2}K_{a3}[H^+] + K_{a1}K_{a2}K_{a3}K_{a4}}\right] \quad (3.8)$$

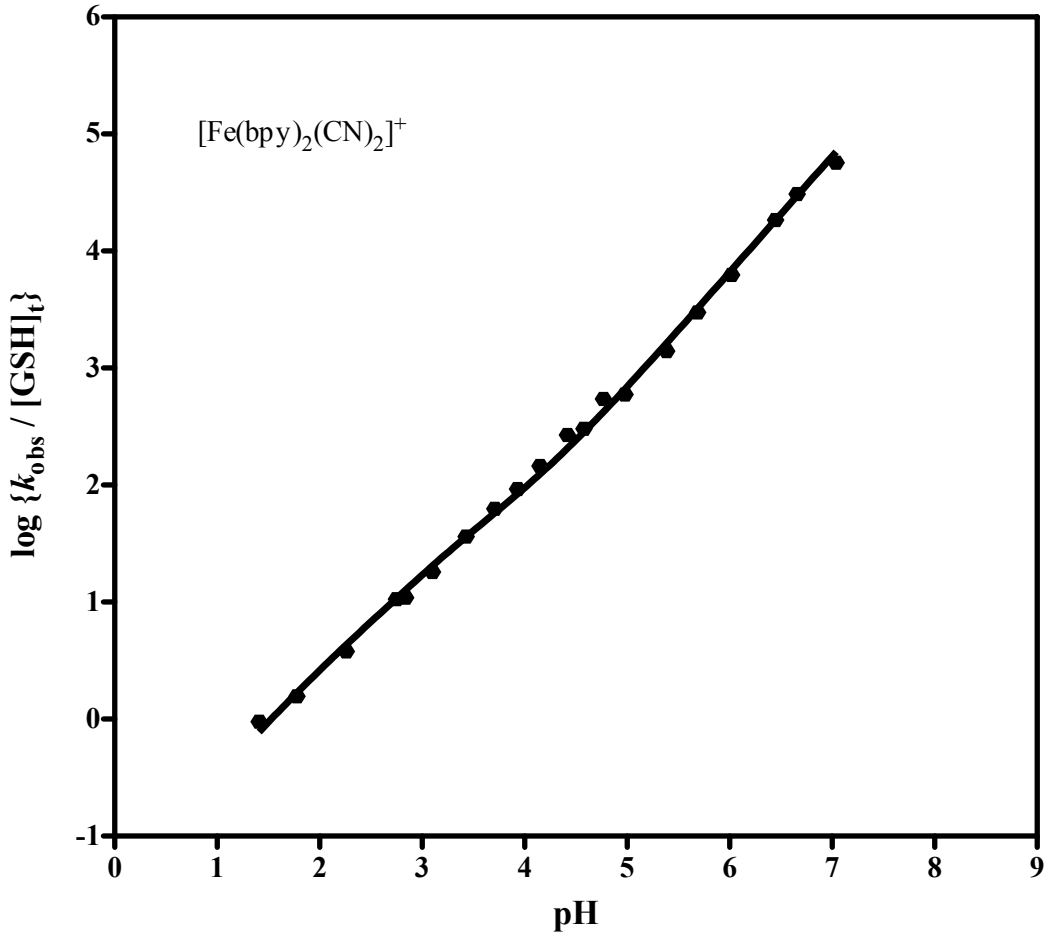

Fig 3.17. pH dependent kinetics fit of the reaction of $[Fe(bpy)_2(CN)_2]^+$ with $[GSH]_t$. [dipic] = 1 mM, [PBN] = 0.1 mM (up to pH 4.4), μ = 0.1 M ($LiClO_4$ below pH 2.7, $NaClO_4$ above pH 2.7), $[Fe^{III}]_0$ = 0.05 mM, $[GSH]_t$ = 1.00 mM. $HClO_4$ (1.4-2.2). Chloroacetate buffer (2.7--3.7), acetate buffer (3.9-4.7) and cacodylate buffer (4.9-7.0).

Table 3.7. pH Dependence of the Kinetics of Reduction of $[Fe(bpy)_2(CN)_2]^+$ by GSH[a]

pH	k_{obs}, s^{-1}	$k_{obs}/[GSH]_t$, M^{-1} s^{-1}	$\log\{k_{obs}/[GSH]_t\}$
1.41[b]	9.52×10^{-4}	0.952	–0.022
1.78[b]	1.57×10^{-3}	1.57	0.196
2.26[b]	3.79×10^{-3}	3.79	0.578
2.75[c]	1.06×10^{-2}	10.6	1.025
2.84[c]	1.08×10^{-2}	10.8	1.037
3.10[c]	1.81×10^{-2}	18.1	1.257
3.43[c]	3.64×10^{-2}	36.4	1.561
3.71[c]	6.26×10^{-2}	62.6	1.796
3.93[d]	9.28×10^{-2}	92.8	1.967
4.15[d]	1.46×10^{-1}	1.46×10^{2}	2.164
4.41[d]	2.69×10^{-1}	2.69×10^{2}	2.429
4.58[d]	3.03×10^{-1}	3.03×10^{2}	2.481
4.77[d]	5.47×10^{-1}	5.47×10^{2}	2.737
4.98[e]	5.93×10^{-1}	5.93×10^{2}	2.773
5.38[e]	1.40	1.40×10^{3}	3.145
5.68[e]	2.99	3.00×10^{3}	3.477
6.02[e]	6.28	6.28×10^{3}	3.797
6.45[e]	18.4	1.84×10^{3}	4.265
6.66[e]	30.6	3.06×10^{3}	4.486
7.04[e]	56.8	5.68×10^{3}	4.75

[a] [Dipic] = 1 mM, [PBN] = 0.1 mM (up to pH 4.4); above this PBN not used. μ = 0.1 M ($LiClO_4$ below pH 2.7, $NaClO_4$ above pH 2.7), $[Fe^{III}]_0$ = 0.050 mM, $[GSH]_t$ = 1.00 mM. [b] $HClO_4$. [c] Chloroacetate buffer. [d] Acetate buffer. [e] Cacodylate buffer.

3.3.4.3. Kinetics with $[Fe^{III}(bpy)(CN)_4]^-$. The oxidation of GSH by $[Fe^{III}(bpy)(CN)_4]^-$ shows general similarities to the oxidations by $[Fe^{III}(bpy)_2(CN)_2]^+$, except that it is generally slower. As a result, it was investigated at higher pH values than the other reaction. The reaction is also more sensitive to copper catalysis, showing significant departures from pseudo-first-order kinetics even with 2 mM dipic (Table 3.3). Experiments on the reaction at pH 6.9 showed that phosphate buffer is ineffective at suppressing copper catalysis. It was found, however, that 5 mM EDTA is effective in suppressing copper catalysis and yields excellent pseudo-first-order kinetics. A typical experimental kinetic trace is depicted in Fig 3.18. Because of the relatively high pH in the kinetics measurements, inhibition by Fe^{II} was quite mild (Table 3.8 & Fig 3.19), and thus no PBN was added to the reactions.

Table 3.8. Product Inhibition Test in the Reaction of $[Fe(bpy)(CN)_4]^-$ with $[GSH]_t$[a]

Expt.	$[Fe(bpy)(CN)_4]^{2-}$, mM	$t_{1/2}$, s	k_{obs}, s^{-1}
1.	0.00	30.4	2.04×10^{-2}
2.	0.10	41.0	1.53×10^{-2}

[a] $[GSH]_t$ = 2.0 mM, $[[Fe(bpy)(CN)_4]^-]$ = 0.05 mM, cacodylate buffer, pH = 6.2, [EDTA] = 5 mM, μ = 0.1 M ($NaClO_4$).

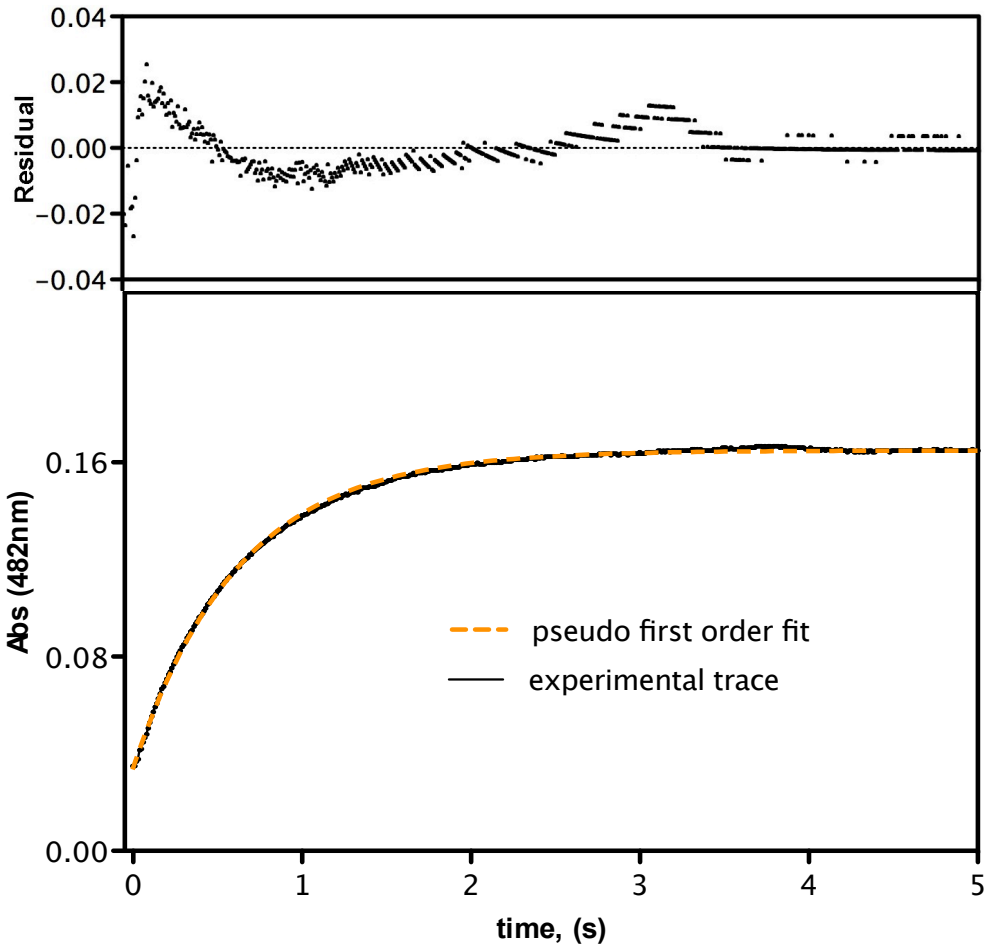

Fig 3.18. Kinetic trace of the reaction of $[Fe(bpy)(CN)_4]^-$ with $[GSH]_t$.

[EDTA] = 5 mM, μ = 0.1 M ($NaClO_4$), pH = 9.0, buffer = gly-gly

$[Fe^{III}(bpy)(CN)_4]^-$ = 0.05 mM $[GSH]_t$ = 0.50 mM. Upper box: residuals and lower box experimental kinetic trace with fit.

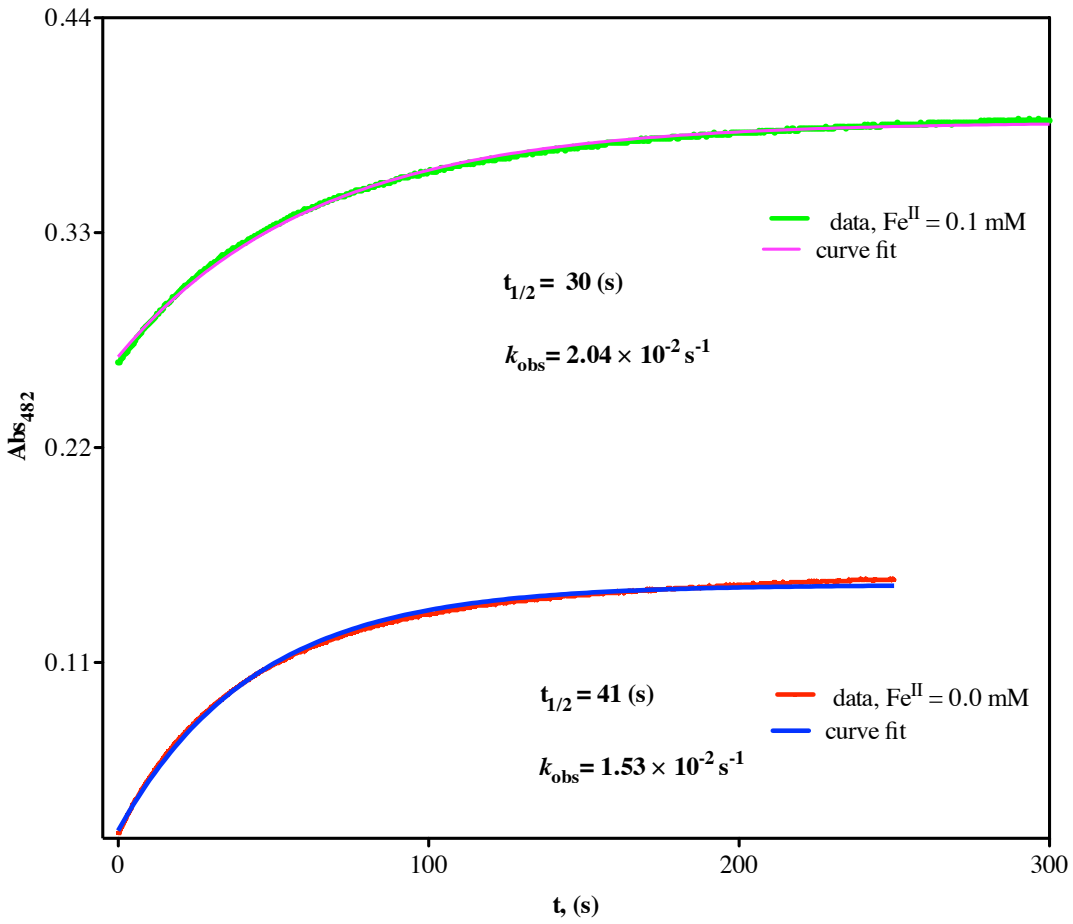

Fig 3.19. Effect of product $[Fe^{II}(bpy)(CN)_4]^{2-}$ in the oxidation of GSH by $[Fe^{III}(bpy)(CN)_4]^{-}$.

$[GSH]_t = 2.0$ mM, $[Fe^{III}]_0 = 0.05$ mM, [EDTA] = 5 mM, cacodylate buffer at pH 6.2 and $\mu = 0.1$ M ($NaClO_4$). $Fe^{II} = K_2[Fe^{II}(bpy)(CN)_4]$.

3.3.4.3.1. GSH Dependence. The dependence of k_{obs} on $[GSH]_t$ was investigated at pH 7.28 (cacodylate buffer) with $[GSH]_t$ = 0.50 – 5.0 mM, $[Fe^{III}]_0$ = 0.05 mM, [EDTA] = 5.0 mM and μ = 0.1 M ($NaClO_4$) (Table 3.9). A linear dependence on $[GSH]_t$ is obtained (Fig 3.20) with a slope of 74.1 ± 1.8 M^{-1} s^{-1} and a negligible intercept of 0.004 ± 0.002 s^{-1}.

Table 3.9. Dependence of k_{obs} on $[GSH]_t$ in the Reaction with $[Fe(bpy)(CN)_4]^{-a}$

Expt.	$[GSH]_t$, mM	k_{obs}, s^{-1}
1.	0.50	0.041
2.	1.0	0.081
3.	1.5	0.115
4.	2.0	0.151
5.	3.0	0.212
6.	4.0	0.302
7.	5.0	0.394

[a] $[Fe^{III}]_0$ = 0.05 mM, $[GSH]_t$ = 0.50 – 5.0 mM, cacodylate buffer at pH 7.28, μ = 0.1 M ($NaClO_4$), [EDTA] = 5 mM.

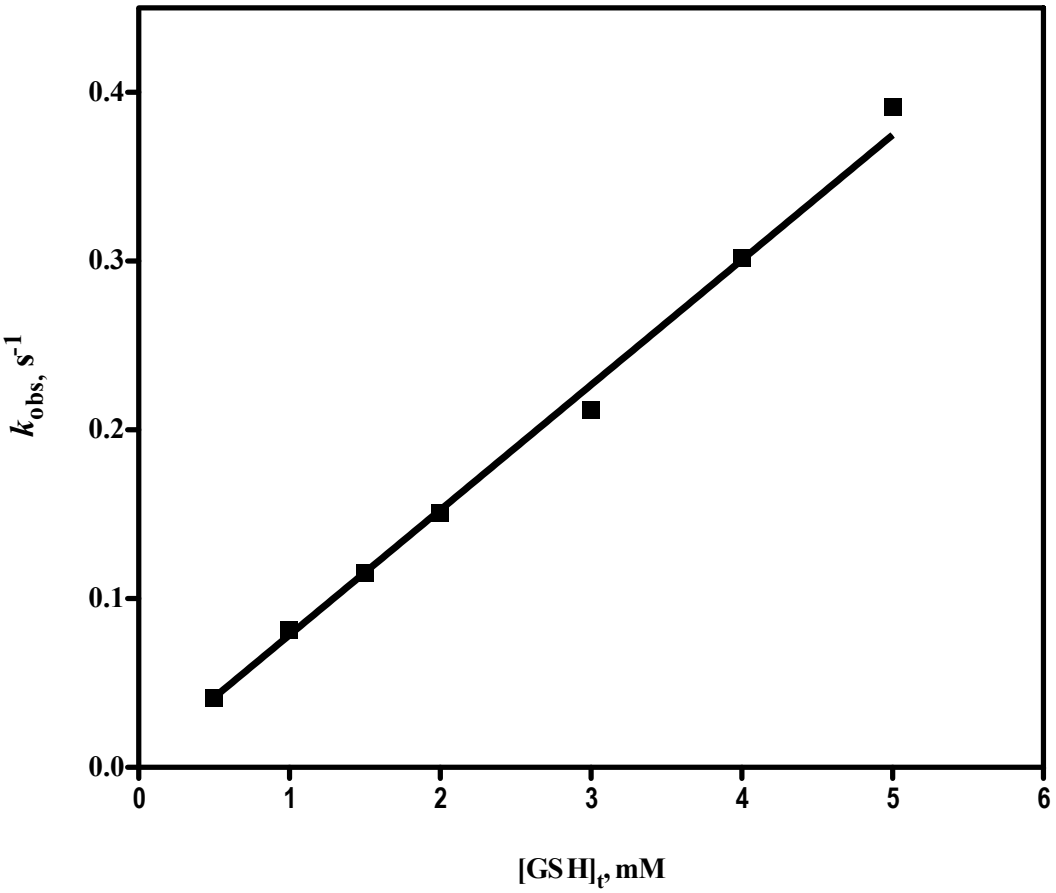

Fig 3.20. $[GSH]_t$ dependence in the reaction between $[Fe(bpy)(CN)_4]^-$ and GSH.

$[Fe(bpy)(CN)_4]^-$ = 0.05 mM, $[GSH]_t$ = 0.50 – 5.0 mM, [EDTA] = 5 mM, cacodylate buffer at pH 7.28, μ = 0.1 M ($NaClO_4$). Slope = (74.1± 1.8) $M^{-1}s^{-1}$ and intercept = (0.004 ± 0.002) s^{-1}.

3.3.4.3.2. pH Dependence. The pH dependence of k_{obs} was studied over the pH range 6.00 - 11.06, with the other conditions being $[Fe^{III}]_0$ = 0.05 mM, $[GSH]_t$ = 0.50 – 2.0 mM, [EDTA] = 5.0 mM and μ = 0.1 M ($NaClO_4$). The kinetic data are summarized in Table 3.10 and displayed in Fig 3.21. An excellent fit of the data with eq 3.5 was achieved by omitting the k_1 and k_2 terms as in eq 3.9, as shown in Fig 3.21. The plot of $\log\left[\frac{k_{obs}}{[GSH]_t}\right]$ vs pH (Fig 3.21) shows that the reactivity increases steadily until a pH of around 9.7, then remains unchanged. The derived second-order rate constants are k_3 = 1.25 ± 0.5 M^{-1} s^{-1}, k_4 = (3.59 ± 0.08) × 10^3 M^{-1} s^{-1} and k_5 = (5.5 ± 0.2) × 10^3 M^{-1} s^{-1} (also collected in Table 3.11). Although the k_3 value is only marginally significant, the k_4 and k_5 values are quite well resolved.

$$\frac{k_{obs}}{[GSH]_t} = \left[\frac{k_3K_{a1}K_{a2}[H^+]^2 + k_4K_{a1}K_{a2}K_{a3}[H^+] + k_5K_{a1}K_{a2}K_{a3}K_{a4}}{[H^+]^4 + K_{a1}[H^+]^3 + K_{a1}K_{a2}[H^+]^2 + K_{a1}K_{a2}K_{a3}[H^+] + K_{a1}K_{a2}K_{a3}K_{a4}}\right] \qquad (3.9)$$

These observations clearly reveal that only the di-anionic (k_4 term) and tri-anionic (k_5 term) forms of the $[GSH]_t$ are kinetically active at the pH values higher than 6. A summary of pH-resolved rate constants for the oxidation of GSH by $[Fe(bpy)_2(CN)_2]^+$ and $[Fe(bpy)(CN)_4]^-$ are given in Table 3.11.

Table 3.10. pH Dependence of the Kinetics of Reaction of $[Fe(bpy)(CN)_4]^-$ with GSH[a]

pH	k_{obs}, s^{-1}	$k_{obs}/[GSH]_t$, $M^{-1}\ s^{-1}$	$\log\{k_{obs}/[GSH]_t\}$	$[GSH]_t$, mM
6.00[b]	1.65×10^{-2}	8.23	0.915	2.00
6.22[b]	2.43×10^{-2}	12.2	1.08	2.00
6.43[b]	3.99×10^{-2}	20.0	1.29	2.00
6.71[b]	6.93×10^{-2}	34.7	1.54	2.00
7.29[c]	$6.16 \times 10^{-}2$	1.23×10^{2}	2.09	0.50
7.67[c]	1.31×10^{-1}	2.63×10^{2}	2.42	0.50
7.97[c]	2.60×10^{-1}	5.21×10^{2}	2.72	0.50
8.23[c]	4.76×10^{-1}	9.53×10^{2}	2.98	0.50
8.35[c]	1.16	1.16×10^{3}	3.06	1.00
8.52[c]	1.50	1.50×10^{3}	3.17	1.00
8.88[c]	1.34	2.68×10^{3}	3.42	0.50
9.00[c]	1.51	3.02×10^{3}	3.48	0.50
9.18[c]	1.75	3.51×10^{3}	3.54	0.50
9.41[c]	2.03	4.06×10^{3}	3.60	0.50
9.56[c]	2.18	4.36×10^{3}	3.64	0.50
9.69[d]	2.17	4.33×10^{3}	3.63	0.50
9.84[d]	2.35	4.71×10^{3}	3.67	0.50
9.97[d]	2.45	4.90×10^{3}	3.69	0.50
10.16[d]	2.46	4.92×10^{3}	3.69	0.50
10.22[d]	2.50	5.01×10^{3}	3.70	0.50
10.77[d]	2.57	5.14×10^{3}	3.71	0.50
11.08[d]	2.58	5.16×10^{3}	3.71	0.50

[a] $[Fe^{III}]_0 = 0.05$ mM, [EDTA] = 5.0 mM, $\mu = 0.1$ M ($NaClO_4$). [b] Cacodylate buffer. [c] Gly-gly buffer. [d] HCO_3^-/NaOH buffer.

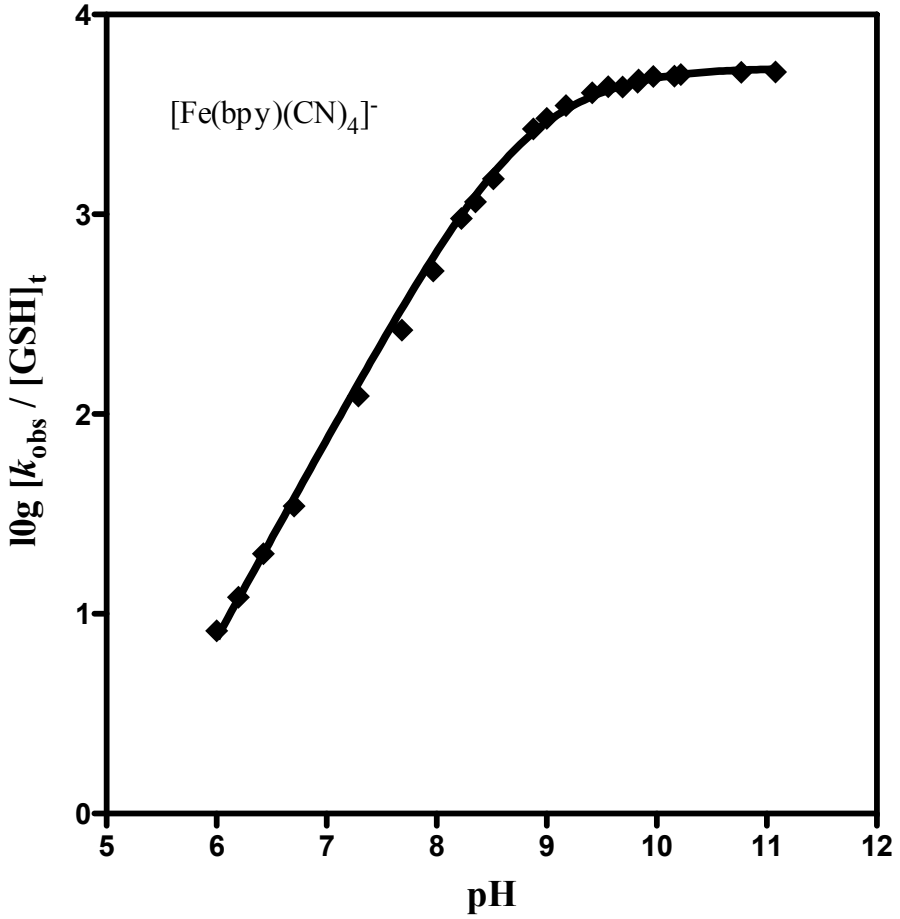

Fig 3.21. pH dependence of the kinetics of reaction of $[Fe(bpy)(CN)_4]^-$ with GSH. $[[Fe^{III}(bpy)(CN)_4]^-] = 0.05$ mM, $[GSH]_t = 0.5\text{-}2.0$ mM, [EDTA] = 5 mM, $\mu = 0.1$ M ($NaClO_4$), pH (6.0- 6.7) cacodylate, pH (7.3 – 9.56) gly-gly, and pH (9.6 - 11) HCO_3^- / NaOH buffers.

3.3.4.4. Kinetics with $[Fe^{III}(CN)_6]^{3-}$. The reaction of GSH with $[Fe(CN)_6]^{3-}$ was examined briefly, monitoring the consumption of $[Fe(CN)_6]^{3-}$ at 420 nm by conventional UV-vis spectrophotometry. When a reaction mixture was prepared containing 2.5 mM GSH and 0.10 mM $[Fe(CN)_6]^{3-}$ in 0.1 M phosphate buffer at pH 7.1, the reaction was rapid, with a half-life of less than 5 s. Under the same conditions except for the addition of 1 mM dipic the reaction was much slower, with a half-life of about 200 s. Because of the slowness of the reaction and the potential for catalysis by ligated metal ions,[44] further studies were not performed.

Table 3.11. Summary of pH-Resolved Rate Constants for the Oxidation of GSH[a]

Parameter	$[Fe(bpy)_2(CN)_2]^+$	$[Fe(bpy)(CN)_4]^-$
k_2, M^{-1} s^{-1}	4.4 ± 0.5	
k_3, M^{-1} s^{-1}	59 ± 6	1.25 ± 0.5
k_4, M^{-1} s^{-1}	$(3.3 \pm 0.2) \times 10^6$	$(3.59 \pm 0.08) \times 10^3$
k_5, M^{-1} s^{-1}		$(5.5 \pm 0.2) \times 10^3$

[a] 25.0 °C, μ = 0.1 M.

3.4. Discussion.

A notable trend in the oxidations of GSH by $[IrCl_6]^{2-}$(described in Chapter 2), $[Fe^{III}(bpy)_2(CN)_2]^+$, and $[Fe(bpy)(CN)_4]^-$ is the increasing degree of over-oxidation with increasing $E°$ of the oxidant. An analogous trend is obtained in the oxidation of cysteine by $[Mo(CN)_8]^{3-}$, $[Fe^{III}(bpy)_2(CN)_2]^+$, and $[Fe(bpy)(CN)_4]^-$, although the over-oxidation product is cysteine sulfinic acid rather than the sulfonate.[34,42] In the case of oxidation of thioglycolate by $[IrCl_6]^{2-}$ and $[Mo(CN)_8]^{3-}$ it is again only the stronger oxidant ($[IrCl_6]^{2-}$) that causes over-oxidation, and in this case the product is the sulfonate.[40,41]

Glutathione has four acid/base sites and the pH dependence of the kinetics is accounted for by a model in which the various protonation states of GSH react with the Fe^{III} compounds to generate thiy radicals in a similar way these reacts with $[IrCl_6]^{2-}$ (Chapter 2) and formation of the thiyl radicals are the rate limiting steps:

$$GSH^0 + Fe^{III} \longrightarrow GS\bullet + Fe^{II} \qquad k_2 \qquad (3.10)$$

$$GSH\text{-}H^- + Fe^{III} \longrightarrow GS\bullet + Fe^{II} \qquad k_3 \qquad (3.11)$$

$$GSH\text{-}2H^{2-} + Fe^{III} \longrightarrow GS\bullet + Fe^{II} \qquad k_4 \qquad (3.12)$$

$$GSH\text{-}3H^{3-} + Fe^{III} \longrightarrow GS\bullet + Fe^{II} \qquad k_5 \qquad (3.13)$$

A general mechanism for reaction of GSH with the oxidants $[Fe^{III}(bpy)_2(CN)_2]^+$ and $[Fe(bpy)(CN)_4]^-$ is given below.

$$Fe^{III} + GSH \rightleftharpoons Fe^{II} + GS\bullet + H^+ \quad (3.14)$$

$$GS\bullet + GSH \rightleftharpoons GSSG\bullet^- + H^+ \quad (3.15)$$

$$Fe^{III} + GSSG\bullet^- \longrightarrow Fe^{II} + GSSG \quad (3.16)$$

$$2GS\bullet \longrightarrow GSSG \quad (3.17)$$

$$GS\bullet + PBN \longrightarrow GSPBN\bullet \quad (3.18)$$

Reaction 3.14 is the predominant rate-limiting step, which generates the well-known glutathione thiyl radical. Reversibility in this reaction is indicated because of the observed kinetic inhibition by Fe^{II}. Production of H^+ in this step accounts in part for the enhanced inhibition by Fe^{II} in solutions that are more acidic. Reversible association of GS• with GSH to form $GSSG\bullet^-$ in the next step (eq 3.15) is quite well established,[28,45,46] and its pH dependence also affects the kinetic inhibition by Fe^{II}. Two routes to GSSG are depicted in reactions 3.16 and 3.17. The first of these, oxidation of $GSSG\bullet^-$ by Fe^{II}, is expected to have a large rate constant and to be predominant at higher pH. At lower pH, where reaction 3.15 is unfavorable, dimerization of GS• could become significant. Reaction 3.18 is the scavenging of GS• by the spin trap PBN,[47] which is rapid enough to compete with the reverse of eq 3.14 and thus prevent kinetic inhibition by Fe^{II}.

We were unable to find evidence for reaction of $HGSH^+$ (k_1) with these oxidants. On the other hand, reaction via thiolate ($GSH\text{-}3H^{3-}$) species is demonstrated by the well-resolved value of k_5 for $[Fe(bpy)(CN)_4]^-$. It is inferred that the values of k_2, k_3, and k_4 in

Table (3.11) all refer to reactions of the Fe^{III} complexes with the associated thiolate forms of glutathione. Since the dianion GSH-$2H^{2-}$ is primarily in the thiolate form, the values of k_4 are the actual bimolecular rate constants for the thiolate. The thiolate forms for the species GSH^0 and GSH-H^- are tautomers (eq 3.19 and 3.20) and lead to the relationships $k_2 = k_{2a}K_{Tn}$ and $k_3 = k_{3a}K_{Ta}$.

$$HS–(NH_3^+)(COOH)(COO^-) \rightleftharpoons {}^-S–(NH_3^+)(COOH)_2 \qquad K_{Tn} \qquad (3.19)$$

$$HS–(NH_3^+)(COO^-)_2 \rightleftharpoons {}^-S–(NH_3^+)(COOH)(COO^-) \qquad K_{Ta} \qquad (3.20)$$

$$^-S–(NH_3^+)(COOH)_2 + Fe^{III} \longrightarrow \bullet S–(NH_3^+)(COOH)_2 + Fe^{II} \qquad k_{2a} \qquad (3.21)$$

$$^-S–(NH_3^+)(COOH)(COO^-) + Fe^{III} \longrightarrow \bullet S–(NH_3^+)(COOH)(COO^-) + Fe^{II} \qquad k_{3a} \qquad (3.22)$$

Applying the values for pK_{a2} and pK_{a3}, a value of about 10^{-5} can be estimated for K_{Tn} and K_{Ta}. Values of the corrected bimolecular rate constants for the thiolate forms with $[Fe^{III}(bpy)_2(CN)_2]^+$ and $[Fe(bpy)(CN)_4]^-$ are presented in Table 3.12.

Table 3.12. Rate Constants for the Oxidation of the Thiolate Forms of GSH[a]

Parameter	$[Fe(bpy)_2(CN)_2]^+$	$[Fe(bpy)(CN)_4]^-$
E_f, V vs NHE	0.77	0.55
k_{11}, M^{-1} s^{-1}	6×10^5[b]	6×10^5[b]
k_{2a}, M^{-1} s^{-1}	4×10^5	
k_{-2a}, M^{-1} s^{-1}	2.8×10^6	
k_{3a}, M^{-1} s^{-1}	6×10^6	1×10^5
k_{-3a}, M^{-1} s^{-1}	4×10^7	5×10^9
k_4, M^{-1} s^{-1}	3.3×10^6	3.6×10^3
k_5, M^{-1} s^{-1}		5.5×10^3

[a] 25.0 °C, μ = 0.1 M. Values for k_{2a} and k_{3a} derived from the values for k_2 and k_3 by adjusting for tautomerization. Likewise, k_{-2a} and k_{-3a} from the relation $k_{2/3a}/ k_{-2/3a} = K_{eq}$.
[b] Reference [34].

The electron-transfer mechanism assigned above to the reactions of the thiolate forms of GSH is based on the observation that the Fe^{III} complexes are reduced by one electron while retaining their coordination spheres intact. Further evidence for an electron-transfer mechanism is the kinetic inhibition by the reduced metal complex and the effects of the radical scavenger PBN. An estimate for the electron-transfer

equilibrium constants can be made, making use of the $E°$ values for the oxidants (shown in Table 3.9) and $E°(GS•/GS^-)$ for the GSH thiyl radical. This latter quantity is estimated to be about 0.82 ± 0.02 V vs NHE.[48] Values for the derived electron-transfer equilibrium constants are 0.14 for $[Fe(bpy)_2(CN)_2]^+$ and 2×10^{-5} for $[Fe(bpy)(CN)_4]^-$. Values for the rate constants for reverse electron transfer can be calculated from the forward rate constants in Table 3.12 and the equilibrium constants. In the case of $[Fe(bpy)_2(CN)_2]^+$, k_{-3a} is 4×10^7 M^{-1} s^{-1} which is well below the limits of diffusion control and $[Fe(bpy)(CN)_4]^-$ has a value of 5×10^9 M^{-1} s^{-1} for k_{-3a}, which is right at the diffusion limit for a reaction of this charge type. These calculations provide further evidence that these reactions have an electron-transfer mechanism.

The cross relationship of Marcus theory should apply to the rate constants if the electron-transfer reactions follow an outer-sphere mechanism. Qualitatively, the rate constants in Table 3.12 decrease with decreasing $E°$ for the oxidants, as expected from the Marcus cross relationship. When this relationship is applied in the usual form including work terms,[49] we calculate a self-exchange rate constant of 3.6×10^6 M^{-1} s^{-1} for the GSH-$2H^{2-}$/GS• redox couple. This calculation is based on the value for k_4 in Table 3.12 i.e. 3.6×10^3 M^{-1} s^{-1}; for $[Fe(bpy)(CN)_4]^-$, a self-exchange rate constant of 6×10^5 M^{-1} s^{-1} for $[Fe(bpy)(CN)_4]^{-/2-}$, and radii of 5.33 Å for $[Fe(bpy)(CN)_4]^-$, and 3 Å for GSH. Given the considerable uncertainties involved, this calculated self-exchange rate constant is quite similar to the value of 7×10^6 M^{-1} s^{-1} that was reported for the analogous cysteine self-exchange rate constant.[34]

In the case of $[Fe(CN)_6]^{3-}$, a publication describes the results of a pH-dependent study in which a rate constant corresponding to k_3 of 300 M^{-1} s^{-1} was obtained;[13] however, no precautions were taken to prevent copper-ion catalysis. In view of the rate constants in Table 3.12 and the low $E°$ for $[Fe(CN)_6]^{3-}$, the value for k_3 seems to be too large by several orders of magnitude. Our brief observations on this reaction (described above) show that it is highly sensitive to metal-ion catalysis and that when dipic is added the rates are at least a factor of 500 slower than those reported previously.[13]

3.5. Conclusions.

Two Fe(III) complexes, $[Fe^{III}(bpy)_2(CN)_2]^+$ and $[Fe^{III}(bpy)(CN)_4]^-$ have been prepared and characterized by UV-vis and CV methods. Copper ions catalyze the oxidation of GSH by these Fe^{III} compounds, which can be suppressed with 1 mM dipic for the $[Fe^{III}(bpy)_2(CN)_2]^+$ reaction and by EDTA for the $[Fe^{III}(bpy)(CN)_4]^-$ reaction. The rate laws are first order in GSH and Fe^{III} with complex pH dependent kinetics. Both oxidants show mild kinetic inhibition by the product, [Fe(II)] and can be controlled with 0.1 mM PBN at low pH. Disulfide (GSSG) is the major product formed by the two oxidants with an increasing degree of over-oxidation with stronger oxidant. The rate constants increase with increasing potential (E^0) of the oxidants. The rate limiting steps involve reversible electron transfer from various protonation states of the thiolate forms of GSH.

References.

1. Sies, H. *Free Rad. Biol. Med.* **1999**, *27*, 916.

2. Meister, A.; Anderson, M. E. *Ann. Rev. Biochem.* **1983**, *52*, 711.

3. Chakravarthi, S.; Jessop, C. E.; Bulleid, N. J. *EMBO reports*, **2006**, *7*, 271.

4. Everse, J.; Kujundzic, N. *Biochemistry* **1979**, *18*, 2668.

5. Hamed, M. Y.; Silver, J.; Wilson, M. T. *Inorg. Chim. Acta* **1983**, *78*, 1.

6. Scarpa, M.; Momo, F.; Viglino, P.; Vianello, F.; Rigo, A. *Biophys. Chem.* **1996**, *60*, 53.

7. Ayoko, G. A.; Olatunji, M. A. *Inorg. Chim. Acta* **1983**, *80*, L15-L17, 287.

8. Labuda, J.; Vanickova, M.; Pavlishchuk, V. V.; Kolchinskii, A. G. *Chem. Papers* **1994**, *48*, 78.

9. Bose, R. N.; Moghaddas, S.; Gelerinter, E. *Inorg. Chem.* **1992**, *31*, 1987.

10. Ayoko, G. A.; Iyun, J. F.; Ekubo, A. T. *Indian J. Chem.* **1993**, *32A*, 616.

11. Ayoko, G. A.; Iyun, J. F.; Ekubo, A. T. *Transition Met. Chem.* **1993**, *18*, 6.

12. Chatterjee, D.; Pal, U.; Ghosh, S.; van Eldik, R. *Dalton Trans* **2011**, *40*, 1302.

13. Stochel, G.; Martinez, P.; van Eldik, R. *J. Inorg. Biochem.* **1994**, *54*, 131.

14. Campanali, A. A.; Kwiecien, T. D.; Hryhorczuk, L.; Kodanko, J. J. *Inorg. Chem.* **2010**, *49*, 4759.

15. Gangopadhyay, S.; Ali, M.; Dutta, A.; Banerjee, P. *J. Chem. Soc., Dalton Trans.* **1994**, 841.

16. Perez-Benito, J. F.; Arias, C. *J. Phys. Chem. A* **1998**, *102*, 5837.

17. Frasca, D. R.; Clarke, M. J. *J. Am. Chem. Soc.* **1999**, *121*, 8523.

18. Nayak, S.; Brahma, G. S.; Reddy, K. V. *Aust. J. Chem.* **2012**, *65*, 113.

19. Sami, P.; Anand, T. D.; Premanathan, M.; Rajasekaran, K. *Transition Met. Chem.* **2010**, *35*, 1019.

20. Ison, A.; Odeh, I. N.; Margerum, D. W. *Inorg. Chem.* **2006**, *45*, 8768.

21. Ford, E.; Hughes, M. N.; Wardman, P. *Free Rad. Biol. Med.* **2002**, *32*, 1314.

22. Abedinzadeh, Z.; Gardes-Albert, M.; Ferradini, C. *Radiat. Phys. Chem.* **1991**, *38*, 1.

23. Zhao, R.; Lind, J.; Merényi, G.; Eriksen, T. E. *J. Am. Chem. Soc.* **1994**, *116*, 12010.

24. Chen, S.-N.; Hoffman, M. Z. *Radiat. Res.* **1973**, *56*, 40.

25. Eriksen, T. E.; Fransson, G. *Radiat. Phys. Chem.* **1988**, *32*, 163.

26. Candeias, L. P.; Folkes, L. K.; Dennis, M. F.; Patel, K. B.; Everett, S. A.; Stratford, M. R. L.; Wardman, P. *J. Phys. Chem.* **1994**, *98*, 10131.

27. Winterbourn, C. C.; Metodiewa, D. *Free Rad. Biol. Med.* **1999**, *27*, 322.

28. Mezyk, S. P. *J. Phys. Chem.* **1996**, *100*, 8861.

29. Huston, P.; Espenson, J. H.; Bakac, A. *Inorg. Chem.* **1992**, *31*, 720.

30. Schöneich, C.; Asmus, K. D.; Bonifacic, M. *J. Chem. Soc., Faraday Trans.* **1995**, *91*, 1923.

31. Folkes, L. K.; Trujillo, M.; Bartesaghi, S.; Radi, R.; Wardman, P. *Arch. Biochem. Biophys.* **2011**, *506*, 242.

32. Schilt, A. A. *J. Am. Chem. Soc.* **1960**, *82*, 3000.

33. Wang, X.; Stanbury, D. M. *Inorg. Chem.* **2006**, *45*, 3415.

34. Wang, X.; Stanbury, D. M. *Inorg. Chem.* **2008**, *47*, 1224.

35. Lescouezec, R.; Lloret, F.; Julve, M.; Vaissermann, J.; Verdaguer, M. *Inorg. Chem.* **2002**, *41*, 818.

36. Sawyer, D. T.; Sobkowiak, A.; Roberts, J. L. *Electrochemistry for Chemists, 2nd ed,* John Wiley and Sons: New York, 1995; pp 192.

37. *Prism 5,* GraphPad Software, Inc.: San Diego, CA, 2010;

38. Agarwala, B. V.; Ramanathan, K. V.; Khetrapal, C. L. *J. Coord. Chem.* **1985**, *14*, 133.

39. Hung, M.; Stanbury, D. M. *Inorg. Chem.* **2005**, *44*, 9952.

40. Saha, B.; Hung, M.; Stanbury, D. M. *Inorg. Chem.* **2002**, *41*, 5538.

41. Sun, J.; Stanbury, D. M. *J. Chem. Soc., Dalton Trans.* **2002**, 785.

42. Hung, M.; Stanbury, D. M. *Inorg. Chem.* **2005**, *44*, 3541.

43. Krezel, A.; Bal, W. *Org. Biomol. Chem.* **2003**, *1*, 3885.

44. Bridgart, G. J.; Wilson, I. R. *J. Chem. Soc., Dalton Trans.* **1973**, 1281.

45. Hoffman, M. Z.; Hayon, E. *J. Phys. Chem.* **1973**, *77*, 990.

46. Mezyk, S. P.; Armstrong, D. A. *J. Chem. Soc., Perkin Trans. 2* **1999**, 1411.

47. Polovyanenko, D. N.; Plyusnin, V. F.; Reznikov, V. A.; Khramtsov, V. V.; Bagryanskaya, E. G. *J. Phys. Chem. B* **2008**, *112*, 4841.

48. Madej, E.; Wardman, P. *Arch. Biochem. Biophys.* **2007**, *462*, 94.

49. Zuckerman, J. J. *Inorganic Reactions and Methods, vol. 15,* VCH: Deerfield Beach, FL, 1986; pp 13.

Chapter 4

Oxidation of Cysteine Sulfinic Acid ($CysSO_2H$) by $[IrCl_6]^{2-}$

4.1. Introduction

Cysteine sulfinic acid ($CysSO_2H$, Scheme 4.1a), a naturally occurring water-soluble alkane sulfinic acid, is found in all living systems and is linked to cysteine metabolism.[1,2] Cellular proteins contain ca 5% of their cysteines in the form of $CysSO_2H$ or $CysSO_3H$.[3] It is also produced as the oxidation product of thiols, for instance, cysteine dioxygenase acts as a catalyst to oxidize cysteine to $CysSO_2H$ in the biosynthesis of taurine (2-aminoethane sulfonic acid, Scheme 4.1b).[4] Direct oxidation of cysteine by $[Mo(CN)_8]^{3-}$ also produces $CysSO_2H$.[5] The over-oxidation products of thiols are shown in Scheme 4.2.

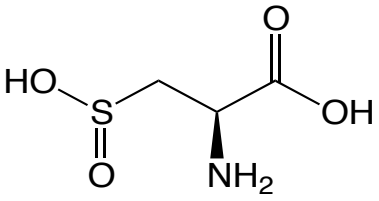

a. Cysteine sulfinic acid

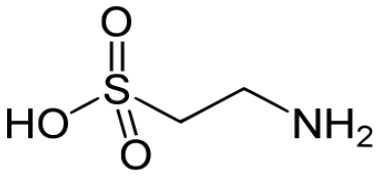

b.Taurine

Scheme 4.1

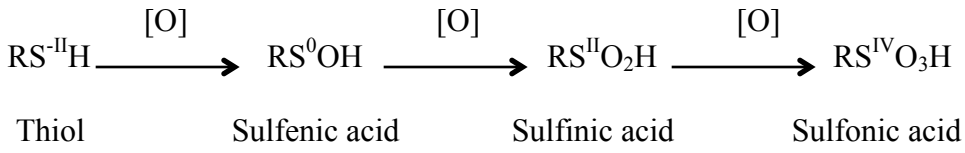

Scheme 4.2. Oxo-products of thiols.

$CysSO_2H$ has three pK_as: 1.50, 2.38, and 9.24,[6] and between pH 4 and 8, this compound exists predominantly in the sulfinate anion form shown in Scheme 4.3a. The four protonation states are presented in Scheme 4.3b.

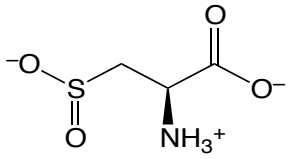

Scheme 4.3a

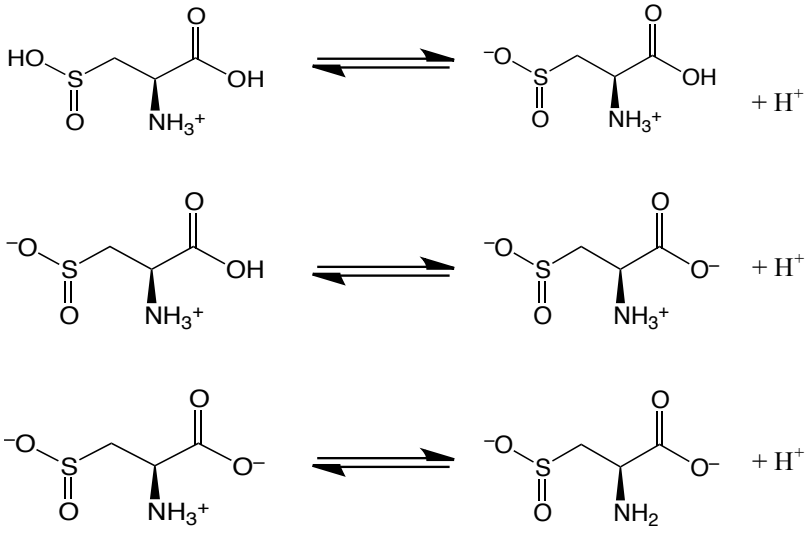

Scheme 4.3b. The four protonation states of $CysSO_2H$.

The resonance structures of the anionic form are shown in Scheme 4.4

Scheme 4.4

Alhough the sulfinate seems to be stabilized through resonance, this anion undergoes alkylation and nucleophilic additions as well.[7] Many functional roles of modifications of sulfinic acids in numerous proteins such as D-amino acid oxidase,[8] Cu-Zn superoxide dismutase,[9] Parkinson's disease protein Dj-1,[10] iron-containing nitrile hydratase,[11] Peroxiredoxin-II(Prx-II),[12-14] etc. have been identified. $CysSO_2H$ has also been reported to act as a neurotransmitter.[15] The sulfinic acid was believed to form irreversibly, but recent findings have shown that this acid can be reduced back to the sulfenic acid or thiol under *in vivo* conditions. Scheme 4.5 illustrates the reversibility of reduction of $CysSO_2H$. The protein Sulfiredoxin(Srx1) catalyzes the reduction.[16,17]

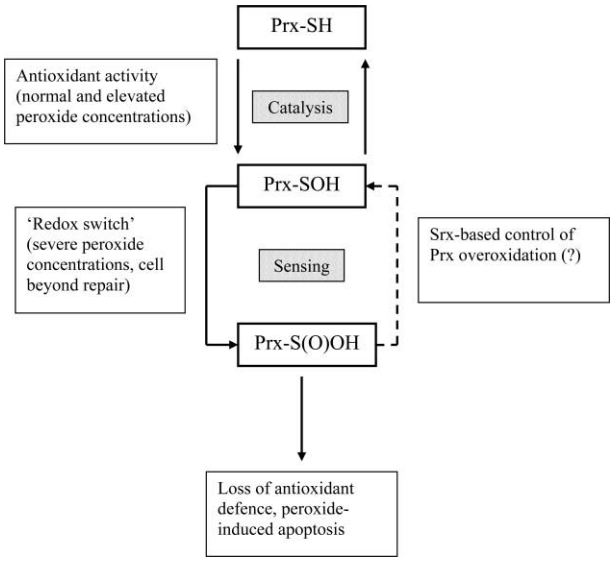

Scheme 4.5[16]. Sulfiredoxin(Srx1) protein reduces $CysSO_2H$.

Reduction of sulfinates to thiols is a challenge to achieve under physiological conditions *in vitro*.[16]

Oxidation of thioglycolate[18] and glutathione[19] by Ir^{IV} produces the respective sulfonate (RSO_3^-) products. Fawcett, et. al.[20] have reported electro-oxidation of $CysSO_2H$ to $CysSO_3H$ using a gold electrode. Identification of Srx1 and its role has inspired more work on thiol as well as on sulfinic acid-based redox switches in proteins.[16,21,22] To study the redox behavior of sulfinates could be helpful to understand the mechanism underlying it. In this project we hypothesize that the sulfonate is formed through the oxidation of the cysteine sulfinic acid. Thus, we have initiated a study of the oxidation of sulfinates by the typical one-electron oxidant, $[IrCl_6]^{2-}$.

4.2. Experimental Sections

4.2.1. Reagents and solutions.

NH_4Cl (Fisher), acetic acid (Fisher), $(NH_4)_3IrCl_6 \bullet H_2O$ (Aldrich), D_2O (Sigma), $CuSO_4 \bullet 5H_2O$ (Fisher), $(NH_4)_2Fe(SO_4)_2 \bullet 6H_2O$ (Fisher), $HCl_{(aq)}$ (Fisher), NaOH pellets ("SigmaUltra", Sigma-Aldrich), N-tert butyl α-phenylnitrone (PBN, Aldrich), 2-6-pyridine dicarboxylic acid (Aldrich), cysteic acid ($CysSO_3H$, Aldrich), cysteine sulfinic acid ($CysSO_2H$, Aldrich), 3-(trimethylsilyl)-1-propane sulfonic acid sodium salt (DSS, Aldrich), Cl_2 gas (Matheson gas product), Dowex 50-X8 resin (J.T. Baker), 5,5-dimethyl-1-pyroline N-oxide (DMPO, TCI), $Na_2C_2O_4$ (Fisher) were used without further purification. $(NH_4)_2IrCl_6$, (Aldrich) and $NaClO_4$ (Fisher) were used after recrystallization.

$NaClO_4$ standardization. An aliquot of solution of the recrystallized $NaClO_4$ was run through a cation exchange column which was regenerated with HCl and packed with Dowex 50-X8 resin. The stock solution was standardized with a standard $NaOH_{(aq)}$ solution.

$(NH_4)_2IrCl_6$ recrystallization. To a hot saturated solution of $(NH_4)_2IrCl_6$ (100 mg/ 14 mL H_2O) was added a saturated solution of NH_4Cl. After cooling the mixture in an ice bath, it was filtered, and the crystals were washed with 20% $NH_4Cl_{(aq)}$ solution. The crystals were again washed with 95% ethanol two times (10 mL at a time) and finally with diethyl ether (10 mL portion two times). The crystals were air dried first and then vacuum dried.[23] Yield was 85%.

Deionized water was purified with a Barnstead Nano-pure Infinity Ultrapure water system and used to prepare all solutions used in the experiments. Freshly prepared

solutions were used in all experiments except $NaClO_4$, $HClO_4$, HCl and buffers. In all reactions (kinetic, stoichiometric and product analysis) the reactant solutions were purged with argon gas prior to the reactions.

4.2.2. Methods. A HP-8453 diode array spectrophotometer equipped with a Brinkman Lauda RM6 thermostated system was used to record all UV-vis spectra at 25 ± 0.1 ^{0}C. All pH measurements were performed on a Corning 450 pH/ion meter with a Mettler Toledo Inlab 421 pH electrode (filled with 3 M Nacl solution) using the relationship pH = -log[H^+]. ^{1}H- NMR spectra were obtained on a Brucker AV 400 MHZ spectrometer. Chemical shift (δ-value) in D_2O were relative to DSS.

Kinetic studies were done at 25 ± 0.1^{0}C on a Hi-Tech SF-51 stopped flow spectrophotometer with Olis 4300 data acquisition and analysis software. All kinetic data of the reaction between Ir^{IV} and $[CysSO_2H]_t$ were monitored at 488 nm. The concentration of $[CysSO_2H]_t$ was kept in at least a 10-fold excess over the oxidant $[Ir^{IV}]_0$. All 2nd order observed rates, k_{obs2} values, reported are the average of at least four runs unless and otherwise stated.

4.3. Results

4.3.1. Qualitative Features of the $CysSO_2H$ Reaction with Ir^{IV}. A general reaction was performed to observe the kinetic behavior of Ir^{IV} with excess $CysSO_2H$ on a UV-vis diode array spectrophotometer. When 1.5 mL of 0.1 mM Ir^{IV} solution prepared in acetate buffer at pH 4.5 was mixed with 1.5 mL of 1.0 mM $CysSO_2H$ kept in a sealed cuvette, by means of an air-tight syringe, the absorbance of Ir^{IV} at 488 nm decreased quickly with non-pseudo first-order kinetics. The reactant solutions were deoxygenated

with Ar gas and the ionic strength was maintained with 0.1 M ($NaClO_4$). 0.5 mM $[IrCl_6]^{3-}$ was added to this experiment. The decay pattern together with the corresponding kinetic trace are shown in Fig 4.1.

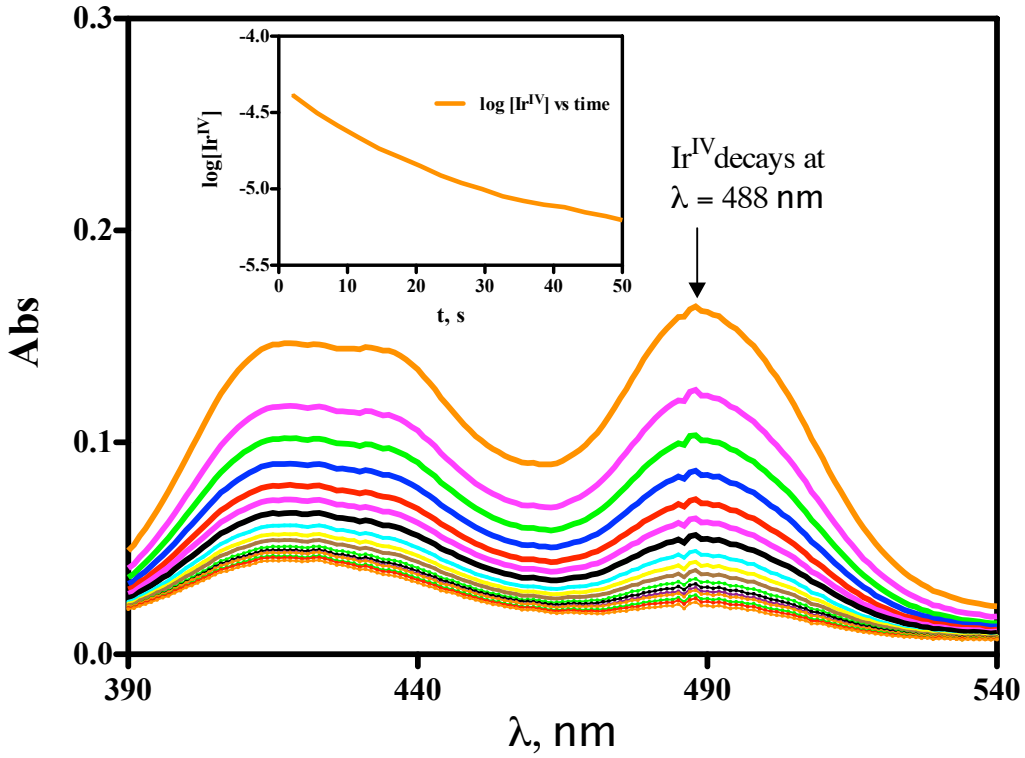

Fig 4.1. The absorbance decay of Ir^{IV} with excess $CysSO_2H$. $[Ir^{IV}]_0$ = 0.05 mM with 0.5 mM $[Ir^{III}]$, $[CysSO_2H]_0$ = 0.5 mM, acetate buffer (10 mM) at pH 4.5 and μ = 0.1 M ($NaClO_4$). Inset: kinetic trace with non-pseudo first-order kinetics. Run time = 50 second with cycle time = 3 second.

4.3.2. Metal Catalysis. Trace metal catalysis is ubiquitous and has been reported to be typical of thiol oxidations.[24-31] Although cysteine sulfinic acid is not a thiol, its reactions may also be catalyzed by impurity level metal ions. So to test for the catalysis, a

set of experiments was conducted in the reaction of $CysSO_2H$ with Ir^{IV} maintaining the conditions 1.0 mM $[CysSO_2H]_0$, 0.1 mM Ir^{IV}, acetate buffer at pH 4.3 and ionic strength (μ) = 0.1 M $NaClO_4$. 1 mM dipicolinic acid and sodium oxalate each were tested as inhibitor. The data are presented in Table 4.1. The half-lives for all reactions, even with added 5 μM Cu^{2+} and Fe^{2+}, were identical within error. These results show that the reaction of $CysSO_2H$ with Ir^{IV} is unaffected by metal-ion catalysis.

Table 4.1. Kinetic Data for Cu^{2+} and Fe^{2+} Catalysis Test in the Reaction of Ir^{IV} with $[CysSO_2H]_t$.[a]

Expt	$[Cu^{2+}]$ μM	$[Fe^{2+}]$ μM	$[C_2O_4^{2-}]$ mM	[dipic] mM	$t_{1/2}$ s
1.	0.0	0.0	0.0	0.0	0.18
2.	0.0	0.0	1.0	0.0	0.19
3.	0.0	0.0	0.0	1.0	0.19
4.	5.0	0.0	0.0	0.0	0.18
5.	0.0	5.0	0.0	0.0	0.19

[a] Cysteine sulfinic acid ($[CysSO_2H]_t$) = 1.0 mM, hexachloroiridate ($[Ir^{IV}]_0$) = 0.1 mM, $C_2O_4^{2-}$ = sodium oxalate salt, acetate buffer (10 mM), pH = 4.3 and ionic strength (μ) = 0.1 M ($NaClO_4$).

4.3.3. Product Inhibition. The reaction of $CysSO_2H$ with Ir^{IV} is greatly inhibited by the metal product $[IrCl_6]^{3-}$. The experimental data produced from the reaction of 1.0

mM $CysSO_2H$ and 0.11 mM Ir^{IV} at pH 4.6 acetate buffer with the maintenance of 0.1 M ionic strength and 1 mM dipic are presented in Table 4.2. The half-life of the reaction with no addition of $[IrCl_6]^{3-}$ to it was 0.28 s whereas it was 3.3 s with 10 fold addition of the same.

Table 4.2. Product Inhibition Test in the Reaction of Ir^{IV} with $CysSO_2H$ [a]

Expt.	$[Ir^{III}Cl_6^{3-}]$, mM	$t_{1/2}$, s
1.	0.0	0.3
2.	1.2	3.3

[a] $[CysSO_2H]_t$ = 1.0 mM, $[Ir^{IV}]_0$ = 0.11 mM, acetate buffer, pH = 4.6, μ = 0.1 M ($NaClO_4$).

4.3.4. Spin trap test. Two spin traps,[19,28-30,32,33] (Scheme 4.6), N-tert butyl α-phenylnitrone (PBN) and 5,5-dimethyl-1-pyroline N-oxide (DMPO) were employed to examine their effects on the kinetics of the $CysSO_2H$/ Ir^{IV} reaction. These spin traps are well-known to scavenge free radicals produced during reaction and eliminate the inhibition effect of the product ($[IrCl_6]^{3-}$ in this work). Trapping the radicals helps correct potential departure from pseudo-first order kinetics due to metal product inhibition. In the first set of reactions varied amount of PBN were used (Table 4.3) with the experimental parameters of 1.0 mM $CysSO_2H$, 0.1 mM Ir^{IV}, acetate buffer at pH = 4.3, μ = 0.1 ($NaClO_4$) and [dipic] = 1 mM. All these reactions took place with the same half-life (0.2

s) and bad pseudo-first order fits. In another set, DMPO was present with a 10 fold excess of $[IrCl_6]^{3-}$ added to 0.05 mM Ir^{IV}, other conditions being the same as in the PBN experiment. Dipic was not used. Again the reactions occurred with constant half-life of 1.6 s (Table 4.3). Thus, the use of these spin traps did not offer significant effect on the reaction. Accordingly, no spin trap or chelator was further employed in the kinetic measurements.

$$R^{\bullet} + \text{PBN/DMPO} \rightarrow \text{spin adduct-}R^{\bullet}$$

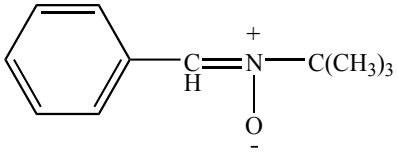

PBN

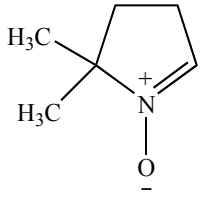

DMPO

Scheme 4.6

Table 4.3. PBN and DMPO Effects in the Reaction of $CysSO_2H$ with Ir^{IV}[a]

PBN[a]			DMPO[b]		
[PBN], mM	$t_{1/2}$, s	[dipic], mM	[DMPO], mM	k_{obs2}, M^{-1} s^{-1}	$t_{1/2}$, s
0.0	0.19	0.0	0.0	1.58×10^4	1.6
0.0	0.19	1.0	1.0	1.50×10^4	1.6
1.0	0.19	1.0	2.0	1.40×10^4	1.7
2.0	0.20	1.0			
5.0	0.20	1.0			

[a] $[Ir^{IV}]_0 = 0.1$ mM, $[CysSO_2H]_t = 1.0$ mM, acetate buffer at pH = 4.3 , $\mu = 0.1$ ($NaClO_4$) and [dipic] = 1 mM. [b] $[Ir^{IV}]_0 = 0.05$ mM, $[CysSO_2H]_t = 1.0$ mM, acetate buffer at pH = 4.4 , $\mu = 0.1$ ($NaClO_4$), $[IrCl_6^{3-}] = 0.5$ mM and no dipic.

4.3.5. Stoiochiometry with Ir^{IV} and Product Analysis. ^{1}H-NMR spectroscopy was used to identify the reductant ($CysSO_2H$) related product. The sample was prepared as follows: 3.0 mM and 1.4 mM solutions of Ir^{IV} and $CysSO_2H$ were prepared respectively in D_2O. Both of these were purged with Ar gas. 1 mL of each solution was mixed together and 0.07 mM DSS was added as an internal standard. The sample was un-buffered (pH 2.7). 0.7 mL of this sample mixture (product) was analyzed. In Fig 4.2a the chemical shift (δ) at 4.23, 3.57 and 3.33 are characteristic of $CysSO_3H$. It was justified by adding cysteic acid ($CysSO_3H$) to the product (Fig 4.2b)**.** Quantitative conversion of $CysSO_2H$ to $CysSO_3H$ was evident from the ^{1}H-NMR spectra. The integration values for the respective peaks were found to be increased in the spectrum with added cysteic acid.

The integrated area 1.0, 1.2 and 1.3 for the peaks at (δ) = 4.23, 3.57 and 3.33 respectively increased to 1.6, 1.8 and 1.8 for the same peaks after spiking the product with cysteic acid showing that the $CysSO_2H$ is oxidized to $CysSO_3H$.

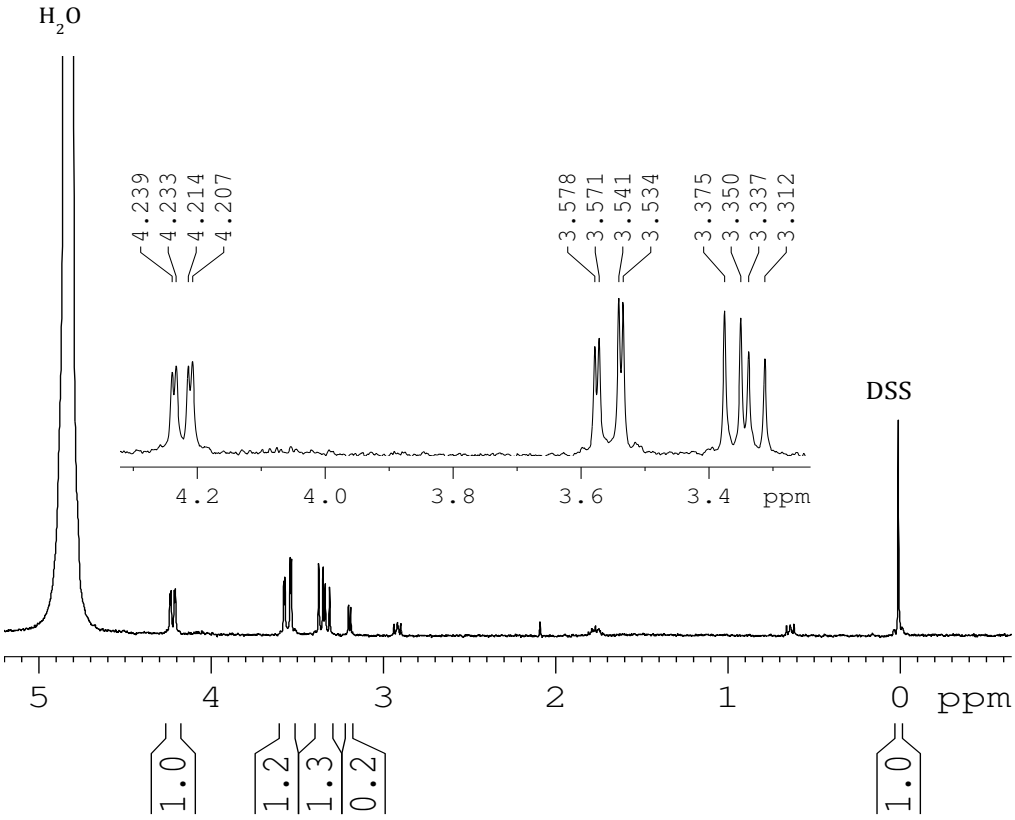

Fig 4.2. a. ^{1}H-NMR spectrum of product in the reaction of $CysSO_2H$ and Ir^{IV}. Inset highlighted peaks of the product. DSS = 2,2-dimethyl-2-silapentane -5-sulfonate sodium salt.

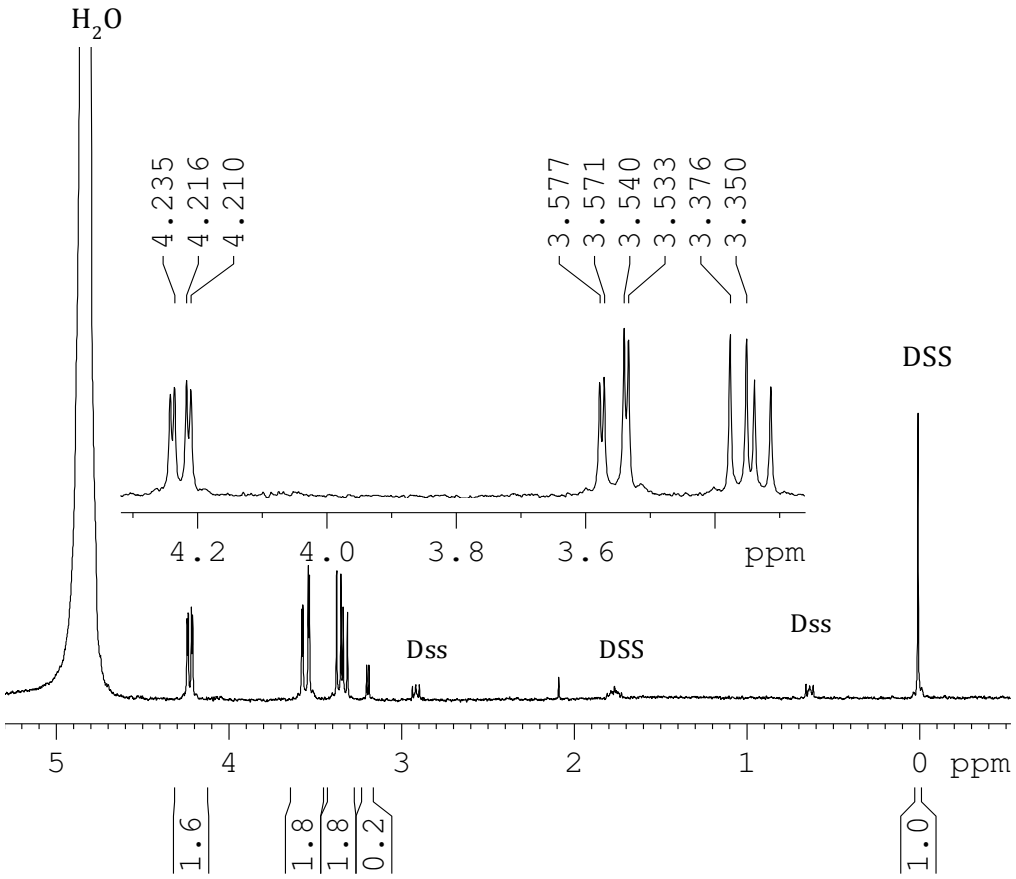

Fig 4.2. b. ^{1}H-NMR spectra of the product spiked with cysteic acid in the reaction of $CysSO_2H$ and Ir^{IV}. Inset highlighted peaks of the spiked product.

4.3.5.1. Stoichiometry. To determine the stoichiometric ratio of the reaction between $CysSO_2H$ and Ir^{IV}, a spectrophotometric titration was conducted. 2.04 mM and 0.508 mM stock solutions of Ir^{IV} and $CysSO_2H$ were prepared respectively in acetate buffer at pH 4.7 and bubbled with Ar gas to remove oxygen. 2.0 mL $CysSO_2H$ was transferred to a cuvette and 0.1 mL aliquots of Ir^{IV} were added to it using a syringe. The absorbance was monitored at 488 nm. A sharp increase of absorbance indicated the end point, and at this point, 0.93 mL Ir^{IV} was found to be consumed by 2.0 mL of 0.508 mM $CysSO_2H$. Titration data are shown in Table 4.4 and titration spectra with plot of the data in Fig 4.3.

According to which the end point is calculated:

Moles Ir^{IV} = (0.93 mL × 2.04 mM) = 1.90 mmol and moles $CysSO_2H$ = (2.0 mL × 0.508 mM) = 1.02 mmol.

Stoichiometric ratio $= \frac{n[Ir^{IV}]}{n[CysSO_2H]} = \frac{1.9\ mmol}{1.02\ mmol} = 1.9 \pm 0.1$

Table 4.4. Absorbance Data from a Spectrophotometric Titration for the Stoichiometry Determination in the Reaction of $[Ir^{IV}]$ with $[CysSO_2H]_t$[a]

Expt	Vol (Ir^{IV}), mL	Abs (λ = 488 nm)
1.	0.00	1.60×10^{-3}
2.	0.10	5.10×10^{-3}
3.	0.20	8.10×10^{-3}
4.	0.30	9.10×10^{-3}
5.	0.40	1.11×10^{-2}
6.	0.50	1.44×10^{-2}
7.	0.60	1.67×10^{-2}
8.	0.70	1.84×10^{-2}
9.	0.80	2.85×10^{-2}
10.	0.90	3.36×10^{-2}
11.	1.00	1.08×10^{-1}
12.	1.10	1.95×10^{-1}
13.	1.20	3.72×10^{-1}

[a] Ir^{IV} = (0.93 mL × 2.04 mM) and $CysSO_2H$ = (2.0 mL × 0.508 mM), acetate buffer at pH 4.7.

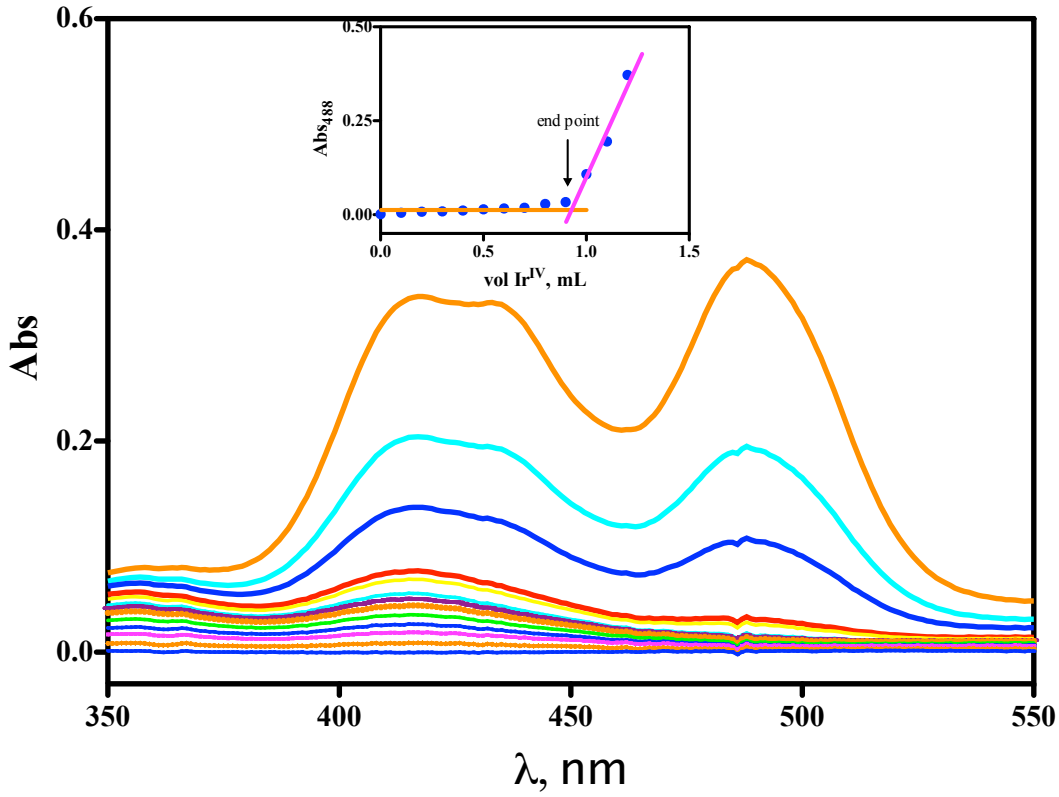

Fig 4.3. Spectrophotometric titration of $CysSO_2H$ with Ir^{IV} for the stoichiometry Determination. 2.0 mL of 0.508 mM $CysSO_2H$ in acetate buffer at pH 4.7 titrated with 2.04 mM Ir^{IV}.

4.3.5.2. Analysis of Metal Product. 1.0 mL of 0.22 mM Ir^{IV} was mixed with 1.0 mL of 2.3 mM $CysSO_2H$ in a cuvette to get the products resulting from the oxidation of $CysSO_2H$ by Ir^{IV}. The colorless product's absorbance at 488 nm was 7.0×10^{-3} which is similar to the absorbance of 0.11 mM (6.9×10^{-3}) of Ir^{III} pure sample. The product was subjected to chlorination to oxidize Ir^{III} (supposed to be formed as product) back to Ir^{IV}. The chlorinated product yielded the identical absorbance of reactant Ir^{IV} at 488 nm with 2% error.

Acetate buffer at pH 4.6 was used to prepare the reactant solution. Ionic strength was maintained at 0.1 M by $NaClO_4$. Both of the reactant solutions were degased with Ar prior to the mixing. To make the environment similar to that of the product solution, $NaClO_4$ and $CysSO_2H$ were added to the $IrCl_6^{3-}$ sample. Fig 4.5 displays all the spectra of these observations as per which the only metallic product formed is $IrCl_6^{3-}$ with the co-ordination sphere of Ir intact.

Abs_{488} of 0.11 mM Ir^{IV} (0.22 mM stock diluted to 0.11 mM) as reactant, before mixing = 0.410 and Abs_{488} of Ir^{IV} as recovered from the product, after chlorination = 0.419.

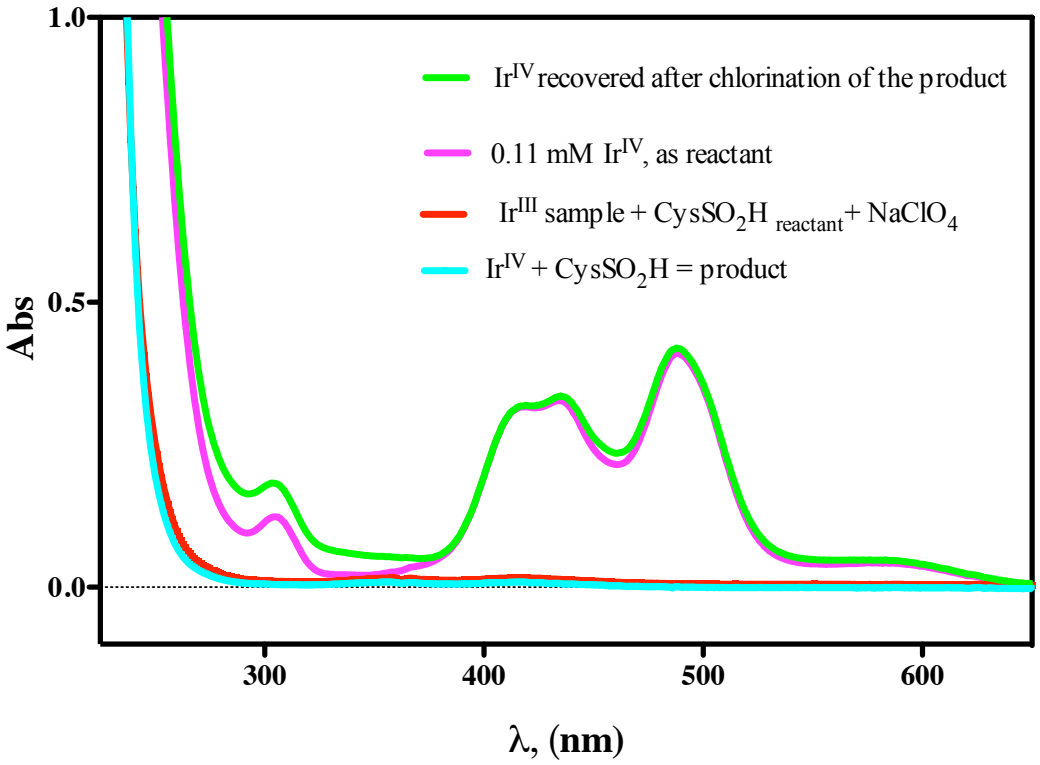

Fig 4.4. Quantitative conversion of $[IrCl_6]^{2-}$ to $[IrCl_6]^{3-}$ by UV-vis. $[Ir^{IV}]$ = 0.11 mM, $[Ir^{III}]$ = 0.11 mM, $[CysSO_2H]$ = 1.2 mM, acetate buffer at pH 4.6 and μ = 0.1 M ($NaClO_4$).

Considering the results of the spectrophotometric titration and UV-vis analysis described above, the stoichiometric reaction between $CysSO_2H$ and Ir^{IV} is described by eq 4.1:

$$2[IrCl_6]^{2-} + CysSO_2H + H_2O \rightarrow 2[IrCl_6]^{3-} + CysSO_3H + 2H^+ \quad (4.1)$$

4.4. Kinetics. Comparison of a typical kinetic trace fitted to first and second order rate laws are shown in Fig 4.5. This trace was obtained when a solution containing 1.0 mM $CysSO_2H$ was mixed with 0.05 mM Ir^{IV} along with 0.52 mM Ir^{III}. The conditions were acetate buffer at pH 3.2 and 0.1 M ($NaClO_4$) ionic strength. The pseudo-first order fit was not perfect but the 2nd order was in good agreement with the data (fit eqn 4.4). A semi log plot (log[Ir^{IV}] vs t) failed to yield a straight line showing that the reaction is not first order. The reaction is significantly inhibited by the product Ir^{III} (Table 4.2) so we used a 10-fold excess of Ir^{III} in all kinetic experiments. The rate law is given by the eq 4.2.

$$\text{Rate} = -\frac{d[Ir^{IV}]}{dt} = k_{obs2}[Ir^{IV}]^2 \quad (4.2)$$

Where k_{obs2} (2nd order rate constant) = $k_{prog} \cdot \varepsilon_{eff} \cdot \iota$; ε_{eff} = molar extinction coefficient of Ir^{IV} at 488 nm and ι = path length. The eqn 4.2 develops to eqn 4.3.

$$-\frac{d[Ir^{IV}]}{dt} = k_{prog} \cdot \varepsilon_{eff} \cdot \iota\, [Ir^{IV}]^2 \quad (4.3)$$

Fitting equation for pseudo-second order reaction was derived which is given in eqn 4.4.

$$Abs_t = \left(\frac{Abs_0}{1+\left(\frac{Abs_0}{\epsilon.\iota}\right).k_{obs}.t}\right) + b \quad (4.4)$$

k_{prog} has relationship with absorbance at required wavelength (λ, nm) as per OLIS fitting routines available within the OLIS software packages:

$$\frac{-d(A_t - A_\infty)_\lambda}{dt} = k_{prog}(A_t - A_\infty)^2_\lambda \quad (4.5)$$

The k_{prog} values generated by these fits are in terms of absorbance. These values are relative to the path length of the instrument i.e. if a instrument with different path length is used, k_{prog} values differ.

The k_{prog} values reported here are average values taken over four measurements and 2nd order rate constants are calculated using the relationship as described above which is,

$$k_{obs2} = k_{prog} \cdot \varepsilon_{eff} \cdot \imath$$

Molar extinction coefficient of Ir^{IV} at 488 nm is, $\varepsilon_{488} = 3.98 \times 10^3\ M^{-1}\ cm^{-1}$.

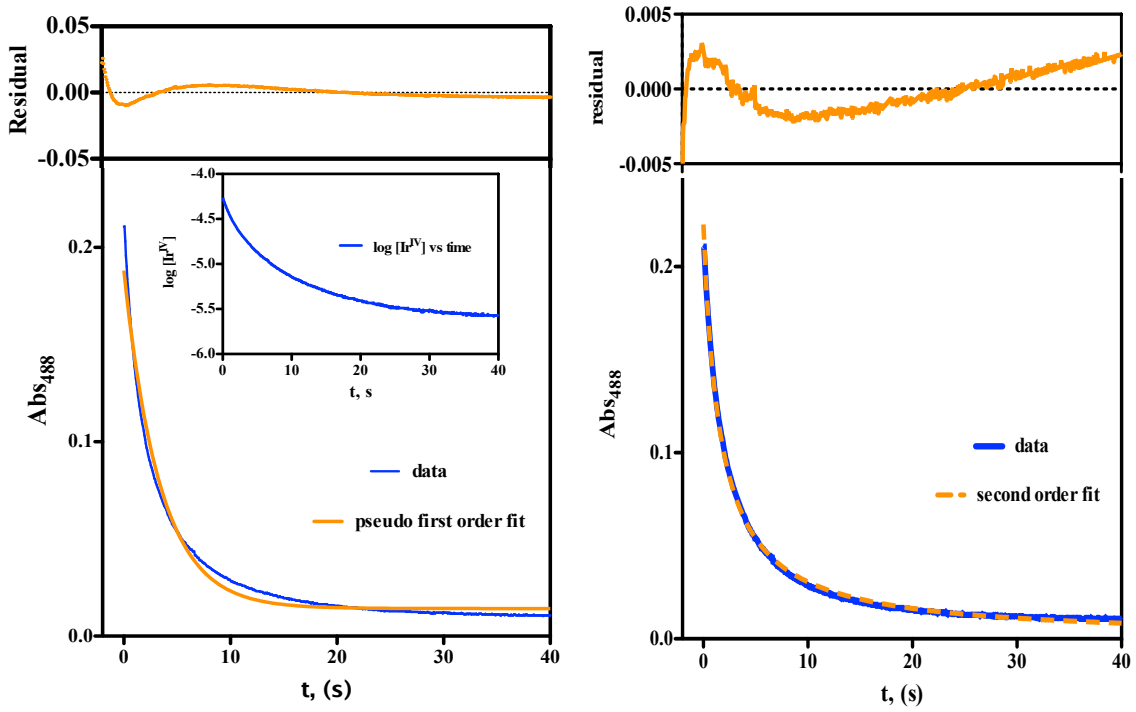

Fig 4.5. With excess $CysSO_2H$ and $[IrCl_6]^{3-}$, Ir^{IV} decays with second order kinetics. Left lower box: pseudo-first order fit. The blue is data, orange line is fit. Inset: log $[Ir^{IV}]$ vs t plot. Right: 2nd order fit of the same data. Upper boxes, residual plots. Conditions: $[Ir^{IV}]_0$ = 0.05 mM, $[Ir^{III}]$ = 0.52 mM, $[CysSO_2H]_0$ = 1.0 mM, acetate buffer at pH 3.2 and μ = 0.1 M ($NaClO_4$).

4.4.1. Inverse Dependence on $[IrCl_6]^{3-}$. A set of experiments with varied $[Ir^{III}]$ was performed keeping 1.0 mM $CysSO_2H$, 0.05 mM Ir^{IV}, μ = 0.1 M ($NaClO_4$) and acetate buffer at pH 4.5. In these, the k_{obs2}, M^{-1} s^{-1} decreased with the added Ir^{III} (Table 4.5). A plot of [$1/k_{obs2}$, M^{-1} s^{-1}] vs $[Ir^{III}]$, Fig 4.6, explains this feature. Likewise, Fig 4.7 depicts the slowing of the decay of Ir^{IV} with increased addition of Ir^{III}. These results prove that the rate of reaction of $CysSO_2H$ with Ir^{IV} is inversely dependent on $[IrCl_6^{3-}]$ as

in eq 4.6. The k_{obs2}, $M^{-1}\ s^{-1}$ values were derived from 2nd order fit (k_{obs2}, $M^{-1}\ s^{-1} = k_{prog}$. ι . ε (Ir^{IV}_{488}). Solid salt of Ir^{III} i.e. $(NH_4)_3IrCl_6 \bullet H_2O$, was weighed separately and added to the individual 10 mL Ir^{IV} solution for each experiment just before running the experiment. Due to instability of Ir^{III} compound, no stock solution of it was prepared.

$$\text{Rate} = -\frac{d[IrCl_6^{2-}]}{dt} \propto \frac{1}{[IrCl_6^{3-}]} \qquad (4.6)$$

Table 4.5. The observed 2nd order rates (k_{obs2}) are Inversely Dependent on $[IrCl_6]^{3-}$.[a]

Expt	$[Ir^{III}]$, mM	k_{prog}, s^{-1}[b]	k_{obs2}, $M^{-1}\ s^{-1}$[c]	$1/k_{obs2}$, $M^{-1}\ s^{-1}$
1.	0.000	29.1	1.16×10^5	8.63×10^{-6}
2.	0.520	3.21	1.28×10^4	7.83×10^{-5}
3.	0.855	1.93	7.68×10^3	1.30×10^{-4}
4.	1.56	1.12	4.46×10^3	2.24×10^{-4}

[a] Cysteine sulfinic acid (1 mM), Ir^{IV} (0.05 mM), Ir^{III} (0.00 – 1.56 mM), μ = 0.1 M ($NaClO_4$), acetate buffer pH 4.5. [b] k_{prog} s^{-1} is taken only in terms of absorbance. [c](k_{obs2}, $M^{-1}\ s^{-1} = k_{prog}$, s^{-1}. ι . ε (Ir^{IV}_{488}) where ε (Ir^{IV}_{488}) = 3980 $M^{-1}\ cm^{-1}$.[19]

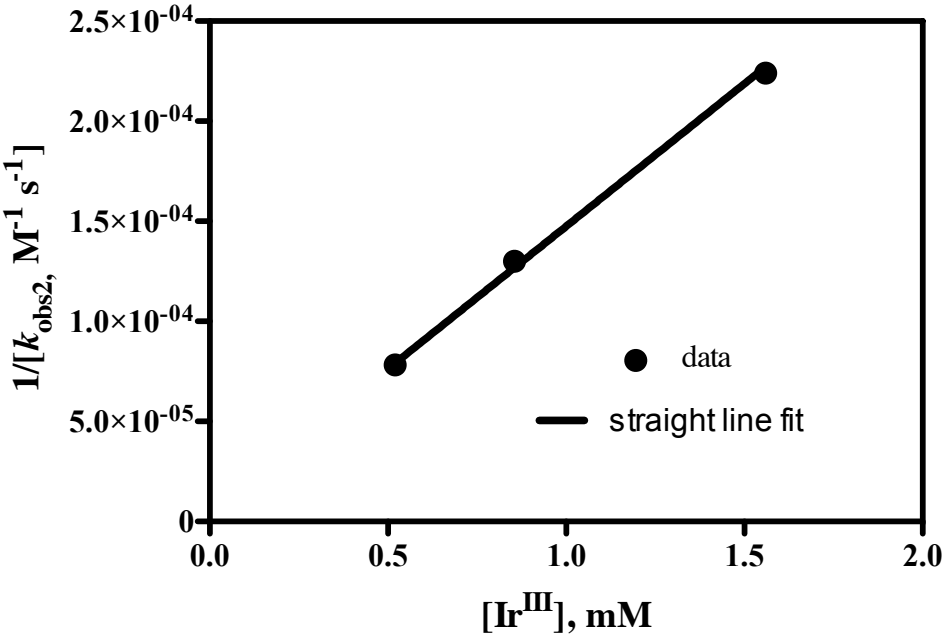

Fig 4.6. Inverse dependence k_{obs2} on $[IrCl_6^{3-}]$. $CysSO_2H$ (1 mM), Ir^{IV} (0.05 mM), Ir^{III} (0.52 – 1.56 mM), μ = 0.1 M ($NaClO_4$), acetate buffer, pH 4.5.

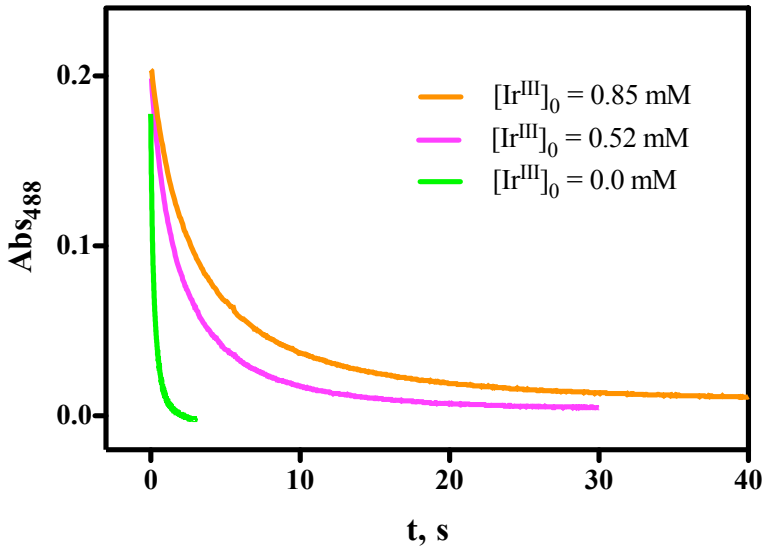

Fig 4.7. Reaction inhibition by $[IrCl_6]^{3-}$. $[CysSO_2H]_0$ = 1.0 mM, $[Ir^{IV}]_0$ = 0.05 mM, $[Ir^{III}]_0$ = 0.0 – 0.85 mM, μ = 0.1 M ($NaClO_4$), acetate buffer pH 4.5.

4.4.2. $[CysSO_2H]_t$ Dependence. In the presence of excess Ir^{III}, the oxidations of $CysSO_2H$ by Ir^{IV} were conducted varying the concentration of $CysSO_2H$ from 0.50 – 5.0 mM in acetate buffer at pH 4.6 and ionic strength 0.1 M ($NaClO_4$). All the data are displayed in Table 4.6. The second order rates, k_{obs2}, were obtained by multiplying the k_{prog} (obtained from 2nd order fit) with the molar absorptivity (ε_{488}) of Ir^{IV}. $k_{obs2,}$ plotted against $[CysSO_2H]_t$ (Fig 4.8) increased linearly indicating first order dependence on $[CysSO_2H]_t$ (eq 4.7).

$$k_{obs2} = \frac{k[\mathrm{CysSO_2H}]_t}{[\mathrm{IrCl_6^{3-}}]} \qquad (4.7)$$

Table 4.6. $[CysSO_2H]_t$ Dependence Kinetics[a]

Expt	$[CysSO_2H]_t$, mM	k_{prog}, s^{-1}	k_{obs2}, $M^{-1}\,s^{-1}$
1.	0.50	1.64	6.54×10^3
2.	1.0	3.98	1.58×10^4
3.	2.0	6.22	2.48×10^4
4.	3.0	10.2	4.05×10^4
5.	4.0	13.8	5.50×10^4
6.	5.0	16.7	6.65×10^4

[a]Cysteine sulfinic acid (0.50 – 5.0 mM), $[Ir^{IV}]_0$ = 0.05 mM, $[Ir^{III}]_0$ = 0.50 mM, μ = 0.1 M ($NaClO_4$), acetate buffer, pH 4.6. (k_{obs2}, $M^{-1}\,s^{-1} = k_{prog}$, s^{-1} . ι . ε ($Ir^{IV}{}_{488}$).

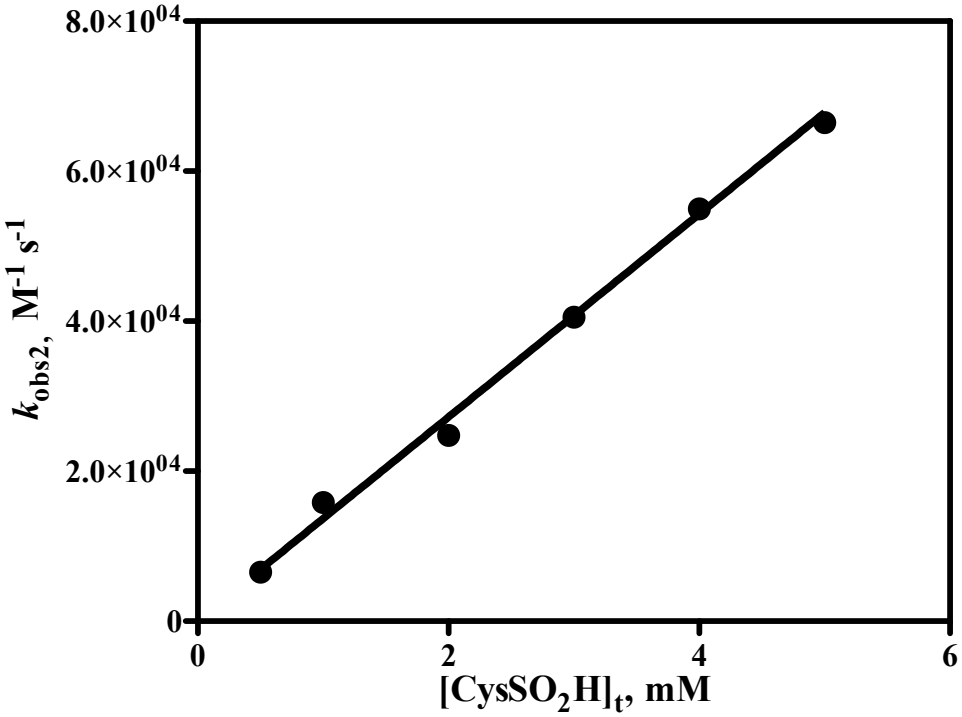

Fig 4.8. Dependence of k_{obs2} on $[CysSO_2H]_t$ in the presence of excess Ir^{III}.

$[CysSO_2H]_t$ = 0.50 – 5.0 mM, $[Ir^{IV}]_0$ = 0.05 mM, $[Ir^{III}]_0$ = 0.50 mM, μ = 0.1 M ($NaClO_4$), acetate buffer, pH 4.6.

4.4.3. pH Dependence. A series of oxidations of $CysSO_2H$ by Ir^{IV} in th pH range 3.15 – 5.63 (acetate buffer) were performed with the other conditions being 0.52 mM Ir^{III} and 0.1 M ionic strength ($NaClO_4$). The data are introduced in the Table 4.7. Basically, these reactions seem to be indifferent to the pH. The log k_{obs2} at pH 3.12 is 4.05 and 4.20 at pH 5.63. The increase of log k_{obs2} (ca. 5%) in more than two pH units may fall within the error limit but the trend seems to be definite, so there could be some other reasons for

such increase. Consequently a plot of log k_{obs2} vs pH showed straight horizontal line with a slope of 0.066 ± 0.009, shown in Fig 4.9.

Table 4.7. pH Dependence Kinetics[a]

pH	$k_{prog,}$ s^{-1}	k_{obs2}, M^{-1} s^{-1}	log k_{obs2}
3.15	2.82	1.12×10^4	4.05
3.35	2.92	1.16×10^4	4.07
3.81	2.84	1.13×10^4	4.05
4.20	3.81	1.26×10^4	4.10
4.57	3.65	1.45×10^4	4.16
5.03	3.74	1.49×10^4	4.17
5.63	3.97	1.58×10^4	4.20

[a]Cysteine sulfinic acid (1.0 mM), $[Ir^{IV}]_0 = 0.05$ mM, $[Ir^{III}]_0 = 0.52$ mM, $\mu = 0.1$ M ($NaClO_4$), acetate buffer, pH (3.12 – 5.63).

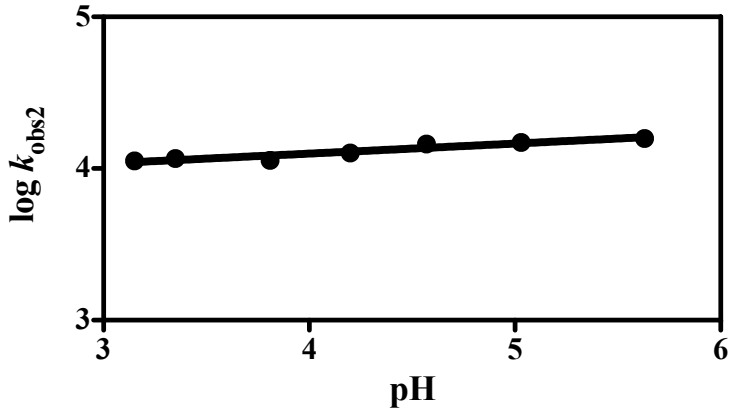

Fig 4.9. pH Dependent Plot of the Reaction of $CysSO_2H$ and Ir^{IV}.

$[[CysSO_2H]_t] = 1.0$ mM, $[Ir^{IV}]_0 = 0.05$ mM, $[Ir^{III}]_0 = 0.52$ mM, $\mu = 0.1$ M ($NaClO_4$), acetate buffer pH (3.12 – 5.63). Straight line fit with a slope = 0.066 ± 0.009.

Combining equations 4.2, 4.6 and 4.7, the overall rate law is described by eqn 4.5.

$$\text{Overall rate} = -\frac{d[IrCl_6^{2-}]}{dt} = \frac{k[IrCl_6^{2-}]^2[CysSO_2H]_t}{[IrCl_6^{3-}]} \quad (4.8)$$

$$\text{and} \quad k_{obs2} = \frac{k[CysSO_2H]_t}{[IrCl_6^{3-}]} \quad (4.9)$$

Rearranging eqn 4.9 gives eqn 4.10 to calculate rate constant '*k*'.

$$k = \frac{k_{obs2}\,[IrCl_6^{3-}]}{[CysSO_2H]_t} \quad (4.10)$$

Inserting the concentrations of $CysSO_2H$, $[Ir^{III}]$ and k_{obs2} (Table 4.5 and 4.6) into eqn 4.10 gives:

$$k = (6.7 \pm 0.09) \times 10^3\ M^{-1}\ s^{-1}.$$

4.4.4. Proposed Mechanism.

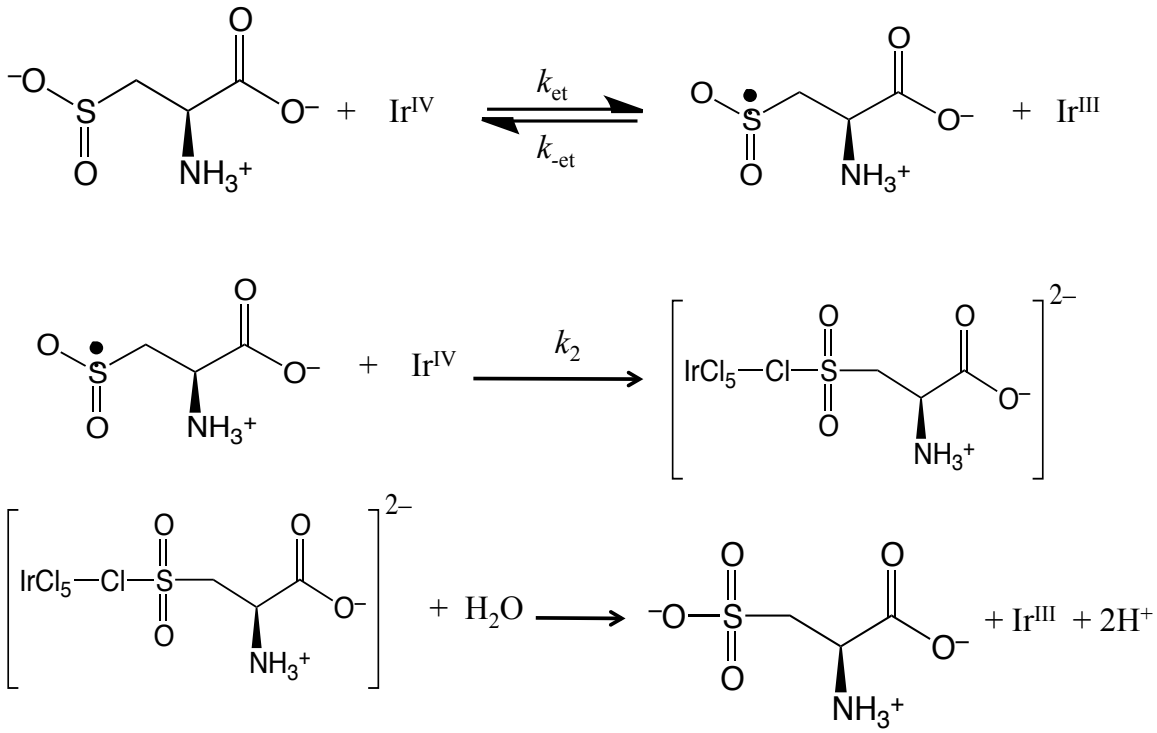

$Ir^{IV} = [IrCl_6]^{2-}$; $Ir^{III} = [IrCl_6]^{3-}$

Rate of formation of $RSO_2^{\bullet} = \frac{d[RSO_2^{\bullet}]}{dt} =$

$$k_{et}[Ir^{IV}][CysSO_2H]_t - k_{-et}[Ir^{III}][RSO_2^{\bullet}] - k_2[Ir^{IV}][RSO_2^{\bullet}] \qquad (4.11)$$

and formation of product (consumption of Ir^{IV})

$$-\frac{1}{2}\frac{d[Ir^{IV}]}{dt} = \frac{d[CysSO_3^-]}{dt} = k_2\,[Ir^{IV}][RSO_2^{\bullet}] \qquad (4.12)$$

Applying steady-state approximation to find $RSO_2^{\bullet}$ and solving eq 4.11 turns to eq 4.13)

$$[\mathrm{RSO_2^{\bullet}}] = \frac{k_{\mathrm{et}}[\mathrm{CysSO_2H}]_{\mathrm{t}}[\mathrm{Ir^{IV}}]}{k_{-\mathrm{et}}[\mathrm{Ir^{III}}] + k_2[\mathrm{Ir^{IV}}]} \tag{4.13}$$

From eq 4.12 and 4.13,

$$-\frac{d[\mathrm{Ir^{IV}}]}{dt} = \frac{2k_{\mathrm{et}}k_2[\mathrm{CysSO_2H}]_{\mathrm{t}}[\mathrm{Ir^{IV}}]^2}{k_{-\mathrm{et}}[\mathrm{Ir^{III}}] + k_2[\mathrm{Ir^{IV}}]} \tag{4.14}$$

For $k_{-et}[Ir^{III}] >> k_2[Ir^{IV}]$, eq 4.14 reduces to eq 4.15 (which is overall rate law already mentioned in eq 4.5.

$$-\frac{d[\mathrm{Ir^{IV}}]}{dt} = \frac{2k_{\mathrm{et}}k_2[\mathrm{Ir^{IV}}]^2[\mathrm{CysSO_2H}]_{\mathrm{t}}}{k_{-\mathrm{et}}[\mathrm{Ir^{III}}]} \tag{4.15}$$

$$k = \frac{2k_{et}k_2}{k_{-et}} \tag{4.16}$$

4.5. Conclusions.

- The oxidation of cysteine sulfinic acid by Ir^{IV} is unaffected by the metal ions Fe^{2+}, Cu^{2+} catalysis.
- The rate laws are first order in $[CysSO_2H]_t$ and 2nd order in $[Ir^{IV}]$ with simple pH independent kinetics but inversely dependent on $[Ir^{III}]$.
- The $1e^-$ reduction of metal compound is without any perturbation to its co-ordination sphere.
- Cysteine sulfinic acid is oxidized to its corresponding sulfonic acid with Ir^{IV}.

References.

1. Lavine, T. F. *J. Biol. Chem.* **1936**, *113,* 583.
2. Rohde, M.; Senning, A. *Sulfur Reports.* **1993**, 14, 391.
3. Hamann, M.; Zhang, T. Hendrich, S.; Thomas, J. A. *Methods Enzymol.* **2002**, *348*, 146.
4. McCoy, J. G.; Baily, L. J.; Bitto, E.; Bingman, C. A.; Aceti, D. J.; Fox, B. G.; Phillips, Jr. G. N. *PNAS.* **2006**, *103*, 3084.
5. Hung, M.; Stanbury D. M. *Inorg. Chem.*, **2005**, *44*, 3541-3550.
6. Palmieri, F.; Stipani, I.; Lacobazzi, V. *BBA*, **1979**, *555*, 531.
7. Reddie, K. G. and Carrol, K. S. *Current Opinion in chemical Biology,* **2008,** *12*, 746.
8. Nidetzky, B. *Biochem. Soc. Trans*. **2007**, *35*, 1588.
9. Cozzolino, M.; Amori, I.; Pesaresi, M. G.; Ferri, A.; Nencini, M.; Carri, M. T. *J. Biol. Chem.* **2008**, *283*, 866.
10. Choi, J.; Sullards, M. C.; Olzmann, J. A.; Rees, H. D.; Weintraub, S. T.; Bostwick, D. E.; Gearing, M.; Levey, A. I.; Chin, L. S.; Li, L. *J. Biol. Chem.* **2006**, *281*, 10816.
11. Jacob, C.; Giles, K. M.; Giles, N. M.; Sies, H. *Angew. Chem., Intl. Ed. Engl.* **2003**, *42*, 4742.
12. Woo, H. A.; Chae, H. Z.; Hwang, S. C.; Yang, K. S.; Kang, K. K.; Rhee, S. G. *Science*, **2003**, *300*, 653.
13. Wood, J. A.; Poole, L. B.; Karplus, P. A. *Science*, **2003**, *300*, 650.
14. Schroder, E.; Littlechild, J. A.; Lebedev, A. A.; Errington, N.; Vagin, A. A.; Inpov, M. N. *Structure*, **2000**, *8*, 605.
15. Baba, A. *Japan J. Pharmacol*. **1987**, *43*, 1.
16. Jacob, C.; Holme, A. L.; Fry, F. H. *Org. Biomol. Chem*. **2004**, *2*, 1953.

17. Biteau, J. L.; Labarre, J; Toledano, M. B. *Nature* **2003**, *425*, 980.

18. Sun, J. F.; Stanbury, D. M. *J. Chem. Soc., Dalton Trans.* **2002,** 785.

19. Bhattarai, N.; Stanbury, D. M. *Inorg. Chem.* **2012**, *51*, 13303.

20. Fawcett, W. R.; Fedurco, M.; Kovacova, Z.; Borkowska, Z. *J. Electroanal. Chem*. **1994**, *368*, 265.

21. Brandes, N.; Schmitt, S.; Jakob, U. *Antioxid. Redox Signal*. **2009**, *11*. 997.

22. Budanov, A. V.; Sablina, A. A.; Feinstein, E.; Koonin, E. V.; Chumakov, P. M. *Science*, **2004**, *304*, 596.

23. Kauffman, G. B.; Teter, L. A. *Inorg. Synth.* **1966**, *8*, 223.

24. Shaikh, N.; Panja, A.; Banerjee, P. *Int. J. Chem. Kinetics* **2004**, *36*, 170.

25. Yordanov, N. D.; Antov, L.; Grampp, G. *Inorg. Chim. Acta* **1998**, *272*, 291.

26. Bagiyan, G. A.; Koroleva, I. K.; Soroka, N. V.; Ufuntsev, A.V. *Russian Chemical Bulletin, International Edition* **2003**, *52*, 1135.

27. Fornaro, A.; Coichev, N. *J. Coord. Chem.* **1999**, *46*, 519.

28. Hung, M.; Stanbury, D. M. *Inorg Chem*. **2005**, *44,* 3541.

29. Saha, B., Hung, M.; Stanbury, D. M.,*Inorg. Chem*. **2002**, *41*, 5538.

30. Wang, X.; Stanbury, D. M. *Inorg. Chem.* **2008**, *47 (3)*, 1224.

31. Sun, J.; Stanbury, D. M. *J. Chem.Soc., Dalton Trans.* **2002**, 785.

32. Song, N.; Stanbury, D. M. *Inorg Chem*. **2011**, *50,* 12762.

33. Konak, R.; Sakata, S. *Chem. Lett*. **1982**, 411.

Chapter 5

Oxidation of 2, 2-Dimethylhydroxylamine Hydrochloride by Hexachloroiridate(IV)

5.1. Introduction.

N,N-dimethylhydroxylamine (DMH) is a di-substituted derivative of hydroxylamine, the crystal structure of which is shown in Scheme 5.1.[1] It can be useful in the separation of radioactive metals. The increased energy demand of developed society has forced to generate more nuclear power as a source of clean energy. This energy is produced from nuclear fuel. The spent fuel contains uranium (U) and plutonium (Pu) along with other fission products (for example Np). U and Pu are separated by applying the well known PUREX (Plutonium Uranium Reduction and Extraction, Scheme 5.2 with extended PUREX process) method which uses tri-butyl phosphate (TBP) to extract the target species from nitric acid solution.[2, 2a] DMH could play an effective role as a salt-free reductant in the reprocessing of spent nuclear fuel. DMH not only reduces Pu^{IV} to Pu^{III} and Np^{VI} to Np^{IV} but also offers a high separation factor for Pu and Np from U. [2,3]

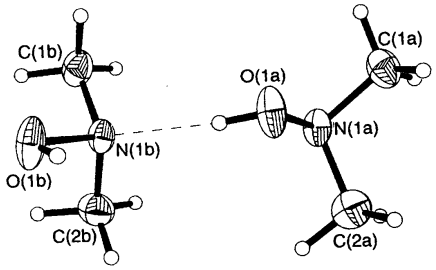

Scheme 5.1

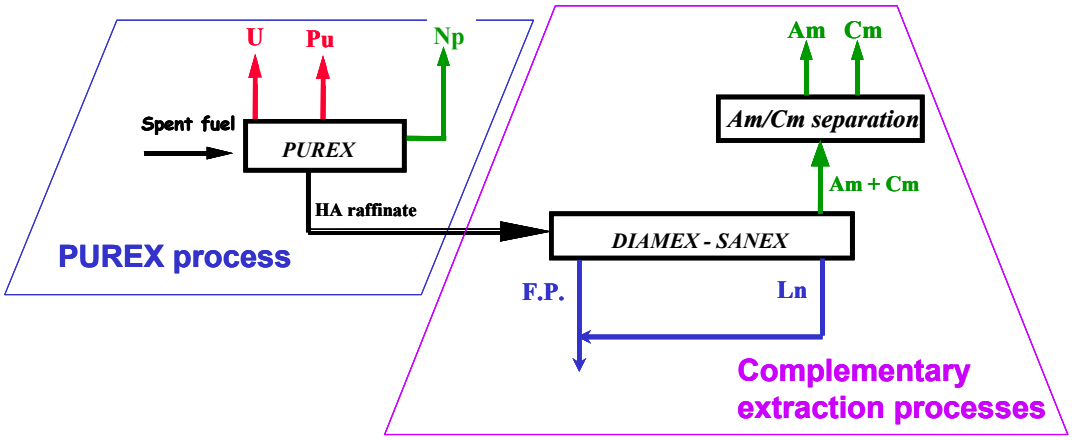

Scheme 5.2. PUREX process with its extended form[2a].

Reports on the kinetics and mechanism of redox reactions involving DMH include HNO_2,[3] H_2O_2 (MTO catalyzed),[4] DPPH,[4a] vanadium(V),[5] plutonium(IV) and neptunium(VI).[6-9] Radiation degradation[10] and radiolysis[11] of DMH are also published. One common feature in the reported mechanisms of DMH oxidations is formation of the dimethyl nitroxyl radical, $(CH_3)_2N^{\bullet}O$ as an intermediate. In this chapter, the kinetics and mechanism of oxidation of DMH with the substitution-inert transition-metal complex, $[IrCl_6]^{2-}$, is described.

5.2. Experimental Section.

5.2.1. Reagents and Solutions. NH_4Cl, acetic acid, monochloroacetic acid, $CuSO_4{\bullet}5H_2O$, $(NH_4)_2Fe(SO_4)_2{\bullet}6H_2O$, cacodylic acid ($(CH_3)_2AsO_2H$), D_2O, and glycylglycine hydrochloride (gly-gly), (all from Sigma), 3-(trimethylsilyl)-1-propane sulfonic acid sodium salt (DSS), and $(NH_4)_3IrCl_6{\bullet}H_2O$ (from Aldrich) $Na_2C_2O_4$ (Fisher)

were used as purchased. Cl_2 gas (Matheson), NaOH pellets ("SigmaUltra", Sigma-Aldrich), HCl, ethanol, diethyl ether and Dowex 50-X8 resin (J. T. Baker) were used without further purification. $NaClO_4$ (Fisher) was recrystallized from hot water. Anhydrous Na_3PO_4 was prepared from $Na_3PO_4 \cdot 12H_2O$ (99.6% Fisher) by melting it in a muffle furnace at 150 °C followed by cooling, pulverization, and repeated heating at 150 °C for several hours.

$(NH_4)_2IrCl_6$ (Aldrich) was recrystallized by adding a saturated solution of NH_4Cl to a hot saturated solution of $(NH_4)_2IrCl_6$ (100 mg/14 mL H_2O). After cooling the mixture in an ice bath, the crystals were collected by vacuum filtration and washed with 20% $NH_4Cl_{(aq)}$ solution. Crystals were again washed with 95% ethanol two times (10 mL at a time) and finally with diethyl ether (10 mL portion two times). The crystals were air dried first and then vacuum dried.[12] Yield = 85%.

N,N-dimethylhydroxylamine hydrochloride (≥98%, Sigma) was recrystallized by dissolving it in isopropyl alcohol (literature[8] uses ethanol) at 50 ^{0}C in water bath. The hot solution was filtered through suction and cooled in ice. The crystals were collected and dried in vacuum dessicator.

Deionized water was purified with a Barnstead Nanopure Infinity system and used to prepare all solutions. Freshly prepared solutions were used to run all experiments except for stock solutions of $NaClO_4$, HCl and some buffers. For all studies the reactant solutions were purged with argon gas on a bubbling line prior to use and transferred via glass syringes with Teflon or Pt needles, except where noted.

Stock solution of $NaClO_4$ was standardized by titration. An aliquot was passed through a cation exchange column which had been packed with Dowex 50-X8 resin and regenerated with conc HCl. The eluate was then titrated with standard $NaOH_{(aq)}$ solution.

5.2.2. Methods. A HP-8453 diode array spectrophotometer equipped with a Brinkman Lauda RM6 thermostated system was used to record all UV-vis spectra at 25 ± 0.1 °C; 10 mm quartz cells were used. All pH measurements were performed on a Corning 450 pH/ion meter with a Mettler Toledo Inlab 421 combination pH electrode (3 M NaCl), calibrated with standard buffers.

^1H NMR spectra were obtained on Brucker AV 400 and 600 MHz spectrometers. Chemical shifts (δ, ppm) in D_2O are relative to DSS.

Electrochemical measurements were conducted on a BAS 100B electrochemical analyzer equipped with a BAS C3 cell stand provided with an N_2 purging and stirring system. The cell used a 3.2 mm diameter glassy carbon disc as a working electrode, a Ag/AgCl (3 M NaCl) reference electrode ($E°$ = 0.205 V vs NHE),[13] and a Pt wire auxiliary electrode. Electrochemistry was performed to check the purity of Ir^{IV} as described in Chapter 2.

Kinetic studies were performed at 25 ± 0.1 °C on a Hi-Tech SF-51 stopped-flow spectrophotometer in the 1 cm path length configuration with Olis 4300 data acquisition and analysis software. The reaction of DMH with $(NH_4)_2IrCl_6$ was monitored at 488, always maintaining at least a 10-fold molar excess of DMH relative to the Ir^{IV}. All rate

constants reported are the average of at least four runs unless otherwise stated. Least-squares fits of the pseudo-first-order rate constants were performed with the Prism 5 software package,[14] weighting the data proportionally to the inverse square of k_{obs}. When fitting the pH-dependent rate laws, proton concentrations were calculated with the approximation $[H^+] = 10^{-pH}$.

5.3. Results.

5.3.1. Characterization of N,N-dimethylhydroxylamine (DMH). This compound was recrystallized as described in **Sec. 5.2.1**. and subjected to ^{1}H-NMR, ^{13}C-NMR and UV-vis tests. Fig 5.1a and b presents NMR spectra.

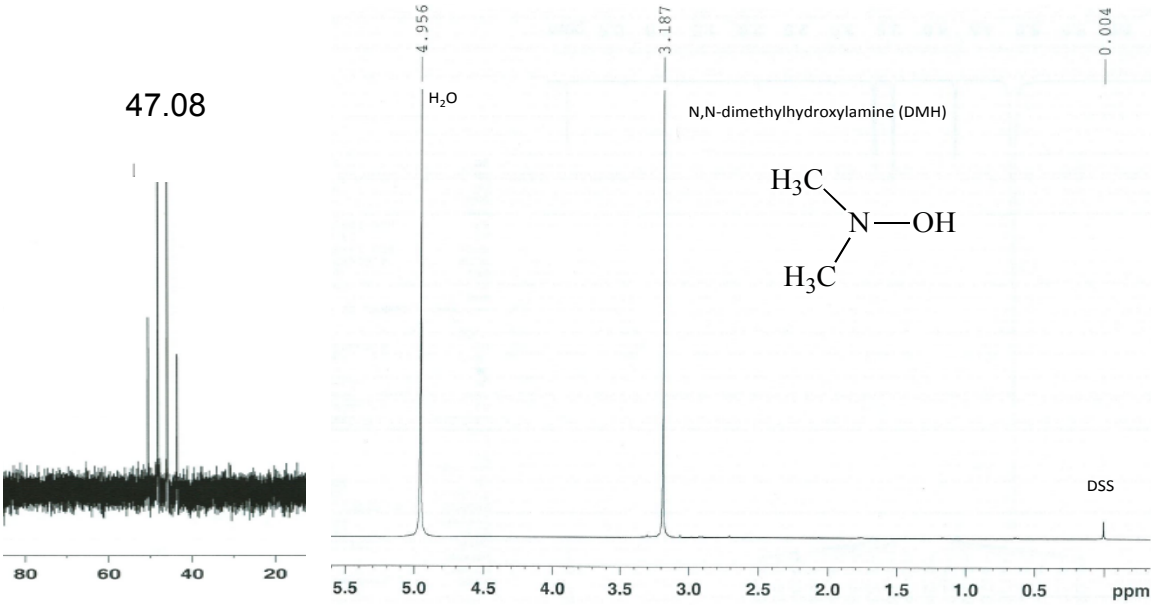

Fig 5.1 a. ^{13}C-NMR: H-coupled b. ^{1}H-NMR

The quartet at δ = 47.08 in the ^{13}C-NMR (Fig 5.1a) and the singlet at 3.18 in the ^{1}H-NMR spectrum (Fig 5.1b) show that the DMH is pure, δ = 4.95 corresponds to water peak. Likewise, the UV-vis spectrum is shown in Fig 5.2.

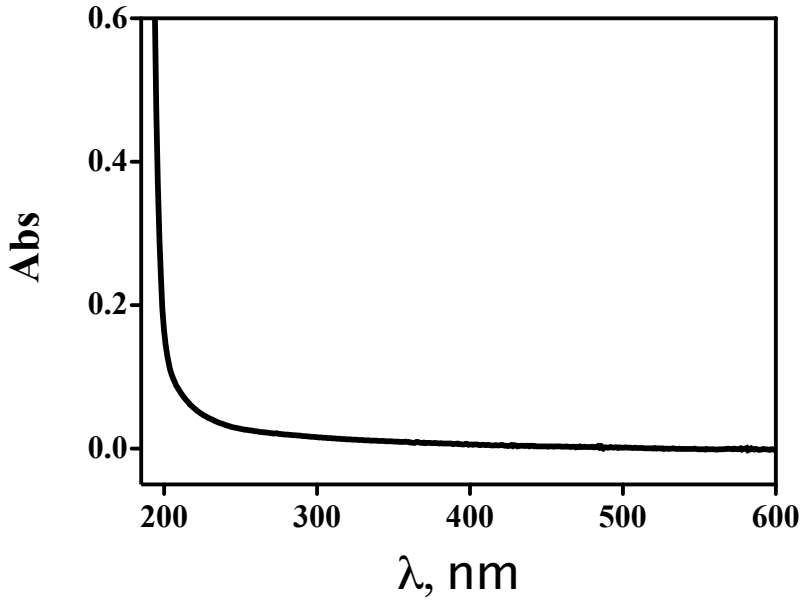

Fig 5.2. UV-vis spectrum of 2 mM aqueous DMH.

5.3.2. Qualitative Features of DMH Reactions with $[IrCl_6]^{2-}$. Rapid color changes take place upon mixing solutions of DMH with $[IrCl_6]^{2-}$. Reduction of Ir^{IV} is signaled by the loss of absorbance at 488 nm. Fig 5.3 illustrates the kinetic decay spectra for the reaction of 0.05 mM Ir^{IV} with 0.5 mM DMH including 1 mM $C_2O_4^{2-}$, 0.1 M $NaClO_4$ acetate buffer at pH 3.8. These results were obtained using a diode array spectrophotometer. The inset shows the kinetic trace for the reaction. Oxygen was eliminated by passing Ar gas through the reactant solutions. 2.0 ml 0.75 mM DMH was transferred to a cuvette and 1.0 mL of 0.15 ml Ir^{IV} was mixed with a syringe making the resulting volume 3.0 ml.

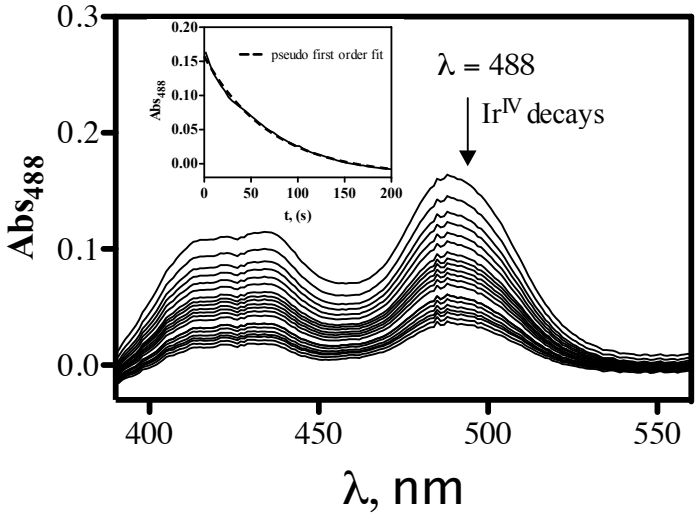

Fig 5.3. Kinetic decay of Ir^{IV} in the reaction of DMH.

$[Ir^{IV}]_0$ = 0.05 mM, [DMH] = 0.5 mM, $[C_2O_4^{2-}]$ = 1 mM, acetate buffer at pH 3.8, μ = 0.1 M ($NaClO_4$). Run time and cycle time equal to 250 and 4 seconds respectively. Inset: kinetic trace of the reaction.

5.3.2.1. Metal Catalysis. Metal-ion catalysis is observed in the oxidation of hydroxylamine[15,16] but no such catalysis has been reported in DMH reactions. Investigations of metal-ion catalysis were conducted with 1 mM DMH, $[Ir^{IV}]$ = 0.1 mM at ionic strength (μ) = 0.1 M ($NaClO_4$) in an acetate buffer at pH 4.7. Various conditions were maintained during tests for the effects of metal ions (Cu^{2+} and Fe^{2+}), Table 5.1. The half-lives for the reactions with 1, 3 and 5 μM Cu^{2+} added were 3.9, 3.2 and 2.4 s respectively. Similarly for the same amounts of added Fe^{2+} the half-lives were 1.1, 0.56 and 0.36 s. In another experiment under the same conditions 1 mM sodium oxalate was applied to test its effectiveness to inhibit the catalysis. The result was that 1 mM $C_2O_4^{2-}$ completely inhibited the catalytic effect of even the added 5 μM Cu^{2+} and Fe^{2+} resulting in good pseudo first-order fits, Fig 5.4 and 5.5. This means that divalent metal ions

present as impurities catalyze the reaction and 1 mM sodium oxalate, (a redox-inert chelator with formation constants[17] for Cu^{2+}/ $C_2O_4^{2-}$: log K_1= 4.85 and log K_2 = 8.85; and Fe^{2+}/ $C_2O_4^{2-}$: log K_1= 3.05 and log K_2 = 5.08) is a perfect choice for the control of such adventitious catalysis. A separate set of experiments was performed to determine the effect of concentration of sodium oxalate on the reaction with the conditions $[Ir^{IV}]_0$ = 0.1 mM, $[DMH]_t$ = 1.0 mM, cacodylate buffer at pH = 5.86 , μ = 0.1 ($NaClO_4$). All the data are listed in Table 5.2. The concentration of $Na_2C_2O_4$ had no affect on the reaction and 1 mM of this salt if added to the reaction, is adequate to suppress the catalysis (Fig 5.6). All further investigations were performed in the presence of 1 mM oxalate as an chelator to inhibit the catalysis by metal-ion impurities.

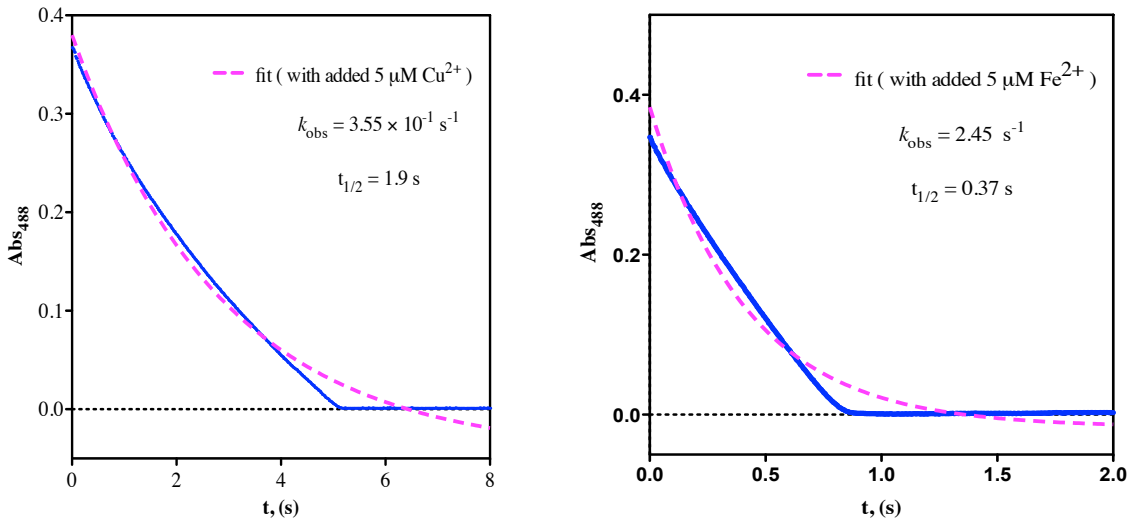

a. added 5 μM Cu^{2+} b. added 5 μM Fe^{2+}

Fig 5.4. The effect of metal ions in the reaction of DMH with Ir^{IV}**.** N,N-Dimethylhydroxylamine [DMH] = 1.0 mM, hexachloroiridate $[Ir^{IV}]_0$ = 0.1 mM, acetate buffer (10 mM), pH = 4.7 and ionic strength (μ) = 0.1 M ($NaClO_4$). Fe^{2+} = $Fe(NH_4)_2(SO_4)_2$**.** $6H_2O$ and Cu^{2+} = $CuSO_4$.

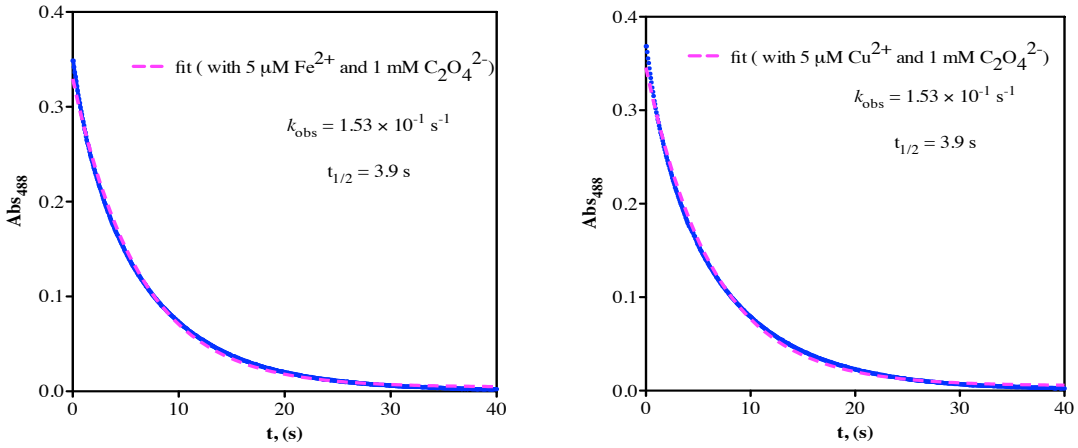

a. 5 μM added Fe^{2+} with 1 mM $C_2O_4^{2-}$ b. 5 μM added Cu^{2+} with 1 mM $C_2O_4^{2-}$

Fig 5.5. 1 mM sodium oxalate is adequate to inhibit the catalysis by added metal ions.

[DMH] = 1.0 mM, $[Ir^{IV}]_0$ = 0.1 mM, $[C_2O_4^{2-}]$ = sodium oxalate salt, acetate buffer (10 mM), pH = 4.7 and ionic strength (μ) = 0.1 M ($NaClO_4$). Fe^{2+} = $Fe(NH_4)_2(SO_4)_2.6H_2O$ and Cu^{2+} = $CuSO_4$.

Table 5.1. Kinetic Data for Cu^{2+} and Fe^{2+} Catalysis Test in the Reaction of Ir^{IV} with $[DMH]_t$.[a]

Expt	$[Cu^{2+}]$, μM	$[Fe^{2+}]$, μM	$[C_2O_4^{2-}]$, mM	$t_{1/2}$, s	k_{obs}, s^{-1}	fit
1.	0.0	0.0	0.0	3.8	1.57×10^{-1}	good
2.	0.0	0.0	1.0	3.9	1.50×10^{-1}	good
3.	1.0	0.0	0.0	3.2	2.07×10^{-1}	bad
4.	3.0	0.0	0.0	2.4	2.59×10^{-1}	bad
5.	5.0	0.0	0.0	1.9	3.55×10^{-1}	bad
6.	5.0	0.0	1.0	3.9	1.53×10^{-1}	good
7.	0.0	1.0	0.0	1.1	9.19×10^{-1}	bad
8.	0.0	3.0	0.0	0.56	1.89	bad
9.	0.0	5.0	0.0	0.37	2.45	bad
10.	0.0	5.0	1.0	3.9	1.53×10^{-1}	good

[a] Dimethylhydroxylamine, $[DMH]_t$ = 1.0 mM, hexachloroiridate $[Ir^{IV}]_0$ = 0.1 mM, $C_2O_4^{2-}$ = sodium oxalate, acetate buffer (10 mM), pH = 4.7 and ionic strength (μ) = 0.1 M ($NaClO_4$).

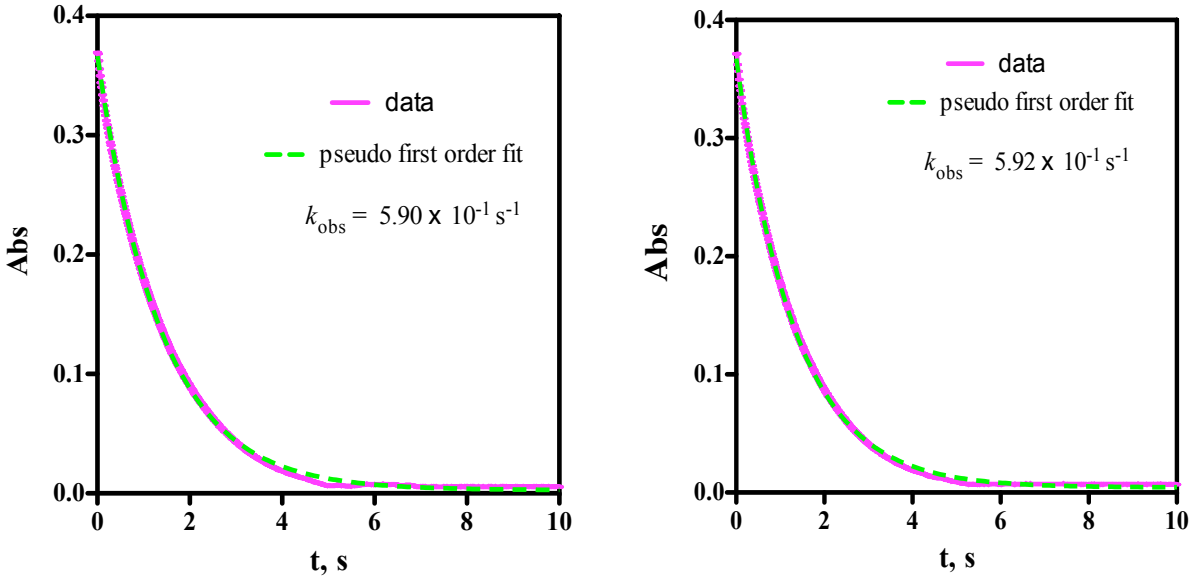

a. 1 mM $C_2O_4^{2-}$ **b**. 4 mM $C_2O_4^{2-}$

Fig 5.6. Concentration of sodium oxalate ($Na_2C_2O_4$) has no effect in the reaction of DMH and Ir^{IV} $[Ir^{IV}]_0 = 0.1$ mM, $[DMH]_t = 1.0$ mM, cacodylate buffer at pH = 5.86 , $\mu = 0.1$ ($NaClO_4$)

Table 5.2. Kinetic Data for the Effect of Sodium Oxalate ($Na_2C_2O_4$) Concentration in the Reaction of Ir^{IV} with [DMH].[a]

Expt	$[C_2O_4^{2-}]$, mM	$t_{1/2}$, s	k_{obs}, s^{-1}	fit	pH
1.	0.0	0.93	7.71×10^{-1}	good	5.90
2.	1.0	1.2	5.90×10^{-1}	good	5.86
3.	2.0	1.2	5.89×10^{-1}	good	5.86
4.	4.0	1.2	5.92×10^{-1}	good	5.86

[a] $[Ir^{IV}]_0 = 0.1$ mM, $[DMH]_t = 1.0$ mM, cacodylate buffer at pH = 5.86, $\mu = 0.1$ M ($NaClO_4$).

5.3.3. Product Analysis and Stoichiometry.

5.3.3.1 Product Analysis. A ^{1}H-NMR experiment was performed on a solution of 1.0 mM DMH, 2.0 mM Ir^{IV}, and 1 mM $C_2O_4^{2-}$ with 0.07 mM DSS in D_2O that was allowed to react. Ir^{IV}, DSS and $C_2O_4^{2-}$ were dissolved in D_2O, the resulting solution was sparged with Ar gas in a bubbling flask and then a weighed amount of solid DMH was added to it. The ^{1}H NMR spectrum of the product mixture (Fig 5.7) shows distinct peaks at δ = 3.74, 6.78 and 6.87 ppm which are characteristic of methyl and methylene groups of nitrone $(CH_3N(O)\text{-}CH_2)^4$ respectively The peak at δ = 2.98 ppm was identified as N-methylhydroxylamine (CH_3NHOH), which was confirmed by spiking the product with authentic sample of N-methylhydroxylamine because the integration value of the peak at δ = 2.98 ppm after adding CH_3NHOH to the product increased from 0.95 to 12.95, Fig 5.8. The peak at δ = 3.18 ppm corresponds to residual N,N-dimethylhydroxylamine (DMH). The nitrone was found to be stable until 24 hours. The spectra of the authentic samples of DMH and N-methylhydroxylamine are given in the appendix.

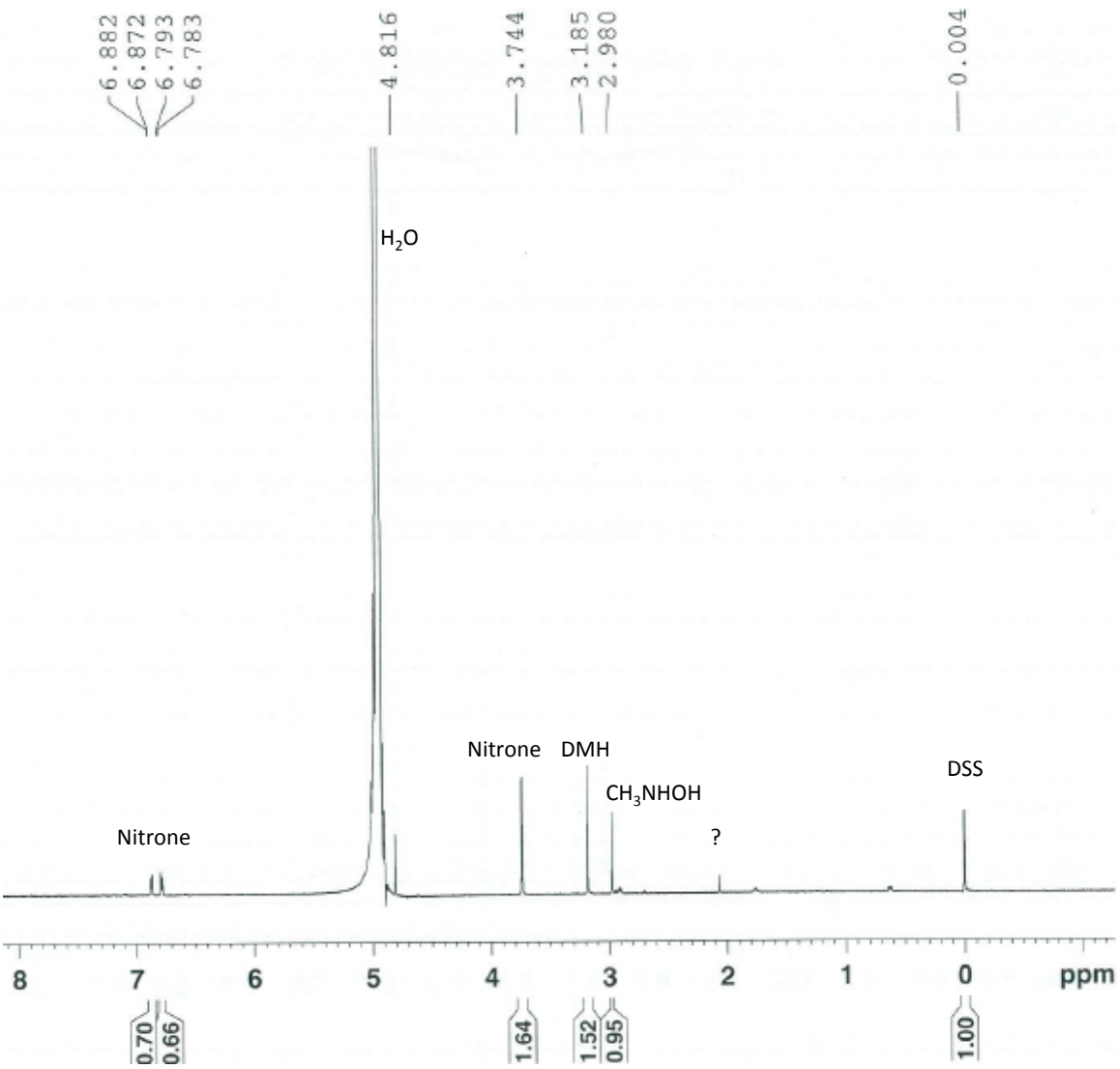

Fig 5.7. ^{1}H NMR spectrum of the product in the reaction of DMH with Ir^{IV}.

1.0 mM DMH, 2.0 mM Ir^{IV}, and 1 mM $C_2O_4^{2-}$ with 0.07 mM DSS in D_2O at pH 3.3.

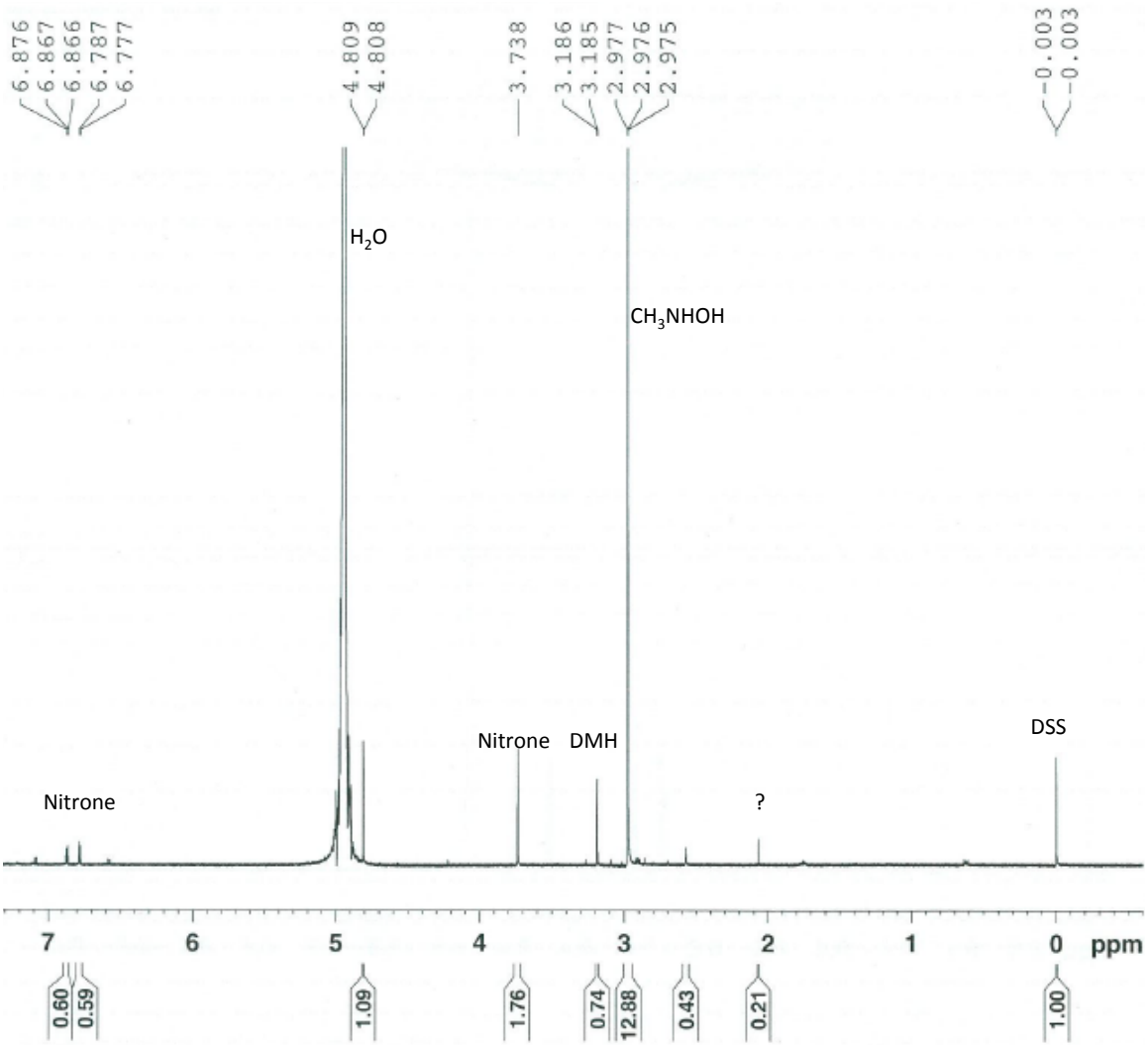

Fig 5.8. ^{1}H NMR spectrum of the product spiked with N-methylhydroxylamine (CH_3NHOH) in the reaction of DMH with Ir^{IV}. 1.0 mM DMH, 2.0 mM Ir^{IV}, and 1 mM $C_2O_4^{2-}$ with 0.07 mM DSS in D_2O.

Using excess DMH (1.1 mM) over Ir^{IV} (0.1 mM), the Ir-containing product was identified and determined from UV-vis spectroscopy. For the UV-vis study, a buffered solution of 0.10 mM Ir^{IV} at 4.8 pH (acetate) with 1 mM $C_2O_4^{2-}$ and 0.1 M $NaClO_4$ was

prepared and its spectrum was recorded, orange spectrum in the Fig 5.9. The green spectrum is the resulting product of the mixture of Ir^{IV} and DMH. Similarly, the red represents the DMH sample before mixing with Ir^{IV} and green after mixing, i.e. product. Purple is authentic sample of $[Ir^{III}Cl_6]^{3-}$ with DMH. The Ir^{III} sample spectrum (purple) is quite similar to the product spectrum obtained from the reaction of DMH and Ir^{IV}. This demonstrates that the $Ir^{IV}$is reduced to Ir^{III} by DMH.

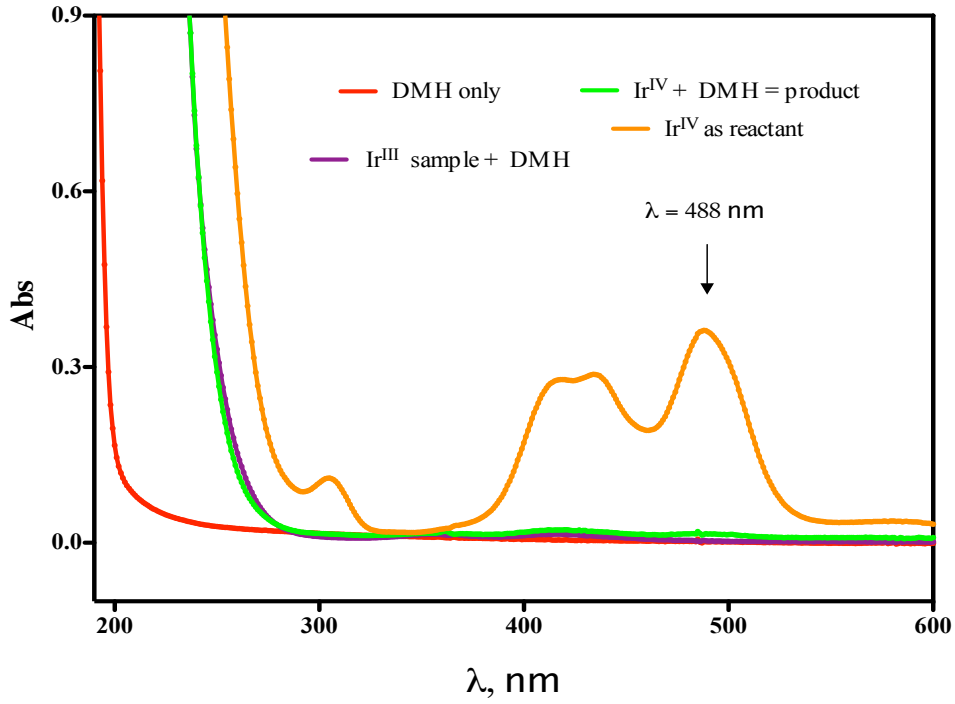

Fig 5.9. UV-vis spectral changes in the reaction of DMH with Ir^{IV}. Orange = Ir^{IV}, green = product solution, purple = Ir^{III} and red = DMH.

$[DMH]_0$ = 1.1 mM, $[Ir^{IV}]$ = 0.10 mM, acetate buffer at pH 4.8. $C_2O_4^{2-}$ (1 mM) and $NaClO_4$ (0.1 M) were added to Ir^{IV}.

Further evidence of reduction of Ir^{IV} to Ir^{III} is provided by the quantitative recovery of Ir^{IV} by chlorination of the product solution (supposed to be Ir^{III}) given in Fig 5.10. For example, the absorbance of 0.1 mM Ir^{IV}(as reactant) at 488 nm was 0.363 and the absorbance of the recovered Ir^{IV} at the same wavelength was 0.369. This is within 2% error.

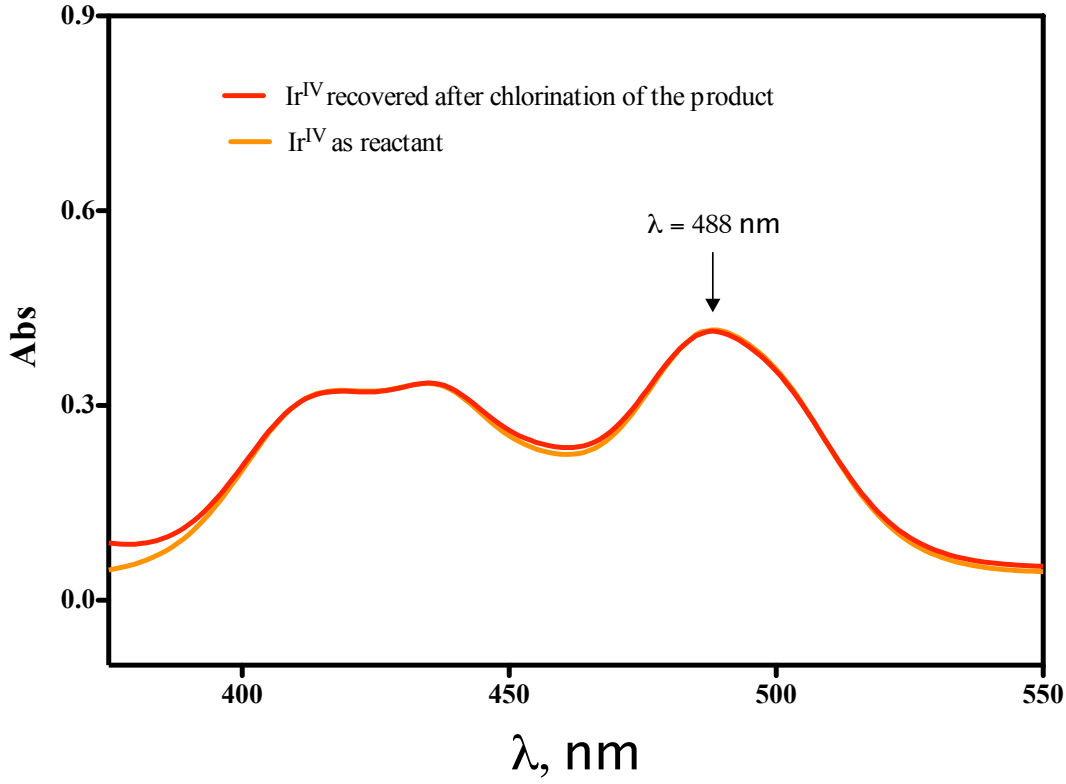

Fig 5.10. Quantitative conversion of Ir^{IV} to Ir^{III} in the reaction of Ir^{IV} with DMH. $[DMH]_0 = 1.1$ mM, $[Ir^{IV}]_0 = 0.10$ mM, acetate buffer at pH 4.8. $C_2O_4^{2-}$ (1 mM) and $NaClO_4$ (0.1 M) were added to Ir^{IV}.

5.3.3.2 Stoichiometry. A spectrophotometric titration was performed at pH 4.2 (buffer maintained with DMH/NaOH) with 1 mM oxalate. 2.0 mL of 0.493 mM DMH was transferred to a cuvette and titrated under Ar with a 2.19 mM solution of Ir^{IV} (Fig 5.11). A fixed aliquot of Ir^{IV} solution was added each time to the cuvette with a syringe. These spectra show a weak absorbance increase at 420 nm connected with the formation of $[Ir^{III}Cl_6]^{3-}$,[18,19] at the endpoint the spectra begin to show a much larger absorbance increase which is due to the accumulation of excess Ir^{IV}. At the end point, 0.986 mmol DMH consumed 1.86 mmol Ir^{IV} and according to which the consumption ratio ($\Delta[Ir^{IV}]/\Delta[DMH]_t$) was found to be 1.9 ± 0.1. All titration data are presented in Table 5.3.

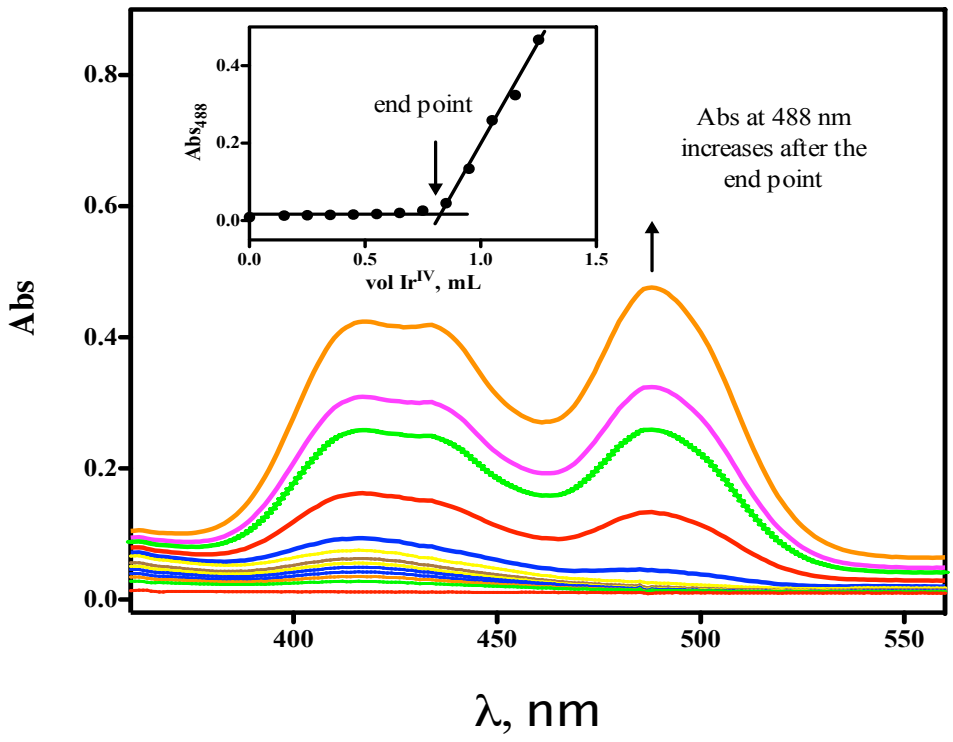

Fig 5.11. Stoichiometry determination (spectrophotometric titration) between the reaction of Ir^{IV} and DMH at pH 4.2 (DMH/NaOH buffer). Inset: plot of titration data. 1 mM oxalate, 2.0 mL of 0.493 mM DMH and 2.19 mM Ir^{IV}. End point 0.85 mL of Ir^{IV}.

From the above results, the overall oxidation of DMH by $[IrCl_6]^{2-}$ under

anaerobic conditions is given by eq 5.1.

$$(CH_3)_2NOH + 2[IrCl_6]^{2-} \longrightarrow H_3CN(O)CH_2 + 2[IrCl_6]^{3-} + 2H^+ \quad (5.1)$$

$$H_3CN(O)CH_2 + H_2O \rightleftharpoons H_3CNHOH + CH_2O \quad (5.1a)$$

Table 5.3. Spectrophotometric Titration Data for the Stoichiometry Determination in the Reaction of $[Ir^{IV}]$ with $[DMH]_t$[a]

Expt.	$V(Ir^{IV})$, mL	Absorbance (λ = 488 nm)
1.	0.00	9.30×10^{-3}
2.	0.15	1.30×10^{-2}
3.	0.25	1.43×10^{-2}
4.	0.35	1.45×10^{-2}
5.	0.45	1.62×10^{-2}
6.	0.55	1.75×10^{-2}
7.	0.65	1.98×10^{-2}
8.	0.75	2.60×10^{-2}
9.	0.85	4.52×10^{-2}
10.	0.95	1.34×10^{-1}
11.	1.05	2.59×10^{-1}
12.	1.15	3.24×10^{-1}
13.	1.25	4.76×10^{-1}

[a][Anaerobic titration of DMH by Ir^{IV}. pH = 4.2 (DMH/NaOH buffer), [oxalate] = 1 mM. $[Ir^{IV}]$ = 2.19 mM and 2.0 mL of 0.493 mM $[DMH]_t$. Endpoint at 0.85 mL of Ir^{IV}.

5.3.4. Kinetics. A typical kinetic trace of the reaction of DMH with $[IrCl_6]^{2-}$ is shown with its pseudo-first order fit in Fig 5.12. This trace was obtained when 1.0 mM DMH was mixed with 0.1 mM Ir^{IV}. The conditions were cacodylate buffer at pH 5.8, 0.1 M ($NaClO_4$) ionic strength and 1 mM oxalate. The pseudo-first order fit was in good agreement with the data. At least a 10-fold excess of DMH over $[IrCl_6]^{2-}$ and 1 mM oxalate were used in all kinetic experiments.

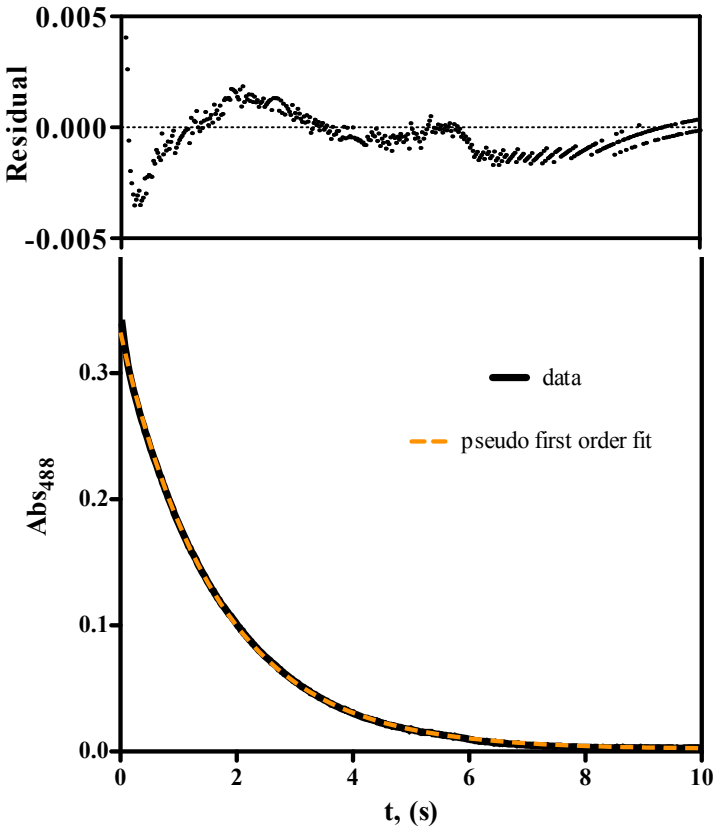

Fig 5.12. Kinetic trace in the reaction of DMH with Ir^{IV}.

Upper box: residuals. Lower box: kinetic trace with pseudo-first order fit. 1 mM DMH with 1 mM $C_2O_4^{2-}$, pH 5.88 (cacodylate buffer), $[Ir^{IV}]_0 = 0.1$ mM, $\mu = 0.1$ M ($NaClO_4$).

The pseudo-first order rate law is given by the eq 5.2.

$$-\frac{d[\mathrm{Ir^{IV}}]}{dt} = k_{obs}\,[\mathrm{Ir^{IV}}] \qquad (5.2)$$

5.3.4.1. DMH Dependence. Oxidations of DMH by Ir^{IV} were conducted varying the concentration of DMH from 0.50 – 5.0 mM in acetate buffer at pH 4.8, 1 mM oxalate and ionic strength 0.1 M ($NaClO_4$). All the data are listed in the Table 5.4. $k_{obs,}$ plotted against $[DMH]_t$ (Fig 5.13) increases linearly indicating a first-order dependence on $[DMH]_t$ in accordance with eq 5.3.

Table 5.4. Data for the DMH Dependent Kinetics with Ir^{IV} [a]

Expt.	$[DMH]_t$, mM	k_{obs} , s^{-1}
1.	0.5	0.111
2.	1.0	0.193
3.	2.0	0.237
4.	3.0	0.487
5.	4.0	0.575
6.	5.0	0.743

[a] $[Ir^{IV}]_0$ = 0.063 mM, $[DMH]_t$ = (0.50 – 5.0) mM, acetate buffer at pH 4.8, μ = 0.1 M ($NaClO_4$), $[C_2O_4^{2-}]$ = 1 mM.

$$k_{obs} = k[DMH]_t \quad (5.3)$$

where, $k[DMH]_t = k_1[DMH] + k_2[DMH\text{-}H^-]$ because

$[DMH]_t$ has two kinetically active species: [DMH] and $[DMH\text{-}H^-]$

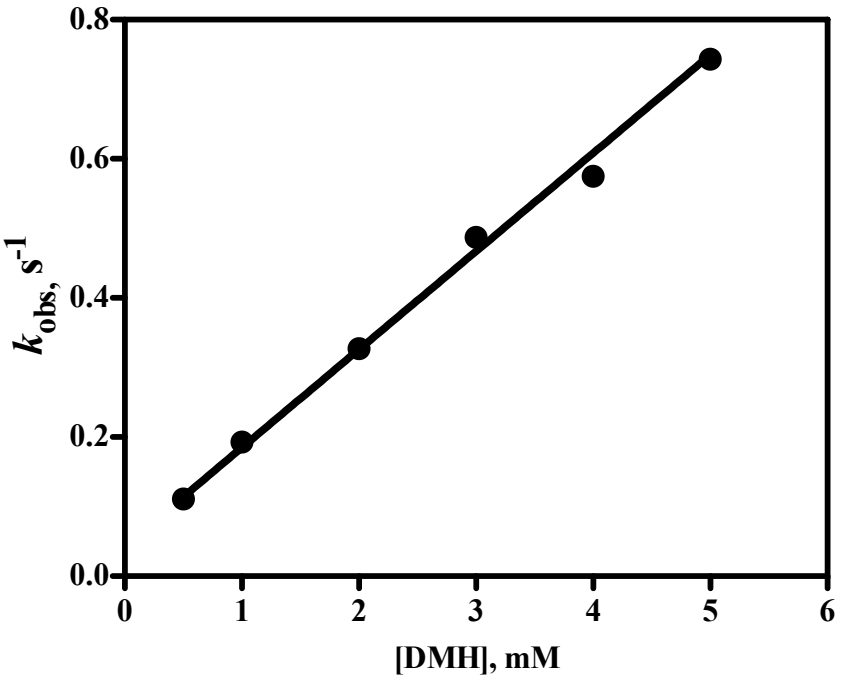

Fig 5.13. DMH dependent kinetics in the reaction of DMH with Ir^{IV}

$[Ir^{IV}]_0$ = 0.063 mM, $[DMH]_t$ = (0.50 – 5.0) mM, acetate buffer at pH 4.8, μ = 0.1 M ($NaClO_4$). $[C_2O_4^{2-}]$ = 1 mM. Slope = (1.4 ± 0.04) × 10^2 M^{-1} s^{-1} and intercept = 0.044 ± 0.006 s^{-1}

5.3.4.2. pH Dependence. An investigation of the pH dependence of k_{obs} was performed over a range of pH (3.68- 7.86) with $[Ir^{IV}]_0$ = 0.1 mM, $[DMH]_t$ = 0.5-7.0 mM, $[C_2O_4^{2-}]$ = 1 mM and μ = 0.1 M ($NaClO_4$) with appropriate buffers. The kinetic data are summarized in Table 5.4. An excellent fit of the data with the eq 5.20 was obtained for a

plot log{k_{obs}/DMH]$_t$}vs pH. The fit equation was obtained considering the pK_a = 5.2[20] and applying the approximation [H^+] = 10^{-pH}. The fit (Fig 5.14) demonstrates that the rate increases with the increase of pH showing a plateau region around pH 6. The pH resolved 2nd order rate constants are k_1 = (5.19 ± 0.15) × 10^2 M^{-1} s^{-1} and k' = (4.45 ± 0.28) × 10^{-5} s^{-1}.

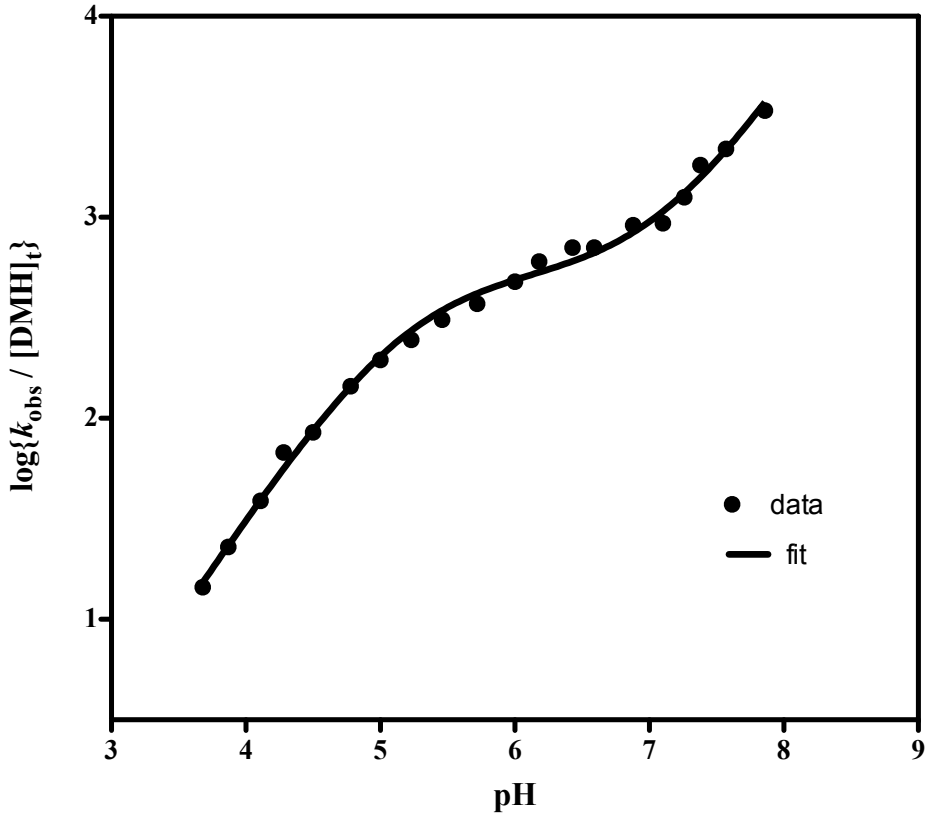

Fig 5.14. pH dependent kinetic reactions of Ir^{IV} with [DMH]$_t$. pH 5.9 - 7.33 (cacodylate), 7.0 - 7.8 (gly-gly), 3.6 - 4.28 (chloroacetate) and 4.3 - 5.7 (acetate) buffer used. DMH molarity varies, [Ir^{IV}]$_0$ = 0.1 mM, ionic strength = 0.1 M ($NaClO_4$) and [$C_2O_4^{2-}$] = 1 mM.

Table 5.5. pH Dependent Kinetic Reactions of Ir^{IV} with $[DMH]_t$ [a]

pH	k_{obs} s^{-1}	$[DMH]_t$	k_{obs} / $[DMH]_t$	$\log\{k_{obs} / [DMH]_t\}$
	s^{-1}	mM	M^{-1} s^{-1}	
3.68	7.25×10^{-2}	5.0	14.5	1.16
3.87	1.14×10^{-1}	5.0	22.8	1.36
4.11	1.96×10^{-1}	5.0	39.2	1.59
4.28	3.35×10^{-1}	5.0	67.0	1.83
4.50	5.95×10^{-1}	7.0	85.0	1.93
4.78	7.26×10^{-1}	5.0	1.45×10^{2}	2.16
5.00	9.91×10^{-1}	5.0	1.98×10^{2}	2.29
5.23	1.24	5.0	2.48×10^{2}	2.39
5.46	1.55	5.0	3.10×10^{2}	2.49
5.72	1.87	5.0	3.74×10^{2}	2.57
6.00	2.42	5.0	4.48×10^{2}	2.68
6. 18	6.06×10^{-1}	1.0	6.06×10^{2}	2.78
6.43	7.14×10^{-1}	1.0	7.14×10^{2}	2.85
6.59	7.50×10^{-1}	1.0	7.05×10^{2}	2.85
6.88	9.27×10^{-1}	1.0	9.27×10^{2}	2.96
7.10	9.36×10^{-1}	1.0	9.36×10^{2}	2.97
7.26	1.26	1.0	1.26×10^{3}	3.10
7.38	9.01×10^{-1}	0.5	1.80×10^{3}	3.20

Table 5.5. pH Dependent Kinetic Reaction of Ir^{IV} with $[DMH]_t$ Contd…

pH	k_{obs}, s^{-1}	$[DMH]_t$, mM	k_{obs} / $[DMH]_t$, M^{-1} s^{-1}	log{k_{obs} / $[DMH]_t$}
7.57	2.18	1.0	2.18×10^3	3.34
7.86	3.36	1.0	3.36×10^3	3.53

[a]pH from 3.6 - 4.28, chloroacetate; 4.3 - 5.7, acetate; 5.9 - 7.3, cacodylate and 7.5 – 7.8, gly-gly buffer (Buffer concentration = 10 mM). μ = 0.1 M ($NaClO_4$), [Ir^{IV}] = 0.10 mM. and [$C_2O_4^{2-}$]= 1 mM, [DMH] = 0.5 – 7.0 mM

Fit equation.

$$\frac{k_{obs}}{[DMH]_t} = \frac{k_1 K_{a1}}{[H^+] + K_{a1}} + \frac{k' K_{a1}}{[H^+]\{[H^+] + K_{a1}\}}$$

Adjusting K_{a1} (pK_a = 5.2 and $K_a = 10^{-pKa}$) in the above eqn gives

$$\frac{k_{obs}}{[DMH]_t} = [(\{k_1(10^{-X}) \text{ x } 6.31e\text{-}6\} + k' \text{ x } 6.31e\text{-}6)/ ((10^{-X}) \{(10^{-X}) + 6.31e\text{-}6\})]$$

Where X = pH

Fit values

$k_1 = (5.19 \pm 0.15) \times 10^2$ M^{-1} s^{-1}

$k' = (4.45 \pm 0.28) \times 10^{-5}$ s^{-1}

5.3.5. Proposed Mechanism. Electron transfer schemes with $1e^-$ oxidant can be postulated as follows:

$$(CH_3)_2NOH \; - \; e^- \longrightarrow (CH_3)_2NO^{\bullet} \; + \; H^+ \qquad (5.4)$$

$$(CH_3)_2NO^{\bullet} \; - \; e^- \longrightarrow H_3CN(O)CH_2 \; + \; H^+ \qquad (5.5)$$

Further details,

Mechanism of the k_1 Term:

$$(CH_3)_2NOH_2^+ \rightleftharpoons (CH_3)_2NOH \; + \; H^+ \qquad K_{a1} \qquad (5.6)$$

$$(CH_3)_2NOH \; + \; Ir^{IV} \longrightarrow (CH_3)_2NOH^{\bullet +} \; + \; Ir^{III} \qquad k_1 \qquad (5.7)$$

$$(CH_3)_2NOH^{\bullet +} \longrightarrow (CH_3)_2NO^{\bullet} \; + \; H^+$$

$$(CH_3)_2NO^{\bullet} \; + \; Ir^{IV} \longrightarrow H_3CN(O)CH_2 \; + \; Ir^{III} \; + \; H^+ \qquad k'_1, \text{ fast} \qquad (5.8)$$

The product nitrone hydrolyses to give N-methylhydroxylamine and formaldehyde

$$H_3CN(O)CH_2 \; + H_2O \rightleftharpoons H_3CNHOH \; + \; CH_2O \qquad (5.9)$$

Mechanism of the k_2 Term:

$$(CH_3)_2NOH \rightleftharpoons (CH_3)_2NO^- \; + \; H^+ \qquad K_{a2} \qquad (5.10)$$

$$(CH_3)_2NO^- \; + \; Ir^{IV} \longrightarrow (CH_3)_2NO^{\bullet} \; + \; Ir^{III} \qquad k_2 \qquad (5.11)$$

Derivation of eqn 5.12.

According eqn 5.3

$$k_{obs} = k[DMH]_t$$

$$= k_1[DMH] + k_2[DMH\text{-}H^-]$$

$$\text{where,} \quad k = \frac{k_1 K_{a1}}{[H^+] + K_{a1}} + \frac{k' K_{a1}}{[H^+]\{[H^+] + K_{a1}\}} \qquad (5.12)$$

In acidic medium protonated DMH is in equilibrium

$$HDMH^+ \rightleftharpoons DMH + H^+ \qquad K_{a1} \qquad (5.13)$$

$$\text{and} \quad [HDMH^+] = \frac{[H^+][DMH]}{K_{a1}} \qquad (5.14)$$

Similarly, at higher pH DMH equilibrates as

$$DMH \rightleftharpoons DMH\text{–}H^- + H^+ \qquad K_{a2} \qquad (5.15)$$

$$\text{and} \quad [HDM-H^-] = \frac{K_{a2}[DMH]}{[H^+]} \qquad (5.16)$$

$[DMH]_t$ includes protonated and neutral DMH, eqn 5.17

$$[DMH]_t = [HDMH^+] + [DMH] \qquad (5.17)$$

Putting the value of $[HDMH^{+}]$ from eqn 5.14 in eqn 5.17 and solving it leads to eqn 5.18.

$$[DMH]_t = \frac{[H^+][DMH]}{K_{a1}} + [DMH]$$

$$= [DMH]\left[\frac{[H]^+}{K_{a1}} + 1\right]$$

$$\text{and } [DMH] = \frac{K_{a1}[DMH]_t}{[H^+] + K_{a1}} \qquad (5.18)$$

DMH reacts with Ir^{IV} to generate the radical ($DMH^{\bullet}$) per eqns 5.7 and 5.11, according to which, the rate law is:

$$-\frac{d[Ir^{IV}]}{dt} = k_1\,[Ir^{IV}][DMH] + k_2\,[Ir^{IV}]\left[DMH - H^-\right] \qquad (5.19)$$

From eqns 5.3 and 5.16 and 5.18 gives eqn 5.20.

$$k_{obs} = \frac{k_1 K_{a1}[DMH]_t}{[H^+] + K_{a1}} + \frac{k_2 K_{a2}[DMH]}{[H^+]}$$

$$= \frac{k_1 K_{a1}[DMH]_t}{[H^+] + K_{a1}} + \frac{k_2 K_{a2}\left(\frac{K_{a1}[DMH]_t}{[H^+] + K_{a1}}\right)}{[H^+]}$$

$$= \left(\frac{k_1 K_{a1}}{[H^+] + K_{a1}} + \frac{k' K_{a1}}{[H^+]\{[H^+] + K_{a1}\}}\right)[DMH]_t \text{ where, } k' = k_2\,K_{a2} \qquad (5.20)$$

5.4. Conclusions.

The reaction of N,N-dimethylhydroxylamine hydrochloride with Ir^{IV} is catalyzed by Cu^{2+} and Fe^{2+} and such catalysis can be inhibited with 1 mM sodium oxalate. The rate law is first order with respect to each reactant. The electron transfer process is supposed to proceed through the intermediate dimethyl nitroxyl radical leading to the product nitrone.

References.

1. Mitzel, N. W.; Smart, B. A.; Parsons, S.; Robertson, H. E.; Rankin, D.W. *J. Chem. Soc., Perkin Trans. 2*, **1996**, 2727.
2. Liu, J.; He, H.; Tang, H.; Chen, Y. *J. Radioanal. Nucl. Chem.* **2011**, *288,* 351.

2a. http://www.oecd-nea.org/science/docs/2012/nsc-wpfc-doc2012 15.pdf

3. Gaoliang, L.; Hui, H. *J. Radioanal. Nucl. Chem.* **2011**, *287,* 673.
4. Zauche,T. H.; Espension, H. *Inorg. Chem*. **1997**, *36*, 5257.

4a. Sayo, H.; Ozaki, S.; Masui, M. *Chem. Pharm. Bull.* **1973**, *21,* 415.

5. Zhang, A.; Xiao, G.; Hu, J.; He, H. *J. Radioanal. Nucl. Chem.* **2003**, *256,* 587.
6. Zuo, C.; Yan, T.; Zheng, W.; Li, C.; Wang, X. *J. Radioanal. Nucl. Chem.* **2010**, *283,* 417.
7. Chen, Y.; Tang, H.; Liu, J.; He, H. *J. Radioanal. Nucl. Chem.* **2011**, *289,* 41.
8. Koltunov, V. S.; Baranov, S. M.; Shapovalov, M. P. *Radiochemistry*, **1993**, *35*, 422.
9. Koltunov, V. S.; Baranov, S. M.; Zharova, T. P.; Abramina, E. V. *Radiochemistry*, **1993**, *35*, 408.
10. Wang, J. H.; Wu, M. H.; Bao, B. R.; Li, Zh.; Wang, Q. Y.; Ye, G. A. *J. Radioanal. Nucl. Chem.* **2007**, *273,* 371.
11. Wang, J. H.; Li, Q.; Wu, M. H.; Xu, G; Li, Ch.; Bao, B. R.; Zheng, W. F.; He, H.; Zhang, Sh. D. *J. Radioanal. Nucl. Chem.* **2012**, *292,* 249.

12. Kauffman, G. B.; Teter, L. A. *Inorg*. *Synth*. **1966**, *8*, 223.

13. Sawyer, D. T.; Sobkowiak, A.; Roberts, J. L. *Electrochemistry for Chemists, 2nd ed*, John Wiley and Sons: New York, 1995; pp 192.
14. *Prism 5,* GraphPad Software, Inc.: San Diego, CA, 2010.

15. Makarycheva-Mikhailova, A. V.; Stanbury, D. M.; Mckee, M. L. *J. Phys. Chem. B* **2007**, *111*, 6942.

16. Hung, M. L.; Mckee, M. L.; Stanbury, D. M. *Inorg. Chem*. **1994**, *33*, 5108.

17. Martell, A. E.; Smith, R. M.; Motekaitis, R. J.; *NIST Critically Selected Stability Constants of Metal Complex Database, 7.0;* U.S. Department of Commerce: Gaithersburg, MD, 2003.

18. Bhattarai, N.; Stanbury, D. M. *Inorg Chem*. **2012**, *51*, 13303.

19. Poulsen, I. A.; Garner, C. S. *J. Am. Chem. Soc*. **1962**, *84*, 2032.

20. Bissot, T. C.; Parry, R. W.; Campbell, D. H. *J. Am. Chem. Soc.* **1957**, *79*, 796.

Appendix A

Further Experimental Details Relating to Chapters 2 - 5

Table A-1. Spectrophotometric Titration Data for the Stoichiometry Determination in the Reaction of $[Ir^{IV}]$ with $[GSH]_t$[a]

Expt.	Vol Ir^{IV}, mL	Absorbance (λ = 488 nm)
1.	0.00	1.8×10^{-2}
2.	0.10	1.9×10^{-2}
3.	0.20	2.2×10^{-2}
4.	0.30	2.5×10^{-2}
5.	0.40	2.8×10^{-2}
6.	0.50	2.8×10^{-2}
7.	0.60	2.9×10^{-2}
8.	0.70	3.1×10^{-2}
9.	0.80	3.3×10^{-2}
10.	0.90	0.277
11.	1.00	0.763
12.	1.10	1.34

[a][Anaerobic titration of GSH by Ir^{IV}. pH = 4.8 (acetate buffer), [dipic] = 1 mM. $[Ir^{IV}]$ = 4.67 mM and 2.0 mL of 0.276 mM $[GSH]_t$. Endpoint at 0.84 mL Ir^{IV}.

Table A-2. The Reaction of GSSG with $[IrCl_6]^{2-}$ [a]

sample	Abs (488, nm)	*t*, min.
GSSG (0.15 mM + 1 mM dipic)	3.21×10^{-4}	
Ir^{IV} 0.17 mM	0.585	
Ir^{IV} + GSSG, fresh	0.615	0.0
Ir^{IV} + GSSG	0.614	5.0
Ir^{IV} + GSSG	0.609	24
Ir^{IV} + GSSG	0.608	60

[a] [GSSG] = 0.15 mM, $[Ir^{IV}]$ = 0.17 mM with 1 mM dipic. Ir^{IV} solution prepared in cacodylate buffer at pH 5.0

Table A-3. Data for the Blank Test with Ir^{IV}.[a]

Expt	vol Ir^{IV}, mL	$[Ir^{IV}]$, mM	$Abs_{corrected}$ (λ = 488 nm)
1.	0.00	0.00	9.0×10^{-3}
2.	0.25	2.96×10^{-2}	1.18×10^{-1}
3.	0.50	5.95×10^{-2}	2.37×10^{-1}
4.	0.75	9.02×10^{-2}	3.59×10^{-1}
5.	1.0	1.23×10^{-1}	4.83×10^{-1}

[a] 20 mM acetate buffer, μ = 0.1 M ($NaClO_4$), 1 mM dipic, no GSH.
$[Ir^{IV}]$ = 0.24 mM (0.25 mL aliquot of 0.24 mM Ir^{IV} added to 2.0 mL blank solution (without GSH) kept in a cuvette at a time).

Table A-4. Data for the Stability Check of the Aqueous $[Fe^{III}(bpy)_2(CN)_2]^+$

Fe(III) solution 's age	Abs at (nm)		
	394	522	544
Fresh	0.449	9.02×10^{-2}	9.16×10^{-2}
15 minutes	0.444	8.99×10^{-2}	9.15×10^{-2}
45 minutes	0.443	9.12×10^{-2}	9.26×10^{-2}
70 mimutes	0.442	9.16×10^{-2}	9.29×10^{-2}
2 hrs	0.447	9.23×10^{-2}	9.29×10^{-2}
24 hrs	0.456	1.17×10^{-1}	1.12×10^{-1}

$[[Fe^{III}(bpy)_2(CN)_2]^+] = 3.4 \times 10^{-4}$ M in water.

Table A-5. Data for the Stability Check of the Aqueous $[Fe^{III}(bpy)(CN)_4]^-$

Fe(III) sol 's age	Abs at (nm)		
	375	416	482
Fresh	0.896	0.575	6.87×10^{-2}
10 minutes	0.895	0.575	6.88×10^{-2}
2 hrs	0.898	0.575	7.03×10^{-2}

$[[Fe^{III}(bpy)(CN)_4]^-] = 5.8 \times 10^{-4}$ M / H_2O

Table A-6. Data for the Stability Check of the Aqueous $[Fe^{III}(bpy)(CN)_4]^-$ with EDTA[a]

Solution (with time)	Abs (λ = 482 nm)
Fresh	1.63×10^{-2}
1 hr	1.98×10^{-2}
2 hrs	2.28×10^{-2}
3 hrs	2.52×10^{-2}
4 hrs	2.85×10^{-2}
overnight	5.36×10^{-2}

[a] $[[Fe^{III}(bpy)(CN)_4]^-] = 8.4 \times 10^{-5}$ M, [EDTA] = 5.0×10^{-4} M, $[NaClO_4]$ = 0.1 M and pH = 6.0 (cacodylate buffer, 20 mM).

Table A-7. $[Fe(bpy)_2(CN)_2]NO_3$ vs $[GSH]_t$ Stoichiometry Determination Spectrophotometric Titration[a]

Expt	$[Fe(bpy)_2(CN)_2]^+$, mL	Abs $_{(550\,nm)}$	Dilution correction [b]
1.	0.10	0.394	0.414
2.	0.20	0.804	0.884
3.	0.30	1.16	1.33
4.	0.40	1.48	1.78
5.	0.50	1.76	2.20
6.	0.60	2.03	2.64
7.	0.70	2.15	2.90
8.	0.80	2.18	3.05
9.	0.90	2.15	3.12
10.	1.0	2.10	3.15

[a] $[[Fe(bpy)_2(CN)_2]NO_3]$ = 2.45 mM, 2.0 mL of 0.495 mM GSH, acetate buffer at pH 4.7 and [dipic] = 1 mM.

[b] Dilution correction; Abs $_{(550)}$ × {2.0 + (Fe^{III} vol)}/2.

Moles $[Fe(bpy)_2(CN)_2]NO_3 = [2.45 \times 10^{-3}\ M \times 6.2 \times 10^{-4}\ L] = 1.5 \times 10^{-6}$ moles

Moles $[GSH]_t = [4.95 \times 10^{-4}\ M \times 2.0 \times 10^{-3}\ L] = 9.9 \times 10^{-7}$ moles

Stoichiometry ratio = $\frac{n[Fe^{III}]}{n[GSH]t} = 1.5 \pm 0.5$

Table A-8. $[Fe(bpy)(CN)_4]^-$ vs $[GSH]_t$ Stoichiometry Determination

Spectrophotometric Titration[a]

Expt	$[Fe(bpy)(CN)_4]^-$, mL	Abs (λ = 482 nm)
1.	0.00	0.002
2.	0.10	0.319
3.	0.20	0.674
4.	0.30	0.979
5.	0.40	1.25
6.	0.50	1.56
7.	0.60	1.82
8.	0.70	2.08
9.	0.80	2.17
10.	0.9	2.20
11.	1.0	2.24
12.	1.1	2.28

[a] $[[Fe(bpy)(CN)_4]^-]$ = 3.5 mM, 2.0 mL of 1.0 mM GSH, cacodylate buffer at pH 6.3 and [dipic] = 1 mM.

Moles $[Fe(bpy)(CN)_4]^-$ = [3.5×10^{-3} M × 6.9×10^{-4} L] = 2.41×10^{-6} moles.

Moles $[GSH]_t$ = [1.0×10^{-3} M × 2.0×10^{-3} L] = 2.0×10^{-6} moles.

Stoichiometry ratio = $\frac{n[Fe(\mathrm{III})]}{n[GSH]t}$ = [2.41×10^{-6} moles] ÷ [2.0×10^{-6} moles] = 1.2 $\pm$ 0.2

Table A- 9. Kinetic Data for the PBN (a Spin Trap) Optimization in the Reaction of $[Fe(bpy)_2(CN)_2]^+$ with $[GSH]_t$ at Low pH.[a]

Expt	[PBN], mM	$t_{1/2}$, s	k_{obs}, s^{-1}	fit
1.	0.00	40.1	1.59×10^{-2}	bad
2.	0.05	52.0	1.31×10^{-2}	good
3.	0.10	51.0	1.35×10^{-2}	good
4.	0.20	51.0	1.36×10^{-2}	good
5.	0.40	50.0	1.37×10^{-2}	good

[a] $[GSH]_t$ = 0.50 mM, $[[Fe(bpy)_2(CN)_2]^+]$ = 0.05 mM, acetate buffer, pH = 3.2, [dipic] = 1 mM, μ = 0.1 M ($NaClO_4$).

Table A-10. PBN is not Required above pH 4.5[a]

Expt	[PBN], mM	$t_{1/2}$, s	k_{obs}, s^{-1}	fit
1.	0.00	2.26	2.97×10^{-1}	good
2.	0.10	2.26	3.03×10^{-1}	good

[a] $[GSH]_t$ = 1.0 mM, $[[Fe(bpy)_2(CN)_2]^+]$ = 0.05 mM, acetate buffer, pH = 4.5, [dipic] = 1 mM, μ = 0.1 M ($NaClO_4$).

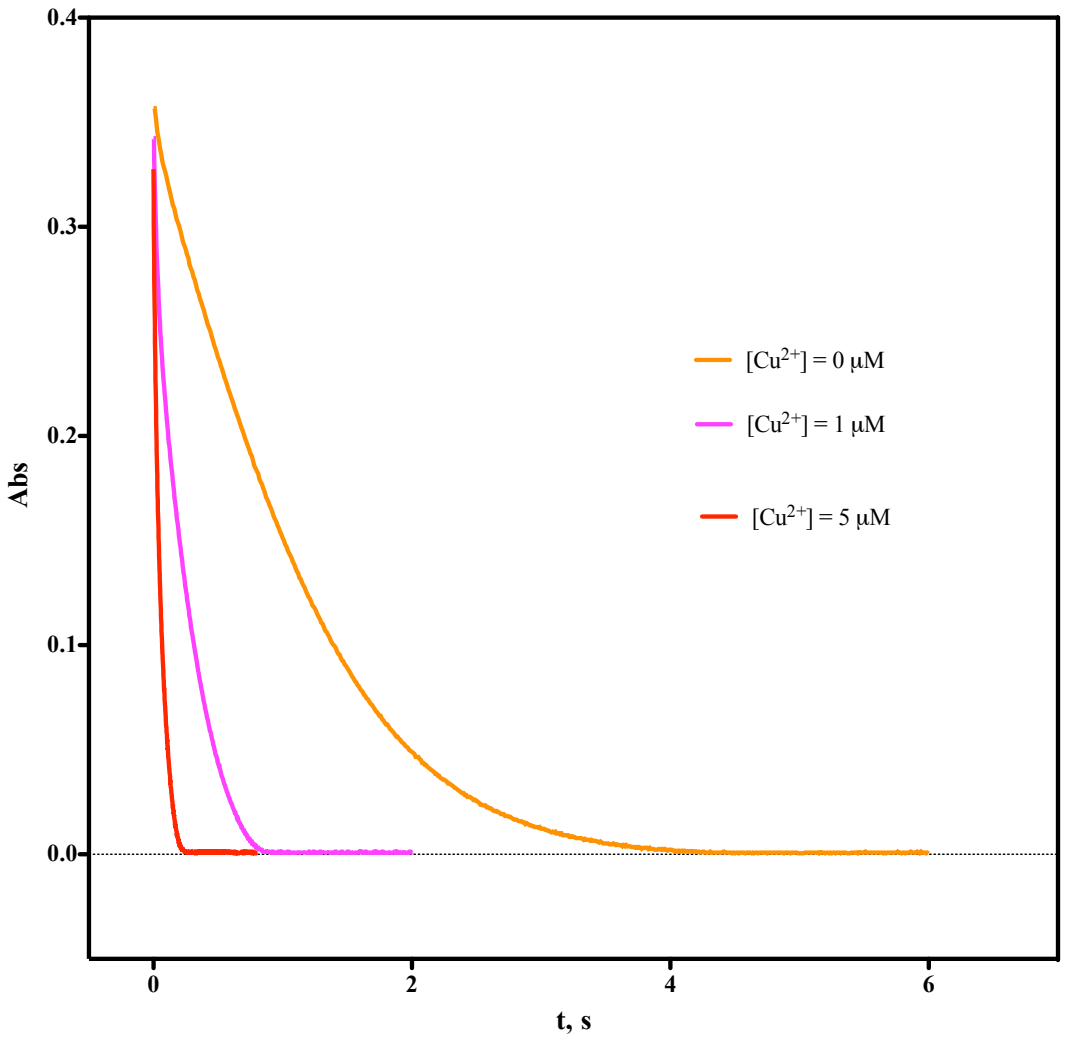

Fig A-1. Kinetic traces of the Cu^{2+} catalysis with fits in the reaction of GSH with Ir^{IV}.

$[IrCl_6^{2-}] = 0.10$ mM, [GSH] = 1.0 mM, $[Cu^{2+}] = 0$, 1 and 5 μM,

pH = 4.6, acetate buffer, $\mu = 0.1$ M ($NaClO_4$) .

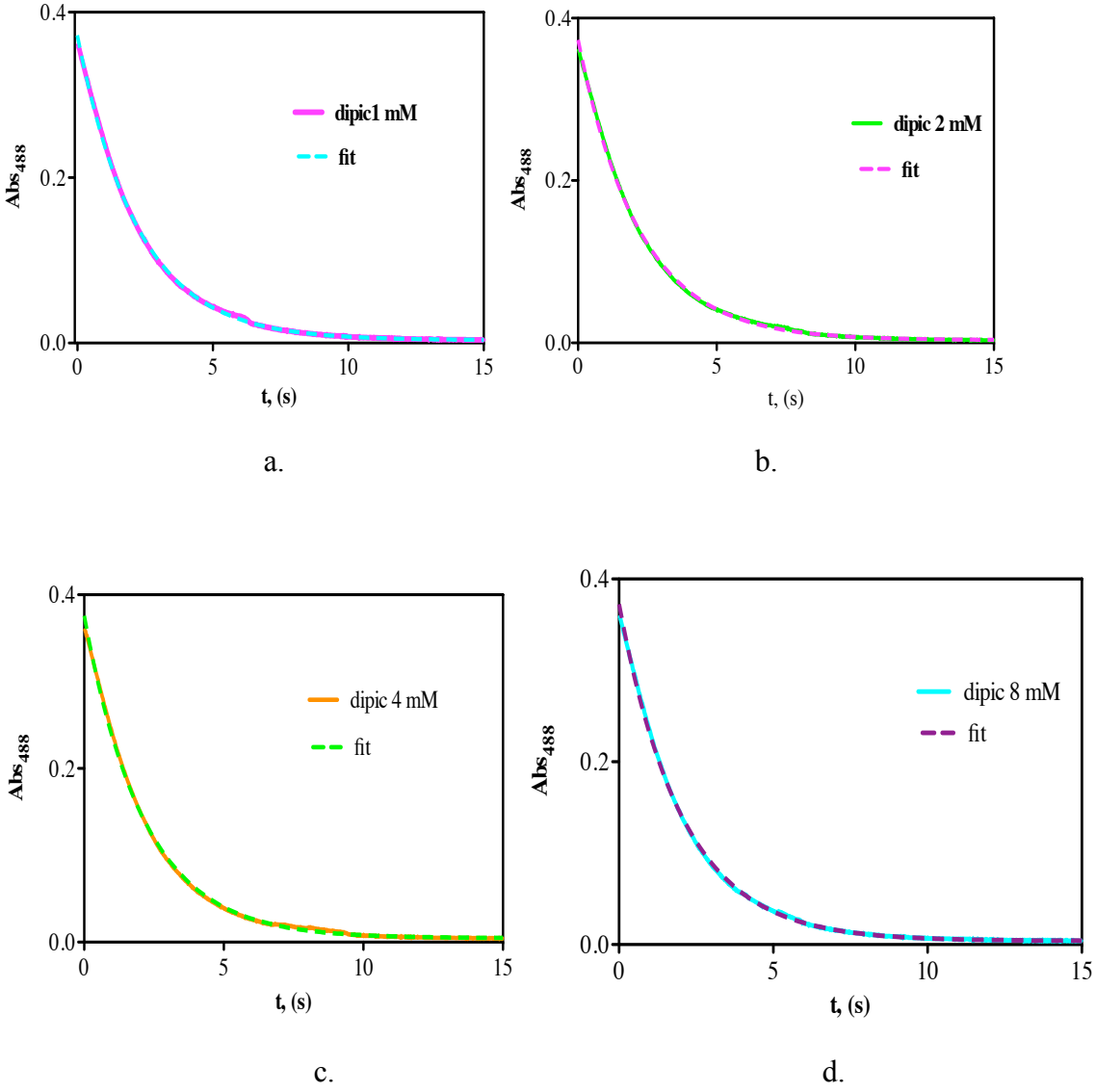

Fig A-2. Kinetic traces for the test (with pseudo-first order fits) of dipicolinic acid effect in the reaction of Ir^{IV} with $[GSH]_t$.

$[Ir^{IV}]_0 = 0.10$ mM, $[GSH]_t = 1.0$ mM, acetate buffer at pH = 4.6, $\mu = 0.1$ ($NaClO_4$).

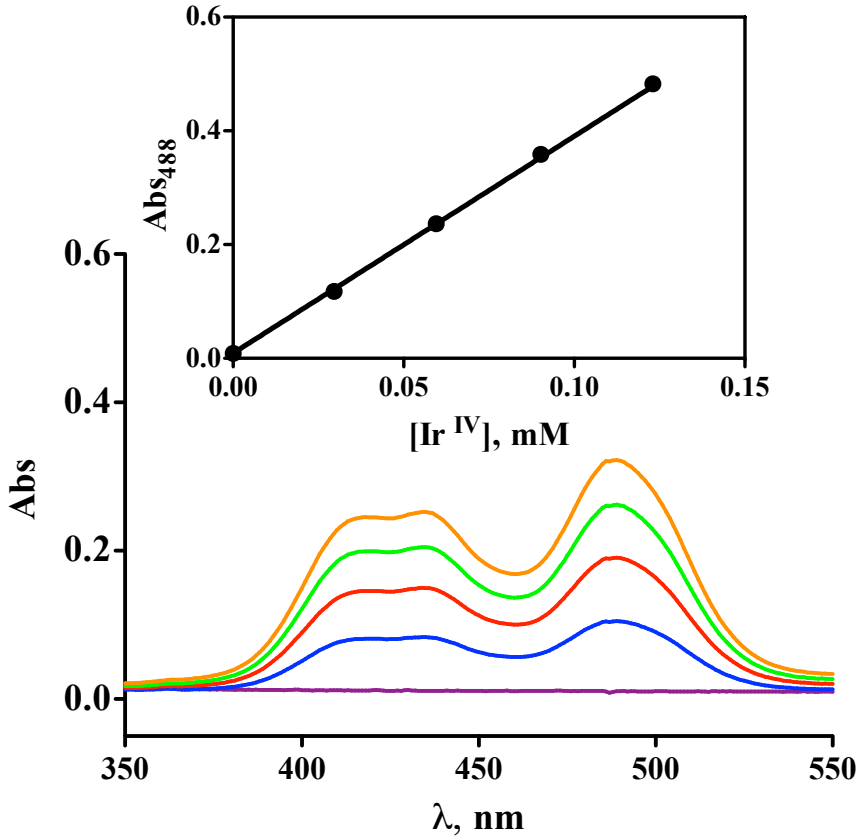

Fig A-3. 20 mM acetate buffer, 0.1 M ($NaClO_4$), 1 mM dipic and no GSH. $[Ir^{IV}]$ = 0.24 mM stock. 0.25 mL aliquot of 0.24 mM Ir^{IV} added to the 2.0 mL blank solution kept in a cuvette at a time.

This test was performed to investigate if buffer, dipic and sodium perchlorate in the absence of GSH consume Ir^{IV}. The result shows that Ir^{IV} does not react with buffer, dipic and $NaClO_4$.

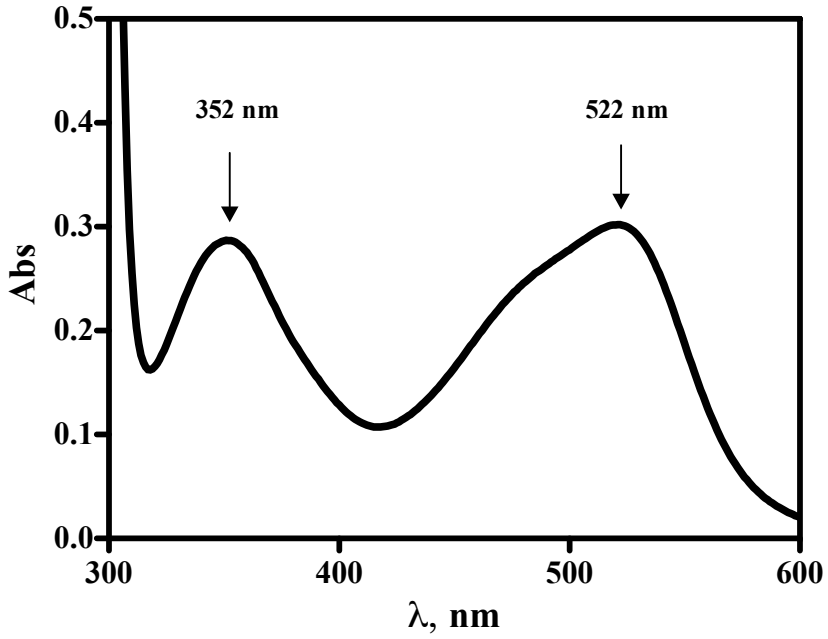

Fig A-4 UV-vis spectrum of dicyanobis(bipyridine)iron(II).

$[Fe^{II}(bpy)_2(CN)_2] = 5.16 \times 10^{-5}$ M in water

A 5.16×10^{-5} M of $[Fe^{II}(bpy)_2(CN)_2]$ solution in water was used to record the UV-vis spectrum and according to which the two absorbance peaks were observed at 352 and 522 nm with molar extinction coefficient 5556 and 5848 M^{-1} cm^{-1} respectively.[37]

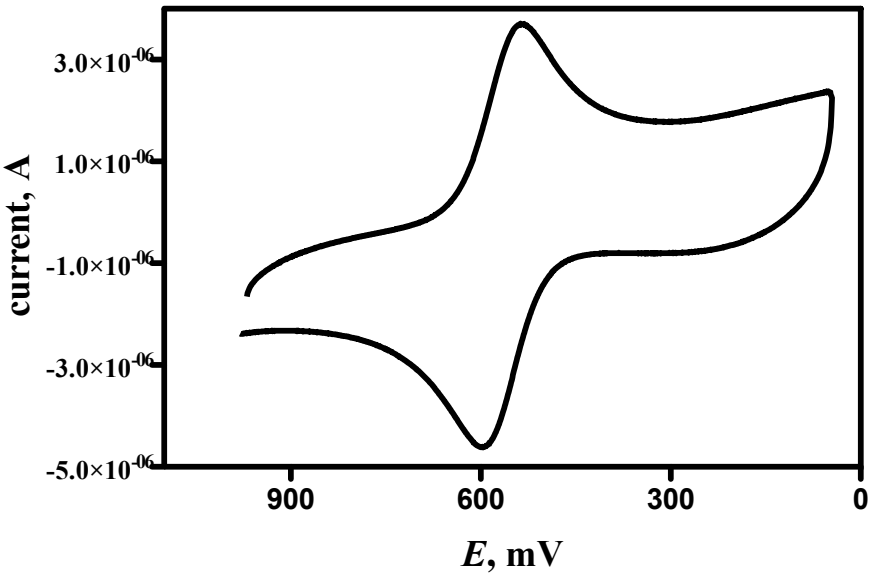

Fig A-5. Cyclic voltammogram of dicyanobis(bipyridine)iron(II).

$[Fe^{II}(bpy)_2(CN)_2] = 1 \times 10^{-3}$ M in 0.1 M $NaCF_3SO_3$

$\Delta E_{p/p} = 60$ mV

$E_{1/2} = 566$ mV; E_f, V vs NHE = 566 + 205 = 771 mV = 0.77 V

CV analysis was performed taking 1×10^{-3} M aqueous solution of it in 0.1 M $NaCF_3SO_3$. The cyclic voltammogram shows $[Fe^{II}(bpy)_2(CN)_2]$ to be quite reversible with $\Delta E_{P/P} = 60$ mV and $E_{1/2} = 566$ mV.[34]

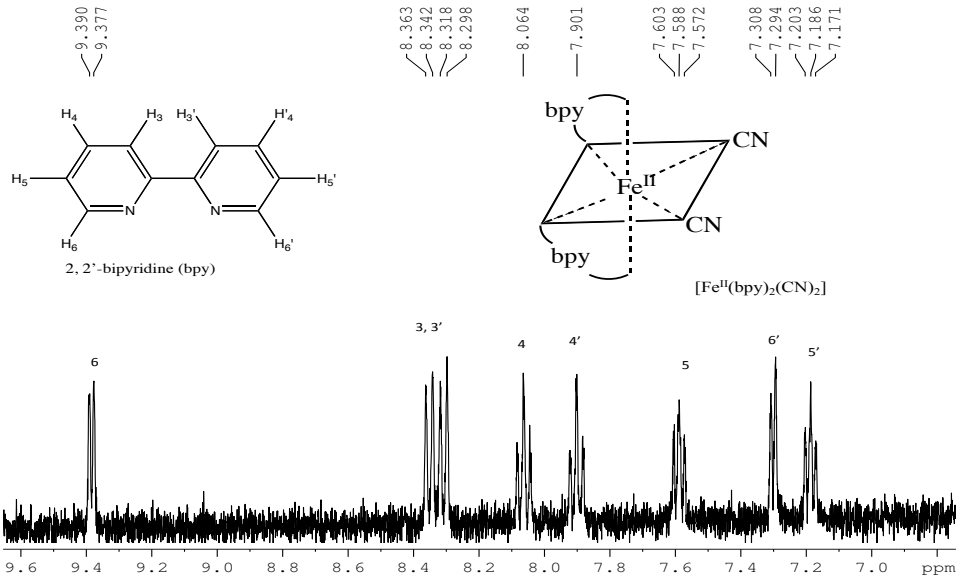

Fig A-6. ^{1}H-NMR spectrum of dicyanobis(bipyridine)iron(II).

$[Fe^{II}(bpy)_2(CN)_2] = 1 \times 10^{-3}$ M in D_2O

^{1}H-NMR : 1×10^{-3} M solution of $[Fe^{II}(bpy)_2(CN)_2]$ was prepared in D_2O with a little DSS and was subjected to analysis. The obtained ^{1}H-NMR spectrum was very consistent with the published literature.[39]

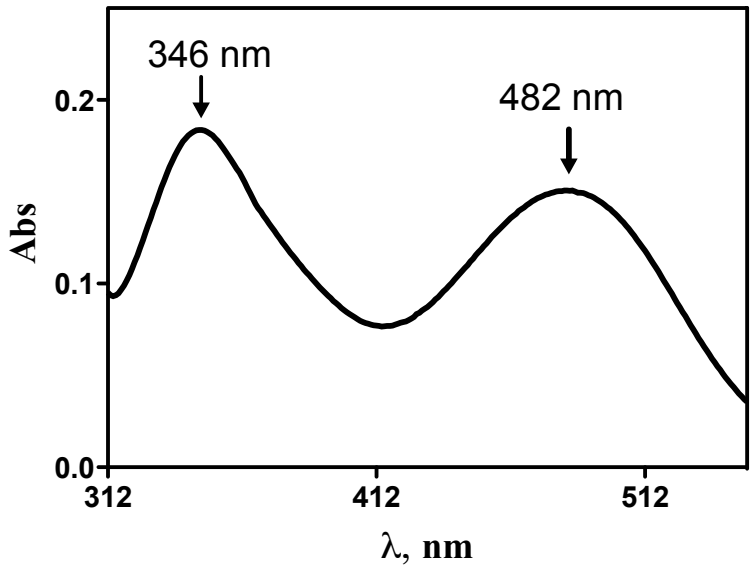

Fig A-7. UV-vis spectrum of potassium tetracyano(bipyridine)iron(II)

$[K_2[Fe^{II}(bpy)(CN)_4]] = 5.2 \times 10^{-4}$ M in water

When 5.2×10^{-4} M aqueous solution of $K_2[Fe^{II}(bpy)(CN)_4]$ was analyzed by UV-vis, two peaks were obtained at 346 and 482 nm with $\varepsilon_{346} = 3200$ and $\varepsilon_{482} = 2624$ M^{-1} cm^{-1} respectively which are characteristic of the compound $K_2[Fe^{II}(bpy)(CN)_4]$.

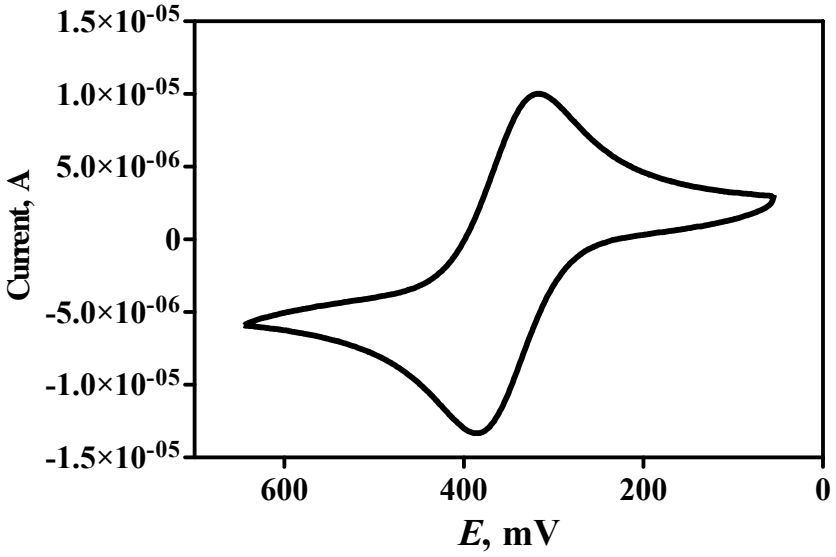

Fig A-8. Cyclic voltammogram of potassium tetracyano(bipyridine)iron(II).

$[K_2[Fe^{II}(bpy)(CN)_4]] = 1 \times 10^{-3}$ M aqueous solution in 0.1 M $NaCF_3SO_3$.

Cyclic voltametry experiment (1×10^{-3} M /0.1M $NaCF_3SO_3$) showed $K_2[Fe^{II}(bpy)(CN)_4]$ to have reversible electrochemistry with $\Delta E_{p/p} = 67$ mV and $E_{1/2} = 351$ mV.

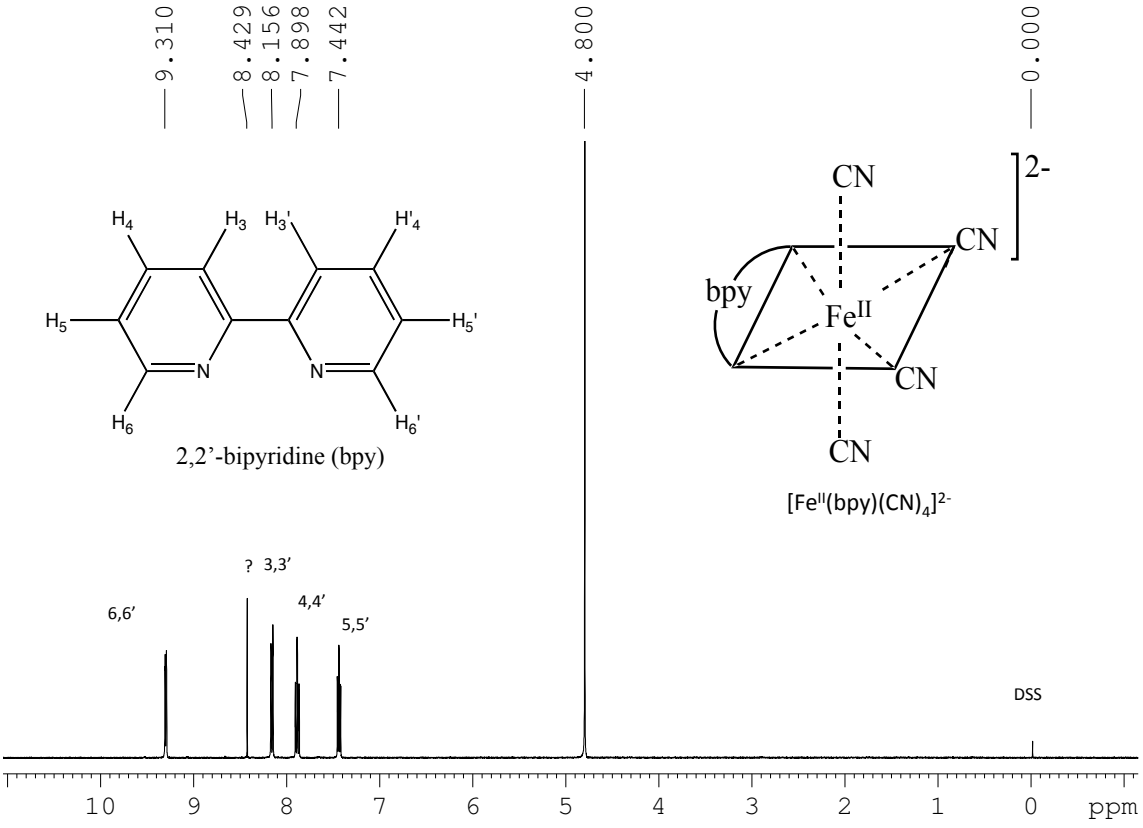

Fig A-9. ^{1}H-NMR spectra of potassium tetracyano(bipyridine)iron(II).

$[Fe^{II}(bpy)_2(CN)_2] = 2 \times 10^{-3}$ M in D_2O

^{1}H-NMR test was done dissolving a small amount of the compound (2×10^{-3} M) in D_2O with DSS in it. The NMR spectra are in accordance with the literature.

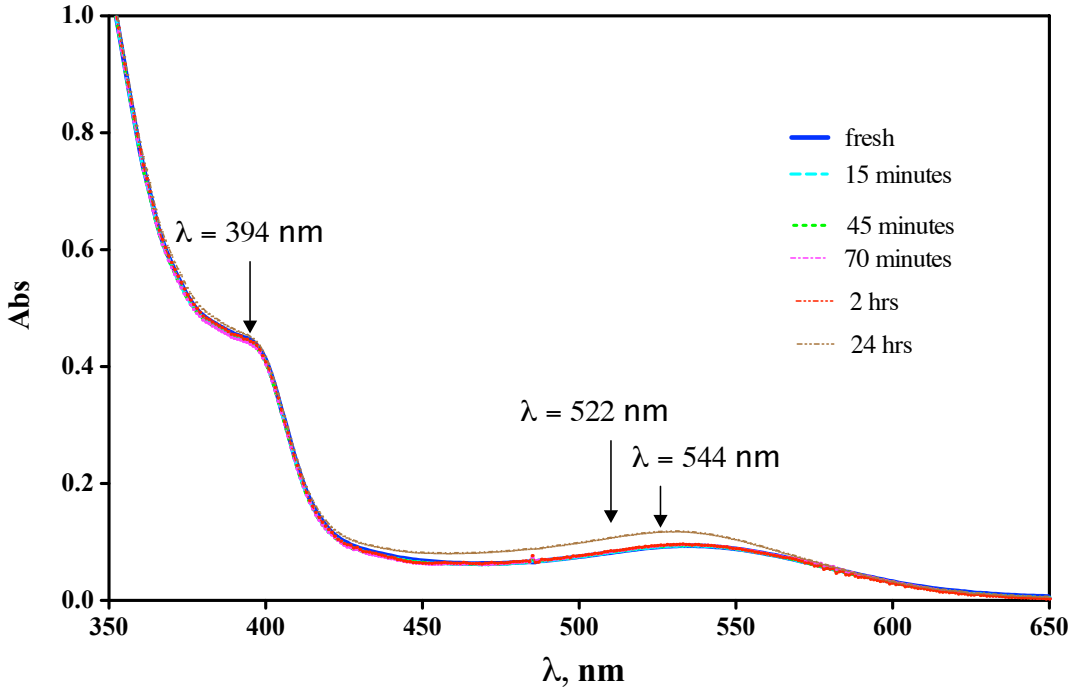

Fig A-10. UV-vis spectra for the stability of aqueous $[Fe^{III}(bpy)_2(CN)_2]^+$.

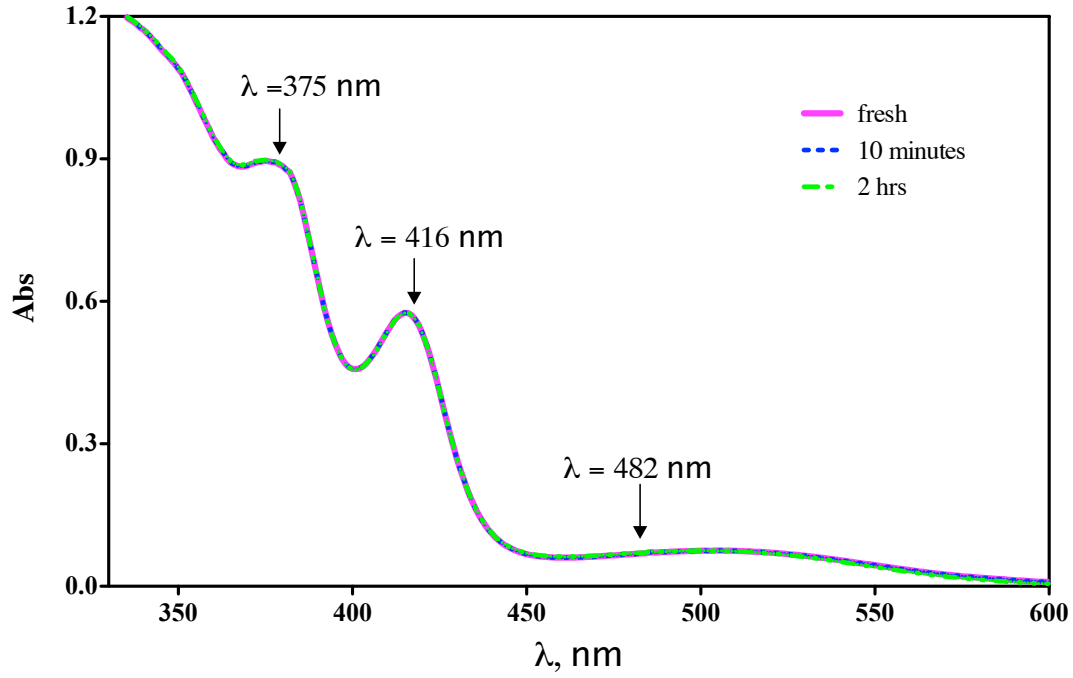

Fig A-11. UV-vis spectra for the stability of aqueous $[Fe^{III}(bpy)(CN)_4]^-$.

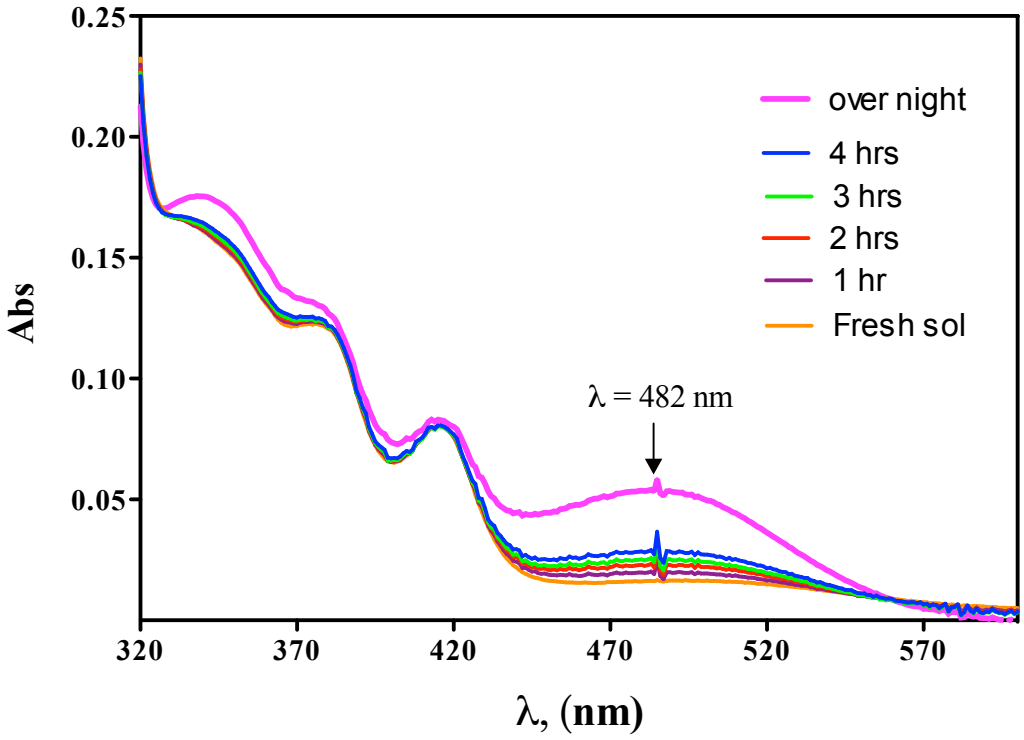

Fig A-12. UV-vis spectra for the stability of aqueous $[Fe^{III}(bpy)(CN)_4]^-$ with EDTA $[[Fe^{III}(bpy)(CN)_4]^-] = 8.4 \times 10^{-5}$ M, [EDTA] = 5.0×10^{-4} M, $[NaClO_4]$ = 0.1 M and pH = 6.0 (cacodylate buffer, 20 mM)

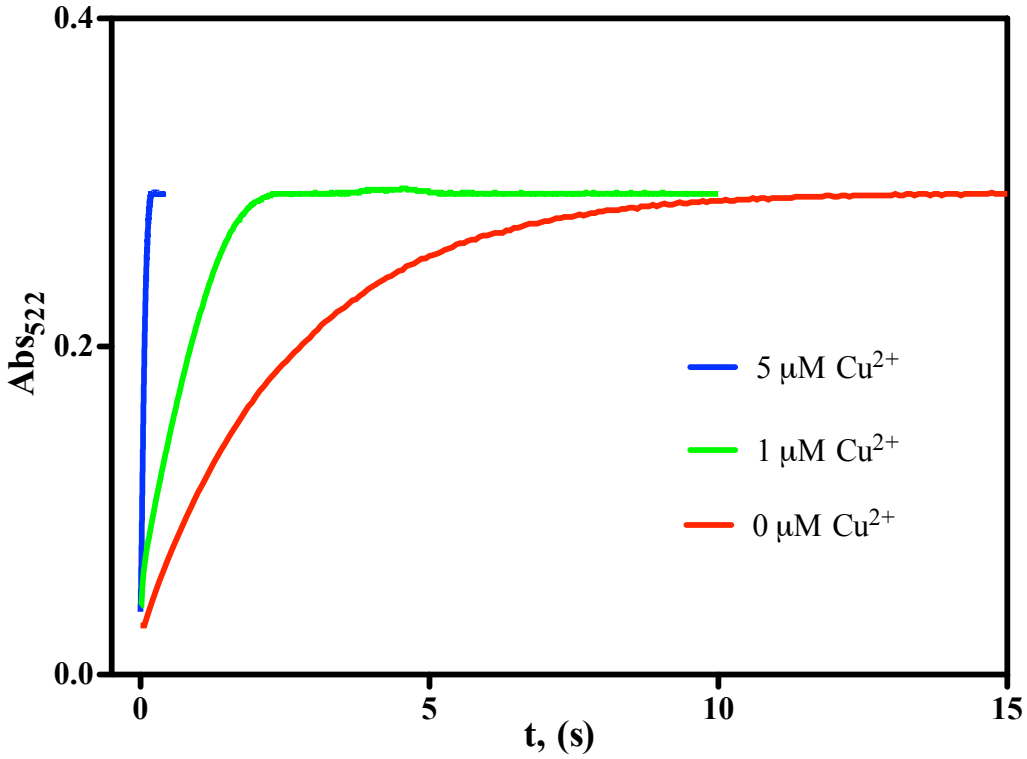

Fig A-13. Comparative kinetic traces of Cu^{2+} ion catalysis in the reaction of $[Fe^{III}(bpy)_2(CN)_2]^+$ with $[GSH]_t$.

$[GSH]_t$ = 0.50 mM, $[[Fe^{III}(bpy)_2(CN)_2]^+]$= 0.05 mM, acetate buffer (10 mM) at pH 4.7. Ionic strength (μ) = 0.1 M ($NaClO_4$).

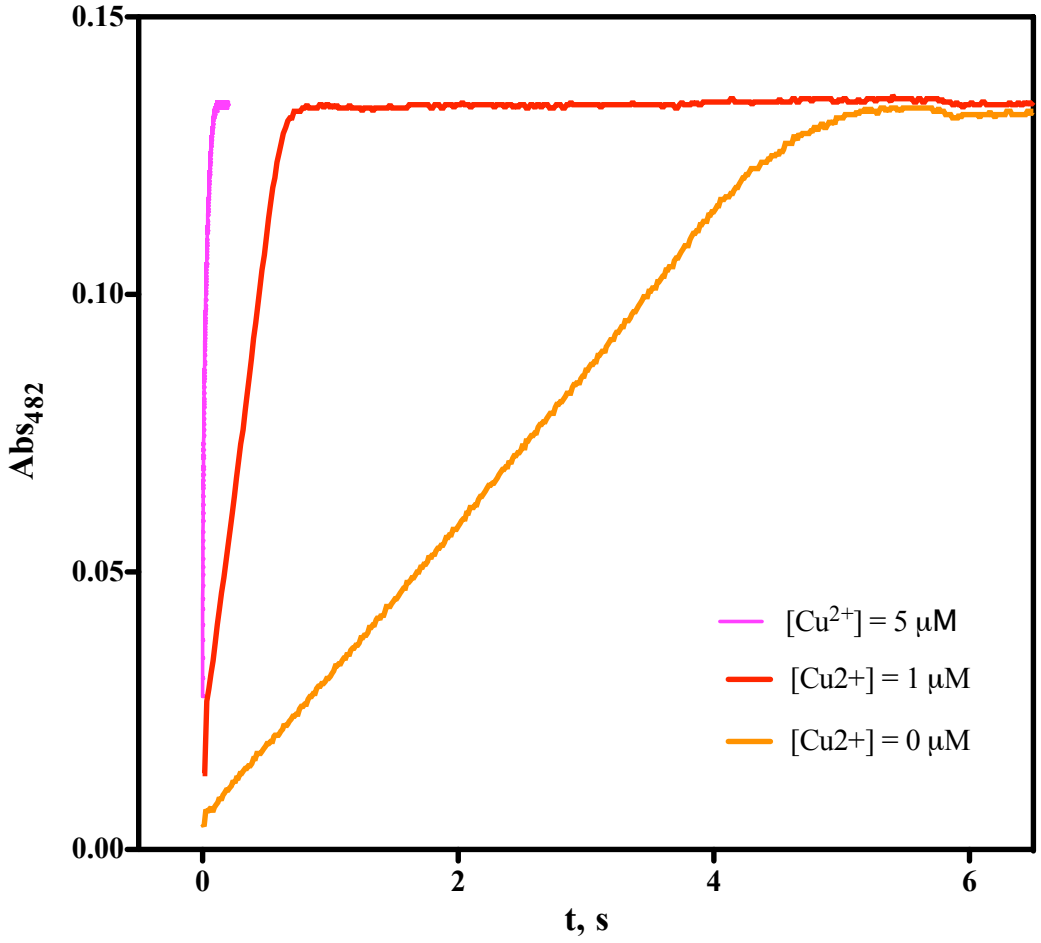

Fig A-14. Kinetic traces for Cu^{2+} catalysis test in the reaction of $[Fe(bpy)(CN)_4]^-$ with $[GSH]_t$.

$[GSH]_t$ = 0.50 mM, $[Fe(bpy)(CN)_4]$ = 0.05 mM, cacodylate buffer at pH = 7.0 , ionic strength (μ) = 0.1 M ($NaClO_4$).

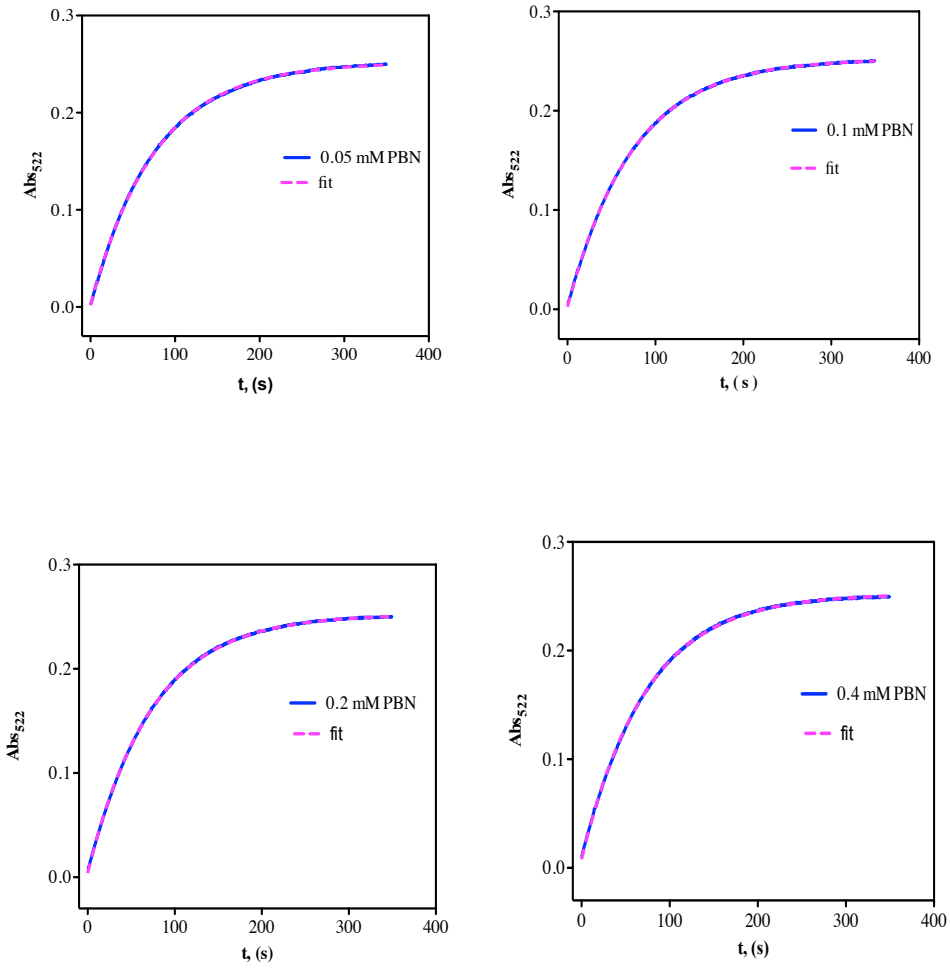

Fig A-15. Kinetic traces for the comparison of PBN effect in the reaction of $[Fe^{III}(bpy)_2(CN)_2]^+$ with GSH at pH 3.2 , acetate buffer.

$[Fe(bpy)_2(CN)_2]^+$ = 0.05 mM, $[GSH]_t$ = 0.50 mM, μ = 0.1 M ($NaClO_4$) and [dipic] = 1 mM. Result: concentration of PBN does not have any significant effect in the reaction.

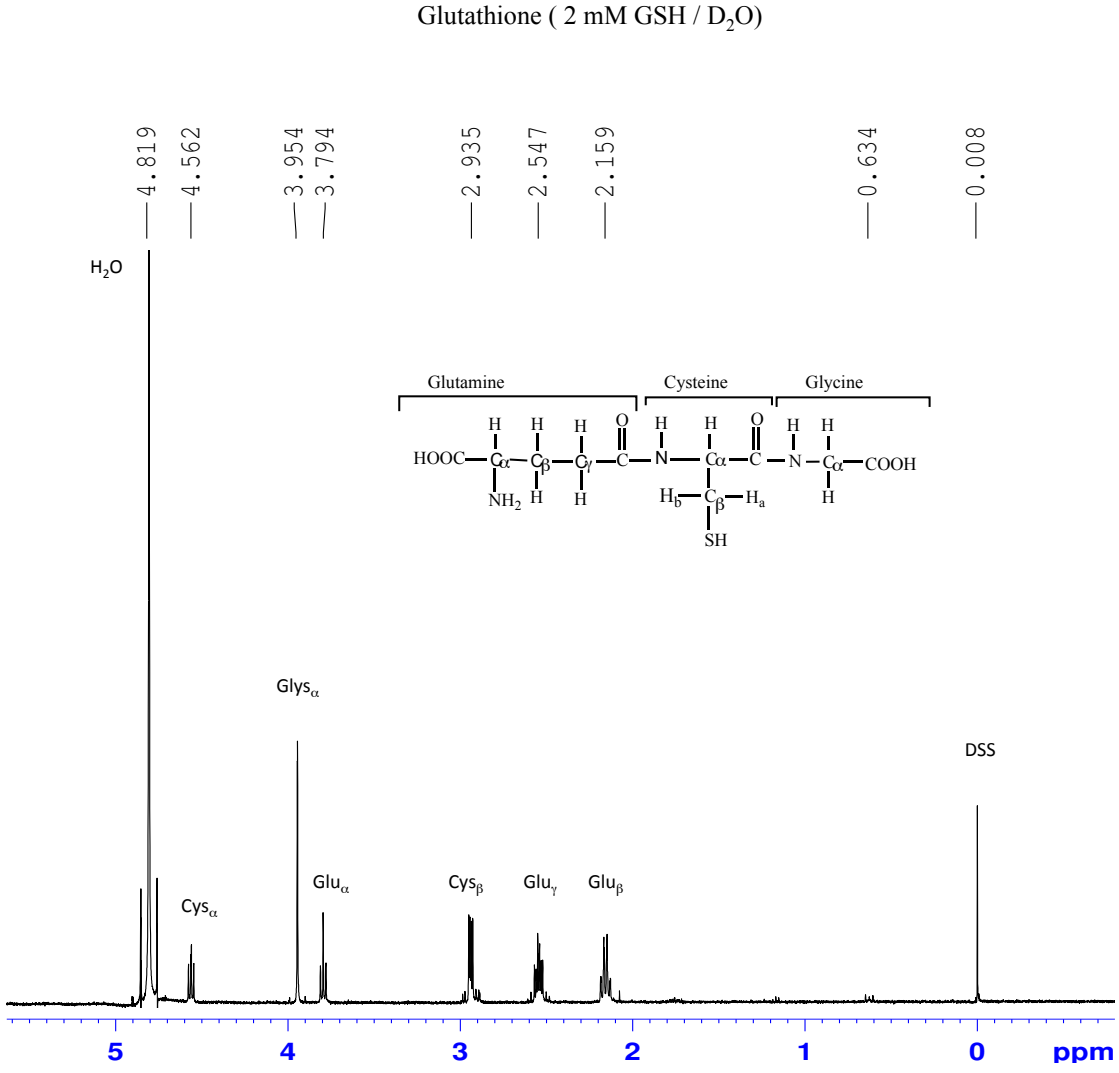

Fig A-16. ^{1}H-NMR spectrum of authentic sample of reduced glutathione (GSH). 2 mM GSH/D_2O.

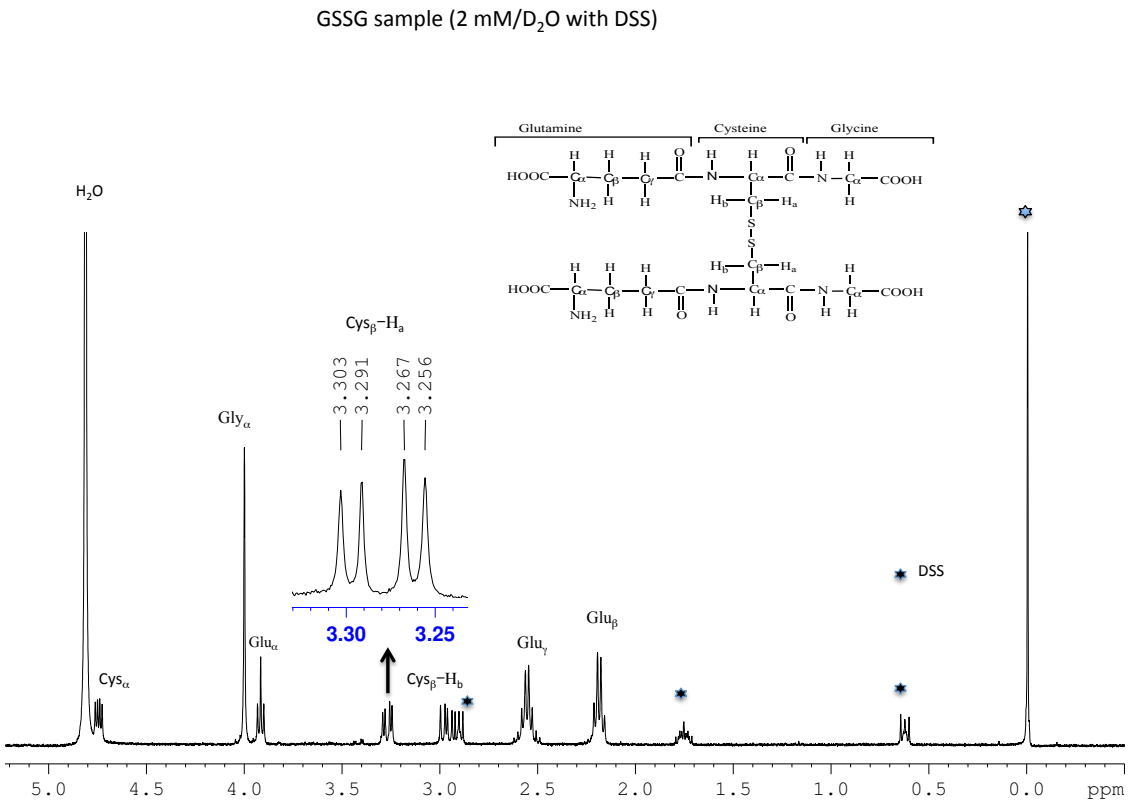

Fig A-17. ^{1}H-NMR spectrum of authentic sample of oxidized glutathione (GSSG). 2 mM GSSG/D_2O.

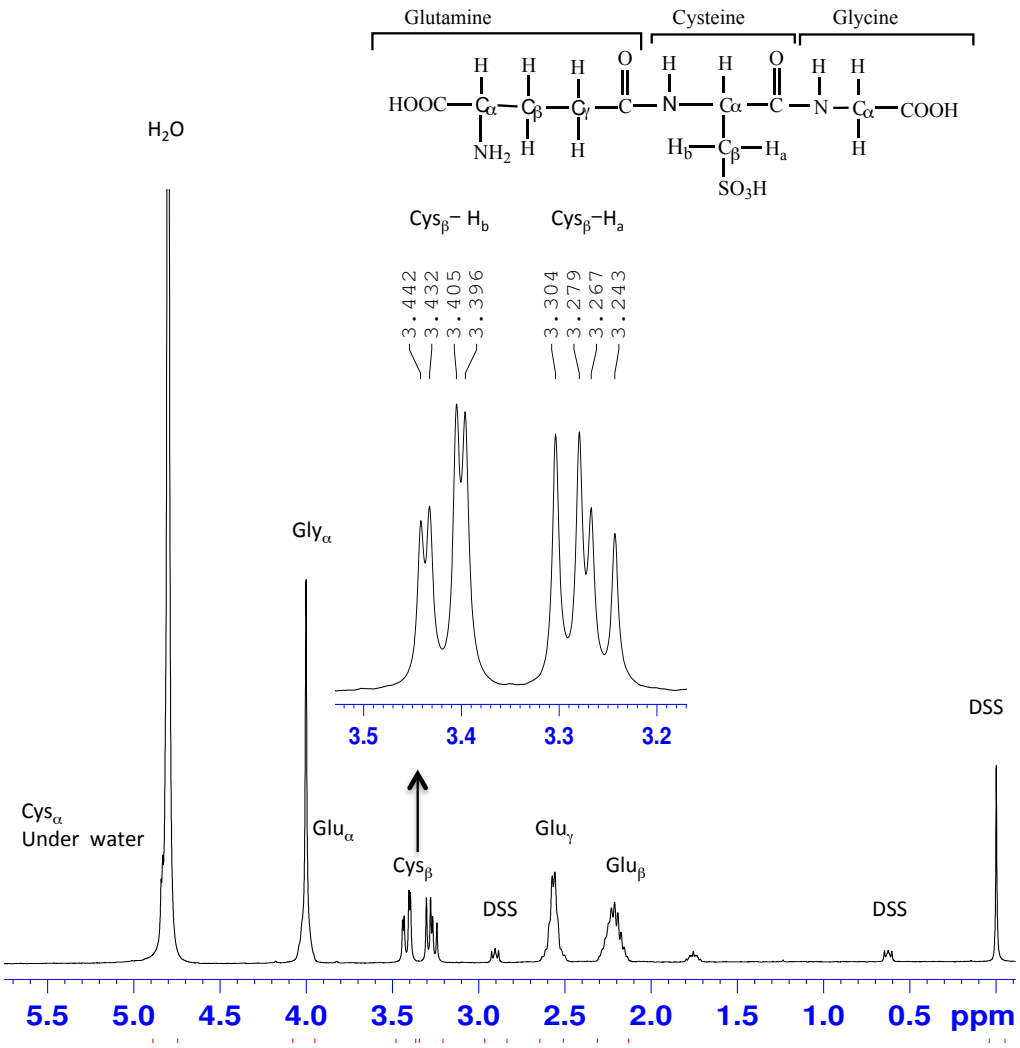

Fig A-18. ^{1}H-NMR spectrum of authentic sample of glutathione sulfonic acid (GSO_3H). 2 mM GSO_3H /D_2O

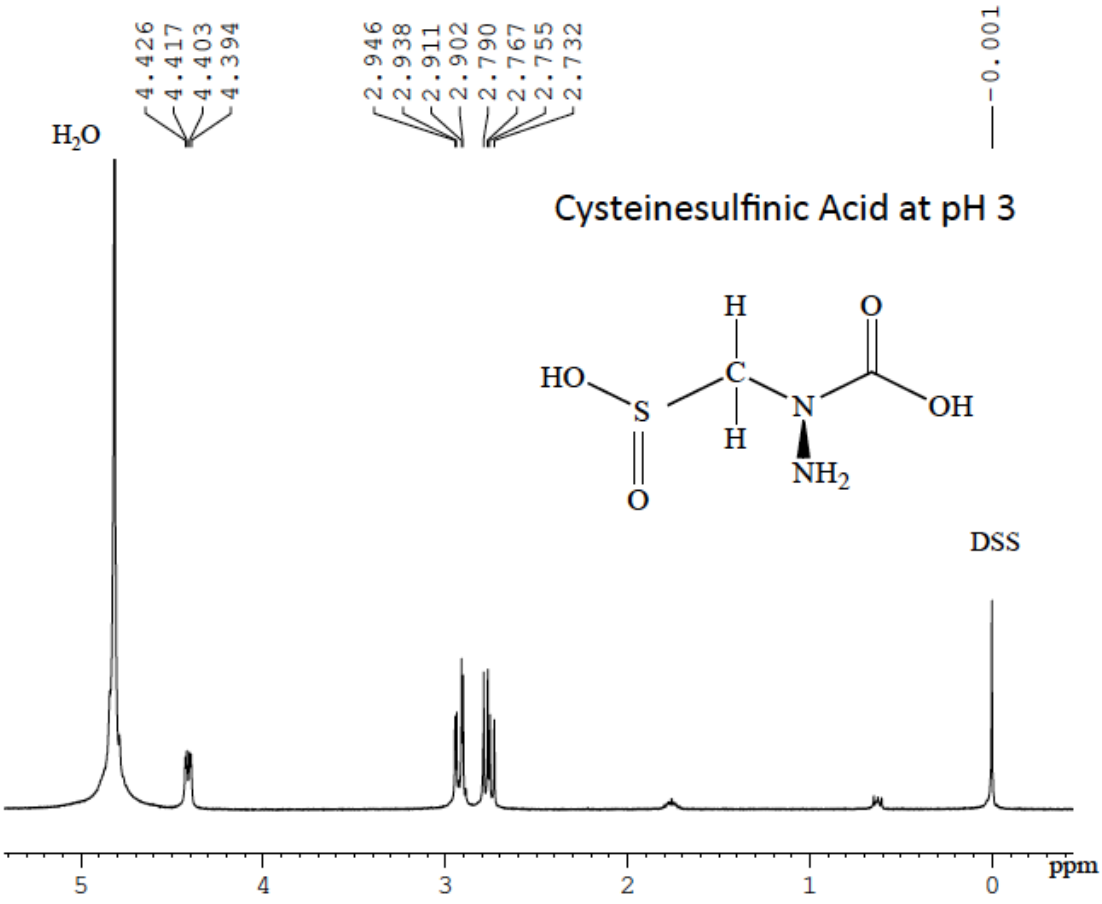

Fig A-19. ^{1}H-NMR spectrum of authentic sample of cysteinesulfinic acid ($CysSO_2H$).

2 mM $CysSO_2H$ /D_2O

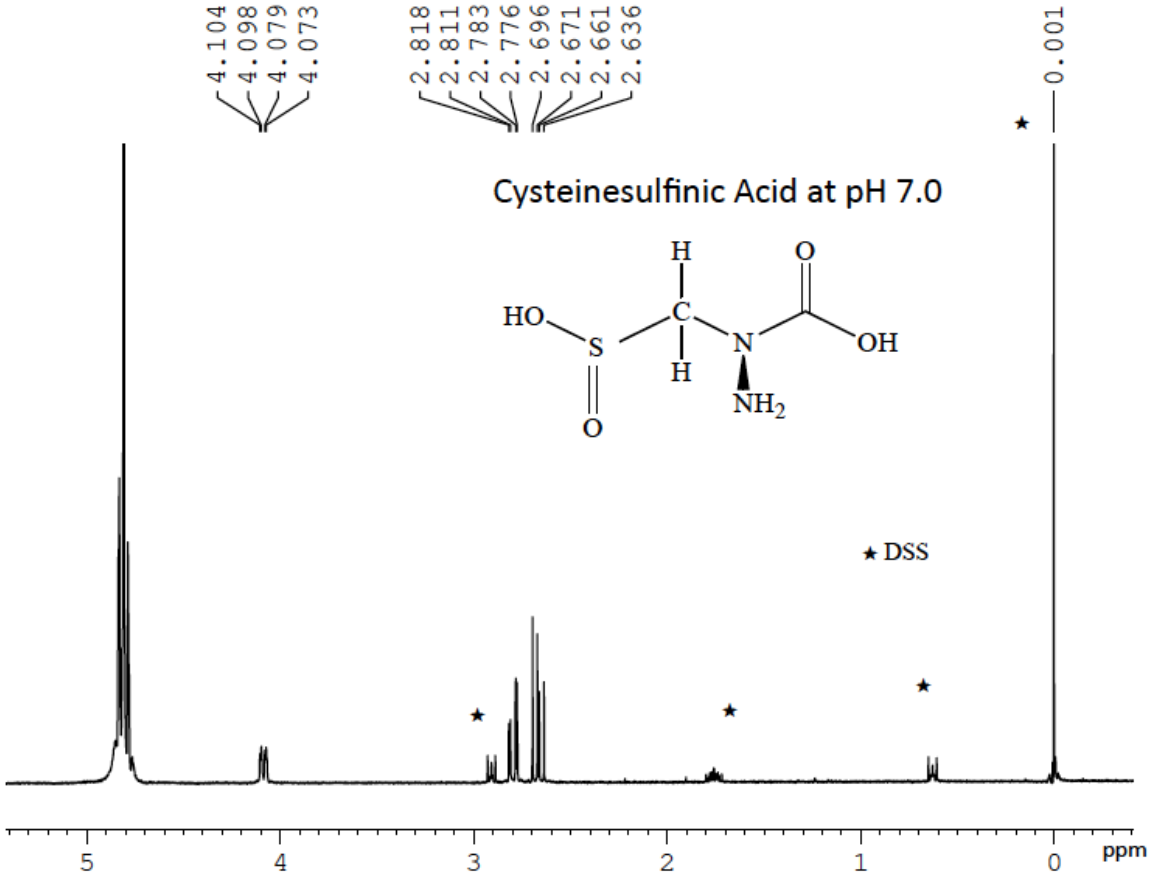

Fig A-20. ^{1}H-NMR spectrum of authentic sample of cysteinesulfinic acid ($CysSO_2H$). 2 mM $CysSO_2H$ /D_2O.

These spectra show the chemical shift value (δ) of cysteinesulfinic acid ($CysSO_2H$) depends on pH.

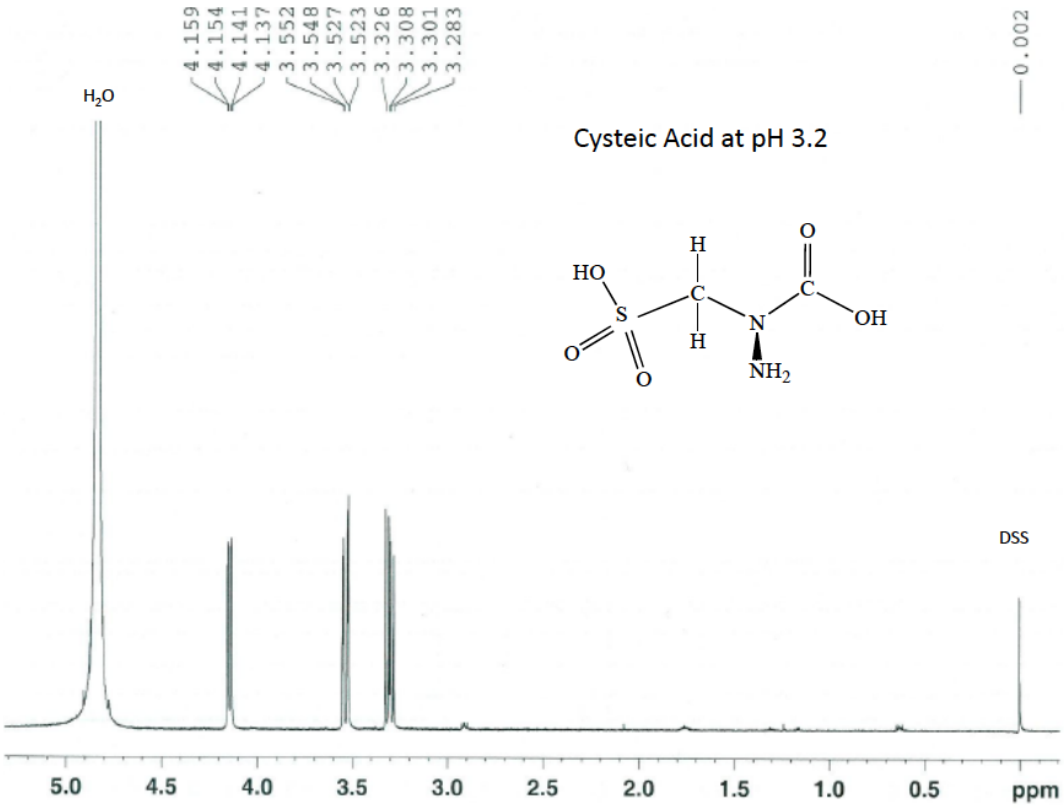

Fig A-21. ^{1}H-NMR spectrum of authentic sample of cysteic acid ($CysSO_3H$). 2 mM $CysSO_3H$ /D_2O.

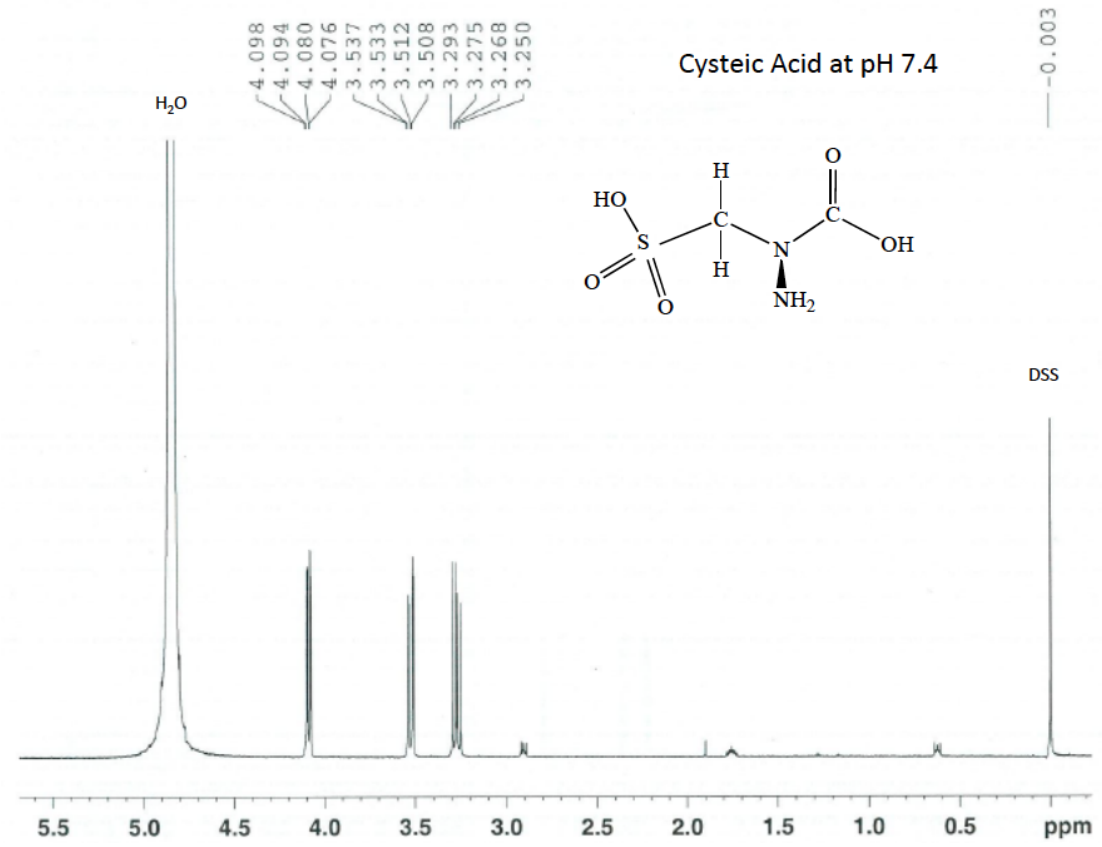

Fig A-22. ^{1}H-NMR spectrum of authentic sample of cysteic acid ($CysSO_3H$). 2 mM $CysSO_3H$ /D_2O.

These spectra show that the chemical shift value (δ) of cysteic acid ($CysSO_3H$) also depends on pH.

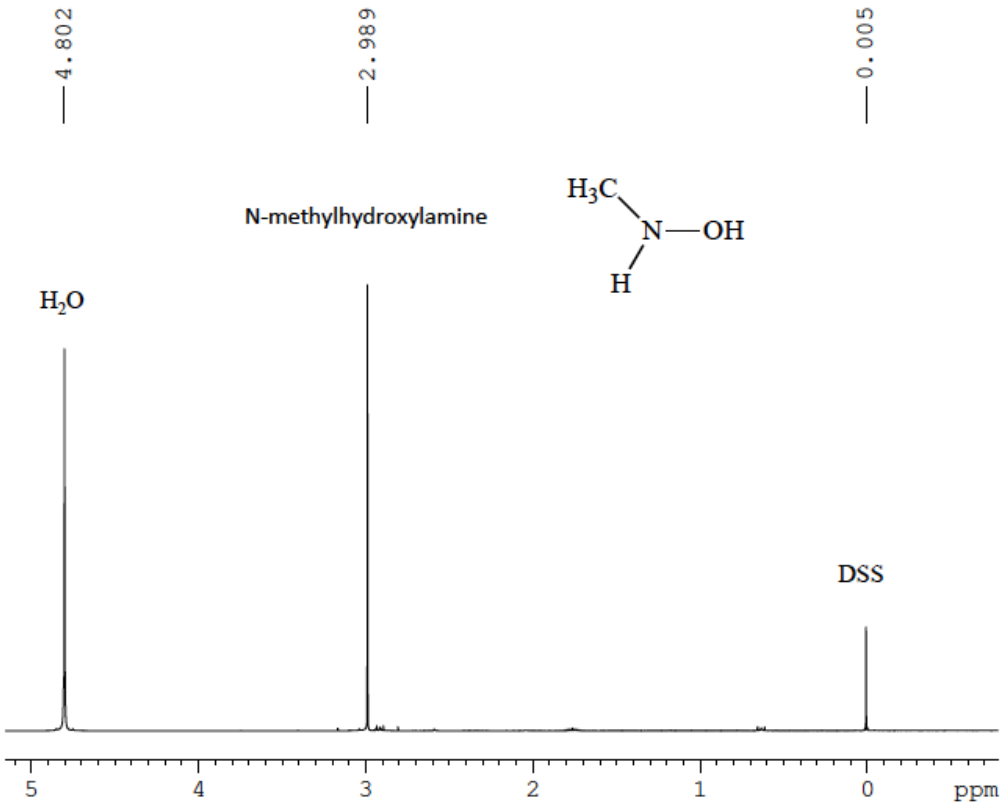

Fig A-23. ^{1}H-NMR spectrum of authentic sample of N-methylhydroxylamine (CH_3NHOH)

20 mM CH_3NHOH /D_2O.

Appendix B

Study of Effects of Buffer Catalysis in Kinetics

Table B-1. Buffer Catalysis Tests in the Reaction of GSH with Ir^{IV}[a]

Buffer	[Buffer], mM	$t_{1/2}$, s	k_{obs}, s^{-1}	pH	[Dipic], mM	[Cu^{2+}], μM
Succinic acid	5	0.032	21.9	5.64	0.0	0.0
Succinic acid	35	0.033	22.1	5.60	0.0	0.0
Succinic acid	5	0.036	19.3	5.62	1.0	0.0
Succinic acid	35	0.035	20.9	5.60	1.0	0.0
Succinic acid	35	0.005	135.6	5.68	0.0	1.0
Succinic acid	5	0.005	133.4	5.60	0.0	1.0
Cacodylic acid	5	0.045	15.3	5.54	1.0	0.0
Cacodylic acid	35	0.05	13.9	5.55	1.0	0.0

[a] [GSH] = 3.0 mM, $[Ir^{IV}]_0$ = 0.08 mM, [dipic] = 1 mM, μ = 0.1 M ($NaClO_4$). No buffer catalysis observed. Reproducible with cacodylate buffer, little lower k_{obs} value may be due to 0.1 unit lower pH than in succinic acid buffer.

Table B-2. Buffer Catalysis Tests in the Reaction of GSH with Ir^{IV} at higher ionic strength (μ) = 1 M (NaCl) [a]

Buffer	[Buffer], mM	k_{obs}, s^{-1}	pH	[Dipic], mM	[NaBr], mM
Succinic acid	5	1.58×10^2	5.74	1.0	0.0
Succinic acid	35	1.68×10^2	5.85	1.0	0.0
Succinic acid	5	1.70×10^2	5.79	1.0	10

[a] [GSH] = 3.0 mM, [Ir^{IV}] = 0.08 mM, [dipic] = 1 mM, μ = 1 M (NaCl).

Ir^{IV} was prepared in buffer and NaCl was added to it. Dipic and NaBr were mixed with GSH. pH was adjusted with NaOH.

Table B-3. Buffer Catalysis Tests in the Reaction of GSH with Ir^{IV} at higher ionic strength (μ) using $NaCl/NaClO_4$ (1 M) [a]

Buffer	[Buffer], mM	k_{obs}, s^{-1}	pH	[Dipic], mM	μ = 1 M
Succinic acid	5	1.74×10^2	5.37	1.0	NaCl
Succinic acid	35	1.17×10^2	5.34	1.0	NaCl
Succinic acid	5	60.3	5.35	1.0	$NaClO_4$
Succinic acid	35	62.0	5.42	1.0	$NaClO_4$
Succinic acid	5 (10 mM NaBr added to GSH)	1.77×10^2	5.38	1.0	NaCl

[a][GSH] = 3.0 mM, $[Ir^{IV}]_0$ = 0.07 mM, [dipic] = 1 mM, μ = 1 M ($NaCl/NaClO_4$). $NaCl/ NaClO_4$ was added to Ir^{IV}. Dipic, buffer and NaBr were mixed with GSH. pH was adjusted with NaOH.

These results show that buffers do not catalyze the reactions between GSH and $[IrCl_6]^{2-}$.